

*Volume 15, No. 1*

*May, 1964*

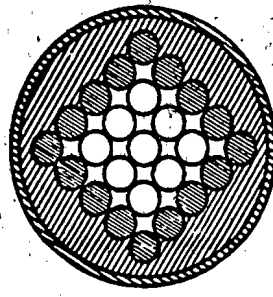
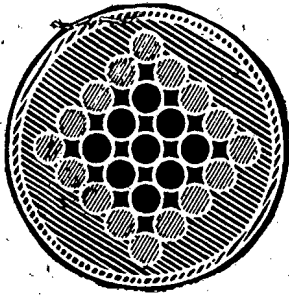
# **SOVIET ATOMIC ENERGY**

**АТОМНАЯ ЭНЕРГИЯ  
(АТОМНАЯ ЭНЕРГИЯ)**

**TRANSLATED FROM RUSSIAN**



**CONSULTANTS BUREAU**



## NUMERICAL METHODS FOR NUCLEAR REACTOR CALCULATIONS

by G. I. Marchuk

"As stated in the foreword, this book is 'an attempt at a systematic exposition of numerical methods for the calculation of thermal, intermediate and fast neutron-reactors.' The author has admirably succeeded in this goal, his exposition of numerical methods for reactor calculations being the most complete yet published. . . . The reviewer was impressed with the thoroughness and skill of the author's presentation. The adjoint reactor equations are applied throughout the text with originality and effectiveness. Similarly, perturbation theory is skillfully developed while its limitations are clearly recognized and defined. In short, the book should appeal not only to the applied mathematician, who is involved in reactor calculations, but also to the general reactor physicist or engineer."

NUCLEONICS

"... completely self-contained. He [Marchuk] derives all the basic equations of reactor theory, develops the most important approximations, and then shows how the reactor equations (in their various approximate forms) can be solved numerically. . . . The advantages are clear. . . . The book has many fine features."

NUCLEAR SCIENCE AND ENGINEERING

Entirely devoted to a systematic exposition of numerical methods of calculation of thermal, intermediate, and fast neutron reactors. Particular attention is devoted to the problems of critical mass, the space-energy neutron flux distribution, and the neutron importance (iterated fission probability). The book gives effective methods for reducing the basic and adjoint reactor equations to a set of multi-group diffusion equations. These equations are then successfully solved by the method of difference factorization. Perturbation theory is used to calculate small effects. Considerable space is devoted to heterogeneous reactor calculations by effective homogenization methods, and in treating fast-neutron reactors, particular attention is paid to numerical methods for solving the kinetic equations. Corresponding to every set of equations derived, an adjoint set of equations is also obtained.

While guaranteeing a given accuracy, these calculations are still sufficiently versatile and convenient to be used in a wide variety of problems, thus making the book particularly valuable to graduate students in physics, doctoral candidates, engineers, and scientific workers specializing in this type of calculation.

293 pages Translated from Russian \$60.00

## THEORY AND METHODS OF CALCULATING NUCLEAR REACTORS

Edited by G. I. Marchuk

Greatest attention is devoted to neutron transport theory and to methods of designing reactors. The general problems of neutron transport theory are discussed and special attention is directed to solving the problem of a point source in an infinite homogeneous medium.

Papers included in the volume discuss such pertinent subjects as: the transmission of a radiation flux near a point source — in which the author develops a numerical method of calculating the radiation field — followed by an analytic solution of the problem; an application of the  $S_n$  method to the solution of the neutron transport equations; as well as methods of calculating nuclear reactor kinetics, including the placement of burnable poisons. Further development of the theory of resonance neutron capture includes such discussions as: numerical methods of calculating the effective resonance integral in homogeneous uniform media, and a method of finding the multi-group cross sections in the resonance region, a theoretical discussion of the mathematical treatment of nuclear physics experiments, and a treatment of resonance parameters, nuclear decay times, etc. The collection employs unified methods of analysis based on a strict mathematical approach, with a subsequent application of the fundamental results to practical solutions.

### CONTENTS

- Application of the Spherical Harmonics to Transport Theory Problems. General Properties of the  $P_n$  Approximations.
- Application of Spherical Harmonics to Transport Theory Problems. The  $P_2$  Approximation.
- One-Velocity Problem of the Angular Distribution of Neutrons Emitted by a Point Isotropic Source at the Center of a Sphere.
- Spatial and Angular Distribution of the Neutrons from a Point Source Considering Anisotropic Scattering.
- Space-Energy Distribution of Fast Neutrons in Hydrogen.
- The Application of One-Group Theory to Reactor Calculations.
- A Two-Group Method for Intermediate-Thermal Reactor Calculations.
- Solution of the Kinetic Equations by the  $S_n$  Method.
- Calculation of Poison Burnup in Reactors.
- Thermal Neutron Spectrum in a Homogeneous Mixture of Moderators at Differing Temperatures.
- Monte Carlo Calculations of the Energy and Angular Distributions of  $\gamma$ -Quanta Penetrating a Plane-Parallel Layer of Finite Thickness.
- Neutron Resonance Absorption in Homogeneous Media.
- Effect of Potential and Resonance Scattering Interference on Neutron Resonance Absorption.
- Neutron Resonance Capture in an Annular Lump.
- Method for Constructing Multi-Group Constants in the Resonance Region Taking Heterogeneous Effects into Account.
- Some Problems in the Statistical Treatment of Nuclear Physics Measurements.
- Optical Model Calculations of the Transport Cross Section.
- Inelastic Scattering of Neutrons by Iron.

180 pages Translated from Russian \$40.00



CONSULTANTS BUREAU 227 W. 17th St., New York, N. Y. 10011

ATOMNAYA ÉNERGIYA  
EDITORIAL BOARD

A. I. Alikhanov	A. I. Leipunskii
A. A. Bochvar	M. G. Meshcheryakov
N. A. Dollezhal'	M. D. Millionshchikov
K. E. Erglis	( <i>Editor-in-Chief</i> )
V. S. Fursov	I. I. Novikov
I. N. Golovin	V. B. Shevchenko
V. F. Kalinin	A. P. Vinogradov
N. A. Kolokol'tsov	N. A. Vlasov
( <i>Assistant Editor</i> )	( <i>Assistant Editor</i> )
A. K. Krasin	
I. F. Kvartskhava	M. V. Yakutovich
A. V. Lebedinskii	A. P. Zefirov

# SOVIET ATOMIC ENERGY

A translation of **ATOMNAYA ÉNERGIYA**  
A publication of the Academy of Sciences of the USSR

© 1964 CONSULTANTS BUREAU ENTERPRISES, INC.  
227 West 17th Street, New York 11, N. Y.

Vol. 15, No. 1

May, 1964

## CONTENTS

	PAGE	
	ENG.	RUSS.
Ion Cyclotron Resonance in a Moving Plasma - I. I. Bakaev, Yu. G. Zalesskii, N. I. Nazarov, A. M. Ukrainskii, and V. T. Tolok. . . . .	655	3
The Kinetic Energy of Fragments and Alpha Particles in the Ternary Fission of U <sup>235</sup> - V. N. Dmitriev, K. A. Petrzhak, and Yu. F. Romanov. . . . .	659	6
Distribution of the Number of Counts on a Neutron Detector Placed in a Reactor - V. G. Zolotukhin and A. I. Mogil'ner. . . . .	664	11
Attenuation of Pile Neutron Flux in Polyethylene - V. N. Avaev, G. A. Vasil'ev, A. P. Veselkin, Yu. A. Egorov, Yu. V. Orlov, and Yu. V. Pankrat'ev. . . . .	671	17
Spectra of Fast Pile Neutrons in Passage Through Polyethylene - V. N. Avaev, G. A. Vasil'ev, A. P. Veselkin, Yu. A. Egorov, Yu. V. Orlov, and Yu. V. Pankrat'ev. . . . .	675	20
The Separation of Zr <sup>95</sup> , Nb <sup>95</sup> , and Ru <sup>106</sup> from a Mixture of Fission Products by Extraction with Tributyl Phosphate - N. E. Brezhneva, V. I. Levin, G. V. Korpusov, E. K. Bogacheva and N. M. Man'ko. . . . .	678	23
The Effect of Neutron Irradiation on the Structure and Mechanical Properties of Alloy Steels - Sh. Sh. Ibragimov, I. M. Voronin, and A. S. Kruglov. . . . .	685	30
The Corrosive Effect of Fuel Element Solvents on Structural Materials - M. M. Kurtenov and E. N. Mirolyubov. . . . .	692	37
Radiation Dosimeters Based on Thermoluminescence Measurements in Aluminum Phosphate Glass (IKS Dosimeters) - I. A. Bochvar, A. A. Vasil'eva, I. B. Keirim-Markus, T. I. Prošina, Z. M. Syritskaya, and V. V. Yakubik. . . . .	704	48
Monitoring Ionizing Radiations Resulting from Nitrogen Reactions - M. T. Dmitriev. . . . .	709	52
LETTERS TO THE EDITOR		
Oscillations in a Spatially Nonuniform Plasma in a Magnetic Field - V. G. Davidovskii. . . . .	717	60
New Ways of Increasing the Efficiency of the Microtron - K. A. Belovintsev, A. Ya. Belyak, V. I. Gridasov, and P. A. Cherenkov. . . . .	720	62
Fast Neutron Polarization Apparatus - N. V. Alekseev, U. R. Arifkhanov, N. A. Vlasov, V. V. Davydov, and L. N. Samoïlov. . . . .	722	62
The Number of Prompt Neutrons and the Kinetic Energy of Fragments During Low-Energy Fission of U <sup>235</sup> - Yu. A. Blyumkina, I. I. Bondarenko, V. F. Kuznetsov, V. G. Nesterov, V. N. Okolovich, and G. N. Smirenkin. . . . .	725	64
The Optimum Condition for Biological Shielding Against a Number of Radiation Sources - G. A. Lisochkin. . . . .	729	67

(continued)

Annual Subscription: \$95

Single Issue: \$30

Single Article: \$15

All rights reserved. No article contained herein may be reproduced for any purpose whatsoever without permission of the publisher. Permission may be obtained from Consultants Bureau Enterprises, Inc., 227 West 17th Street, New York City, United States of America.

**CONTENTS** (continued)

	<b>P A G E</b>	
	<b>ENG.</b>	<b>RUSS.</b>
The Structure of the Gamma Radiation Field from an Isotropic Point Source in Aluminum with Barrier Geometry—V. A. Vorob'ev . . . . .	732	68
The Ratio of the Thermal Neutron Flux in Water to the Power of a Point Source—E. A. Garusov and Yu. V. Petrov . . . . .	736	71
The Effectiveness of a System of Absorber Rods Arbitrarily Distributed in a Reflected Reactor—V. I. Nosov. . . . .	737	71
Frequency Analysis in a System which Includes a Runaway Reactor—A. R. Mirzoyan and I. N. Brikker. . . . .	741	74
Calculation of the Temperature of Regenerative Preheating of Water in Two-Circuit Atomic Power Plants—D. Grecov. . . . .	744	76
An Investigation of Critical Heat Fluxes During Forced Movement of Monoisopropyl Diphenyl Heated Below the Saturation Temperature—G. N. Karavaev, A. D. Leongardt, and Yu. P. Shlykov. . . . .	747	77
Determination of the Permeability of Pipe Walls with Respect to Helium—I. S. Lupakov, Yu. S. Kuz'michev, and Yu. V. Zakharov . . . . .	750	79
The Fluorination of Uranium Sulfate by Chlorine Trifluoride—N. S. Nikolaev and Yu. D. Shishkov. . . . .	753	81
<b>NEWS OF SCIENCE AND TECHNOLOGY</b>		
XIII All-Union Conference on Nuclear Spectroscopy—V. P. Rudakov. . . . .	754	82
Geochemical Conference Dedicated to the Centennial of V. I. Vernadskii—A. I. Tugarinov. . . . .	755	82
New Trends in Research and Applications for Rare Earths—L. Polyakov . . . . .	758	84
Conference on Nuclear Power Development in the Czechoslovak Socialist Republic—S. Medonos . . . . .	760	86
Conference of the Plasma Physics Section of the American Physical Society . . . . .	761	87
Status of the Uranium Industry in the Capitalist Countries as of 1962—V. D. Andreev. . . . .	763	88
USAEC Delegation Visits the Soviet Union . . . . .	769	91
<b>BRIEF COMMUNICATIONS</b> . . . . .	772	93
<b>FROM THE EDITOR</b>		
The Introduction of an International System of Units in the USSR—V. Korotkov . . . . .	774	96
<b>BIBLIOGRAPHY</b>		
New Literature . . . . .	779	99
Articles from the Periodical Literature . . . . .	780	99



## ION CYCLOTRON RESONANCE IN A MOVING PLASMA

I. I. Bakaev, Yu. G. Zalesskii, N. I. Nazarov,  
A. M. Ukrainskii, and V. T. Tolok

Translated from *Atomnaya Énergiya*, Vol. 15, No. 1,  
pp. 3-6, July, 1963

Original article submitted September 22, 1962

The generation and absorption of ion cyclotron waves in moving plasma bunches was observed. Absorption of high-frequency power occurred at two frequencies which were the result of a Doppler shift in both directions from some mean frequency. It was shown that magnetic beaches play an important role in the damping of ion cyclotron waves. Thus, in the absence of one beach, the second absorption peak was not observed. Measurements of the Doppler shift and resonant frequencies made it possible to determine the mean bunch velocity and the plasma density ( $6.7 \cdot 10^6$  cm/sec and  $7 \cdot 10^{12}$  cm<sup>-3</sup>, respectively).

In most cases, experiments investigating plasma containment in magnetic traps obviously would prefer to work with plasma at a maximum high temperature. If the plasma is created by means of external sources, there exists the possibility of additionally heating it before injection into a trap. It is obvious that a sufficiently rapid heating method is required to heat moving plasma bunches. Ion cyclotron resonance may prove to be such a method.

In fact, no more than  $10^{-5}$  sec are required for a significant acceleration of plasma ions [1-3] under present-day conditions for performing experiments on heating a stationary plasma by ion cyclotron resonance. Therefore, with bunch velocities of the order of  $10^7$  cm/sec, the length of a heating section will have reasonable dimensions (no more than 1 m). Besides the heating effect, one can probably expect some improvement in the conditions for ion capture in a magnetic trap because of the increased ion velocity which is directed perpendicularly to the magnetic lines of force. Comparing resonance high-frequency heating in stationary and moving plasmas, it is appropriate to note still another consideration. In the first case, the plasma completely fills the volume of the dielectric chamber where the heating must occur. The internal surface of the wall of the cylindrical chamber to which the coil of the high-frequency circuit is attached is subject to the action of high-frequency electrical discharge since the electrical field intensity is a maximum at the wall. In such a situation, it is difficult to insure the absence of a large quantity of impurities from chamber wall materials in the heated plasma.

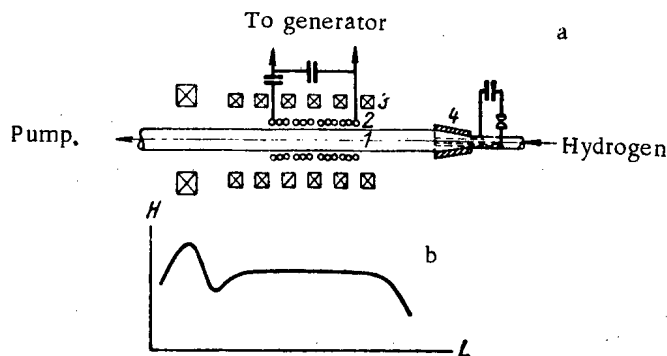


Fig. 1. Diagram of the experimental apparatus (a) and magnetic field topography (b): 1) plasma tube; 2) heating coil; 3) solenoid; 4) plasma gun.

In the case where there is heating of plasma bunches which are moving in a high vacuum along a magnetic field, it is possible to isolate them from the chamber walls during their time of flight if the cross section of a bunch

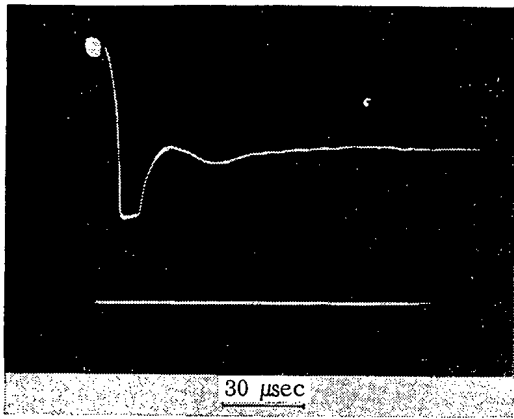


Fig. 2. Oscillogram of the non-resonant loading introduced into the high-frequency circuit by a bunch.

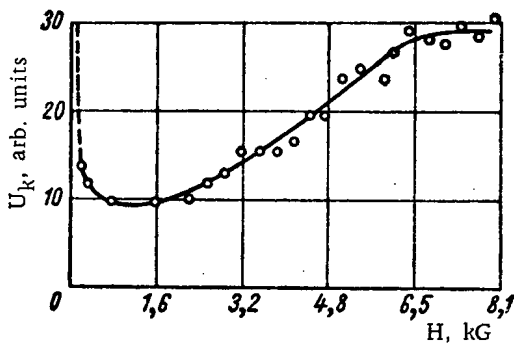


Fig. 3. High-frequency circuit voltage as a function of magnetic field intensity.

are injected into it from an electrodeless plasma gun. The gun is located at a distance of 45 cm from the edge of the uniform portion of the magnetic field and in a region where the magnetic field intensity is close to zero. Admission of the gas is accomplished by a pulsed valve (not shown in Fig. 1). The working gas is hydrogen which passes into the valve through a palladium filter.

The timing of all the elements of the equipment was so chosen that the bunches reached the heating coil at the time of maximum intensity of the longitudinal magnetic field.

In the experiments, the velocity of the bunches which moved along the longitudinal magnetic field and the dependence of the high-frequency circuit voltage on magnetic field intensity were measured.

The bunch velocity,  $V_z$ , was measured with an electrical probe, placed in the plasma; it was measured by means of photomultipliers, and it was also evaluated from the rise rate of the loading introduced into the high-frequency circuit by the bunches. All these methods gave approximately the same result:  $V_z \approx 6 \cdot 10^6$  cm/sec.

The shape of the loading introduced into the high-frequency circuit by a bunch is shown in the oscillogram in Fig. 2 for the case where the magnetic field intensity was less than the cyclotron value. Here, the straight line indicates the base line, the point at the top—the magnitude of the voltage in the circuit prior to the appearance of a bunch within the heating coil. The loading has a rise time approximately  $6 \mu\text{sec}$  long. Considering that the loading rise time is equal to the time during which the bunch fills the entire heating coil, one can evaluate the bunch velocity in the magnetic field. It was equal to  $\sim 7 \cdot 10^6$  cm/sec. From the curve in Fig. 3, one can make some judgement about bunch loading of the high-frequency circuit as a function of magnetic field intensity. There is a certain optimal region of magnetic field intensity values from 1.0 to 2.5 kG where the loading is maximal.

entering the chamber is less than the cross section of the chamber itself. Further, there is no need for the creation of high-frequency discharge at the chamber walls since a vacuum no poorer than  $10^{-7}$  mm Hg can be maintained in this situation. If a bunch passes into the high vacuum along the axis of the heating high-frequency coil so that it doesn't touch the windings, then the dielectric chamber becomes unnecessary. Thus, the entire heating system can be located within a heated metallic casing. Besides assuring sufficiently good vacuum conditions, in such a case it is possible to ensure a high degree of electrical safety for the high-frequency heating circuit and, consequently, to have the possibility of increasing the power supplied to the plasma.

The considerations presented above will serve as subjects for investigation in future experiments. In this paper, only the first experiments on the observation of ion cyclotron resonance in plasma bunches are described.

The experimental equipment is schematically shown in Fig. 1a. The magnetic field is created by a solenoid during the time a condenser bank is discharged through it. The topography of the magnetic field is shown in Fig. 1b. There is a uniform portion 50 cm long where the nonuniformity does not exceed 1%; there are two magnetic beaches and a plug at the system exit. The half-life of the magnetic field is 20 msec. High-frequency power is introduced into the plasma by means of the heating coil which is an inductance in the high-frequency circuit and which has a wave length  $\lambda_z = 20$  cm. The high-frequency circuit, designed for a frequency of 10 Mc, is supplied from a generator with a power of 100 kW. The plasma tube, located along the solenoid axis, is in the form of a molybdenum glass tube 75 mm in diameter and 2 m long. A vacuum of the order  $10^{-6}$  mm Hg is maintained in the tube. Plasma bunches

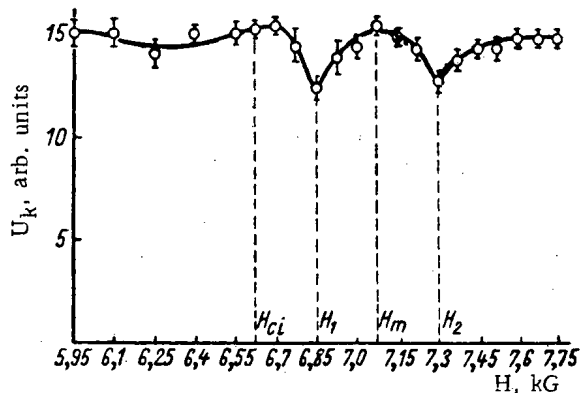


Fig. 4. High-frequency circuit voltage as a function of magnetic field intensity (two magnetic beaches).

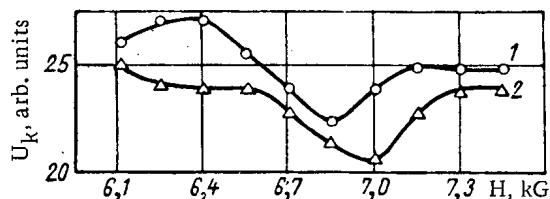


Fig. 5. Resonance loading for two different portions of a bunch depending on the generation of waves with frequency  $\omega_1$  (one magnetic beach).

For weak fields, the loading is small because of low bunch density on account of particle loss at the tube walls. With increasing fields, the loading increases and reaches a maximum for the value  $H=1.6$  kG. With further increase in the field, it falls; this probably occurs both because of the reduction in bunch radius with consequent weakening of its coupling with the heating coil and because of reduction in bunch density resulting from particle reflection at the entrance to the longitudinal magnetic field.

After protracted break-in of the chamber by high-frequency discharge, the measurements that were made indicated the presence of two absorption peaks (Fig. 4) symmetrically located with respect to some value  $H_M$ , and the existence of a large value  $H_{Ci}$  corresponding to ion cyclotron resonance for individual ions. The shift of the high-frequency power absorption peak from  $H_{Ci}$  in the direction of larger magnetic fields is evidence of power consumption by the generation of ion cyclotron waves [4]. One can determine plasma density from the magnitude of this shift. With our experimental conditions, the cyclotron absorption of high-frequency power was small in comparison with nonresonance absorption, obviously because of the weakening of the coupling between plasma and high-frequency circuit at higher values of the magnetic field. Such a dependence was repeated from experiment to experiment, and the curve in Fig. 4 is typical.

The existence of two absorption peaks can be explained by a Doppler shift in the frequency of the generated ion cyclotron waves which are propagated in both directions from the heating coil—along the moving bunch and in the opposite direction. These two frequencies should equal, respectively

$$\omega_1 = \omega_0 - k_z V_z, \text{ and } \omega_2 = \omega_0 + k_z V_z,$$

where  $\omega_0$  is the resonant frequency of the circuit;  $k_z = \frac{2\pi}{\lambda_z}$  is the component of the wave vector directed along the axis;  $\lambda_z$  is the excitation wave length, equal to the wave length of the heating coil.

Having the experimental value  $\Delta\omega = \omega_2 - \omega_1$ , one can determine the bunch velocity averaged over the length of the heating coil.

For the bunch velocity, we have the formula

$$V_z = \frac{\left( \frac{eH_2}{Mc} - \frac{eH_1}{Mc} \right) H_{ci}}{2k_z H_M},$$

which is obtained from the equality  $\Delta\omega = \omega_2 - \omega_1$  with consideration being given to the dispersion relation for ion cyclotron waves [4]. Here,  $H_1$  and  $H_2$  are the magnetic field intensities for which cyclotron waves are generated with frequencies  $\omega_1$  and  $\omega_2$ , respectively;  $H_{ci}$  is the magnetic field intensity for which the resonance condition for individual hydrogen ions in a stationary plasma is fulfilled;  $H_M$  is the value of the magnetic field intensity for which cyclotron waves are generated in a stationary plasma;  $e$ ,  $M$ ,  $c$ , are, respectively, ion charge, ion mass, and the velocity of light. For the values of  $H_1$ ,  $H_2$ ,  $H_{ci}$ , and  $H_M$  shown in Fig. 4, the bunch velocity  $V_z$  equals  $\sim 6.7 \cdot 10^6$  cm/sec. This is in agreement with bunch velocity measurements by other methods.

The bunch density,  $n_i$ , averaged over the length of the heating coil was calculated from the dispersion relation for a stationary plasma [4]

$$n_i \approx \left[ \left( \frac{H_m}{H_{ci}} \right)^2 - 1 \right] \cdot \frac{1}{5 \cdot 10^{-17} \lambda_2^2}$$

and was  $\sim 7 \cdot 10^{12} \text{ cm}^{-3}$ . Note that probing a bunch with an 8 mm microwave signal indicated the existence of a plasma with a density not less than  $1.6 \cdot 10^{13} \text{ cm}^{-3}$  under these conditions. It appears reasonable that bunch parameters change with time; therefore, all comparisons of plasma parameters must be carried out for a fixed instant.

The curves shown in Fig. 5 represent the same functional dependence as in Fig. 4 but for the case where there is no beach at the point where the bunch enters the uniform magnetic field. As can be seen from the curves, absorption of high-frequency power at the frequency  $\omega_2$  is not observed.

In Fig. 5, resonance loading is shown for two different regions of a bunch which are  $\sim 1 \text{ m}$  apart. Curves 1 and 2 correspond to two oscillogram traces. The time interval between them is  $\sim 20 \text{ } \mu\text{sec}$ . The relative shift of the resonance peaks with the field arises, obviously, from a difference in the velocities in the selected regions of the bunch. In this case, the difference amounts to  $\sim 2\%$ . The curves shown illustrate the fact that regions more removed from the forward boundary of a bunch move at lower speeds.

Thus, absorption of high-frequency power was experimentally observed for plasma bunches at two frequencies, shifted by the Doppler effect in both directions from some mean frequency which, in its turn, was shifted toward lower frequencies with respect to the cyclotron frequency for individual hydrogen ions. Such a shift corresponds to the generation of ion cyclotron waves.

Magnetic beaches play an important role in the damping of these waves. With two beaches (at both ends of the heating coil), waves with frequencies  $\omega_1$  and  $\omega_2$  can both be damped, and therefore two high-frequency power absorption peaks are observed. If a steep nonuniformity in the magnetic field replaces one of the beaches, then a wave would be reflected at that point and would return to the coil region. In such a situation, the second absorption peak should not be observed. This was verified experimentally.

Measurements of the amount of Doppler shift make it possible to fix the average velocity of a bunch. Determining  $H_{ci}$  and  $H_m$ , it is possible to obtain information about plasma density. It is obvious that, by getting the time dependence of the quantities mentioned, one can also determine the velocity and density distribution in the plasma along the length of a bunch.

The authors express their deepest gratitude to K. D. Sinel'nikov for discussions of the results.

#### LITERATURE CITED

1. K. D. Sinel'nikov, et al., Zh. tekhn. fiz., 30, 282 (1960).
2. W. Hooke, et al., Phys. of Fluids, 4, 1131 (1961).
3. N. I. Nazarov, et al., Zh. tekhn. fiz., 32, 536 (1962).
4. T. Stix and R. Palladino, Phys. of Fluids, 3, 641 (1960).

---

All abbreviations of periodicals in the above bibliography are letter-by-letter transliterations of the abbreviations as given in the original Russian journal. Some or all of this periodical literature may well be available in English translation. A complete list of the cover-to-cover English translations appears at the back of this issue.

---

THE KINETIC ENERGY OF FRAGMENTS AND ALPHA PARTICLES  
IN THE TERNARY FISSION OF  $U^{235}$

V. N. Dmitriev, K. A. Petrzhak, and Yu. F. Romanov

Translated from *Atomnaya Énergiya*, Vol. 15, No. 1,  
pp. 6-11, July, 1963

Original article submitted August 23, 1962

We measured the energy distributions of ternary fission fragments corresponding to different energy intervals in the spectrum of long-range alpha particles with average energies of 10.6, 16.4, 20.3, and 24.0 MeV. It was found that for  $E_{\alpha} > 15$  MeV the most probable total energy of ternary fission fragments, within the limits of experimental error, was independent of the energy of the alpha particles and that for  $E_{\alpha} = 10.6$  MeV it was about 4 MeV higher.

The results of the measurements are evaluated.

Experimental data on the relation between the kinetic energy of fragments and the energy of long-range alpha particles in the ternary fission of nuclei are of great interest. They are necessary for estimating the degree of deformation of the nucleus when ternary fission takes place and for formulating a hypothesis concerning the mechanism of ternary fission.

Earlier measurements [1], in which we recorded alpha particles over a fairly wide energy range (from 13 to 22 MeV), showed that for  $U^{235}$  the difference between the most probable total kinetic energies of fragments from binary and ternary fission was 15 MeV. It is quite natural that the most probable ternary-fission fragments should be compared with the most probable alpha particles, whose energy, as is known, is 15 MeV. From this it was deduced that

$$E_{\text{bin}} = E_{\text{tern}} + E_{\alpha} \quad (1)$$

On the basis of the previously discovered fact [2] that the average number of neutrons in ternary fission is independent of the energy of the long-range alpha particles, it was assumed that Eq. (1) is valid for less probable fission conditions as well. This assumption was not contradicted by any other experimental data on ternary fission.

In order to verify Eq. (1), in the present study we measured the energies of paired  $U^{235}$  fragments corresponding to separate energy intervals in the spectrum of long-range alpha particles. The experiments were conducted on the reactor of The Leningrad Institute of Physics and Technology of the Academy of Sciences, USSR.

#### The Selection of Energy Intervals in the Spectrum of Long-Range Alpha Particles

The ternary ionization chamber and the electronic equipment used in the study were described in [1, 3]. An important change in the design of the alpha particle recording chamber was the introduction of a shielding grid (Fig. 1), which ensured that the magnitude of the pulse was independent of the angle of incidence of the alpha particle; the signal-to-noise ratio was increased, and the working volume of the chamber was limited. When the grid was introduced, the experiments were conducted at intense neutron fluxes of the order of  $5 \cdot 10^8$  neutrons/cm<sup>2</sup>·sec. The grid consisted of two coaxial rings encircling the collecting electrode and having diameters of 120 and 180 mm; a tungsten wire 0.1 mm in diameter was wound radially around the rings. The inner ring was 8 mm high, the outer ring 12 mm. Fluoroplast uprights were used to attach the entire structure to the annular collector. The chamber was filled with argon (95%) and methane (5%) to a pressure of 1 atmosphere. The addition of methane ensured a constant pulse front ( $\sim 1$   $\mu$ sec) and a stable pulse amplitude (over a period of 10-15 days the amplitude did not vary by more than 2%).

Alpha particles with energies in a fixed interval were isolated by means of pieces of aluminum foil separating the volume of the alpha chamber from the volumes of the fission chambers. Since the latter were of finite dimensions, an alpha particle was braked both in the foil and in the volume of the fission chambers. The amplitude of the pulse in the alpha chamber is maximum in the case when the end of the path of an alpha particle coincides with the boundary of the working volume of the alpha chamber. By using an amplitude discriminator it is possible to re-

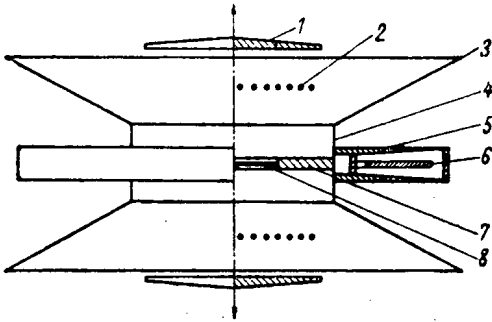


Fig. 1. Schematic diagram of the electrodes of the ternary ionization chamber: 1) fission chamber collector; 2) fission chamber grid; 3) conical electrode of alpha particle recording chamber; 4) aluminum foil; 5) alpha chamber grid; 6) alpha chamber collector; 7) common electrode of fission chamber; 8) target.

as well as the necessary discrimination threshold. Table 1 shows the thicknesses of the foils used, the selected energy intervals, and the average energies of the alpha particles, obtained from a known energy distribution [4].

TABLE 1. Average Energies ( $\bar{E}$ ) of the Selected Groups of Alpha Particles

Foil thickness, mg/cm <sup>2</sup>	$E_1 - E_2$ , MeV	$\bar{E}$ , MeV
—	9—12	10,6
21	15—18	16,4
36	19—22	20,3
51	23—26	24,0

cord the alpha particles whose pulse amplitudes are greater than a fixed value  $A_1$ . Pulses with amplitudes between  $A_{\max}$  and  $A_1$  will correspond to alpha particles whose initial energy lies between  $E_1$  and  $E_2$ . Thus, the selection of an energy interval in the spectrum of long-range alpha particles reduces to the choice of the appropriate thickness of aluminum foil and the choice of a specific discrimination threshold in the alpha channel.

To determine the necessary discrimination threshold one must know the working volume of the alpha chamber. This was found by measuring the spectra of natural alpha particles from  $U^{233}$  at reduced gas pressure; a  $U^{233}$  source with high alpha activity was put in the place of the  $U^{235}$  source. By comparing the calculated values with the experimentally determined variation of pulse amplitude as a function of gas pressure, we found that the effective working volume of the alpha chamber was between  $r_1 = 6$  cm and  $r_2 = 8.5$  cm. We calculated the amplitude distribution of the pulses from long-range particles at a gas pressure of 1 atmosphere and varying thicknesses of foil,

TABLE 2. Number of Recorded Ternary Fissions

Foil thickness, mg/cm <sup>2</sup>	$N_{\text{tern}}$	$N_{\text{tern}}/N_{\text{bin}} \times 6400$	$n_{\text{tern, exper.}}$	$n_{\text{tern, calc.}}$
—	6400	0,36	0,78	0,80
21	4300	0,46	1,00	1,00
36	4400	0,24	0,52	0,51
51	3400	0,096	0,19	0,15

The resolving power of the alpha chamber was determined chiefly by the finite dimensions of the source. At a pressure of 29 cm Hg the half-width of the line from the natural  $U^{233}$  alpha particles was about 25%. If we take account of the fact that 1.6 MeV was released in the working volume of the chamber, we may assume that the energy of an alpha particle can be measured to within 0.2 MeV at a pressure of 29 cm Hg and about 0.5 MeV at 1 atmosphere. These accuracies for the measurement of long-range alpha particle energies were sufficient, since no energy intervals narrower than 4 MeV could be distinguished under the experimental conditions. These conditions relate primarily to the "single-channel" nature of the experiment, the comparatively small solid angle of the alpha chamber with respect to the target (about 8%), and the low probability of production of alpha particles with energies greater and less than 15 MeV.

#### Results of the Measurements

In the experiments we used  $U^{235}$  targets with thicknesses ranging up to  $20 \mu\text{g}/\text{cm}^2$  and an area of  $1.5 \text{ cm}^2$ . The backing for the target was an organic plate with a thickness of  $5 \mu\text{g}/\text{cm}^2$  and coated on both sides with gold layers having a combined thickness of  $10 \mu\text{g}/\text{cm}^2$ . The number of binary fissions reached values up to 120,000 per minute.

Table 2 shows the number of ternary fissions recorded for each of four alpha particle energy intervals, the ratio of the number  $N_{\text{tern}}$  of ternary fissions to the number  $N_{\text{bin}}$  of binary fissions, the relative count values  $n_{\text{tern}}$  and the relative probability of finding an alpha particle in a given interval, as obtained from the energy spectrum of long-range alpha particles [4].

The agreement between the experimental and calculated values of  $n_{\text{tern}}$  indicates that the selected energy intervals in the spectrum of long-range alpha particles were correctly determined. For the interval with an average energy of 24 MeV we obtained a somewhat high count value, which may be explained by the following: it is known

[5] that for alpha particles with energies of more than 20 MeV the angular distributions of the fragment divergence lines is nearly isotropic. Under the conditions of the experiment described above, alpha particles with an isotropic angular distribution are recorded with a higher probability than alpha particles which have the characteristic anisotropic distribution with a maximum near 90°. In view of this the count value for a foil thickness of 51 mg/cm<sup>2</sup> is less surprising.

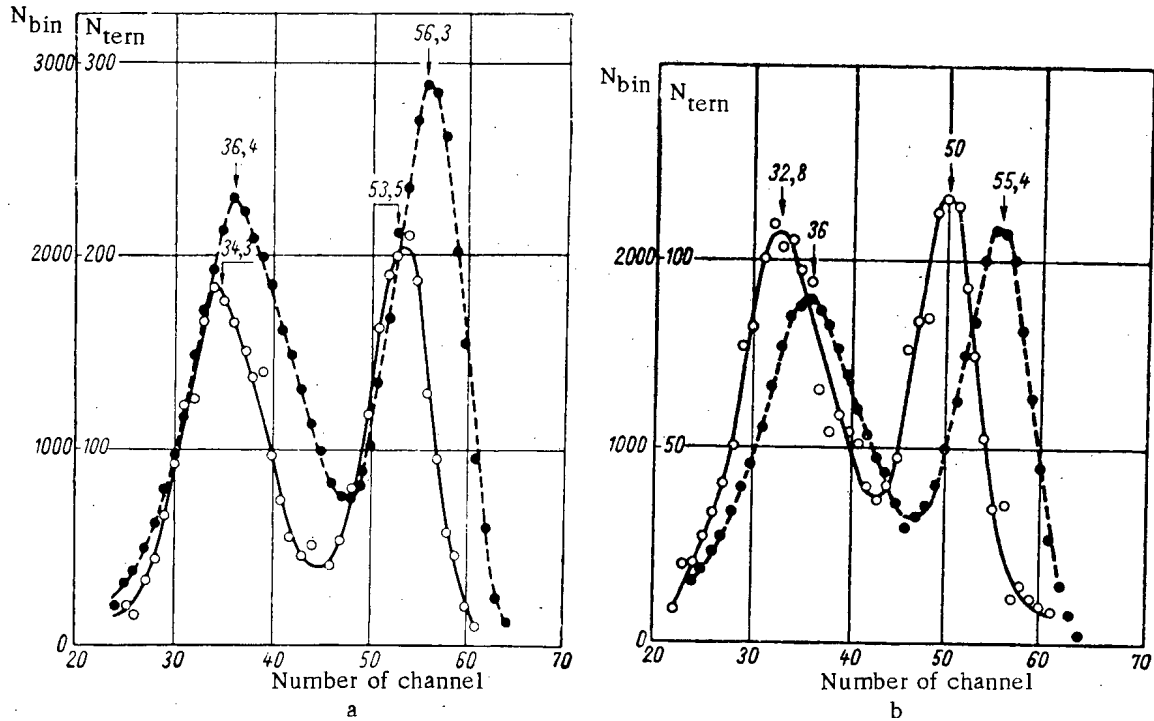


Fig. 2. "Two-humped" energy distribution of binary-fission fragments  $N_{bin}$  (---) and ternary-fission fragments  $N_{tern}$  (—): a)  $\bar{E}_\alpha = 10.6$  MeV; b)  $\bar{E}_\alpha = 24.0$  MeV.

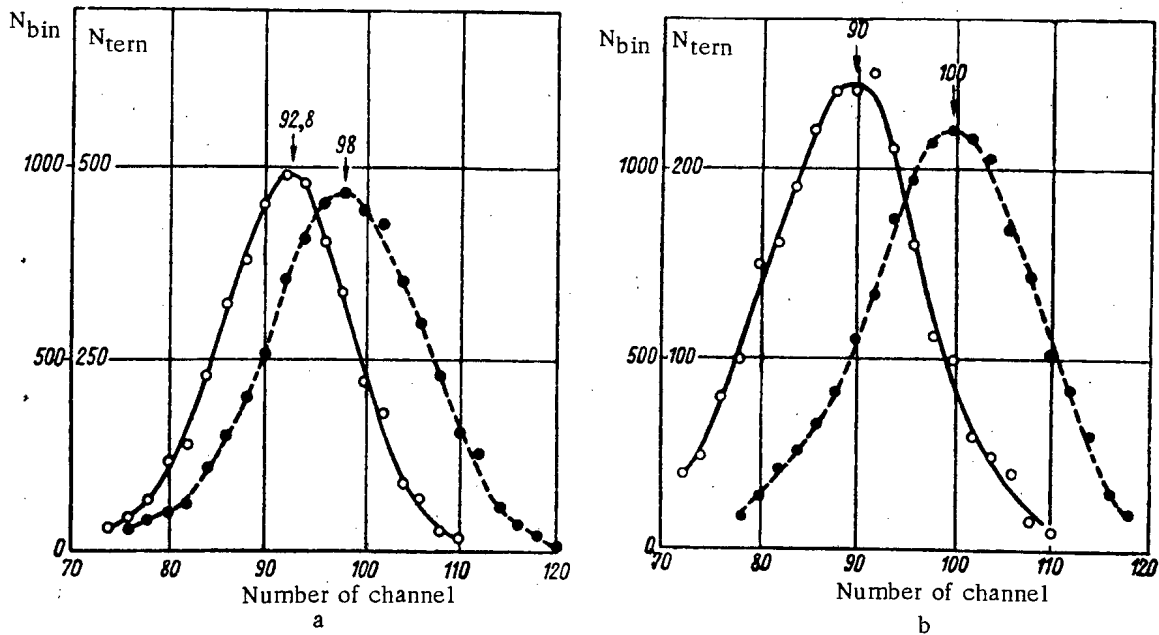


Fig. 3. Number of fissions as a function of the total kinetic energy of the fragments (a and b are the same as in Fig. 2).

To measure the energies of the ternary fission fragments we used both a multichannel amplitude analyzer and a special cathode-ray tube analyzer with a photographic attachment [1, 3]. The energy shifts of the peaks in the "two-humped" distributions of binary and ternary fission fragments were found by means of a multichannel analyzer. As an illustration, Figs. 2a and 2b show the results of one of the series of measurements. In case b we use a thicker target, which produced a reduction in the pulse amplitudes and in the peak-to-trough ratios. This fact is of no great importance, since the measurements are relative. In Figs. 3a and 3b, for the same series of measurements, we show the variation of the number of fissions as a function of the total kinetic energy of the fragments, as obtained from an analysis of the photographic plates. The values of the chosen channels in both cases are arbitrary and are not equal to the analyzer channel value; this is due to the different magnification of the projector.

Table 3 shows the differences between the energies of the most probable light and heavy binary and ternary fission fragments,  $\Delta E_L$  and  $\Delta E_H$ .

TABLE 3. Differences Between the Energies of Light and Heavy Fragments Produced by Binary and Ternary Fission

$\bar{E}_\alpha$ , MeV	$\Delta E_L$ , MeV	$\Delta E_H$ , MeV	$\Delta E_L + \Delta E_H$ , MeV
10,6	$6,0 \pm 0,6$	$4,9 \pm 0,6$	$10,9 \pm 1,2$
16,4	$8,5 \pm 0,6$	$6,5 \pm 0,6$	$15,0 \pm 1,2$
20,3	$9,3 \pm 0,8$	$5,5 \pm 0,8$	$14,8 \pm 1,6$
24,0	$9,6 \pm 0,8$	$5,9 \pm 0,8$	$15,5 \pm 1,6$

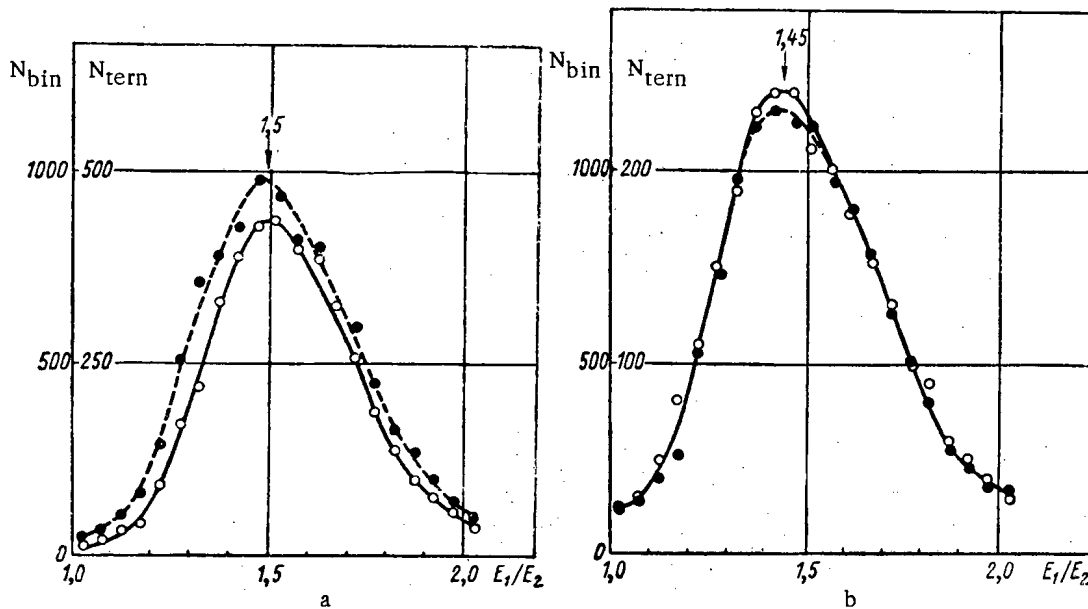


Fig. 4. Number of fissions as a function of fragment energy ratio (a and b are the same as in Fig. 2).

The tabulated data include corrections for ionization caused by the alpha particles in the fission chambers. The last column of the table shows the total energy difference,  $\Delta E_L + \Delta E_H$ . It can be seen from the table that if  $E_\alpha > 16$  MeV, the difference between the energies of binary and ternary fission fragments remains constant, within the limits of experimental error. This means that in ternary fission the total kinetic energy increases as the energy of long-range alpha particles increases and that it may considerably exceed the total energy of the most probable binary fission fragments.

By processing the data corresponding to each alpha particle energy interval, we obtain graphs of the number of ternary fissions as a function of the fragment energy ratio  $E_1/E_2$  ( $E_1/E_2 \approx M_2/M_1$ ). The resulting relationships show that in all cases the mass distributions of ternary fission fragments for different energies of long-range alpha particles



are approximately equal, and the maximum values of the distributions are found for the same mass ratio, about 1.5 (Figs. 4a, b). The difference between the peak-to-trough ratios may be explained by the thickness of the targets used, and the relatively small trough in each case is caused by the absence of a collimator, which could not be used in principle under the conditions of the experiments.

#### Evaluation of Results

The experimental data obtained in the present study indicate that as the alpha particle energy increases from 10.6 MeV to 16.4 MeV, the most probable total kinetic energy of the fragments is reduced by about 4 MeV. This means that Eq. (1) apparently applies only in the region of low alpha particle energies (up to 15 MeV). The energy shifts of the most probable ternary fission fragments in comparison to those of the binary fission fragments indicate that the effect of distance between the fragments at the moment of fission depends on the energy of the alpha particles if  $E_\alpha < 15$  MeV but is independent of it if  $E_\alpha > 15$  MeV. It may be assumed, therefore, that the mechanisms of alpha particle emission in these two regions are different.

From the increase in the total kinetic energy of the fragments and alpha particles as the alpha particle energy increases for  $E_\alpha > 15$  MeV we conclude that the internal excitation energy of ternary fission fragments decreases for high values of  $E_\alpha$ .

From the similarity of the mass distributions of ternary fission fragments for different alpha particle energies it follows that for each chosen interval of mass ratios the energy spectrum of long-range alpha particles must be approximately the same ( $1.1 < M_1/M_2 < 1.8$ ).

#### LITERATURE CITED

1. V. N. Dmitriev, et al., Zh. éksperim. i teor. fiz., 39, 556 (1960).
2. V. F. Apalin, et al., Atomnaya énergiya, 7, 375 (1959).
3. V. N. Dmitriev, et al., Pribory i tekhnika éksperimenta, No. 1, 94 (1962).
4. C. Fulmer and B. Cohen, Phys. Rev., 108, 370 (1957).
5. N. A. Perfilov and Z. I. Solov'eva, Zh. éksperim. i teor. fiz., 37, 1157 (1959).

---

All abbreviations of periodicals in the above bibliography are letter-by-letter transliterations of the abbreviations as given in the original Russian journal. Some or all of this periodical literature may well be available in English translation. A complete list of the cover-to-cover English translations appears at the back of this issue.

---

DISTRIBUTION OF THE NUMBER OF COUNTS ON A NEUTRON DETECTOR  
PLACED IN A REACTOR

V. G. Zolotukhin and A. I. Mogil'ner

Translated from *Atomnaya Énergiya*, Vol. 15, No. 1,  
pp. 11-16, July, 1963

Original article submitted July 18, 1962

A discussion is given in the stochastic process of neutron multiplication and detection in a nuclear reactor. The use of physically justifiable assumptions makes it possible to simplify the mathematically complicated problem and find the productive probability function for the number of counts in a definite interval of time. The distribution found has been confirmed experimentally. Some applications of the theory are indicated for determining the reactor kinetic parameters.

The interest in the theory of reactor noise, due mainly to new experimental possibilities of determining reactor parameters, has stimulated the appearance of a number of theoretical and experimental papers. In the general case, equations are written for the mean values and fluctuations of the neutron density [1], and on the assumption of elementary nuclear reactor theory, expressions have been found for the autocorrelation function of the detector counting rate [2], the dispersion of the number of counts [3-5], and the fluctuation in the total number of neutrons in the reactor [6].

In [7], the question is posed of the distribution of the number of neutron detector counts in a definite interval of time. It turned out, as in the theory of cascade processes, that the Pólya distribution provides a certain approximation to the exact distribution, but is in some respects unsatisfactory.

Knowing the distribution of the number of detector counts is also of practical importance. The statistical methods used at the present time for investigating the kinetic parameters of subcritical reactors, employing the data of a discrete neutron detector, are based on making an experimental determination of the autocorrelation function of the counting rate (Rossi-alpha method) or of the dispersion in the number of counts (Feinman-alpha method). This requires a rather long time for practical measurements, or complicated apparatus for accumulating sufficient information to achieve the required accuracy in the parameters being determined.

In contrast with the above methods, the probability method, the basic ideas of which have been presented in previous papers by the authors [7, 8], is based on knowing the probability distribution law for the number of neutron detector counts. Knowing this law makes possible a great reduction in the time required to accumulate the data. Further, the probability method makes it possible to use relatively simple apparatus, combined with automatic treatment of the information for intervals of different lengths.

This paper gives expressions for the probability  $P_k(t)$  of having  $k$  detector counts in the time  $t$ . This distribution depends on two kinetic parameters of the reactor, which may be found by comparing the distribution found experimentally with the theoretical distribution. The productive function is also found for the distribution of the number of counts in two nonintersecting time intervals, which makes it possible to treat the experimental data. The distribution  $P_k(t)$  is confirmed experimentally, and a description is given of some of the possible applications of one of the forms of the probability method.

Choice of Model and Solution of Equations for the Productive Functions

It is assumed in the discussion that the reactor is subcritical, and that the steady state power level is maintained by an external neutron source of strength  $S$  neutrons/sec, with a Poisson distribution of the emitted neutrons.

Three elementary factors tending to change the number of neutrons in the reactor are important in describing a microscopic reactor model: 1) neutron loss resulting from leakage and pure absorption; 2) counting loss; and 3) fission, with generation of new neutrons. In these processes, an exponential distribution law is assumed for the partial

lifetimes, with the time independent constants,  $\lambda_c$ ,  $\lambda_p$ , and  $\lambda_f$ , respectively. The probabilities  $P_{\nu, f}$  that fission of a fuel nucleus will give  $\nu$  secondary neutrons are known [9]. In the present model, the effect of delayed neutrons is neglected, which is permissible for a detection time much less than the mean lifetime of the delayed neutrons.

Since interactions between neutrons and matter and their detection under small loadings are clearly defined discrete events, it is convenient to use the productive probability function apparatus (abbreviated p.p.f.).

We introduce the following p.p.f.:

1.  $H(x)$  is the p.p.f. of the number of neutrons in the reactor at an arbitrarily chosen instant of time (in the steady state case).
2.  $F_1(x_1, x_2, t)$  is the p.p.f. of the number of neutrons in the reactor at the instant of time  $t$ , and of the number of neutrons detected in the time  $t$ , under the condition that there was one neutron in the reactor at the instant of time  $t=0$ .
3.  $P(x, t) = F_1(1, x, t)$  is the p.p.f. of the number of neutrons detected in time  $t$ , owing their origin to the neutron that was present in the reactor at  $t=0$ .
4.  $\Pi_t(x)$  is the p.p.f. of the number of neutrons detected in the time  $t$ .

Making use of the familiar properties of the p.p.f. and the Poisson distribution, it is not difficult to obtain the following relations:

$$\left. \begin{aligned} H(x) &= \exp \left( S \int_0^{\infty} [F_1(x, 1, \tau) - 1] d\tau \right), \\ \Pi_t(x) &= H(P(x, t)) \exp \left( S \int_0^t [P(x, \tau) - 1] d\tau \right). \end{aligned} \right\} \quad (1)$$

To find the p.p.f.  $F_1(x_1, x_2, t)$ , we make use of the theory of random branching processes developed by A. N. Kolmogorov and N. A. Dmitriev in [10]. This considers  $n$  types of particles,  $T_1, T_2, \dots, T_n$ , with possible conversions of one into the other. The state of the system is given by the  $n$ -dimensional vector  $\alpha$ , with the integral components  $\alpha_1, \alpha_2, \dots, \alpha_n$ , equal to the number of particles of each type. Let one particle of type  $T_k$  have the probability  $P_k(\alpha, t_1, t_2)$  of being converted in the time  $(t_1, t_2)$  into the assembly characterized by the vector  $\alpha$ . If the probability  $P_k(\alpha, t_1, t_1 + \Delta)$  may be represented in the form

$$P_k(\alpha, t_1, t_1 + \Delta) = E_{\alpha}^k + g_k(\alpha, t_1) \Delta + o(\Delta),$$

where

$$E_{\alpha}^k = \begin{cases} 1, & \text{if } \alpha_i = 0, i \neq k, \alpha_k = 1; \\ 0 & \text{in all other cases;} \end{cases}$$

then, for the productive functions in the case of a homogeneous process

$$F_k(x_1, x_2, \dots, x_n, t) = \sum_{\alpha_1=0}^{\infty} \sum_{\alpha_2=0}^{\infty} \dots \sum_{\alpha_n=0}^{\infty} x_1^{\alpha_1} x_2^{\alpha_2} \dots x_n^{\alpha_n} P_k(\alpha, t)$$

we have the equations

$$\left. \begin{aligned} \frac{\partial F_k}{\partial t} &= f_k(F_1, F_2, \dots, F_n), \\ \frac{\partial F_k}{\partial t} &= \sum_{j=1}^n f_j(x_1, x_2, \dots, x_n) \frac{\partial F_k}{\partial x_j} \end{aligned} \right\} \quad (2)$$

with the initial conditions  $F_k(x, 0) = x_k$ . In Eqs. (2),  $f_k(x)$  is the p.p.f.; thus

$$f_k(x) = \sum_{\alpha_1=0}^{\infty} \sum_{\alpha_2=0}^{\infty} \dots \sum_{\alpha_n=0}^{\infty} g_k(\alpha_1, \alpha_2, \dots, \alpha_n) x_1^{\alpha_1} x_2^{\alpha_2} \dots x_n^{\alpha_n},$$

and  $k = 1, 2, \dots, n$ .

Assigning the neutrons present in the reactor to the particles of the first type, and the detected neutrons to the particles of the second type, using the present model, we obtain

$$\begin{aligned} f_1(x_1, x_2) &= \lambda_c(1 - x_1) + \lambda_p(x_2 - x_1) + \\ &+ \lambda_f[y(x_1) - x_1]; \\ f_2(x_1, x_2) &= 0, \end{aligned} \quad (3)$$

where  $y(z) = \sum_{h=0}^{\infty} P_h f z^h$  is the p.p.f. of the number of prompt fission neutrons.

Noting that  $F_2(x_1, x_2, t) = x_2$ , we obtain for  $F_1(x_1, x_2, t)$

$$\frac{\partial F_1}{\partial t} = \lambda_c(1 - F_1) + \lambda_p(x_2 - F_1) + \lambda_f[y(F_1) - F_1], \quad (4)$$

and for  $P(x, t) = F_1(1, x, t)$  and  $\tilde{F}(x, t) = F_1(x, 1, t)$

$$\frac{\partial P}{\partial t} = \lambda_c(1 - P) + \lambda_p(x - P) + \lambda_f[y(P) - P]; \quad (5)$$

$$\frac{\partial \tilde{F}}{\partial t} = \lambda_c(1 - \tilde{F}) + \lambda_p(1 - \tilde{F}) + \lambda_f[y(\tilde{F}) - \tilde{F}] \quad (6)$$

[with  $P(x, 0) = 1$  and  $\tilde{F}(x, 0) = x$ ].

For  $H(x)$  we obtain

$$H(x) = \exp\left(S \int_0^{\infty} [F_1(x, 1, \tau) - 1] d\tau\right) = \exp\left(S \int_x^1 \frac{(r-1) dr}{\lambda_c(1-r) + \lambda_p(1-r) + \lambda_f[y(r) - r]}\right). \quad (7)$$

Further, from (1) and (7) we find

$$\begin{aligned} \ln \Pi_t(x) &= S \int_1^{P(x,t)} \frac{(r-1) dr}{(\lambda_c + \lambda_p)(1-r) + \lambda_p(x-1) + \lambda_f[y(r) - r]} + \\ &+ S \int_{P(x,t)}^1 \frac{(r-1) dr}{(\lambda_c + \lambda_p)(1-r) + \lambda_f(1-r)}. \end{aligned}$$

Taking  $\lambda_c + \lambda_p = \lambda'_c$ , and differentiating  $\ln \Pi_t(x)$  with respect to  $t$ , using (5) we find

$$\frac{\partial \ln \Pi_t}{\partial t} = \frac{S [P(x, t) - 1] \lambda_p (1 - x)}{\lambda'_c (1 - P) + \lambda_f [y(P) - P]},$$

from which

$$\Pi_t(x) = \exp\left(S \lambda_p (x - 1) \times \int_0^t \frac{[1 - P(x, \tau)] d\tau}{\lambda'_c [1 - P(x, \tau)] + \lambda_f [y(P) - P]}\right). \quad (8)$$

For  $P(x, t)$ , we obtain from (5)

$$\begin{aligned} t &= \int_1^{P(x,t)} \frac{dz}{(\lambda'_c + \lambda_f)(1-z) + \lambda_p(x-1) + \lambda_f[y(z) - z]} = \\ &= \int_1^{P(x,t)} \frac{dz}{\alpha \left\{ 1 - z + \frac{\lambda_p}{\alpha}(x-1) + \frac{\lambda_f}{\alpha}[y(z) - 1 - \bar{v}(1-z)] \right\}}, \end{aligned} \quad (9)$$

where  $\bar{v} = \frac{dy(z)}{dz} \Big|_{z=1}$  is the mean number of secondary fission neutrons,  $\alpha = \frac{1 - K_p}{l_0}$  is the Rossi constant,  $K_p$  is the fast neutron multiplication factor, and  $l_0$  is the mean neutron lifetime.

Although the p.p.f.  $y(z)$  may, with good approximation, be taken in the form

$$y(z) = \left(1 + \frac{\bar{v}(1-z)}{m}\right)^m,$$

where  $m = 5-7$ , the problem of making an explicit solution of (8) and (9) for  $\Pi_t(x)$  is exceedingly complicated. However, there is no need for using the exact form of the function  $y(z)$ . Under actual conditions, the probability of detecting one or more neutrons owing their origin to the one original neutron is exceedingly small as a result of the smallness of the detecting efficiency. It is hence clear that the function  $P(x, t)$  is very close to unity for all values  $0 < |x| < 1$ . Accordingly, in the expression under the integral sign in (9), we can limit ourselves to an expansion of  $y(z)$  in Taylor's series keeping the first three terms, and then, after evaluating the integral in (9), and solving for  $P(x, t)$ , we obtain

$$P(x, t) = 1 - \frac{1}{2A} \frac{(\varphi-1)(1-e^{-\alpha t\varphi})}{\left(1 + \frac{\varphi-1}{\varphi+1} e^{-\alpha t\varphi}\right)}, \quad (10)$$

where

$$A = \frac{\bar{v}(\bar{v}-1)}{\alpha\tau_f}; \quad \varphi = \sqrt{1 + 2z(1-x)};$$

$$z = \frac{\bar{v}(\bar{v}-1)R}{(\alpha\tau_f)^2};$$

$$\tau_f = \frac{1}{\lambda_f}; \quad R = \lambda_p\tau_f.$$

The quantity  $R$  is the detector efficiency for fission counts in the volume of the reactor. In the denominator of the expression under the integral sign in (8), we can also limit ourselves to three terms of the expansion of  $P(x, t)$  in Taylor's series, so that

$$\ln \Pi_t(x) = \frac{S\lambda_p(x-1)}{\alpha} \int_0^t \frac{d\tau}{\left[1 + \frac{\bar{v}(\bar{v}-1)}{\alpha\tau_f} (1-P)\right]},$$

from which, using (10), after integrating and some rearrangements, we obtain

$$\ln \Pi_t(x) = \frac{m}{z} \left\{ 1 - \varphi - \frac{2}{\alpha t} \times \ln \left[ 1 + \frac{(\varphi-1)^2}{4\varphi} (1 - e^{-\alpha t\varphi}) \right] \right\}, \quad (11)$$

where  $\underline{m}$  is the mean number of counts in time  $\underline{t}$ .

The distribution with p.p.f. (1) depends on the three parameters  $\alpha t$ ,  $\underline{z}$ , and  $\underline{m}$ , and has the following central moments:

$$\sigma^2 = m [1 + z\varphi_1(\alpha t)];$$

$$\mu_3 = m [1 + 3z\varphi_1(\alpha t) + 3z^2\varphi_2(\alpha t)];$$

$$\mu_4 = 3\sigma^4 + m [1 + 7z\varphi_1(\alpha t) + 18z^2\varphi_2(\alpha t) + 15z^3\varphi_3(\alpha t)],$$

where

$$\varphi_1(x) = 1 - \frac{1-e^{-x}}{x};$$

$$\varphi_2(x) = 1 + e^{-x} - \frac{2(1-e^{-x})}{x};$$

$$\varphi_3(x) = 1 - \frac{3(1-e^{-x})}{x} + 2e^{-x} + \frac{1}{10} \frac{(1-e^{-x})^2}{x} + \frac{4xe^{-x}}{10}.$$

It may be shown that as  $z \rightarrow 0$ , the distribution of the number of counts reduces to the Poisson distribution. The asymptotic expansion of the probabilities  $P_k$  as  $m \rightarrow 0$  is of the form

$$P_k \approx \frac{e^{-x_k^2/2}}{\sqrt{2\pi\sigma^2}} \left[ 1 - \frac{\gamma_1}{6} H_3(x_k) + \frac{\gamma_2}{24} H_4(x_k) + \frac{\gamma_1^2}{72} H_6(x_k) \right],$$

where

$$\gamma_1 = \frac{\mu_3}{\sigma^3}; \quad \gamma_2 = \frac{\mu_4}{\sigma^4} - 3; \quad x_k = \frac{k-m}{\sigma};$$

and the  $H_k(x)$  are Hermite polynomials.

The quantity  $Q = \frac{1}{m} \ln P_0^{-1}$ , equal, from (11) to

$$Q(t) = 2 \frac{1 + \frac{2}{\alpha t (\varphi_0 - 1)} \ln \left[ 1 + \frac{(\varphi_0 - 1)^2}{4\varphi_0} (1 - e^{-\alpha t \varphi_0}) \right]}{1 + \varphi_0}, \quad (12)^*$$

where  $\varphi_0 = \sqrt{1 + 2z}$ , may be used to find the parameters  $\alpha$  and  $z$ , if there are measurements of  $Q$  for at least two intervals  $t$ .

The exact distribution was compared with the Pólya distribution. For  $\alpha t \rightarrow \infty$ , it is a simple matter, from the p.p.f. (11) to find the recursion relation for the probabilities:

$$P_{k+1} = \frac{m}{(1+k) \sqrt{1+2z}} \sum_{j=0}^k P_{k-j} \frac{(2j-1)!!}{j!} \left( \frac{z}{1+2z} \right)^j,$$

while the Pólya distribution with the correct two moments gives

$$P_{k+1} = P_k \frac{m+kz}{(1+z)(1+k)}; \quad P_0 = (1+z)^{-m/z}.$$

Figure 1 shows these distributions for  $m = 5$ , and  $z = 1$ . The difference between them is small, particularly for small  $z$ .

By following the method presented above, we can find the p.p.f. of the number of counts in two nonintersecting intervals of the same duration  $t$ , separated by the time interval  $T$ :

$$\Pi(x_1, x_2, t, T) = \Pi_t(x_1) \Pi_t(x_2) \times \exp \left\{ -\frac{2m}{\alpha t z} \ln [1 - \gamma(x_1) \gamma(x_2) e^{-\alpha t}] \right\},$$

where

$$\gamma(y) = \frac{\varphi^2 - 1}{4\varphi} \cdot \frac{(1 - e^{-\alpha t \varphi})}{1 + \frac{(\varphi - 1)^2}{4\varphi} (1 - e^{-\alpha t \varphi})}$$

(here  $\varphi(y) = \sqrt{1 + 2z(1-y)}$ ),

and  $\Pi_t(x)$  is given by Eq. (11).

#### Experimental Check on the Distribution

The results obtained in the preceding section are based on an idealized one group and one zone nuclear reactor model. The question of how correctly this model reflects all the essential features of the multiplication process in an actual physical reactor must be solved experimentally.

\* The expression (12) which is a special case of the distribution (11), was obtained independently by L. Pal [11], whose work became known to the authors while they were preparing the present paper for publication. The production function (11) was found in 1960, and was awaiting experimental confirmation.

Measuring the probability  $P_0(t)$  of having no counts in the time  $t$  is a sensitive method of finding the parameter  $\alpha$ , which is of the greatest interest.

An experimental check on the distribution consisted in comparing the values of the quantity  $\alpha$  obtained by the  $P_0$ -method and by the independent method of C. Cohn [12]. The latter is based on a spectrum analysis of the noise in the ionization chamber current which measures the neutron flux in the physical reactor, and is only associated with a type of counting rate autocorrelation function confirmed by numerous experiments.

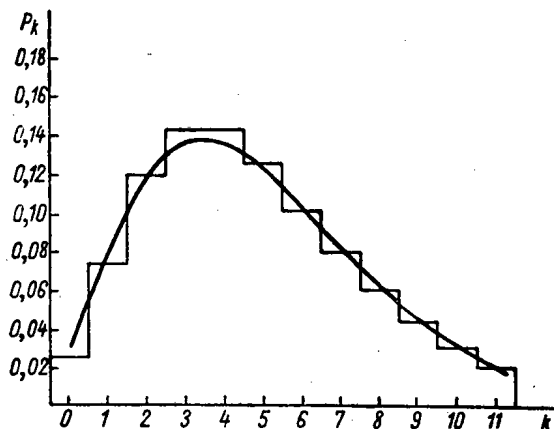


Fig. 1. Distribution of the number of neutron detector counts (histogram), and Pólya distribution (solid curve) for  $m=5$ ,  $z=1$ , and  $\alpha t = \infty$ .

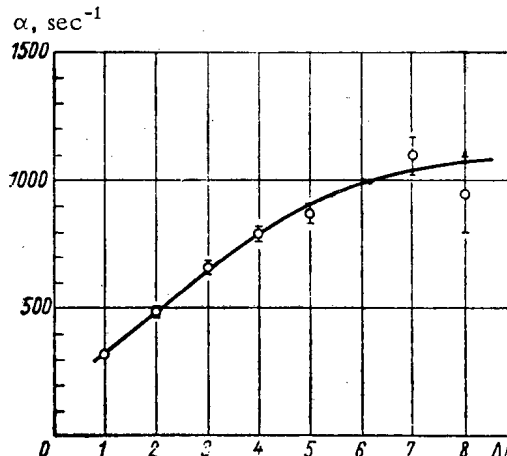


Fig. 2.  $\alpha = \frac{1-K_p}{l_0}$  as a function of the number  $\Delta N$  of fuel channels removed.

The measurements were made on a thermal assembly, the active zone of which contained uranium enriched to 90% in the  $U^{235}$  isotope, with hydrogen moderator and a beryllium reflector. In finding the value of  $P_0(t)$ , use was made of a six channel statistical analyzer employing transistor-ferrite elements, operating on the principle set forth in [8]. In four minutes, each channel analyzed about  $10^6$  time intervals, which gave high statistical accuracy in the results.

The neutron detector was a standard SNMO-5 proportional counter, filled with  $BF_3$  gas having enriched boron. The detector was converted from proportional operation to an ionization chamber by lowering the voltage. In making measurements by C. Cohn's  $\alpha$ -method, the reactor power was increased by means of an external source. After preliminary amplification, the noise in the detector current was passed through a resonance filter. The constant component of the detected signal, taken from the circuit, was recorded on the chart of an automatic ÉPP-09 potentiometer. The spectrum analysis was made in the frequency range 26-125 cps.

The normalized value of the spectral density of the noise in the current is known to be of the form

$$n^2 = A + \frac{B}{\omega^2 + \alpha^2}$$

with constant values of  $A$  and  $B$  ( $\omega$  is the angular frequency). The best value of  $\alpha$  was obtained from a set of experimental values using the method of least squares.

In the  $P_0$ -measurements, the six intervals  $t_k$  were related by the equation  $t_k = t_1 \cdot 2^{k-1}$ , with  $t_1 = 0.32 \cdot 10^{-3}$  sec, where  $k$  is the number of the interval for which the value of  $P_0(t_k)$  was measured. The values found for  $Q(t_k)$  were treated by the method of least squares on a BÉSM-2 computer. The result of the measurements by the  $P_0$ -method was

$$\alpha = (420 \pm 20) \text{ sec}^{-1},$$

and by the spectrum method

$$\alpha = (400 \pm 50) \text{ sec}^{-1}.$$

These values agree with one another within the limits of error shown.

It is interesting to note that using the  $P_0$ -method for eight minutes gave an accuracy of 5%, while the spectrum method (for eight frequency values) only gives an accuracy of 12% for 80 minutes.

#### Determination of Large Subcriticalities by the Probability Method

A description is given of one of the experiments where the  $P_0$ -method was used to measure large negative reactivities in one of the highly enriched uranium-beryllium homogeneous assemblies with a beryllium reflector, and an intermediate neutron spectrum.

The  $P_0$ -method was used to measure the values of  $\alpha$  as the outside fuel channels were successively removed from the active zone. Here it was assumed that in the function  $K_{\text{eff}} = f(N - N_{\text{CR}})$ , where  $N$  is the number of identical operating channels in the active zone and  $N_{\text{CR}}$  is the critical number, there is a linear initial portion obtained by expanding the function in Taylor's series using the first two terms. The value of  $\alpha$  is also related to the reactivity  $\rho$  by the linear equation

$$\frac{\rho}{\beta} = \frac{\alpha}{\alpha_0} - 1,$$

where  $\alpha_0 = \frac{\beta}{l_0}$ . It was accordingly to be expected that as the fuel channels were successively removed from a reactor that was close to critical, the initial portion of the curve  $\alpha(\Delta N)$ , where  $\Delta N$  is the number of channels removed, would be linear.

In making the  $P_0$ -measurements, the apparatus was used which was spoken of in the previous section. The SNMO-5 counter was set up in place of one of the blocks in the beryllium reflector, adjacent to the active zone. "Priming" with the external neutron source was only used at very large subcriticalities to improve the statistics. A preliminary (5% accurate) determination of  $\alpha$  from the set of experimental values of  $Q(t) = \frac{1}{m(t)} \ln \frac{1}{P_0(t)}$  was made graphically [we have previously spoken of a set of  $Q(z, \alpha t)$  curves]. The values of  $\alpha$  was made more accurate on a BESM-2 computer.

The resulting  $\alpha(\Delta N)$  curve shown in Fig. 2 shows that there is an initial linear portion. If it is borne in mind that the effectiveness of one fuel channel on the edge is  $2.3 \beta$ , it may be concluded from the curve of Fig. 2 that the linear portion extends to subcriticalities of  $\sim 10 \beta$ .

Thus, using the present method enables measurements to be made successfully of negative reactivities at least to  $\sim 10 \beta$ , so that in this range, the probability method competes successfully with the pulsed source method [11], with the convenient difference that the apparatus is simpler.

In conclusion the authors express profound gratitude to A. I. Leipunskii and G. I. Marchuk for their interest in the work, to V. A. Kuznetsov for useful discussions and aid, to V. V. Sapozhnikov, who made up the apparatus and took part in the experiments, and to G. P. Krivelev and A. S. Postovalov, who took part in the experiments.

#### LITERATURE CITED

1. L. Paf, *Nuovo Cimento. Suppl.*, 7, 25 (1958).
2. C. Veles, *Nucl. Sci. and Engng.*, 6, 414 (1959).
3. *Scientific and Engineering Bases of Nuclear Power*, Vol. 2, edited by K. Goodman [Russian translation], Moscow, IL, p. 18 (1950).
4. Feynman, D. de Hoffman, and R. Serber, *J. Nucl. Engng.*, 3, 64 (1956).
5. J. Bengston, et al., Paper No. 1783, presented by the USA at the Second International Conference on the Peaceful Uses of Atomic Energy [Russian translation], Geneva (1958).
6. E. Courant and R. Wallase, *Phys. Rev.*, 72, 1038 (1947).
7. V. G. Zolotukhin and A. I. Mogil'ner, *Atomnaya Energiya*, 10, 379 (1961).
8. A. I. Mogil'ner and V. G. Zolotukhin, *ibid.*, 10, 377 (1961).
9. King and Simmons, *Nucl. Sci. and Engng.*, 3, 595 (1958).
10. A. N. Kolmogorov and N. A. Dmitriev, *Dokl. AN SSSR*, 11, 7 (1947).
11. L. Paf, *Statistical Theory of the Chain Reaction in Nuclear Reactors*, Part III [in Russian], Budapest (1961).
12. C. Cohn, *Nucl. Sci. and Engng.*, 5, 331 (1959).



## ATTENUATION OF PILE NEUTRON FLUX IN POLYETHYLENE

V. N. Avaev, G. A. Vasil'ev, A. P. Veselkin, Yu. A. Egorov,  
Yu. V. Orlov, and Yu. V. Pankrat'ev

Translated from *Atomnaya Énergiya*, Vol. 15, No. 1,  
pp. 17-20, July, 1963

Original article submitted August 25, 1962

The relaxation lengths of research reactor neutrons were measured in polyethylene. The findings are in excellent accord with data computed theoretically using the method of moments. The relaxation lengths are ~15% less than in the case of water.

The function of polyethylene in nuclear engineering is as a biological shielding material for neutron shielding [1]. The principal advantage of polyethylene over rival hydrogen-bearing materials is the high density of hydrogen nuclei ( $7.92 \cdot 10^{22}$  per  $\text{cm}^3$ ) combined with a relatively low specific weight ( $0.92 \text{ g/cm}^3$ ). For example, for the dose rate due to 0.33-18 MeV neutrons to be reduced by 10 thousand times, a polyethylene slab of  $\sim 61 \text{ g/cm}^2$  is required [2], while the thickness of an equivalent layer of water would be  $\sim 81 \text{ g/cm}^2$ . In this case, the savings in shielding weight may top 30%.

TABLE 1. Characteristics of Indicators

Indicator	Effective energy cutoff, MeV; resonance energy, eV	Energy range in determination of indicator activity, MeV	Size of indicator, mm
$\text{In}^{115} (n, \gamma)$	1.44 eV	0.9-1.7	Flat $10 \times 10 \times 0.2$
$\text{I}^{127} (n, \gamma)$	30 eV	0.28-0.78	Cylinder, $d = 8, h = 40$
$\text{P}^{31} (n, p)$	2.8 MeV	$\beta$	Cylinder, $d = 8, h = 40$
$\text{Al}^{27} (n, p)$	4.7 MeV	0.41-0.95	Cylinder, $d = 8, h = 50$
$\text{Al}^{27} (n, \alpha)$	7 MeV	1.1-2.85	Cylinder, $d = 8, h = 50$

The physicochemical and chemical properties of polyethylene have been extensively studied and reported on the literature [3]; studies on radiation effects on the properties of polyethylene are continuing. In particular, it has been found that preirradiated polyethylene (up to 15-20 Mrad exposures), known under the name irrathene, is stable at temperatures as high as  $250^\circ\text{C}$ , and its strength at  $110^\circ\text{C}$  is triple that of conventional unirradiated polyethylene at the same temperature [4].

The shielding properties of polyethylene have been investigated by Broder, et al. [5] for neutrons of 4 and 14.9 MeV energy. Goldstein [2] has drawn inferences from findings of studies of the passage of neutrons through polyethylene [2]. However, the amount of experimental data in the literature on the attenuation of pile neutrons by polyethylene is still meager.

#### Experimental Geometry and Conditions

The experiments were carried out in a water-cooled water-moderated research reactor. A polyethylene prism ( $680 \times 680 \times 1000 \text{ mm}^3$ ) was placed in a recess formed in the heavy concrete reactor shield. The prism was made up of square plates 10 and 20 mm thick.

Resonance indicators (indium, iodine) and a  $\text{BF}_3$ -filled counter were used in the measurements of the distributions of thermal and epithermal neutrons. The spatial distribution of fast neutrons was measured with the threshold indicators  $\text{P} (n, p)$ ,  $\text{Al} (n, p)$ ,  $\text{Al} (n, \alpha)$ , and a bantam-size  $\text{ZnS} (\text{Ag})$  scintillation counter. To avoid activation of the threshold and resonance indicators by thermal neutrons, the indicators were sheathed in 1 mm thick cadmium jackets. The characteristics of the indicators employed appear in Table 1.

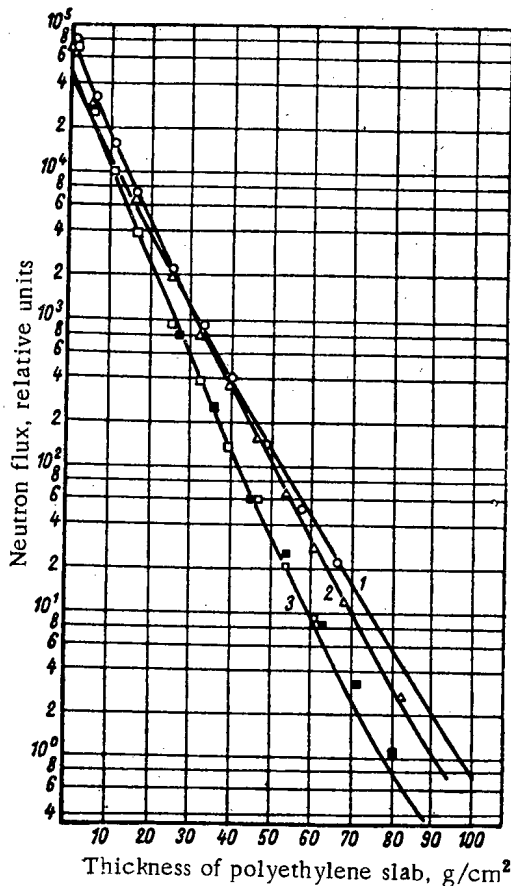


Fig. 1. Fast neutron distribution in polyethylene. Computed data: 1)  $E_n > 7$  MeV; 2)  $E_n > 4.7$  MeV; 3)  $E_n \gg 2.8$  MeV. Empirical data:  $\Delta$  Al (n, p);  $\circ$  Al (n,  $\alpha$ );  $\square$  P (n, p);  $\blacksquare$  ZnS(Ag).

In the course of the measurements, flat indicators were lodged in the spaces between the platelets, and the round cylindrical ones were placed in notches (20 x 20 x 100 mm) in the plates. Four indicators were irradiated at a time, and mutual shielding was averted by shifting them around the axis of the prism at  $\pm 5$  cm spacings.

The activity of the flat indicators was measured using a  $2\pi$ -scintillation counter, and the activity of the cylindrical ones was measured using a  $4\pi$ -scintillation counter. The counters were incorporated into the circuitry of a spectrometer in order to reduce background and impurity effects in the indicators, and instead of the integrated number of pulses, the number of pulses due to the  $\gamma$ -line or group of  $\gamma$ -lines most characteristic of the given indicator was recorded (see Table 1).

The spatial neutron distribution in polyethylene was measured with a ZnS(Ag) scintillation counter ( $d > 20$  cm polyethylene thickness) and a BF<sub>3</sub>-loaded counter (at  $d > 30$  cm). A slit 30 x 30 x 350 mm was cut in one plate to accommodate the counters, and this slit was moved around the prism during the experiment. Measurements were carried out at each point at several different reactor power levels in order to check the counter sensitivity to  $\gamma$ -radiation and in order to ensure more reliable results.

#### Attenuation of Fast Flux

The measured distributions of fast flux (Fig. 1) were compared with the results of a computation of distributions by the method of moments for a point isotropic neutron source with a fission spectrum [2]. The computed differential neutron spectra were integrated according to the formula

$$N(d) = \int_{E_n}^{18 \text{ MeV}} \sigma(E) \cdot \Phi(E, d) dE,$$

where  $\sigma(E)$  is the cross section of the reaction [6] for an indicator of threshold  $E_n$  extrapolated to 18 MeV;  $\Phi(E, d)$  is the differential numerical neutron spectrum in polyethylene at thickness  $d$ ;  $N(d)$  is the flux of neutrons with energies ranging from  $E_n$  to 18 MeV at thickness  $d$ .

TABLE 2. Relaxation Lengths of Fast Neutrons in Polyethylene (cm)

Thickness of polyethylene slab, cm	$E_n > 7$ MeV		$E_n > 4.7$ MeV		$E_n > 2.8$ MeV		ZnS(Ag)	$\lambda_{\text{dose}}$
	Exper.	Theor.	Exper.	Theor.	Exper.	Theor.		
0-30	7,8	9,1	7,8	7,8	6,6	7,5	—	7,1
30-60	9,7	9,7	8,9	8,9	8,2	8,2	8,2	7,4
60-90	—	10,7	9,5	9,5	—	8,8	9,5	8,6

Clearly, in the light of Fig. 1, the experimental data points\* obtained in measurements of the neutron flux distribution with the indicator Al (n, p), i.e., in measuring the distribution of neutrons of energy greater than 4.7

\* The experimental findings reported here take into account geometrical attenuation of neutron flux along the prism. The correction for geometric attenuation was determined experimentally.

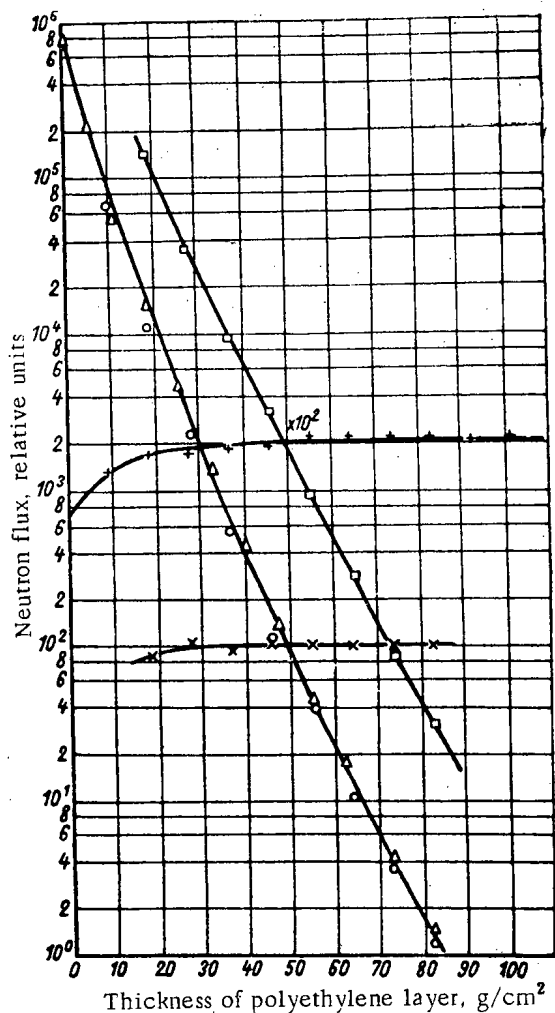


Fig. 2. Distribution of thermal and epithermal neutrons in polyethylene: (O) In; (Δ) I; (□) BF<sub>3</sub> counter; +) cadmium ratio, from results of In measurements; x) cadmium ratio, from results of BF<sub>3</sub> counter measurements.

In Table 2, relaxation lengths determined empirically and read off theoretically predicted curves are compared. The excellent fit between theoretically predicted data and empirical data for all the energies at a polyethylene thickness greater than 30 cm is quite conspicuous, and a substantial divergence is observed at lesser thicknesses in the case of neutrons of energy  $E > 7$  MeV and  $E > 2.8$  MeV. The discrepancies are apparently accountable to some difference in the assumed and the actual spectra of the neutron sources [7] and the geometry (in reference [2], calculations were carried out for a point isotropic source in an "infinite" medium, while the experiment involved a plane source in a "semiinfinite" medium).

Table 2 also lists relaxation lengths for neutron dose rates  $\lambda_{\text{dose}}$  calculated from the data reported in [2]. A comparison of  $\lambda_{\text{dose}}$  and the relaxation lengths for the neutron fluxes clearly reveals that the contribution of neutrons of energies 1-2 MeV to the dose is quite appreciable even at relatively large distances from the source.

In Table 3, relaxation lengths of neutrons in polyethylene and in water, measured under identical conditions, are compared. The relaxation lengths in polyethylene are 12 to 17% less than the relaxation lengths in water.

MeV, fit well on the predicted curve. The results obtained for neutrons of energy greater than 2.8 MeV [indicator P (n, p)] also show a good fit, within the limits of experimental error, with the theoretically predicted data (with the exception of the first two data points).

For neutrons of energy greater than 7 MeV [indicator A1 (n, d)], the agreement between experiment and calculations is observed at a thickness greater than 30 g/cm<sup>2</sup>. At lesser polyethylene thicknesses, sharper attenuation than that anticipated in the calculations is observed (curve 1).

TABLE 3. Relaxation Lengths (cm) of Neutrons in Polyethylene and in Water (Density of Polyethylene 0.92 g/cm<sup>3</sup>, of Water 1 g/cm<sup>3</sup>)

Slab thickness, cm	$E_n > 4,7$ MeV		$E_n > 2,8$ MeV	
	Polyethylene	Water	Polyethylene	Water
0-30	7,8	8,9	6,6	7,7
30-60	8,9	10,0	8,2	9,3
60-90	9,5	11,1	—	—

TABLE 4. Relaxation Lengths (cm) of Thermal and Epithermal Neutrons in Polyethylene and in Water

Layer thickness, cm	Polyethylene		Water [8]
	1,44 and 30eV	Thermal, BF <sub>3</sub>	
0-30	5,5	—	6,1
30-60	6,9	—	6,8
60-90	8,8	9,0	8,5

The neutron distributions measured with a scintillation counter and with the indicator P (n, p) are superposed at 26 g/cm<sup>2</sup> slab thickness, and agree within the limits of experimental error.

Attenuation of Slow Flux

The results of measurements of the spatial distributions of fluxes of neutrons, 1.44 eV (indium) and 30 eV (iodine), are shown in Fig. 2. At close distances from the reactor core, the attenuation curves appear to have a steeper slope than at great distances. The more abrupt attenuation experienced in the first polyethylene layers is due to the absorption of neutrons slowed down in the core and in the water reflector of the reactor. The relaxation lengths computed from the experimental results are given in Table 4, while the geometrical attenuation of the flux is subject to the same correction as that applying to fast neutrons.

The curve describing the thermal flux distribution (see Fig. 2) at polyethylene layer thickness less than 50 g/cm<sup>2</sup> has a gentler slope than the distributions measured by indium and iodine indicators. This is apparently explained by the leakage of scattered neutrons from the concrete shielding from the side of the unshielded end of the BF<sub>3</sub> gas counter.\* At a large polyethylene thickness, satisfactory agreement is observed in the attenuation of thermal and epithermal flux.

The cadmium ratios calculated on the basis of the results of our measurements (see Fig. 2) reveal that the equilibrium spectrum of thermal and epithermal neutrons in polyethylene is established at layer thickness 20 to 30 g/cm<sup>2</sup>.

Table 4 offers, for comparison, relaxation lengths for water, as calculated from the data in reference [8].

The authors take this opportunity to express their gratitude to the staff working on the research reactor and to the laboratory technicians who took part in the experiments.

## LITERATURE CITED

1. Mod. Plastics, No. 10, 97 (1961).
2. H. Goldstein, Fundamental aspects of reactor shielding, Addison Wesley, USA (1959).
3. V. Shifrina and N. Samosatskii, High-pressure polyethylene, Moscow, State Chemical Press [in Russian] (1958).
4. R. Ward, Nucleonics, 19, No. 8 (1961).
5. D. L. Broder, A. A. Kutuzov, and V. V. Levin, Inzhener.-fiz. zhur., 5, 47 (1962).
6. D. Hughes, Neutron Cross Sections, BNL-Upton-New York (1958).
7. V. N. Avaev, et al., JAE, 15, 20 (1963).
8. K. Cooper, D. Johns, and K. Horton, Article in symposium "Shielding of nuclear-propelled vehicles" [Russian translation], Moscow, Foreign Literature Press (1961).

---

All abbreviations of periodicals in the above bibliography are letter-by-letter transliterations of the abbreviations as given in the original Russian journal. *Some or all of this periodical literature may well be available in English translation. A complete list of the cover-to-cover English translations appears at the back of this issue.*

---

\* According to the experimental conditions, polyethylene must not be placed above the counter at the thicknesses mentioned.

## SPECTRA OF FAST PILE NEUTRONS IN PASSAGE THROUGH POLYETHYLENE

V. N. Avaev, G. A. Vasil'ev, A. P. Veselkin, Yu. A. Egorov,  
Yu. V. Orlov, and Yu. V. Pankrat'ev

Translated from *Atomnaya Énergiya*, Vol. 15, No. 1,  
pp. 20-22, July, 1963  
Original article submitted August 25, 1962

A single-transducer fast-neutron spectrometer was used to measure the spectra of fast pile neutrons after passing through polyethylene layers of different thicknesses. The results of measurements at  $E_n > 3$  MeV show excellent agreement with data computed by the method of moments. At  $E_n < 3$  MeV, the discrepancies are accounted for by the difference in the geometry and in the original spectra. Problems involving the correct procedures to be followed in setting up experiments of this type are discussed.

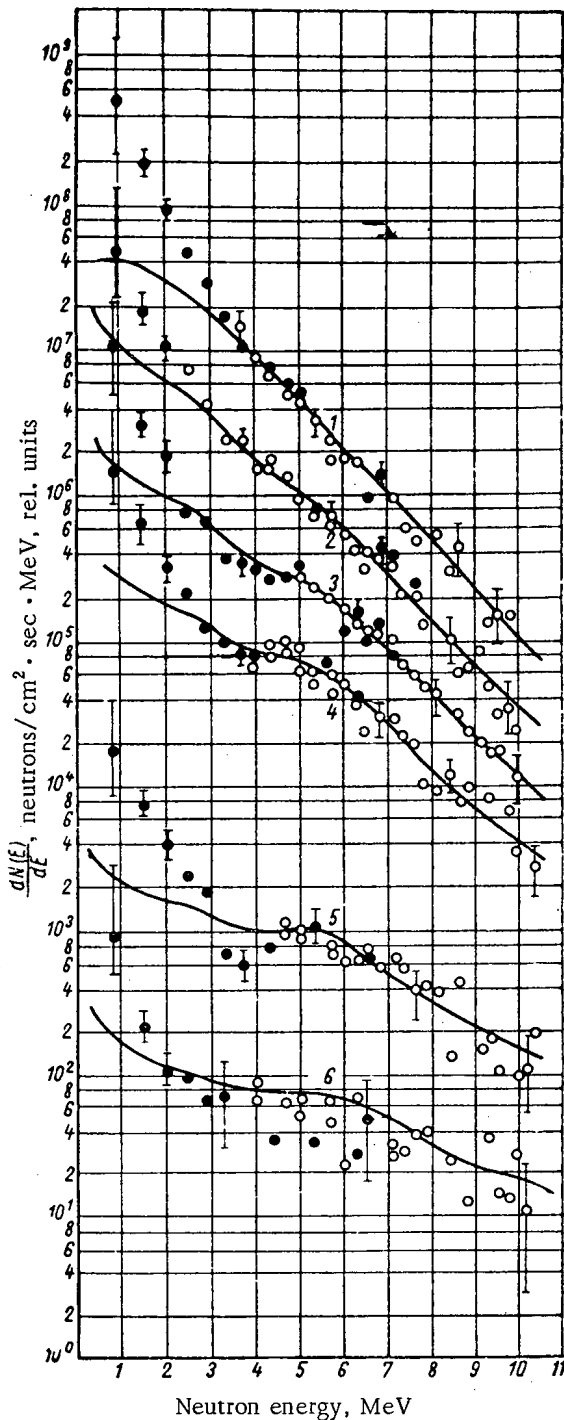
The measurement of the deformation of spectra of fast pile neutrons after their passage through shielding material is a complicated experimental task, and only a scant number of papers have been published throwing any light on the results of experiments in this line [1]. The problem is that the fast flux is accompanied by high-level gamma flux, and until recently no highly efficient fast neutron spectrometer capable of reliable operation in the presence of considerable gamma background was known. Research on the dependence of scintillator deexcitation time on the mode of the emissions being recorded has led to such a spectrometer becoming available [2].

In the experiments conducted by the present authors, the spectra of fast neutrons passed through polyethylene were measured in a barrier-geometry water-cooled water-moderated research reactor. Slabs of polyethylene  $680 \times 680 \times 10$  mm<sup>3</sup> were positioned in recesses in the reactor shielding. The polyethylene slab thickness increased in the direction of the spectrometer transducer in the course of the measurements. Measurements were performed with the aid of a single-transducer fast-neutron scintillation spectrometer, and discrimination of gamma background was carried out by means of the space charge between the last dynode and the anode of the photomultiplier tube [2]. The spectrometer transducer contained a FÉU-33 photomultiplier and a stilbene crystal 30 mm in diameter and 20 mm high. The fast spectrum was determined by the amplitude distribution of pulses due to recoil protons in the stilbene crystal. The amplitude distribution of pulses was transformed into the energy distribution of neutrons through a procedure proposed by Broek and Anderson [3]; corrections for secondary scattering of neutrons in the crystal and for partial leakage of recoil protons out of the crystal were introduced into the energy distribution so obtained.

Investigation of the spectrometer gamma-sensitivity revealed that the spectrometer failed to record gamma emission at a dose rate lower than  $20 \mu\text{r}/\text{sec}$ . A slab of lead 16 cm thick was placed in front of the polyethylene, therefore, with the object of reducing the gamma intensity issuing from the pile, and the spectrometer transducer was placed in paraffin shielding with boron and lead in such a way that it could "see" almost the entire surface of the polyethylene slab. Boron-loaded polyethylene (0.5 wt. %) was employed to reduce capture gamma radiation in the polyethylene and to cut down the thermal flux. In addition, a 5 cm thick layer of bismuth\* was placed directly in front of the transducer.

However, as the thickness of the polyethylene increased, the ratio of neutron flux to gamma flux declined drastically in value, and even at a gamma recording efficiency ( $\text{Co}^{60}$ ) of  $\sim 0.005\%$  and neutron recording efficiency ( $\text{Po} + \text{Be}$ ) of  $\sim 14\%$ , the contribution of pulses due to recording of gamma emission became conspicuous even at polyethylene thicknesses ranging from 30 to 90 cm. It was established in the course of the experiments that the gamma-ray background discrimination level at 1.33 MeV maximum energy is insufficient to discriminate against high-energy gamma photons. Pulses due to electrons of  $\sim 3$  MeV and higher are clearly observed in the amplitude distribution, and their effect was evaluated by means of a paraffin filter 20 cm thick placed in front of the spectrometer transducer.

\* It has been shown experimentally that a slab of bismuth 5 cm thick will not deform the fast neutron spectrum at  $E_n > 2.5$  MeV; at  $E_n < 2.5$  MeV the deformation of the spectrum is not greater than 20%.



Spectra of fast neutrons passed through polyethylene:  
 1) spectrum of fast pile neutrons passed through 16 cm lead; 2, 3, 4, 5, 6) spectrum of fast pile neutrons passed through polyethylene of 10, 20, 30, 60, 80 g/cm<sup>2</sup> thickness, respectively. Filled data points indicate data obtained at  $E_{n1} = 0.6$  MeV; hollow data points denote data obtained at  $E_{n2} = 2.1$  MeV.

\* The spectrometer energy thresholds were determined from the results of measurements of (d, d)-neutron spectra.

† The reactor power level varied by a factor of  $10^4$  during the measurements, depending on the thickness of the polyethylene slab.

In order to avoid any distortions due to the gamma-ray background, and at the same time to measure the spectrum over the broadest possible range of fast-neutron energies, all of the experiments were carried out at the two energy thresholds of the spectrometer:\*  $E_{n1} = 0.6$  MeV and  $E_{n2} = 2.1$  MeV. At the threshold  $E_{n2} = 2.1$  MeV, the pile gamma radiation escaped detection.

After the results were processed, it was found that the spectral distribution obtained at threshold  $E_{n1}$  was slightly lower than that obtained at threshold  $E_{n2}$ , the discrepancy amounted to 15-20% in the 3-5 MeV energy range. The results obtained at  $E_{n2}$  were accepted as the actual values, i.e., when the spectrometer failed to record gamma emission; and the  $E_{n1}$  results were accordingly increased by 15-20%. The differential fast spectra so obtained in the energy region to 10 MeV appear in the accompanying diagram.

Errors in the measurements consisted of statistical errors, errors in determining the energy threshold ( $\pm 0.1$  MeV), errors in determining the reactor power level,† in determining the polyethylene thickness and density, and also of errors related to imprecise calibration of the spectrometer. The errors indicated in the diagram are the sum of the statistical errors and of the errors in determining the energy threshold. Other errors were substantially less in our estimation, and were therefore left out of account.

The measured fast spectra (denoted by points on the diagram) were compared with results predicted by the method of moments [4] on the neutron spectra of a point isotropic fission source in the polyethylene (indicated by solid curves on the diagram). For purposes of comparison, experimental results were normalized with the predicted data at a polyethylene slab thickness of 20 g/cm<sup>2</sup> and neutron energy of 6 MeV.

Clearly, from the diagram, the spectrum of fast neutrons emitted by a reactor and passed through a slab of lead is slightly different from the fission neutron spectrum at  $E_n < 3$  MeV; at  $E_n > 3$  MeV, the measured spectrum agrees with the fission spectrum within the limits of experimental error. The difference between the measured spectrum and the fission spectrum at  $E_n < 3$  MeV may be ascribed to the following factors: 1) distortion of the fission spectrum in the reactor core in response to neutron scattering; 2) the difference between the geometry of the experiment and the geometry adopted in the calculations; and 3) the presence of a lead shield.

However, to judge by the energy dependence of the removal cross section in the case of lead [5], the presence of this shield should not lead to such a distortion of the spectrum.

The measured spectra show excellent agreement, at all polyethylene thicknesses in question, with predicted results at  $E_n > 3$  MeV. At  $E_n < 3$  MeV, a certain discrepancy is observed between the measured and the theoretically predicted spectra, on account of the difference in the initial spectra. The tendency of the spectrum to change in that range of energies as the thickness of the polyethylene increases is the same as that found in the predicted spectra. At neutron energy 3-4 MeV and at polyethylene slab thicknesses greater than  $20 \text{ g/cm}^2$ , a steeper decline is seen in the measured spectra than in the theoretically predicted spectra. This is apparently related to the inaccurate choice of, or averaging of, the cross sections in the calculations. The same steep decline was detected in measurements of neutron spectra in water [1].

The authors take this opportunity to express their gratitude to the reactor operations staff and to the laboratory technicians for their kind assistance in the performance of the experiments herein described.

#### LITERATURE CITED

1. USAEC Manual. Research Reactors (1956).
2. R. Owen, IRE Trans. Nucl. Science, NS-5, 198 (1958).
3. H. Broek and G. Anderson, Rev. Sci. Instr., 31, No. 10 (1960).
4. H. Goldstein, Fundamental aspects of reactor shielding, Addison Wesley, Cambridge, Mass. (1959).
5. B. I. Sinitsyn and S. G. Tsylin, JAE, 12, 306 (1962).

---

All abbreviations of periodicals in the above bibliography are letter-by-letter transliterations of the abbreviations as given in the original Russian journal. *Some or all of this periodical literature may well be available in English translation.* A complete list of the cover-to-cover English translations appears at the back of this issue.

---

THE SEPARATION OF  $Zr^{95}$ ,  $Nb^{95}$ , and  $Ru^{106}$  FROM A MIXTURE  
OF FISSION PRODUCTS BY EXTRACTION WITH TRIBUTYL PHOSPHATE

N. E. Brezhneva, V. I. Levin, G. V. Korpusov,  
E. K. Bogacheva, and N. M. Man'ko

Translated from *Atomnaya Énergiya*, Vol. 15, No. 1,  
pp. 23-30, July, 1963

Original article submitted July 6, 1962

We have studied methods for preparing radiochemically pure isotopes of  $Zr^{95}$ ,  $Nb^{95}$ , and  $Ru^{106}$  by a previously described [1] general scheme for the separation of fragmentary radioactive elements.

We mainly consider regularities which were established in a study of the extraction of zirconium, niobium, and ruthenium by tributyl phosphate (TBP).

Ruthenium is extracted by TBP after preliminary concentration on the sulfides of metals.

Niobium and zirconium are separated by successive reextraction of niobium by hydrogen peroxide and zirconium by oxalic acid.

Methods of Experiments

The extraction of zirconium, niobium, and ruthenium was studied under static conditions by shaking solutions in separating funnels; for the dynamic conditions we used a glass extraction semicounter-current apparatus consisting of 20 sections. We used pure preparations of radioactive isotopes of  $Zr^{95}$ ,  $Nb^{95}$ ,  $Ru^{106}$ ,  $Y^{91}$ ,  $Eu^{152}$ , and  $Eu^{154}$  to label the solutions.

TABLE 1.  $K_{distr}$  of Zirconium and Niobium Between TBP and Aqueous Solutions of Nitric Acid at 20°C

Undiluted TBP									
Zirconium									
Equilibrium concentration of									
$HNO_3$ , M	1,3	3,7	4,6	8,1	9,7	11,2	13,5		
$K_{distr}$	7,5	18	25	66	109	217	270		
Niobium									
Equilibrium concentration of									
$HNO_3$ , M	2,6	4,6	5,4	6,4	7,9	8,5	9,3	9,5	10,5
$K_{distr}$	0,9	1,2	1,5	2,15	3,6	4,3	4,5	4,8	5,9
									11,2
									24
40% solution of TBP in kerosene									
Zirconium									
Equilibrium concentration of									
$HNO_3$ , M	0,9	2,0	5,1	6,2	8,0	9,1	10,2	11,1	12,2
$K_{distr}$	0,03	0,09	1,1	3,4	5,0	9,3	17,3	22,8	85,3
Niobium									
Equilibrium concentration of									
$HNO_3$ , M	1,4	2,4	3,2	4,3	5,6	6,9	7,2	10,3	
$K_{distr}$	0,009	0,02	0,04	0,09	0,13	0,23	0,42	0,93	

In the dynamic experiments the solution under investigation, containing a mixture of isotopes in nitric acid of a certain concentration, was placed in the first section of the extractor described in [1]. We poured wash solutions of the appropriate composition into the remaining sections. TBP which had first been brought to equilibrium with the aqueous phase was passed through the extractor. Samples of solvent leaving the apparatus and also the contents of the extraction cells were subjected to radiometric analysis at the end of the experiment.



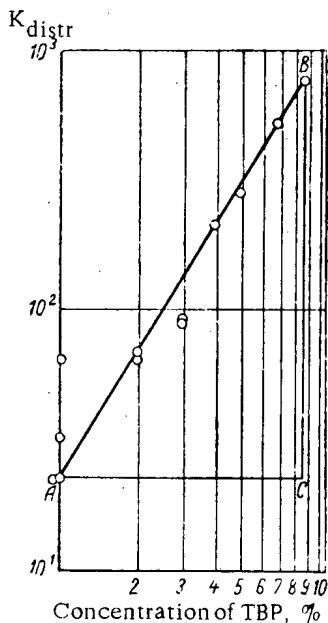


Fig. 1. Dependence of the coefficient of distribution of niobium between nitric acid and a mixture of TBP and benzene on the TBP

concentration ( $\tan \alpha = \frac{BC}{AC} = \frac{154}{96} = 1.64$ ).

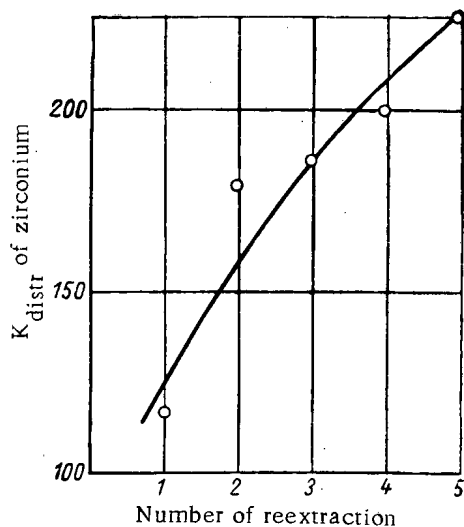


Fig. 2. Distribution coefficient of zirconium during successive reextractions from TBP.

above 5 N for zirconium prevents reextraction. Hydrogen peroxide does not affect the distribution of zirconium.

#### Extraction of Zirconium and Niobium Under Dynamic Conditions

In a glass extractor we experimented on the separation of an artificially prepared mixture of zirconium with niobium. The first section contained a mixture of  $Zr^{95}$  and  $Nb^{95}$  in 10 N  $HNO_3$  in the second and third sections there was 10 N  $HNO_3$ , containing 2%  $H_2O_2$ . Through the system we passed TBP in equilibrium with 10 N  $HNO_3$ . When the experiment was completed we measured the activity of the contents of the sections and obtained absorption curves for the radiation of aqueous phases from sections with  $H_2O_2$  and the last portion of solvent leaving the apparatus. The absorption curves would seem to show that the reextracted niobium does not contain noticeable impurities of zirconium and the latter is not contaminated with niobium.

#### Extraction of $Zr^{95}$ and $Nb^{95}$

We studied the dependence of  $K_{distr}$  of zirconium and niobium in extraction by undiluted TBP and 40% solution of TBP in kerosene (Table 1) on a number of factors. On extraction by diluted TBP,  $K_{distr}$  of niobium increases in proportion to the second power (approximately) of the TBP concentration in the organic phase (Fig. 1). This shows that the extracted complex includes two TBP molecules. Bearing in mind the increase in  $K_{distr}$  with increase in acidity, we can assume that  $HNO_3$  molecules also take part in the formation of the extracted complex.

A feature of the behavior of zirconium and niobium is the apparent irreversibility of the distribution. For example,  $K_{distr}$  during reextraction is much higher than during extraction.

TABLE 2. Dependence of  $K_{distr}$  of Niobium on the Holding Time of the Solution

Holding time, h	$K_{distr}$	
	2,2N $HNO_3$	4,1N $HNO_3$
0	0,49	0,71
24	0,69	0,89
48	0,34	1,05
72	0,25	0,91
96	0,15	0,88
216	0,05	0,59
264	—	0,32

The existence of several chemical forms of zirconium and niobium in solutions is shown by data obtained during extraction and reextraction in successive portions from one solution (Fig. 2). The values of  $K_{distr}$  of niobium in three successive extractions from the same portion of solution are 8.2, 1.4, 0.9, respectively. On the other hand,  $K_{distr}$  of niobium depends on the time the solution is kept (Table 2) after its preparation (by dilution of a solution of niobium in concentrated  $HNO_3$ ).

These data show that both phases contain several chemical forms of zirconium and niobium, the equilibrium between which is established with a relatively low rate. The difficulty in the reextraction of zirconium and niobium is readily overcome by using complex formers: hydrogen peroxide for niobium and oxalic acid for zirconium. Experimental data on reextraction with complex formers are given in Tables 3 and 4. It can be seen that an increase in  $HNO_3$  concentration above 13 N for niobium and above 5 N for zirconium prevents reextraction. Hydrogen peroxide does not affect the distribution of zirconium.

TABLE 3. Reextraction of Zirconium by HNO<sub>3</sub> Containing Complex Formers (1% H<sub>2</sub>O<sub>2</sub> or 0.1% H<sub>2</sub>C<sub>2</sub>O<sub>4</sub>)

Equilibrium concentration of HNO <sub>3</sub> in aqueous phase, M	5,3	8,0	1,0	1,45	2,5	5,3	5,8	6,7	7,7
Complex former	H <sub>2</sub> O <sub>2</sub>	H <sub>2</sub> O <sub>2</sub>	H <sub>2</sub> C <sub>2</sub> O <sub>4</sub>	H <sub>2</sub> C <sub>2</sub> O <sub>4</sub>	H <sub>2</sub> C <sub>2</sub> O <sub>4</sub>	H <sub>2</sub> C <sub>2</sub> O <sub>4</sub>	H <sub>2</sub> C <sub>2</sub> O <sub>4</sub>	H <sub>2</sub> C <sub>2</sub> O <sub>4</sub>	H <sub>2</sub> C <sub>2</sub> O <sub>4</sub>
K <sub>distr</sub> during reextraction	380	400	10 <sup>-3</sup>	0,005	0,004	0,52	1,7	4,7	21,4

TABLE 4. Reextraction of Niobium by HNO<sub>3</sub> Containing Complex Former (1% H<sub>2</sub>O<sub>2</sub>)

Equilibrium concentration of HNO <sub>3</sub> in aqueous phase, M	2,6	6,8	7,3	9,3	10,5	12,0	13,0	14,6	16,5
K <sub>distr</sub> during reextraction	0,11	0,1	0,1	0,1	0,13	0,20	0,35	7,0	11,0
Degree of reextraction, %	90	91	91	91	89	83	74	13	8,3

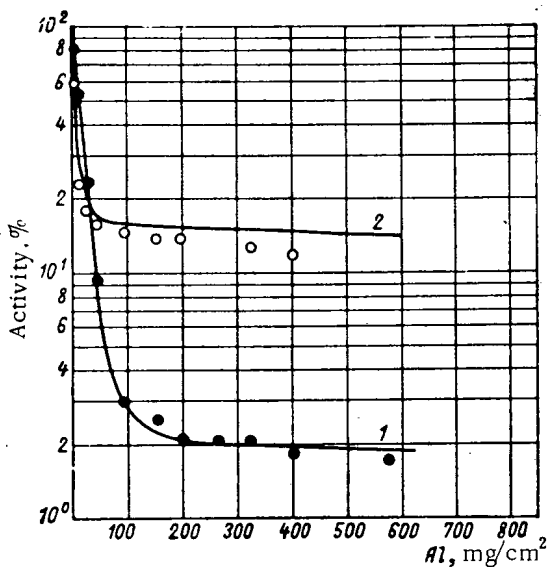


Fig. 3. Curves for absorption of radiation of Zr<sup>95</sup> and Nb<sup>95</sup> preparations obtained in an experiment with an extractor: a) pure Zr<sup>95</sup>; 2) pure Nb<sup>95</sup>; ●) Zr<sup>95</sup> preparation; ○) Nb<sup>95</sup> preparation.

The results formed the basis for the dynamic extraction separation of zirconium and niobium from a nitric acid solution of an iron hydroxide precipitate obtained during the treatment of mixtures of fission products according to the scheme of [1].

For this purpose we used an extractor with 19 sections. The first section contained the initial solution with 9.8 N HNO<sub>3</sub>, the next four contained HNO<sub>3</sub> to remove from the TBP radioactive elements which were extracted less efficiently than zirconium and niobium; the next four sections contained HNO<sub>3</sub> with 2% H<sub>2</sub>O<sub>2</sub> to reextract the niobium. For the reextraction of zirconium, the sections with 1 N HNO<sub>3</sub>, intended for the washing out of impurities, were followed by sections containing 2 N HNO<sub>3</sub> and 1 N oxalic acid. We passed TBP in equilibrium with 9.7 N HNO<sub>3</sub> through the extractor. In Fig. 3 curves for the absorption of radiation of the reextracts, containing zirconium and niobium, are compared with curves for the absorption of radiation of the pure preparations.

An analysis of the wash sections showed that impurities of radioactive cerium and yttrium contained in the initial nitric acid solution are concentrated in them.

#### Extraction of Ru<sup>106</sup>

The main regularities of the distribution of ruthenium during extraction were studied with preparations of pure radioactive ruthenium. To prepare extracted complex of nitrosyl ruthenium we must have oxide of nitrogen or compounds which readily liberate them, for example nitrous acid. Special experiments, the results of which are given in Fig. 4, showed that in the presence of NO<sub>2</sub><sup>-</sup> ions during extraction by TBP from nitric acid solutions K<sub>distr</sub> of ruthenium at first increases and then falls sharply. With increase in the concentration of NO<sub>3</sub><sup>-</sup> ions the value of K<sub>distr</sub> of ruthenium continuously increases (Fig. 5). A study of the distribution of ruthenium as a function of the acidity showed that K<sub>distr</sub> of ruthenium passes through a sharp maximum (Fig. 6). During repeated extraction from the same solution over certain intervals of time K<sub>distr</sub> of ruthenium continuously decreases (Table 5).

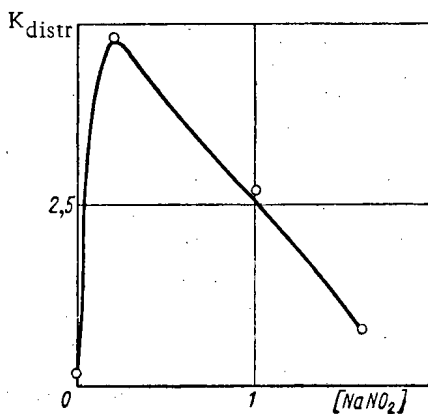


Fig. 4. Dependence of  $K_{distr}$  of ruthenium between TBP and  $HNO_3$  on the nitrite ion concentration in the aqueous phase.

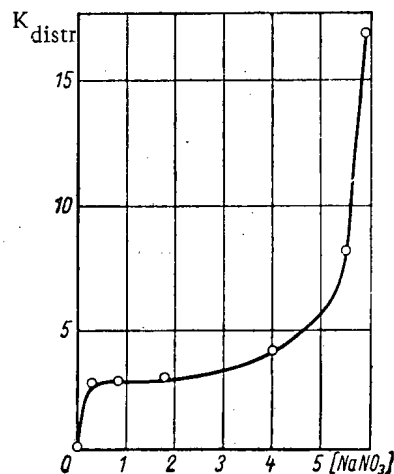


Fig. 5. Dependence of  $K_{distr}$  of ruthenium between TBP and nitric acid solution on the nitrate ion concentration (at constant ionic strength).

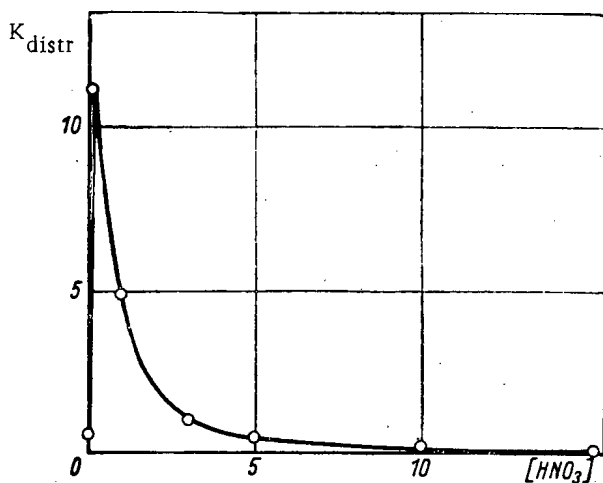


Fig. 6. Dependence of  $K_{distr}$  of ruthenium between TBP and nitric acid on the concentration of the latter.

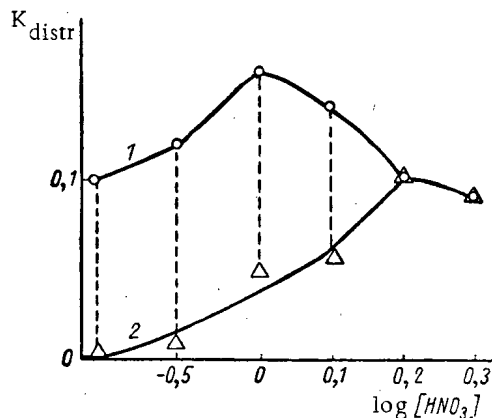


Fig. 7. Extraction of ruthenium by TBP from solutions of varying acidity: 1) primary extraction; 2) secondary extraction.

As can be seen from Table 5 and Fig. 7, with increase in the acidity of the solution the differences in  $K_{distr}$  during primary and repeated extractions decrease and eventually disappear completely.

In successive reextractions from the organic phase after short intervals of time the values of  $K_{distr}$  gradually increase even when an active reextracting medium is used, such as a 2 N solution of ammonium carbonate. In this case  $K_{distr}$  for two successive reextractions is 0.175 and 0.270.

As can be seen from Fig. 8, increasing the concentration of  $HNO_3$  during reextraction leads to a reduction in the values of  $K_{distr}$ . The values of  $K_{distr}$  for ruthenium during extraction increase with increase in the content in TBP of its hydrolysis products, forming intensively, especially during heating with acid.

Concentrating  $Ru^{106}$  on Sulfide Precipitates. The conditions for the occlusion of radioactive ruthenium by precipitates of nickel, copper, and cadmium sulfides were studied as a function of the amount of carrier, the excess concentration of ions of precipitating agent, the temperature and concentration of the added reducing agent. As can be seen from Table 6, the best results are obtained using precipitates of nickel and copper sulfides. Lead sulfide is less convenient due to difficulty in dissolving this precipitate. Adding up to 1 g/liter of hydrazine to the solution does not affect the extraction of ruthenium.

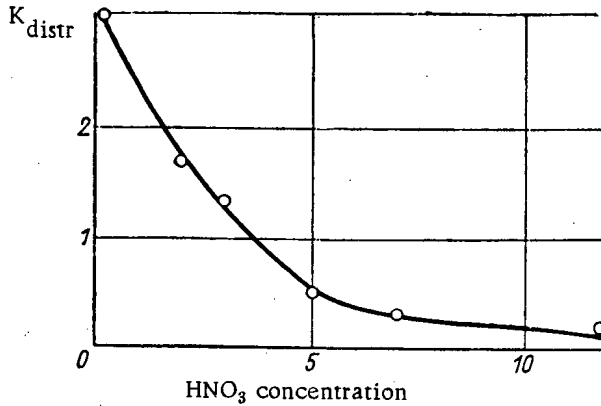


Fig. 8. Values of  $K_{distr}$  for ruthenium between TBP and  $HNO_3$  during reextraction from the organic phase (the  $HNO_3$  concentration in the aqueous phase is plotted along the abscissa axis).

TABLE 5. Change in  $K_{distr}$  of Ruthenium During Repeated Successive Extraction From the Same Solution

Number of extraction	First series of experiments	Second series of experiments
1	0,64	0,58
2	0,27	0,27
3	0,23	0,20
4	0,20	0,66*
5	0,13	

\* Solution treated with 24 N  $HNO_3$ .

TABLE 6. Dependence of the Occlusion of Radioactive Ruthenium by Sulfide Precipitates on the Nature of the Carrier (Concentration of Carrier 3.4 mM)

Carrier	Concentration of sodium sulfide, M	Occlusion of radioactive ruthenium by precipitate, %
Ni	0,1	99,2
Cu	0,1	98,2
Pb	0,1	98,2
Cd	0,1	91,0
Ni	0,02	20
Cu	0,02	24
Pb	0,02	7,5
Cd	0,02	9,0
Bi	0,02	9,0
Sb	0,02	1,5

transfers to the organic phase in the form  $Zr(NO_3)_4 \cdot x TBP$ . However, according to the data of [5],  $K_{distr}$  of zirconium for a constant concentration of  $NO_3^-$  ions increases approximately proportional to the second power of the  $H^+$  ion concentration. The authors of [5] attribute this phenomenon to the suppression of hydrolysis of zirconium or the formation of the complex  $H_2Me(NO_3)_6 \cdot x TBP$ . The first explanation is unlikely since at acid concentrations of 3-5 N, at which the investigation was conducted, microquantities of zirconium are hardly hydrolyzed at all [6, 7]. A. M. Rozen and co-workers explain the regularities of extraction of zirconium at high acidities by the formation of complexes of the type  $Zr(NO_3)_4 \cdot mHNO_3$  [8].

Separation of Radioactive Ruthenium From a Solution of a Mixture of Fission Products. Using the described method, we separated radioactive  $Ru^{106}$  from the decanted oxalate solution obtained in the treatment of a mixture of long-lived radioactive isotopes.

The washed precipitate of nickel sulfide obtained from the decanted oxalate solution was dissolved in  $HNO_3$ ; the acidity was reduced to 0.2 N by the addition of caustic alkali; after adding sodium nitrite to a concentration of 0.2 N, we extracted the solution with TBP in equilibrium with 0.2 N  $HNO_3$ .

The results for the extraction of radioactive ruthenium are given in Table 7; the best results were obtained for nickel and copper sulfides.

A simultaneous study of the extraction of nickel and copper showed that  $K_{distr}$  for these elements is 0.05 and 0.12, respectively.

The degree of extraction of radioactive ruthenium from a sulfide precipitate is therefore not less than 80%.

#### Discussion of Results

The value of  $K_{distr}$  of zirconium between TBP and  $HNO_3$  increases continuously with increase in concentration of the latter, without passing through a maximum, which is the case in the extraction of many other elements. The same regularity was observed by other investigators studying the extraction of zirconium [2-4]. It is of course possible that the maximum nevertheless exists, but that it is beyond the limits of the investigated region of  $HNO_3$  concentrations. Its appearance on the curve for the dependence of  $K_{distr}$  on the acid concentration is usually connected with a reduction in the concentration of free solvent due to its combining with the extracted acid, or with the formation in the aqueous phase of unextractable complexes of the distributing element with the anion of the acid.

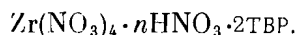
We were unable to obtain sufficiently precise data on the composition of the extracted complex of zirconium. It can be assumed that these complexes are the neutral molecule of  $Me(NO_3)_4$  or the complex acid  $H_2Me(NO_3)_6$ .

Some investigators [2, 4] who have studied the extraction of zirconium believe that this element trans-

TABLE 7. Extraction of Radioactive Ruthenium by TBP From a Solution of Sulfide Precipitates of Various Metals

Carrier	Occlusion of Ru <sup>106</sup> by precipitate, %	K <sub>distr</sub>	Extraction of Ru <sup>106</sup> , %
Ni	98,3	4,6	82
Cu	98,2	4,0	80
Pb	98,0	3,1	76
Cd	91,0	0,45	34

There is disagreement in the literature with regard to the number of TBP molecules in the extracted zirconium complex. According to [2] the number of TBP molecules in the solvate is equal to two. In another paper [4] a formula of  $Zr(NO_3)_4 \cdot (TBP)_3$  is given for the composition of the complex. Data are also favoring the formula  $Zr(NO_3)_4 \cdot TBP \cdot xHNO_3$  [9]. In our opinion the most convincing are the data of [8]; for three nitric acid concentrations (0.5, 4, and 9 M), curves were obtained with the tangent of the slope close to two, indicating the following composition of the extracted complex:



The absence of a maximum on the curve of  $K_{distr}$  versus acid concentration for a complex of this composition points to the relative instability of the higher nitrate complexes of zirconium (for example, compared with similar complexes of cerium or plutonium).

A characteristic feature of the extraction of zirconium is its apparent irreversibility. For the same composition of the phases  $K_{distr}$  of zirconium is much greater if the zirconium was initially in the organic phase (reextraction) than in the case where it was initially added to the aqueous phase (extraction).

These phenomena could be explained by hydrolysis on the basis of the fact that the zirconium forms a stable hydrolytic complex in weakly acid solutions [10-12]. The hydrolysis if accompanied by polymerization and the reverse process of depolymerization of zirconium, like plutonium [14], proceeds slowly and with difficulty. Hydrolysis undoubtedly affects the extraction of zirconium and is very important for low acidities; however, the "irreversibility" is also observed at high  $HNO_3$  concentrations, when the hydrolysis can be neglected. There is more likely to be a strong chemical reaction between the TBP and the extracted zirconium, leading to the formation of stable complexes of zirconium with the decomposition product of TBP—dibutylphosphoric acid. This chemical reaction proceeds at a measurable rate and  $K_{distr}$  during reextraction therefore has unstable values, increasing at each of the subsequent stages of reextraction. The reaction of zirconium with the decomposition products of TBP is also shown by the increase in  $K_{distr}$  with time when an insufficiently purified solvent is used [2].

Niobium is hydrolyzed to a still greater extent than zirconium [15-17]. Equilibrium between various products of hydrolysis and the ionic forms of niobium is sometimes established extremely slowly. Hydrolysis causes a slow reduction in  $K_{distr}$ , lasting many hours and days. In solutions of niobium the unextracted hydrolytic polymers and also colloidal (or pseudocolloidal) forms exist at comparatively high acid concentrations [18]. This is due to the change in  $K_{distr}$  during repeated extractions from the same aqueous solution: after each extraction the fraction of hydrolytic complexes in the solution increases and  $K_{distr}$  decreases. With increase in the  $HNO_3$  concentration the value of  $K_{distr}$  for niobium does not pass through a maximum.

Since the extracted form of ruthenium contains, in addition to the nitrate ion, the nitroso group NO [19, 20], for the formation of a nitrosyl-ruthenium ion  $RuNO^{3+}$  we must evidently have lower oxides of nitrogen or compounds which readily liberate them, for example, nitrous acid. In fact, in the presence of nitrites  $K_{distr}$  for ruthenium increases sharply. However, nitrite ions also have a negative effect on the extraction: with increase in their concentration there is an increase in the fraction of unextracted nitrite complexes of the type  $RuNO(NO_2)_3$  [20-24].  $K_{distr}$  of ruthenium therefore increases at first with increase in the nitrite ion concentration, passes through a maximum and then again decreases.

Among the nitrate complexes formed by nitrosyl ruthenium, the greatest extractability is shown by the saturated neutral complex  $RuNO(NO_3)_3$  [19, 25] the fraction of which naturally increases with the  $HNO_3$  concentration [19-20] and the  $NO_3^-$  ions in general. This explains the increase in extraction of ruthenium with increase in the  $NaNO_3$  concentration.

The extraction of ruthenium is very sensitive to the acidity of the solution. During extraction from  $HNO_3$  solutions of varying concentration  $K_{distr}$  for ruthenium passes through a fairly sharp maximum (see Fig. 6).

From data on the study of extraction it also follows that at low acidity, corresponding to the greatest extraction of ruthenium, the latter is in solution in several chemical forms, equilibrium between which is established

slowly. Similar conclusions are drawn by other investigators [19, 25]. During repeated extraction from the same solution  $K_{\text{distr}}$  for ruthenium continually decreases after short intervals of time (see Table 5) since after each extraction there is a reduction in the content of the most readily extracted forms. The readily extracted form is  $\text{RuNO}(\text{NO}_3)_3$ , and the difficultly extracted forms are the lower nitrate complexes [19, 20] and different stages of hydrolysis of nitrosyl ruthenium and its nitrate complexes [19, 26].

Accordingly, with increase in the acid concentration differences in  $K_{\text{distr}}$  during primary and secondary extractions decrease and finally disappear altogether (see Fig. 7).

In the organic phase ruthenium is also found in various forms with differing stabilities in combination with TBP. During successive reextractions from the organic phase, after short intervals of time the values of  $K_{\text{distr}}$  therefore gradually increase, even when an ammonium-carbonate solution is used.

The extracted complex of ruthenium  $\text{RuNO}(\text{NO}_3)_3$  in the organic phase gradually changes to other compounds which are more firmly combined with the solvent. As in the extraction of zirconium and niobium, we can assume slow extensive reaction of ruthenium with TBP or its decomposition products. This is confirmed by the fact that  $K_{\text{distr}}$  of ruthenium during extraction increases with increase in the content of TBP hydrolysis products in the organic phase.

The results given here for the separation of radioactive zirconium, niobium, and ruthenium from solutions remaining after the separation of a calcium oxalate precipitate indicate that the complex method [1] which we have developed can be used to obtain radiochemically pure preparations of these fission products.

The concentration of zirconium and niobium on a hydroxide precipitate is not an unusual operation. Less usual is the concentrating of ruthenium on sulfides. This method enables ruthenium to be more completely separated from solution. The absorption of radioactive ruthenium by sulfides of metals was also described in [27, 28].

#### LITERATURE CITED

1. N. E. Brezhneva, V. I. Levin, G. V. Korpusov, et al., In: Transactions of the Second International Conference on the Peaceful Uses of Atomic Energy. Report of Soviet Scientists. Vol. 4, Moscow, Atomizdat, p. 57 (1959).
2. K. Alcock, et al., *J. Inorg. and Nucl. Chem.*, **4**, 100 (1957).
3. D. Peppard, et al., *J. Inorg. and Nucl. Chem.*, **3**, 215 (1956).
4. E. Murbach and W. Mc Vey, *Nucl. Sci. Abstr.*, **10**, 18A, 904 (1956).
5. G. F. Egorov, V. V. Fomin, Yu. G. Frolov, and G. A. Yagodin, *Zh. neorganich. khim.*, **5**, 1044 (1960).
6. A. S. Solovkin, *Zh. neorganich. khim.*, **2**, 611 (1957).
7. V. I. Paramonova and A. N. Sergeev, *Zh. neorganich. khim.*, **3**, 215 (1958).
8. N. M. Adamskii, S. M. Karpacheva, I. N. Mel'nikov, and A. M. Rozen, *Radiokhimiya*, **2**, 400 (1960).
9. Z. N. Tsvetkova, A. S. Solovkin, N. S. Povitskii, and I. N. Davydov, *Zh. neorganich. khim.*, **6**, 489 (1961).
10. R. Connick and W. Reas, *J. Amer. Chem. Soc.*, **73**, 1171 (1951).
11. K. Kraus and J. Johnson, *J. Amer. Chem. Soc.*, **75**, 5769 (1953); **78**, 3937 (1956).
12. V. I. Paramonova and A. S. Voevodskii, *Zh. neorganich. khim.*, **1**, 1905 (1956).
13. I. E. Starik, I. A. Skul'skii, and A. I. Yurtov, *Radiokhimiya*, **1**, 66 (1959).
14. A. Brunstad, *Industr. and Engng. Chem.*, **51**, 38 (1959).
15. J. Kanzelmeyer and J. Ryen, *J. Amer. Chem. Soc.*, **78**, 3020 (1956).
16. V. I. Paramonova, et al., *Zh. neorganich. khim.*, **3**, 212 (1958).
17. I. E. Starik and I. A. Skul'skii, *Radiokhimiya*, **1**, 77 (1959).
18. V. I. Paramonova and V. B. Kolychev, *Zh. neorganich. khim.*, **1**, 1896 (1956).
19. J. Fletcher, *Progr. Nucl. Energy, Ser. III, Process Chem.*, **1**, London, p. 105 (1956).
20. A. Wain, P. Brown, and J. Fletcher, *Chem. Ind.*, No. 1, 18 (1957).
21. O. E. Zvyagintsev and S. M. Starostin, *Zh. neorganich. khim.*, **2**, 1281 (1957).
22. J. Fletcher, *J. Inorg. and Nucl. Chem.*, **1**, 378 (1955).
23. J. Fletcher, *J. Inorg. and Nucl. Chem.*, **8**, 287 (1958).
24. F. Martin, et al., *J. Chem. Soc.*, **76** (1959).
25. V. D. Nikol'skii and V. S. Shmidt, *Zh. neorganich. khim.*, **2**, 2746 (1957); **3**, 2967 (1958).
26. I. Jenkins and A. Wain, *J. Inorg. and Nucl. Chem.*, **3**, 28-37 (1956).
27. F. Martin and J. Miles, *Progr. Nucl. Energy, Ser. III, Process Chem.*, **1**, London, p. 369 (1956).
28. F. Martin and J. Miles, *AERE, C/R 2413* (1957).

THE EFFECT OF NEUTRON IRRADIATION ON THE STRUCTURE  
AND MECHANICAL PROPERTIES OF ALLOY STEELS

Sh. Sh. Ibragimov, I. M. Voronin, and A. S. Kruglov

Translated from Atomnaya Énergiya, Vol. 15, No. 1,

pp. 30-37, July, 1963

Original article submitted May 31, 1962

We have studied the effect of neutron irradiation at temperatures of 200-500°C with various integral doses ( $1.5 \cdot 10^{20}$ - $7 \cdot 10^{21}$  neutrons/cm<sup>2</sup>) on the properties and microstructure of some steels with different chemical compositions and initial structures. We have shown the effect of alloying by various elements on the sensitivity of the steel to irradiation and the temperature of annealing of radiation defects of hardening.

In recent years a number of papers have been published [1-6] on the effect of neutron irradiation on the mechanical properties of low- and complex-alloy steels. Nevertheless, the existing data are far from sufficient to explain the effect of alloying by elements and the initial structure of the steel on the change in its properties during irradiation. There is comparatively little information on the change in mechanical properties of steels during irradiation by high integral doses (above  $5 \cdot 10^{20}$  neutrons/cm<sup>2</sup>). To a certain extent the present work extends our ideas in this field.

Material and Irradiation

We studied iron and steel (2Kh2MS, 2Kh6MST, 1Kh12MS, 1Kh16MSB, 1Kh18N9T, and 1Kh18N14MSB), differing considerably from one another in their chemical composition and the phase-structural state.

TABLE 1. Mechanical Properties of Iron and Steel 1Kh16MSB

Material and its state	Irradiation temperatures, °C	Integral flux, neutrons/cm <sup>2</sup>		Strength, kg/mm <sup>2</sup>	Yield point during 0.2% deformation, kg/mm <sup>2</sup>	Relative elongation, %
		Total	Neutrons with E ≥ 1 MeV			
Iron, annealed at 760°C	—	0	0	35,0	29,5	38,5
	200—240	$1,1 \cdot 10^{20}$	$1,1 \cdot 10^{19}$	50,0	49,5	18,5
	200—240	$1,5 \cdot 10^{20}$	$1,5 \cdot 10^{19}$	52,0	51,5	15,5
	200—240	$1,9 \cdot 10^{20}$	$1,9 \cdot 10^{19}$	52,5	51,5	15,0
	200—240	$2,8 \cdot 10^{20}$	$2,8 \cdot 10^{19}$	53,5	52,5	16,0
1Kh16MSB steel, annealed at 900°C	—	0	0	63,0	44,0	26,0
	200—240	$1,5 \cdot 10^{20}$	$1,5 \cdot 10^{19}$	73,0	58,0	19,0
	200—240	$1,9 \cdot 10^{20}$	$1,9 \cdot 10^{19}$	74,0	60,0	12,0
	200—240	$2,8 \cdot 10^{20}$	$2,8 \cdot 10^{19}$	74,5	65,5	8,0
	200—240	$8 \cdot 10^{20}$	$8 \cdot 10^{19}$	75,0	66,0	8,0
	320—360	$1,2 \cdot 10^{21}$	$3,6 \cdot 10^{20}$	74,5	56,0	10,0
	450—500	$7 \cdot 10^{21}$	$2,1 \cdot 10^{21}$	65,5	50,0	24,0

1Kh16MSB steel has a ferrite structure with stable carbides; 2Kh2MS, 1Kh6MST, and 1Kh12MS steels are ferritic perlitic and the remainder are austenitic.

From bars of these materials we prepared small tensile specimens, with a diameter of 3 mm in the calculated part and a total length of 25 mm; the specimens were used for the tensile tests, metallographic analysis, and the de-

terminations of hardness. From steels of some grades specimens were prepared in the form of 2-mm diam wire to study the electric resistance.

All the specimens were annealed before irradiation in the reactor. Furthermore, to find the effect of the initial microstructure on the change in mechanical properties during irradiation specimens of steels of some grades were subjected to varying heat treatment. The heat-treated specimens in special stainless steel containers were loaded into the BR-5 reactor [7, 8]; they were irradiated in the active zone of the reactor and two vertical channels intended for investigation into materials. Irradiation in the active zone was carried out over a fairly "hard" energy spectrum of neutrons (mean neutron energy 0.38 MeV; neutrons with an energy  $\geq 1$  MeV comprised 30%) at temperatures of 320-500°C in the channels the irradiation was conducted in a relatively "soft" spectrum (mean neutron energy 36 keV; neutrons with an energy  $\geq 1$  MeV comprised 10%) at temperatures not exceeding 255°C.

TABLE 2. Mechanical Properties of Austenitic Steels and Nickel

Material	Irradiation temperature, °C	Integral flux, neutrons/cm <sup>2</sup>		Tensile strength, kg/mm <sup>2</sup>	Yield point during deformation by 0.2%, kg/mm <sup>2</sup>	Relative elongation, %
		Total	Neutrons with E $\geq 1$ MeV			
1Kh18N9T steel	—	0	0	58,5	18,0	68,5
	220—255	$3 \cdot 10^{19}$	$3 \cdot 10^{19}$	68,5	42,0	52,0
	220—255	$1 \cdot 10^{21}$	$1 \cdot 10^{20}$	68,0	41,5	51,0
	450—500	$1,7 \cdot 10^{21}$	$0,5 \cdot 10^{21}$	64,0	27,0	50,0
	450—500	$5,2 \cdot 10^{21}$	$1,6 \cdot 10^{21}$	70,0	33,0	58,0
1Kh18N14MSB steel	—	0	0	57,0	22,0	58,0
	220—255	$3 \cdot 10^{20}$	$3 \cdot 10^{19}$	62,0	28,0	50,0
	220—255	$1 \cdot 10^{21}$	$1 \cdot 10^{20}$	68,0	38,0	30,0
	450—500	$1,7 \cdot 10^{21}$	$0,5 \cdot 10^{21}$	61,5	24,5	47,0
	450—500	$5,2 \cdot 10^{21}$	$1,6 \cdot 10^{21}$	59,5	24,0	51,0
Nickel (mean grain size 0.3 mm)	—	0	0	49,0	13,5	47,0
	200—240	$1,1 \cdot 10^{20}$	$1,1 \cdot 10^{19}$	63,5	47,0	29,0
	200—240	$1,9 \cdot 10^{20}$	$1,9 \cdot 10^{19}$	68,5	57,5	26,0
	200—240	$2,8 \cdot 10^{20}$	$2,8 \cdot 10^{19}$	70,5	61,0	24,0

Irradiated and nonirradiated specimens were tested in tension at room temperature with a remote-controlled UMD-5 machine. Each experimental point represents a test of not less than four specimens. The hardness was determined with a diamond pyramid at a load of 10 kg on a Vickers instrument adapted for operation with  $\gamma$ -active specimens. The microstructure of nonirradiated specimens was studied with the MIM-8 microscope; that of irradiated specimens was studied with the remote-controlled MIM-14 metallographic microscope.

#### Results of Experiments and Their Discussion

Iron and 1Kh16MSB Steel. The metallographic investigation of nonirradiated and irradiated specimens showed that there were no noticeable changes in the microstructure of iron and steel. The ferrite grain size in both materials is about the same (mean diameter  $\sim 0.04$  mm). The mechanical properties of the iron and steel are given in Table 1. The data show that neutron irradiation at temperatures of 200-240 and 320-360°C considerably increases the strength and yield point, and reduces the relative elongation of iron and 1Kh16MSB steel. The absolute value of the change in properties depends on the temperature and integral irradiation dose. During irradiation at temperatures of 200-240°C and below [5, 9] an intensive change in the mechanical properties of iron is observed for doses below  $1,1 \cdot 10^{20}$  and of steel at doses up to  $2,8 \cdot 10^{20}$  neutrons/cm<sup>2</sup> (except for the tensile strength—less sensitive to radiation defects of the characteristics). Further changes in the properties are slight; consequently, at doses of about  $1 \cdot 10^{20}$  neutrons/cm<sup>2</sup> for iron and  $3 \cdot 10^{20}$  neutrons/cm<sup>2</sup> for 1Kh16MSB steel there is almost saturation. We notice that the maximum in-



crease in the yield point for both materials for corresponding saturation doses has the same values (22.0-23.0 kg/mm<sup>2</sup>). Such a change in the mechanical properties for iron and steel during neutron irradiation is connected with the formation of radiation defects of hardening in the material. In the investigated steel these defects are completely annealed at temperatures below 500°C [9]. The irradiation of 1Kh16MSB steel at 450-500°C, despite the high integral dose ( $7 \cdot 10^{21}$  neutrons/cm<sup>2</sup>) did not lead to a noticeable change in the mechanical properties.

TABLE 3. Mechanical Properties of 2Kh2MS Steel

Heat treatment	Irradiation temperature, °C	Integral flux neutrons/cm <sup>2</sup>		Tensile strength, kg/mm <sup>2</sup>	Yield point, kg/mm <sup>2</sup>	Relative elongation, %	Hardness, kg/mm <sup>2</sup>
		Total	Neutrons with E ≥ 1 MeV				
Annealing at 1100°C and stepwise cooling	—	0	0	95,0	71,0	16,5	275
	200—240	$8 \cdot 10^{20}$	$8 \cdot 10^{19}$	96,0	86,0	18,0	314
	320—360	$1,2 \cdot 10^{21}$	$3,6 \cdot 10^{20}$	94,5	—	5,2	297
	450—500	$7 \cdot 10^{21}$	$2,1 \cdot 10^{21}$	76,0	67,0	1,0	287
The same, soaking at 400°C for 16 days	—	0	0	91,0	65,0	18,5	270
Quenching from 1050°C in oil and tempering at 650°C for 3 h	—	0	0	121,0	102,0	11,0	370
	200—240	$8 \cdot 10^{20}$	$8 \cdot 10^{19}$	126,5	114,5	8,5	402
	320—360	$1,2 \cdot 10^{21}$	$3,6 \cdot 10^{20}$	135,0	124,0	3,5	446
	450—500	$7 \cdot 10^{21}$	$2,1 \cdot 10^{21}$	120,0	103,0	6,5	392

TABLE 4. Mechanical Properties of 2Kh6MST Steel

Heat treatment	Irradiation temperature, °C	Integral flux, neutrons/cm <sup>2</sup>		Tensile strength, kg/mm <sup>2</sup>	Yield point, kg/mm <sup>2</sup>	Relative elongation, %	Hardness, kg/mm <sup>2</sup>
		Total	Neutrons with E ≥ 1 MeV				
Annealing at 900°C	—	0	0	80,0	52,0	26,5	202
	200—240	$8 \cdot 10^{20}$	$8 \cdot 10^{19}$	82,0	58,0	24,0	254
	320—360	$1,2 \cdot 10^{21}$	$3,6 \cdot 10^{20}$	86,5	60,5	22,5	249
	450—500	$7 \cdot 10^{21}$	$2,1 \cdot 10^{21}$	72,5	46,0	23,0	—
The same, soaking at 400°C for 16 days	—	0	0	71,5	38,5	25,0	203
Quenching from 1000°C in oil and tempering at 650°C for 3 h	—	0	0	96,5	78,5	19,5	284
	200—240	$8 \cdot 10^{20}$	$8 \cdot 10^{19}$	98,5	86,0	19,0	325
	320—360	$1,2 \cdot 10^{21}$	$3,6 \cdot 10^{20}$	101,0	—	15,5	322
	450—500	$7 \cdot 10^{21}$	$2,1 \cdot 10^{21}$	91,5	76,0	18,0	290
The same, soaking at 400°C for 16 days	—	0	0	92,5	71,5	20,0	282

Austenitic Steels and Nickel. Before being loaded into the reactor austenitic steel specimens were quenched in water from 1100°C, and nickel specimens were annealed at 650°C for one hour. A microstructural investigation of nonirradiated specimens showed that the austenitic grain size of the investigated steels was approximately the same

(mean grain diameter  $\sim 0.1$  mm). After irradiation no changes were observed in the microstructure of the steels, only the etchability of the grain changed. It is a characteristic fact that after irradiation twins in the austenitic grains are either not revealed at all or are revealed as traces of boundaries of twin formation which have lost their initial linearity.

TABLE 5. Mechanical Properties of 1Kh12MS Steel

Heat treatment	Irradiation temperature, °C	Integral flux, neutrons/cm <sup>2</sup>		Tensile strength, kg/mm <sup>2</sup>	Yield point, kg/mm <sup>2</sup>	Relative elongation, %	Hardness, kg/mm <sup>2</sup>
		Total	Neutrons with E $\geq 1$ MeV				
Annealing at 900°C	—	0	0	64,5	44,5	29,5	195
	200—240	$2,8 \cdot 10^{20}$	$2,8 \cdot 10^{19}$	72,5	60,0	26,0	—
	200—240	$8 \cdot 10^{20}$	$8 \cdot 10^{19}$	70,5	59,0	27,0	248
	320—360	$1,2 \cdot 10^{21}$	$3,6 \cdot 10^{20}$	74,5	62,0	25,0	243
	450—500	$7 \cdot 10^{21}$	$2,1 \cdot 10^{21}$	80,0	62,5	16,0	254
The same, soaking at 400°C for 16 days	—	0	0	66,5	43,5	28,5	—
Quenching from 1000°C in oil and tempering at 650°C for 3 h	—	0	0	88,5	68,0	21,5	260
	200—240	$8 \cdot 10^{20}$	$8 \cdot 10^{19}$	93,0	82,5	19,0	312
	320—360	$1,2 \cdot 10^{21}$	$3,6 \cdot 10^{20}$	95,5	81,0	20,0	309
	450—500	$7 \cdot 10^{21}$	$2,1 \cdot 10^{21}$	—	81,0	16,0	—
	The same, soaking at 400°C for 16 days	—	0	0	88,5	67,0	21,0

The mechanical properties of austenitic steel and nickel before and after irradiation by various doses at temperatures of 200-500°C are given in Table 2. The data show that changes in the properties of investigated steels after neutron irradiation are determined by the integral dose and the irradiation temperature and, consequently, by the number of formed radiation defects in the material.

A certain regularity is observed in the effect of alloying elements on the sensitivity of steel to neutron irradiation. Complicating the steel composition by alloying with various elements, as in the case of alloying of iron, displaces the integral saturation flux toward a high irradiation dose. The strongest effect is therefore shown by elements such as silicon and molybdenum. Thus, due to irradiation at temperatures of 220-255°C with an integral dose of  $3 \cdot 10^{20}$  neutrons/cm<sup>2</sup> the tensile strength and the yield point 1Kh18N9T steel increase to 10 and 24 kg/mm<sup>2</sup>, and 1Kh18N14MSB steel which, in addition to chromium and nickel, contains  $\sim 1\%$  silicon and  $\sim 2\%$  molybdenum, only increase by 5 and 6 kg/mm<sup>2</sup>, respectively. At a dose of about  $3 \cdot 10^{20}$  neutrons/cm<sup>2</sup> there is almost saturation in the change in the mechanical properties of 1Kh18N9T steel and nickel.\*. For 1Kh18N14MSB steel at doses of  $3 \cdot 10^{20}$  -  $1 \cdot 10^{21}$  neutrons/cm<sup>2</sup> there is an intensive change in the properties and saturation evidently does not occur.

It is a well-known fact [4] that in austenitic steels irradiated at temperatures below 350°C radiation defects of hardening are annealed in the temperature range 430-650°C. During irradiation of 1Kh18N9T and 1Kh18N14MSB steels at 450-500°C some of the radiation defects are therefore annealed and the mechanical properties change somewhat less than in the case of irradiation at temperatures below 350°C (in both cases the integral flux exceeds the saturation dose).

\* When iron is alloyed with chromium and nickel the integral saturation flux is displaced toward a high dose and becomes the same as for nickel; this is apparently connected with the change in the crystal structure of the material as a result of alloying. Data on the change in mechanical properties of iron and nickel as a function of the irradiation dose show (see Tables 1 and 2) that, other conditions being equal, the integral saturation flux depends on the crystal structure of the material.

2Kh2MS, 2Kh6MST, and 1Kh12MS Steels. In contrast to 1Kh16MSB steel and austenitic steels these steels are sensitive to heat treatment; the changes in their properties during irradiation were therefore studied after two forms of preliminary heat treatment. We also found the effect of prolonged (16 days) soaking at 400°C on the structure and properties of these steels.

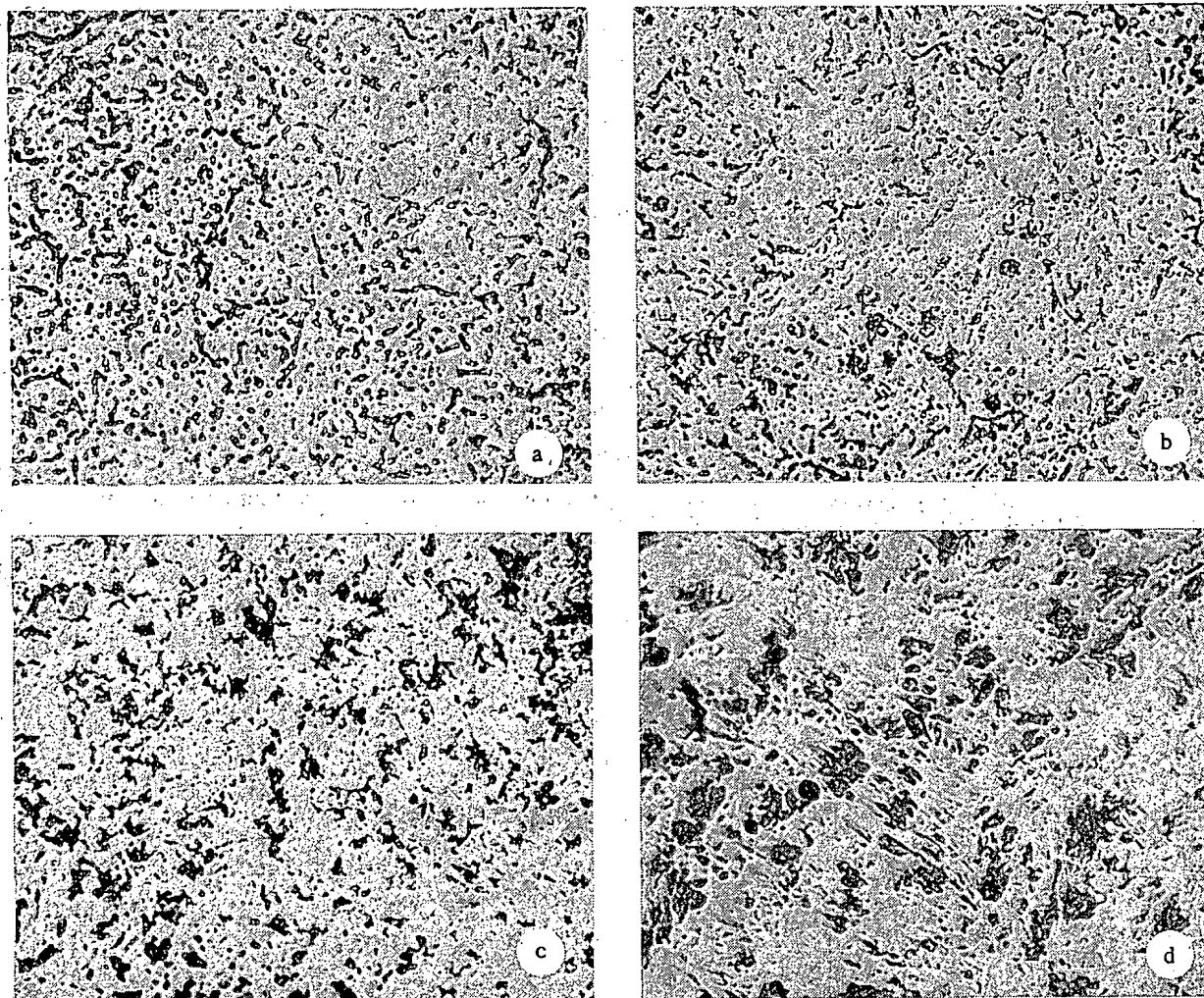


Fig. 1. Microstructure of annealed 2Kh2MS steel ( $\times 800$ ): a) before irradiation; b) after soaking at 400°C for 16 days; c) after irradiation at 320-360°C,  $nvt = 1.2 \cdot 10^{21}$  neutrons/cm<sup>2</sup>; d) after irradiation at 450-500°C,  $nvt = 7 \cdot 10^{21}$  neutrons/cm<sup>2</sup>.

The mechanical properties of these steels are given in Tables 3, 4, and 5; it can be seen that as a result of irradiation at 200-360°C there was an increase in the strength, yield point, and hardness, and a reduction in the relative elongation of the investigated steels. The absolute value of the change in these characteristics due to irradiation at 200-240°C (integral dose  $8 \cdot 10^{20}$  neutrons/cm<sup>2</sup>) was practically independent of the initial structure and properties. As a result of irradiation at 450-500°C the strength characteristics of 2Kh2MS and 2Kh6MST steels decreased somewhat and annealed 2Kh2MS steel almost completely lost its plasticity. Prolonged soaking at 400°C only appreciably affected the properties of 2Kh2MS and 2Kh6MST steels.

A metallographic study of nonirradiated and irradiated specimens showed that irradiation at temperatures of 320-360°C and above in a relatively hard energy spectrum of neutrons considerably affected the microstructure (redistribution, and also change in form and dimensions of the carbide phase) of 2Kh2MS and 2Kh6MST steels (Figs. 1 and 2). For 1Kh12MS steel a certain change in the structure is only observed under the electron microscope and only for the quenched-tempered state. In 2Kh2MS and 2Kh6MST steels changes in the microstructure were also observed

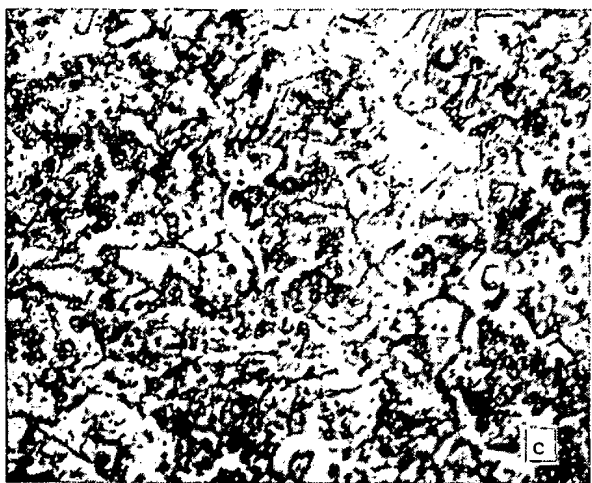
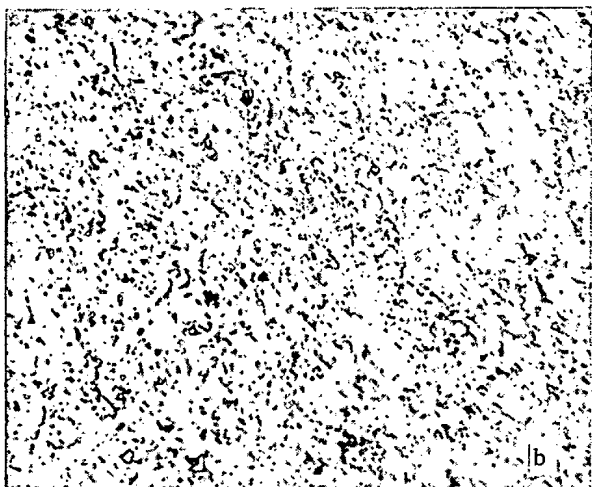
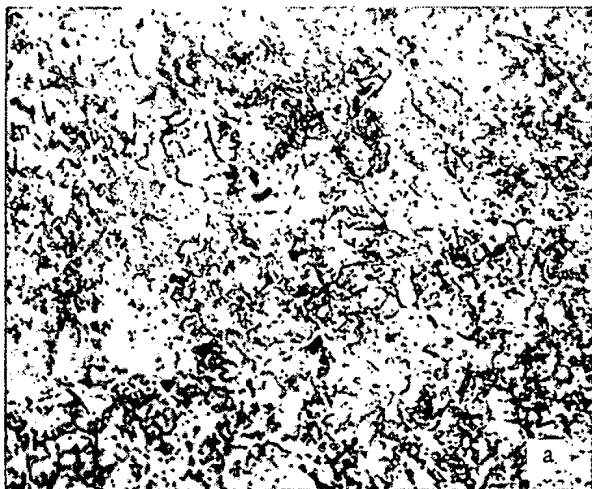


Fig. 2. Microstructure of annealed 2Kh6MST steel ( $\times 800$ ): a) before irradiation; b) after soaking at  $400^{\circ}\text{C}$  for 16 days; c) after irradiation at  $320\text{-}360^{\circ}\text{C}$ ,  $\text{nvt} = 1.2 \cdot 10^{21}$  neutrons/cm $^2$ .

after prolonged soaking at  $400^{\circ}\text{C}$ , but the form and character of these changes differ considerably from the changes in structure due to irradiation.

We can therefore state that a change in the mechanical properties of 2Kh2MS, 2Kh6MST, and 1Kh12MS steels during irradiation at  $200\text{-}240^{\circ}\text{C}$  is due to the formation of radiation defects of hardening; at  $320\text{-}360^{\circ}\text{C}$  and above the change is due to the formation of radiation defects and a change in the structural state of the steel during irradiation. These defects and changes in the microstructure do not have much effect on the electric resistance of the steel. For example, the electric resistance of annealed 2Kh2MS steel before irradiation was  $63.0 \mu \cdot \Omega \cdot \text{cm}$ , and after irradiation at  $320\text{-}360^{\circ}\text{C}$  by an integral dose of  $1.2 \cdot 10^{21}$  neutrons/cm $^2$  it was  $62.5 \mu \cdot \Omega \cdot \text{cm}$ . The radiation defects of hardening in specimens of 2Kh2MS, 2Kh6MST, and 1Kh12MS steels, irradiated at  $200\text{-}240^{\circ}\text{C}$ , are annealed in the same temperature range  $350\text{-}575^{\circ}\text{C}$  (Fig. 3); consequently, the temperature of annealing of the defects, as for austenitic steels [4], is independent of the extent of alloying. We can therefore draw the following conclusions:

1. Irradiation of austenitic steels at temperatures of  $200\text{-}500^{\circ}\text{C}$  by neutrons up to an integral dose of  $7 \cdot 10^{21}$  neutrons/cm $^2$  changes the mechanical properties, due to the formation of radiation defects of hardening.

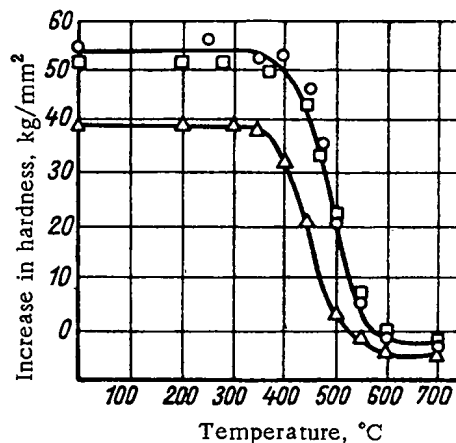


Fig. 3. Change in the increase in hardness of irradiated steel specimens versus annealing temperature:  $\Delta$ ) 2Kh2MS;  $\square$ ) 2Kh6MST;  $\circ$ ) 1Kh12MS.

2. A change in the mechanical characteristics of steels with a ferrite-perlitic structure (2Kh2MS, 2Kh6MST, and 1Kh12MS) during irradiation in a relatively hard energy spectrum of neutrons at temperatures of  $320\text{-}360^{\circ}\text{C}$  and above is due to the formation of radiation defects and a change in the microstructure of steel during irradiation.

3. Complicating the composition of the material by alloying with various elements leads to a displacement of the saturation dose toward high integral fluxes and has no noticeable effect on the annealing temperature of radiation defects of hardening.

LITERATURE CITED

1. L. Trudo, In: Transactions of the Second International Conference on the Peaceful Uses of Atomic Energy. Selected reports of non-Soviet scientists. Vol. 6, Moscow, Atomizdat, p. 427 (1959).
2. N. F. Pravdyuk, et al., In: Transactions of the Second International Conference on the Peaceful Uses of Atomic Energy. Reports of Soviet scientists, Vol. 3, Moscow, Atomizdat, p. 610 (1959).
3. J. Wilson. See [1], p. 391.
4. Sh. Sh. Ibragimov, V. S. Lyashenko, and A. I. Zav'yalov, Atomnaya énergiya, 8, 413 (1960).
5. D. Harries, Nucl. Power, 5, 97, 142 (1960).
6. I. M. Voronin, et al., Atomnaya énergiya, 8, 514 (1960).
7. A. I. Leipunskii, et al., See [2], Vol. 2, p. 215.
8. A. I. Leipunskii, et al., Atomnaya énergiya, 11, 498 (1961).
9. Sh. Sh. Ibragimov and V. S. Lyashenko, Fizika metallov i metallovedenie, 10, 84 (1960).

## THE CORROSIVE EFFECT OF FUEL ELEMENT SOLVENTS ON STRUCTURAL MATERIALS

M. M. Kurtenov and E. N. Mirolyubov

Translated from *Atomnaya Énergiya*, Vol. 15, No. 1,  
pp. 37-48, July, 1963

Original article submitted April 16, 1962

We examined the corrosion resistance of structural materials in boiling solutions of nitric, sulfuric, and hydrofluoric acid, and also nitric acid with additions of fluorides with application to the technological process of dissolution of fuel elements. The obtained data on the nature of the corrosive action of fuel element solvents on structural materials can be used to decide on materials and methods for protecting reactor dissolvers against corrosion.

The numerous technological schemes for the treatment of fuel elements involve very corrosive solutions.

Boiling solutions of nitric acid, nitric acid with small additions of fluorides, and also solutions of hydrofluoric and sulfuric acids, are used as solvents for the cans and cores of various types of fuel elements [1].

A knowledge of the nature of the corrosive effect of various fuel element solvents is a very important factor for a correct choice of structural materials for reactor-dissolvers. However, insufficient attention has been paid to this problem in published papers.

On the basis of a thorough investigation of corrosion processes in structural materials we have shown the extent of corrosive activity of fuel element solvents, the possibility of changing it under the operating conditions of the reactor solvent; we have also developed ideas on the mechanism of corrosion of structural materials in the above solutions.

### General Corrosion Characteristics of Metal Structural Materials

From the papers published in recent years [2-5] it follows that the corrosion of most metals and alloys in various solutions is characterized by a certain general dependence of the steady rate of solution on the potential (Fig. 1). On the diagram corresponding to this general dependence we can separate characteristic regions of potentials for each of which the dissolving of materials has its own features.

Corrosion in the region of the active state (I) is characterized by an increase in the rate of solution with increase in potential. In the region of partial passivation (II), on the other hand, there is a reduction in the rate of corrosion with increase in potential. In the region of the stable passive state (III) the corrosion rate has a minimum value and is independent of the potential; this is due to the chemical dissolution of the passive oxide film. In the region of superpassivation (IV) a new increase is observed in the corrosion rate, caused by oxidation of the protective passive film to higher, more readily soluble oxides. In the region of superpassivation the corrosion rate increases with the potential.

The potentials of passivation ( $\varphi_{\text{pass}}$ ), activation ( $\varphi_a$ ) and superpassivation ( $\varphi_{\text{super}}$ ) bounding these regions, and also the anodic polarizability in the active state ( $\tan \beta$ ) depend on the nature of the material, temperature, and hydrogen ion concentration in the solution.

It therefore follows that the corrosion behavior of structural materials under operating conditions (extent of corrosion, the character of its change with increase in potential and the mechanism of the process) should be determined by the region in which the stationary potential of the material will be located. The location of this potential in a corrosive medium in a given region of potentials depends on the nature of the oxidation-reduction equilibria in the solution, the concentration of the oxidizing agent and the overvoltage of its reduction on materials differing in composition.

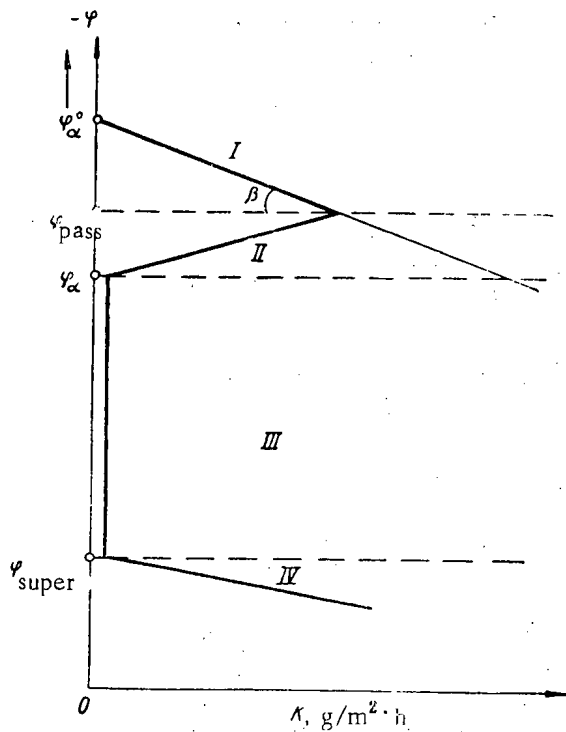


Fig. 1. Dependence of the corrosion rate  $K$  of structural materials on their potential in the regions: I) active state; II) partial passivation; III) stable passive state; IV) superpassivation.

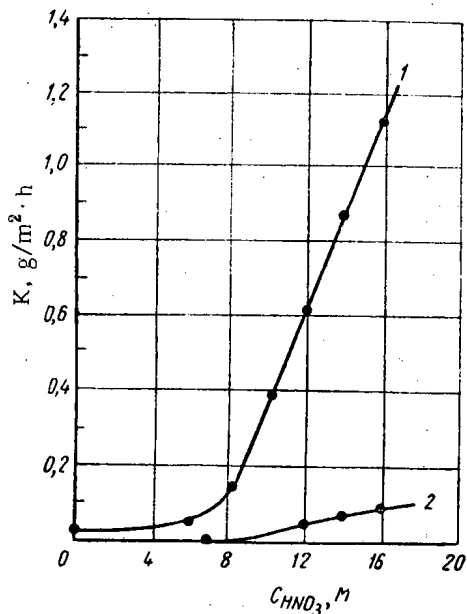


Fig. 2. Corrosion rate of 18-8 steel with titanium versus concentration of HNO<sub>3</sub> solutions and temperature: 1) boiling point; 2) 60°C.

### Solutions of Nitric Acid

Nitric acid solutions with concentrations up to 15.8 M are used to dissolve various types of fuel element [1, 6]. Extensive use is made of 18-8 chrome-nickel steels as structural materials when nitric acid solutions are used. In HNO<sub>3</sub> solutions with concentrations up to 16 M the corrosion rate of this steel at temperatures up to 100°C does not exceed 0.2 g/m<sup>2</sup>·h [7], since the stationary potential of corrosion of the steels corresponds to the region of the passive state. However, at the boiling point the corrosive effect of the HNO<sub>3</sub> solutions increases considerably and at acid concentrations above 6-8 M the corrosion rate of the steels increases sharply (Fig. 2). At these concentrations the oxidation-reduction potential of the medium exceeds the potential of breakdown of the passive state in the region of positive values ( $\varphi_{\text{redox}} > \varphi_{\text{super}}$ ) and according to the mechanism of superpassivation corrosion becomes thermodynamically possible. When the potential of steel in a 14-M solution of HNO<sub>3</sub> is displaced from the stationary state to the region of negative values the corrosion rate decreases (Fig. 3); this is characteristic for corrosion according to the superpassivation mechanism.

An analysis of numerous literature data on the corrosion of 18-8 stainless steels in boiling concentrated solutions of HNO<sub>3</sub> (mainly 10-14 M) [7-12] and the results of experiments carried out leads to the conclusion that corrosion under these conditions proceeds with preferential control\* due to the retarding effect of the reduction of HNO<sub>3</sub> to nitrous acid and N<sub>2</sub>O<sub>4</sub>. Bearing in mind that the reduction of HNO<sub>3</sub> to nitrous acid and N<sub>2</sub>O<sub>4</sub> is autocatalyzed by nitrous acid [13, 14] and, consequently, by oxides of nitrogen which are present with the HNO<sub>2</sub> in rapidly establishing equilibrium, we can understand the reasons for the strong increase in the corrosion rate of steels in concentrated HNO<sub>3</sub> solutions when the acid is saturated with oxides of nitrogen [10], the accumulation in it of products of the corrosion of steel (Fe<sup>3+</sup>, Cr<sup>6+</sup>, etc.) [8, 9], which can be reduced cathodically, and then be oxidized by HNO<sub>3</sub> with the formation of oxides of nitrogen. The acceleration of the corrosion of steels in these cases is due to the retardation of the cathodic reduction of HNO<sub>3</sub>, as in the case when the steels are in contact with metals having a low overvoltage of HNO<sub>3</sub> reduction (contact with platinum in 12 M HNO<sub>3</sub> during boiling intensifies the corrosion of 1Kh18N9T steel by a factor of 50). These facts are clear from the corrosion diagram shown in Fig. 4. Such diagrams are used extensively in work on corrosion [15, 16].

It can be seen from the diagram that when the cathodic process is facilitated due to the accumulation of corrosion products in the solution or the presence of oxides of nitrogen in the acid, and also due to contact with

\* Near the stationary potential the cathodic polarizability is much higher than the anodic polarizability.

platinum, the corrosion potential is displaced toward positive values and the corrosion rate increases. With hindering of the cathodic process, for example when oxides of nitrogen are removed from the acid the potential is reduced and the corrosion rate falls.

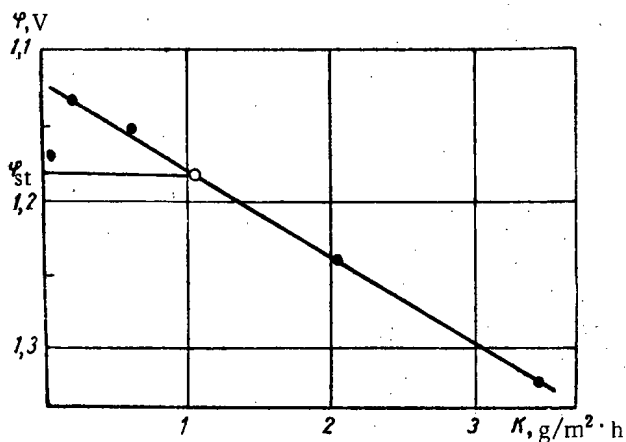


Fig. 3. Corrosion rate of 18-8 steel with titanium in a boiling 14-M  $\text{HNO}_3$  solution versus potential.

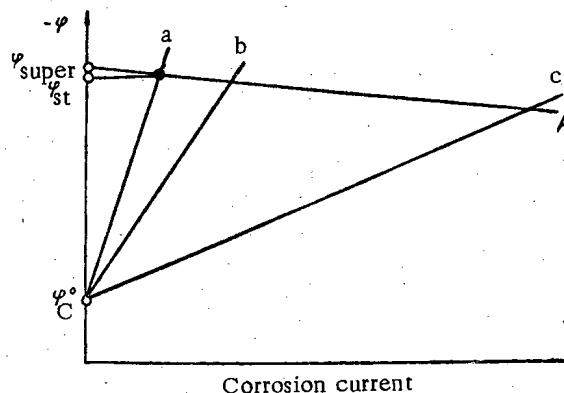


Fig. 4. Corrosion diagram for 18-8 steels in boiling concentrated solutions of  $\text{HNO}_3$ :  $\varphi_{\text{super}}^A$  is the anodic curve. The position of the cathodic curves in the case:  $\varphi_{\text{C}}^0$  a) absence of oxides of nitrogen in the solution;  $\varphi_{\text{C}}^0$  b) presence of corrosion products in the solution;  $\varphi_{\text{C}}^0$  c) contact with platinum.

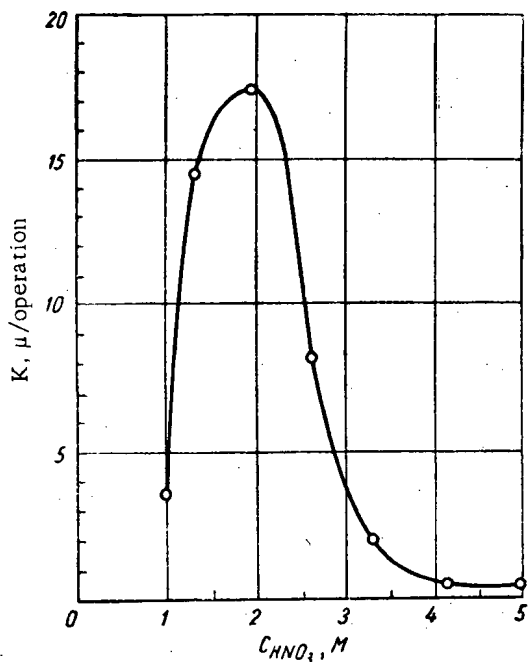


Fig. 5. Corrosion rate of 18-8 steel with titanium making contact with aluminum during dissolution in boiling  $\text{HNO}_3$  solutions in the presence of 0.05% mercuric nitrate.

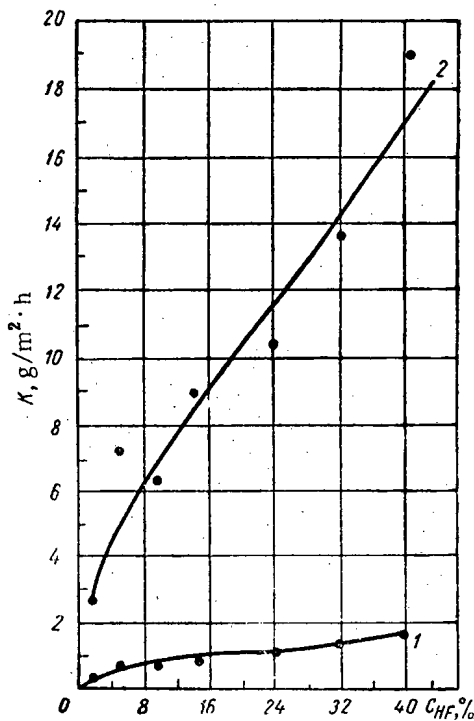


Fig. 6. Corrosion rate of monel metal versus  $\text{HF}$  concentration at  $90^\circ\text{C}$ : 1) in the solution; 2) over the solution.



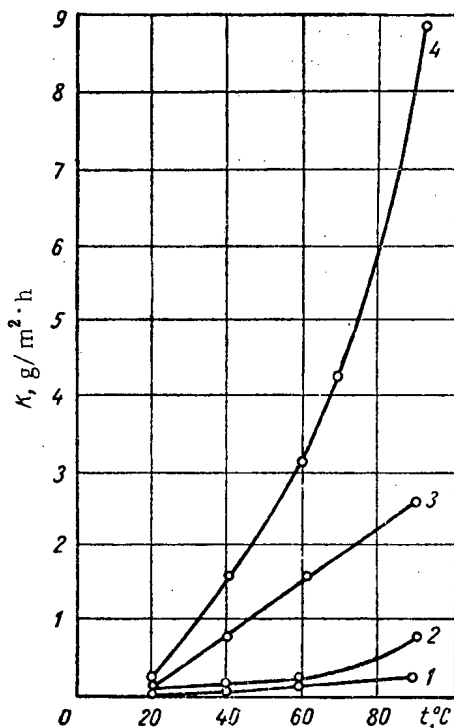


Fig. 7. Corrosion rate of monel metal in HF solutions versus temperatures: 1, 2) inside solution; 3, 4) over solution; 1, 3) 1.6% HF; 2, 4) 14.4% HF.

TABLE 1. Effect of Composition of the Gaseous Medium on the Corrosion Rate of Monel Metal in Boiling 20% HF

Composition of medium	Corrosion rate, g/m <sup>2</sup> ·h	
	Inside solution	Over solution
Air	0.96	15.05
Oxygen	2.86	27.4
Argon	0.05	0.09

ities are observed in the corrosion of copper. A metallographic analysis of monel metal specimens in contact with acid for various intervals of time (Fig. 8) shows that on the surface of the specimens narrow cracks are initially formed; these become wider with time and merge into one another, leading to continuous uneven corrosion of the monel metal.

The corrosion rate of monel metal, like that of copper in HF solutions, depends strongly on the composition of the gaseous medium over the solution (Table 1).

The gas which was passed over the solution was preheated to maintain isothermal conditions in the experiments. The results given in Table 1 and also the increased corrosion rate over the solution, where the oxygen of the air has more easy access to the metal surface than inside the solution, indicate that the corrosion of monel metal in HF solutions proceeds with oxygen depolarization with preferential cathodic control. The process of corrosion over the solution, which develops in the film (more precisely under the drops of condensed water and acid vapors) proceeds at a higher rate than inside the solution; this is caused by the removal of cathodic control due to better

It should be borne in mind that during contacting with fuel elements which are being dissolved in boiling concentrated solutions of HNO<sub>3</sub> under the conditions of the reactor-dissolvers stainless steels should be corroded at lower rates than in the absence of contact with the dissolving metals. There is no doubt that this retardation of the corrosion rate will be observed only if the potential of dissolution of the fuel element in a given solution is more negative than the potential of stainless steel, since only in this case can there be cathodic protection of the steel. However, cathodic polarization of stainless steel due to the contacting with electronegative metals dissolving in HNO<sub>3</sub>, for example aluminum, can also lead to a considerable increase in the corrosion rate of the steel. Figure 5 gives data on the corrosion of 18-8 steel with titanium in the boiling HNO<sub>3</sub> solutions with additions of mercuric nitrate in the case where this steel is in contact with dissolving aluminum. For 1 g of aluminum there was 10 g of acid; the ratio of the aluminum and steel surfaces was 6:1. It follows from Fig. 5 that in 2-M acid the corrosion rate of steel reaches 17 μ during the dissolution operation, which lasts about one hour. The high rate of corrosion is due to displacement of the potential of steel (due to contact with aluminum dissolving at a negative potential, equal to -0.8 V) in a region characterized by dissolution from the active state. An effect similar to cathodic polarization—the breakdown of the passive state of stainless steels in HNO<sub>3</sub> solutions during contact with electronegative metals was detected and studied in detail in [17-20].

#### Hydrofluoric Acid Solutions\*

Hydrofluoric acid solutions are used to dissolve fuel elements of zirconium alloys with a small content of uranium [1]. On the basis of a study of the corrosion stability of various metals and alloys in HF solutions many investigators have chosen monel metal as being the most stable structural material [1, 21-23]. However, the literature contains no information on the mechanism of corrosion of monel metal in HF solutions.

Experiments show that the corrosion rate of monel metal in an HF solution is an order lower than that over the solution (Fig. 6). With increase in the acid concentration and temperature the corrosion rate in the solution and over the solution increases (Fig. 7) but simultaneously remains constant with time. Similar regular-

\* N. N. Bardizh performed the experimental part.

TABLE 2. Corrosion Rate of Monel Metal and Copper ( $\text{g}/\text{m}^2 \cdot \text{h}$ ) in 20% HF Inside the Solution as a Function of the Presence or Absence of Contact with Semi-immersed Specimens

Temp., °C	Monel metal			Copper		
	Without contact (B)	With contact (A)	A/B	Without contact (B)	With contact (A)	A/B
20	0,24	0,31	1,3	—	—	—
40	0,65	1,0	1,5	0,38	0,85	1,5
90	0,82	3,43	4,2	1,5	4,5	3,0

TABLE 3. Stationary Potentials of Corrosion and Rate of Corrosion of Copper in 20% HF Solution. Duration of Experiments 2 h

Atmosphere over solution		Temp., °C		
		20	40	80
Air	$\varphi$ , V	0,23	0,27	0,29
	K, $\text{g}/\text{m}^2 \cdot \text{h}$	0,17	0,34	1,02
Oxygen	$\varphi$ , V	0,27	0,29	0,36
	K, $\text{g}/\text{m}^2 \cdot \text{h}$	0,25	0,83	4,7

aeration of the corroding surface. If the cathodic ionization of oxygen on metal situated above the solution proceeds with a small overvoltage than that inside the solution, i.e., if the metal over the solution is a more effective cathode, then the contacting of the specimen located inside the solution with another semiimmersed specimen should evidently lead to an increase in the corrosion rate of the first specimen; this is confirmed experimentally (Table 2).

Electrochemical measurements show that with increase in temperature and concentration of oxygen in the vapor phase the potential of monel metal and copper is displaced to the region of more positive values. For copper, this follows from the data given in Table 3.

Experiments show that the increase in the corrosion rate of monel metal and copper in hydrofluoric acid solutions with increase in temperature of the solution, acid concentration and oxygen content in the gaseous phase is accompanied by a reduction in the cathodic polarizability of the electrodes.

Experimental data on the corrosive effect of HF solutions with respect to monel metal and copper can therefore be represented in a generalized form by means of a real corrosion diagram, shown in Fig. 9.

The formation of cracks during the corrosion of monel metal is evidently the result of the preferential development of the corrosion process at the sites of local

stress concentration. The annealing of monel metals, relieving local stresses, completely prevents the formation of cracks and the corrosion process develops more uniformly. The previously observed continuous uneven character of corrosion of monel metal and copper in HF solutions is typical for processes of corrosion with oxygen depolarization and with preferential cathodic control [24].

#### HNO<sub>3</sub> Solutions with Additions of Fluorides\*

Concentrated HNO<sub>3</sub> solutions with small additions of fluorides are frequently used to dissolve various types of fuel elements, for example, those containing plutonium, thorium, zirconium, and aluminum. Published papers on the corrosion of structural materials in these solutions did not examine the nature of their high corrosion activity [1, 25].

A study of the corrosion activity of such solutions over a wide range of HNO<sub>3</sub> concentrations and additions of ammonium fluoride up to 0.1 M showed that additions of HF, NaF, KF, etc., affect the corrosion rate of stainless steels in HNO<sub>3</sub> solutions in the same way as ammonium fluoride.

Figures 10 and 11 show the corrosion rates of 18-8 steel with titanium for various temperatures as a function of the ammonium fluoride content in the HNO<sub>3</sub> solutions. Small additions of fluoride causes a sharp increase in the corrosion rate of stainless steel in HNO<sub>3</sub> solutions. In relatively concentrated solutions (above 11 M) containing additions of ammonium fluoride up to 0.1 M, with increase in the fluoride content the corrosion rate changes, passing through a maximum; with increase in the acid concentration and temperature this maximum in the corrosion rate is displaced toward low fluoride contents. The corrosion rate remains constant with time. The corrosion has a continuous uniform character.

The addition of sodium nitrate to concentrated solutions of HNO<sub>3</sub> (>10-11 M) in the presence of fluoride reduces the corrosion rate of stainless steel (Fig. 12). With increase in the HNO<sub>3</sub> concentration, with a constant fluor-

\* N. N. Bardizh and L. M. Zhuk performed the experimental part.

ide content in the solution, the corrosion rate of stainless steels changes, also passing through a maximum (Fig. 13). With increase in the temperature and fluoride content the corrosion rate maximum is displaced to the region of more dilute  $\text{HNO}_3$  solutions.

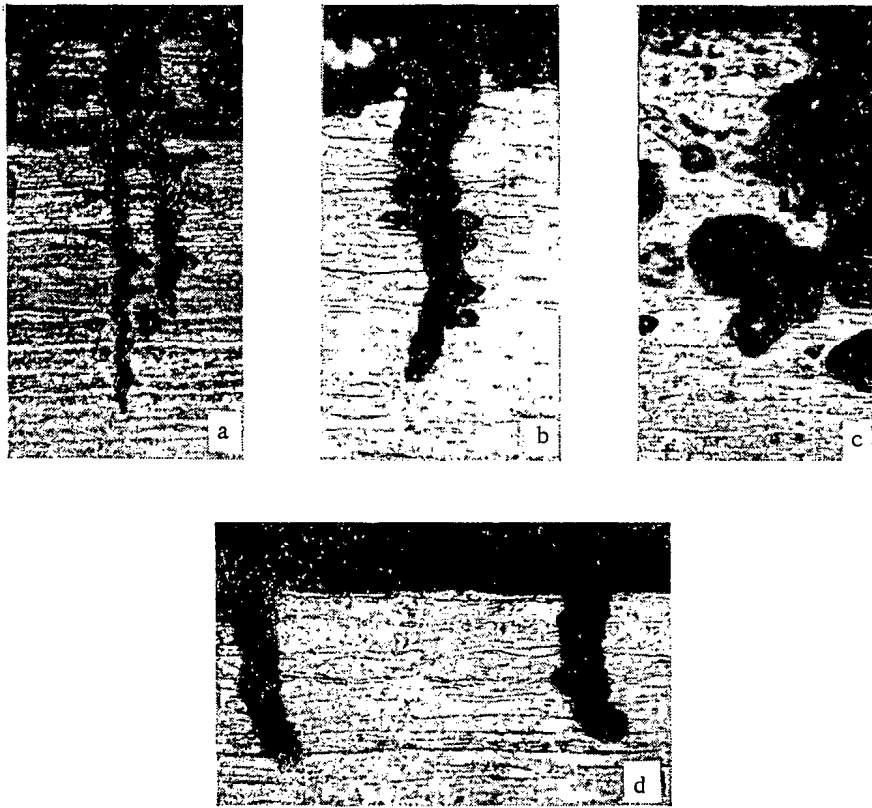


Fig. 8. The character of the corrosion breakdown of monel metal in 5% HF at 90°C with time. Over solution: a) 52 h; b) 112 h; c) 372 h. In solution: d) 372 h.

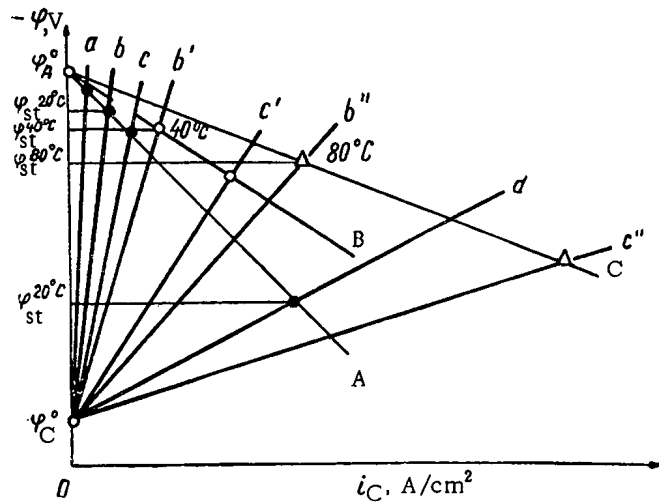


Fig. 9. Corrosion diagram for monel metal in HF solutions. Position of anodic curves for temperatures:  $\phi_A^A$ ) 20°C;  $\phi_A^B$ ) 40°C;  $\phi_A^C$ ) 80°C. Position of cathodic curves for atmospheres: 1) air:  $\phi_C^b$ ) 20°C;  $\phi_C^{b'}$ ) 40°C;  $\phi_C^{b''}$ ) 80°C;  $\phi_C^d$ ) vapor phase; 2) oxygen:  $\phi_C^c$ ) 20°C;  $\phi_C^{c'}$ ) 40°C;  $\phi_C^{c''}$ ) 80°C; 3) nitrogen:  $\phi_C^a$ ) 20°C.

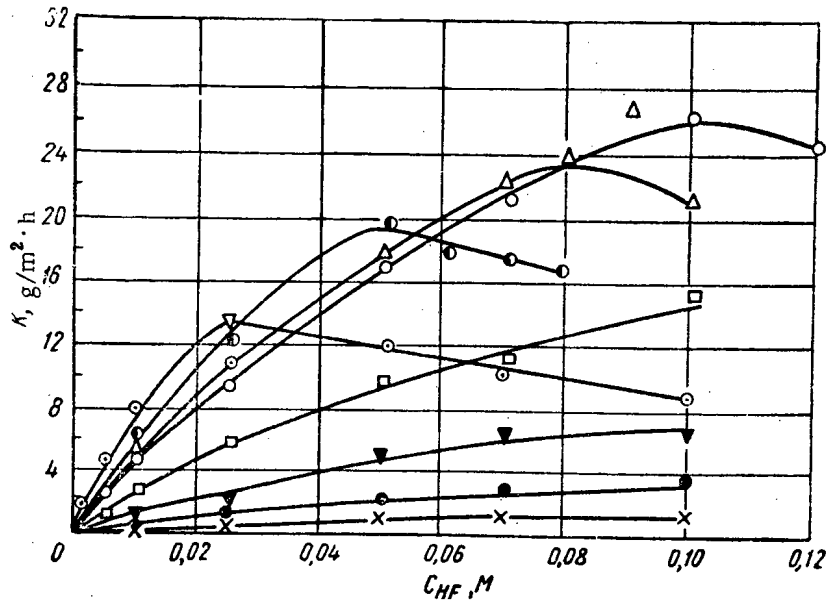


Fig. 10. Effect of ammonium fluoride additions on the corrosion rate of 18-8 steel with titanium in boiling solutions of  $\text{HNO}_3$ : x) 2 M; ●) 4 M; ▼) 6 M; □) 8 M; ○) 11 M; △) 12 M; ◐) 12.5 M; ◑) 14 M.

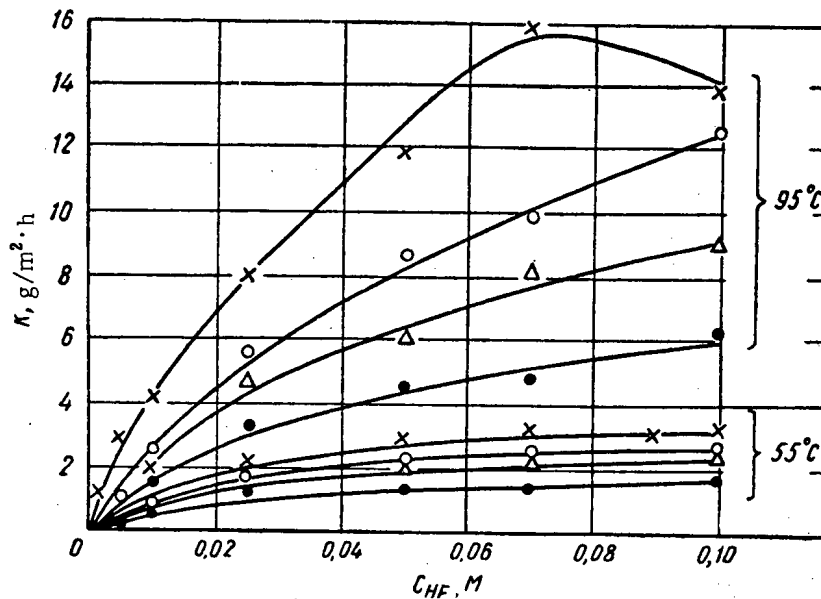


Fig. 11. Effect of ammonium fluoride additions on the corrosion rate of 18-8 steel with titanium in  $\text{HNO}_3$  solutions at 95 and 55°C: ●) 6 M; △) 8 M; ○) 12 M; x) 14 M.

From the results given in Figs. 10-13, it follows that the corrosion rate of stainless steel in  $\text{HNO}_3$  solutions with fluoride additions depends on the hydrogen ion concentration. When the acid concentration is increased above 11 M (see Fig. 10) and, consequently, there is a reduction in the content of hydrogen ions in solution [26], the position of the corrosion rate maximum of steel is displaced toward lower concentrations of fluoride. The addition of nitrate ions to the  $\text{HNO}_3$  solutions reduces the hydrogen ion concentration and the corrosion of steel (see Fig. 12). With increase in temperature, a reduction in the hydrogen ion concentration in  $\text{HNO}_3$  solutions displaces the corrosion rate maximum (see Fig. 13) toward lower  $\text{HNO}_3$  concentrations.

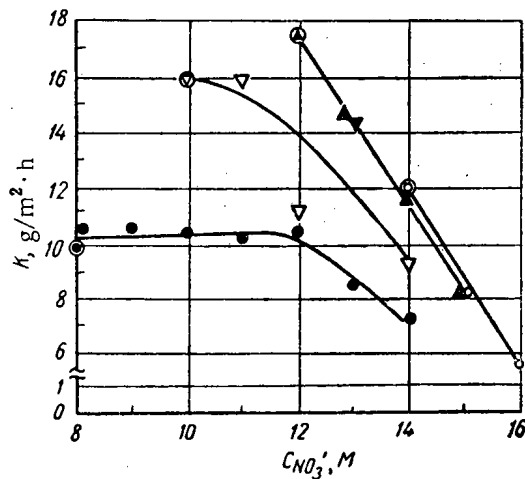


Fig. 12. Corrosion rate of 18-8 steel with titanium in boiling HNO<sub>3</sub> solutions with 0.05 M HF as a function of the addition of sodium nitrate to them: ●) 8 M HNO<sub>3</sub>; ▽) 10 M HNO<sub>3</sub>; ▲) 12 M HNO<sub>3</sub>; ○) 14 M HNO<sub>3</sub>.

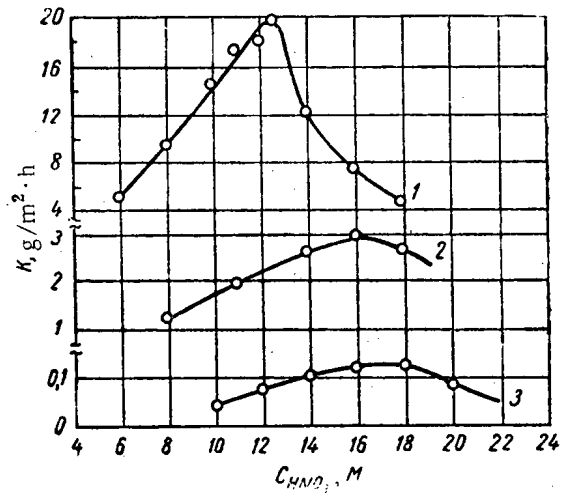


Fig. 13. Corrosion rate of 18-8 steel with titanium in HNO<sub>3</sub> solutions with 0.05 M HF as a function of the acid concentration and temperature: 1) boiling point; 2) 60°C; 3) 20°C.

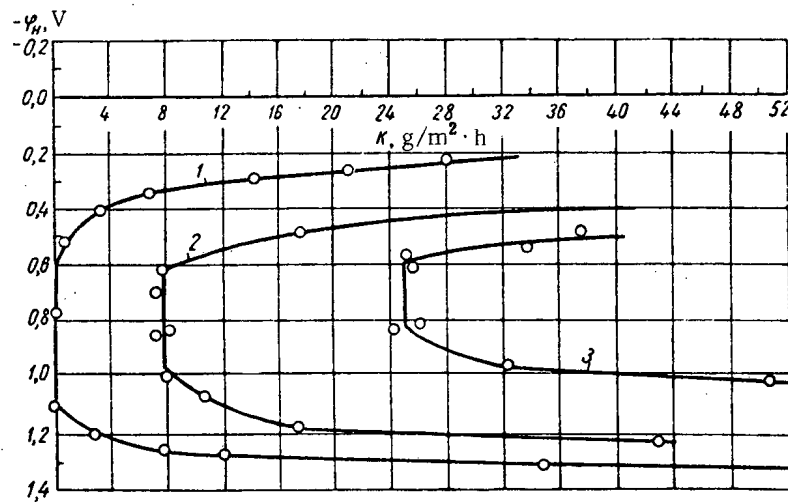


Fig. 14. Corrosion rate of 18-8 steel with titanium as a function of the potential in 10 M HNO<sub>3</sub> solution at 110°C with an addition of sodium fluoride: 1) without addition; 2) 2.5 g/liter; 3) 6 g/liter.

An increase in the corrosion rate of steel with the addition of fluoride to HNO<sub>3</sub> solutions is accompanied by a reduction in the potential of the steel, this reduction being the greater the higher the corrosion rate. This increase in the corrosion rate of stainless steels in HNO<sub>3</sub> solutions with fluoride additions is observed over a wide range of potentials corresponding to the region of active dissolution, the passive state, and superpassivation (Fig. 14).

The most intensive acceleration in the corrosion then occurs in the region of the passive state. Thus, on the addition of 2.5 g/liter of NaF to 10 M HNO<sub>3</sub> the corrosion rate of steel in the region of the passive state increases by a factor of ~80; in the region of active dissolution and superpassivation the factor is only ten. Since fluoride additions accelerate the corrosion of stainless steel to an approximately equal extent over a wide region of potentials (with dissolution in the active state and according to a superpassivation mechanism), we can assume that the corrosion is caused by uncharged particles, for example HF molecules. In actual fact, HF is a weak acid and the concentration of its undissociated molecules will therefore change strongly, depending on the hydrogen ion concentration

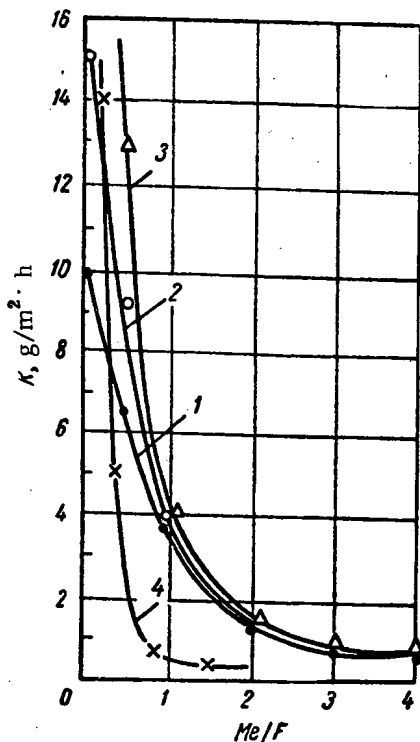


Fig. 15. Corrosion rate of 18-8 steel with titanium in boiling solution of 8 M HNO<sub>3</sub> with additions of HF 0.05 M (1), 0.10 M (2), 0.15 M as a function of the ratio of molar concentrations of aluminum nitrate (1, 2, 3) and zirconium nitrate (4) to fluorine.

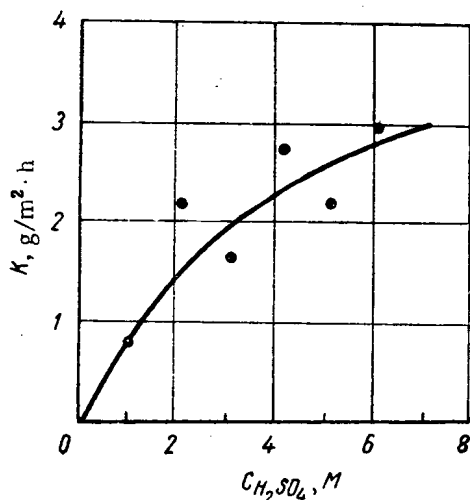


Fig. 16. Effect of the concentration of boiling H<sub>2</sub>SO<sub>4</sub> solutions on the corrosion rate of Kh23N27M3D3T steel.

to form stable complex compounds with the fluorine ions. These metals can be all the elements listed below, arranged in order of increasing stability of their complex compounds with the fluorine ion: iron, beryllium, aluminum, plutonium, thorium, and zirconium [27].

in the system. It readily dissolves oxides of many metals, including those of chromium, iron, and nickel, which exists on the surface of stainless steels in HNO<sub>3</sub> solutions. Consequently, the autocatalytic acceleration of the corrosion of stainless steels in HNO<sub>3</sub> solutions with additions of fluorides is due to the formation of HF molecules from fluorine and hydrogen ions; these molecules dissolve the oxide films on the metal surface. From the condition of a stationary corrosion rate it follows that the rate of dissolution of the oxide film should be equal to its rate of formation. On the addition of HF the increase in the rate of dissolution of oxide films should therefore be compensated by an increase in the growth of their formation. In the absence of anodic polarization by an external current the only source of oxidation of the steel can be the reduction of the oxidizing agent (HNO<sub>3</sub>). The increase in the oxidation rate should therefore be accompanied by an increase in the reduction current of HNO<sub>3</sub> and, consequently, a displacement in the potential of the steel toward negative values, which is observed experimentally. In the passive state the dissolution of steel only proceeds through a film; additions of HF or fluoride therefore accelerate the corrosion process most strongly in the region of potentials which characterize the passive state. Corrosion in HNO<sub>3</sub> solutions with HF additions can therefore be considered as consisting of two stages: chemical dissolution of oxide films by hydrofluoric acid and their formation due to reduction of HNO<sub>3</sub>.

TABLE 4. Instability Constants of Complex Compounds

Reaction	Instability constants
$AlF_6^{2-} \rightleftharpoons AlF_4^- + F^-$	0,37
$AlF_4^- \rightleftharpoons AlF_3 + F^-$	$7,2 \cdot 10^{-2}$
$AlF_3 \rightleftharpoons AlF_2^+ + F^-$	$1,5 \cdot 10^{-4}$
$AlF_2^+ \rightleftharpoons AlF^{2+} + F^-$	$5,0 \cdot 10^{-6}$
$AlF^{2+} \rightleftharpoons Al^{3+} + F^-$	$4,8 \cdot 10^{-7}$

From an analysis of the material given it becomes quite evident that the electrochemical protection of stainless steels in HNO<sub>3</sub> solutions with additions of HF is not possible since in these media steels corrode rapidly even from the passive state. For these aggressive media the choice of structural materials with minimum solubility of the passive oxide films is therefore the main problem.

However, we should bear in mind that under the conditions used to dissolve fuel elements the corrosive activity of HNO<sub>3</sub> solutions with HF additions can decrease considerably in time. This may be due to a reduction in the HNO<sub>3</sub> concentration and due to the accumulation of metal ions in the solution (part of the composition of the fuel elements), able

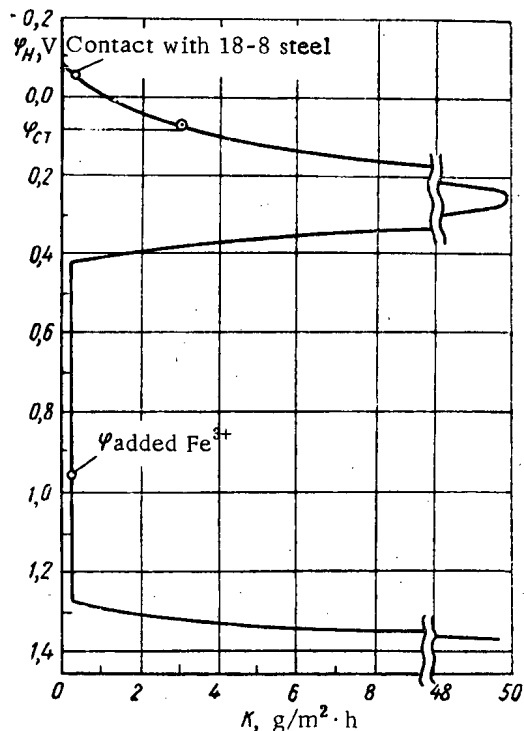


Fig. 17. Dependence of the corrosion rate of Kh23N27M3D3T steel in a boiling solution of 6 M  $H_2SO_4$  on the potential.

be more active in forming complexes with the fluorine ions than the  $Al^{3+}$  ions from the added nitrate salt, i.e., slow down the corrosion of stainless steels more effectively.

It therefore follows that in the dissolution of fuel elements the corrosive effect of  $HNO_3$  solutions with additions of fluorides with respect to structural materials will depend to a considerable extent on the presence, rate of accumulation and final concentration in the solution of ions which form stable complex compounds with the fluorine ions.

#### Sulfuric Acid Solutions\*

To dissolve the cans of stainless steel fuel elements 4-6 M boiling solutions of sulfuric acid are used [1]. Kh23N27M3D3T stainless steels are used to construct the complex chemical apparatus and feed system needed for operation with  $H_2SO_4$  solution [28, 29]. The corrosion rate of these steels in  $H_2SO_4$  solutions with a concentration up to 10 M does not exceed  $0.1 \text{ g/m}^2 \cdot \text{h}$  at temperatures up to  $100^\circ\text{C}$ . However, in boiling  $H_2SO_4$  solutions the corrosion rate of steel increases considerably (Fig. 16) and in 6 M acid it is  $2-3 \text{ g/m}^2 \cdot \text{h}$ . The stationary potential for the corrosion of steel in boiling 6 M  $H_2SO_4$  corresponds to the region of the active state and is equal to  $+0.07 \text{ V}$  (Fig. 17).

It follows from Fig. 17 that the corrosion rate should decrease on contact between Kh23N27M3D3T steel with 18-8 steel which is dissolving at a more negative potential. In fact, in this case the corrosion rate of Kh23N27M3D3T steel decreases to  $0.2 \text{ g/m}^2 \cdot \text{h}$ , and the potential reduces to  $-0.05 \text{ V}$ , i.e., there is cathodic electrochemical protection of the structural material. The main breakdown of reactor-dissolvers made from the considered structural material will evidently occur at the start of the process until there is intensive dissolution of the stainless steel fuel element cans and after completion of the process of dissolution. At these stages of the technological process the corrosion of the material of the reactor-dissolver can evidently slow down. For this purpose it is sufficient to add to the boiling  $H_2SO_4$  solution some oxidizing agent which can displace the potential of the structural material of the reactor to the region of the stable passive state. Experiments show that the addition of  $0.2 \text{ g/liter}$  of  $Fe^{3+}$  ions to boiling 6 M  $H_2SO_4$  solutions displaces the potential of Kh23N27M3D3T steel to  $0.9 \text{ V}$  and the corrosion rate becomes  $0.2 \text{ g/m}^2 \cdot \text{h}$ .

\* The experimental part was performed by N. A. Bozin.

Figure 15 shows results characterizing the corrosion rate of 18-8 steel with titanium in an 8-M solution of  $HNO_3$  with varying content of HF, as a function of the ratio of the molar concentrations of aluminum and zirconium nitrates to fluorine.

The reduction in the corrosive effect of the solution observed in this case is due to a reduction in the HF concentration. It is a well-known fact that  $Al^{3+}$  ions form a series of complex compounds with fluorine ions (Table 4), the instability constants of which fall with increase in the  $Al/F$  ratio.

It follows from Table 4 that with increase in the content of  $Al^{3+}$  ions in the solution more stable complex compounds of aluminum with fluorine can exist; this leads to a reduction in the concentration of free HF in the solution. When the limiting ratio  $Al/F$  is reached in the solution there will evidently only be one compound  $AlF_2^{2+}$  with a minimum instability constant for the system  $Al^{3+}-F^-$ . A further increase in the aluminum concentration in the solution should lead to a smaller reduction in the HF concentration, due to displacement of equilibrium of the last reaction to the left (see Table 4). For an  $Al/F$  ratio above two or three the corrosion rate therefore decreases more slowly. Similarly, we can explain the reduction in corrosion when zirconium nitrate is added to the solution. Since complex compounds of zirconium with fluorine are more stable than aluminum compounds, the zirconium naturally slows down the corrosion process more effectively (curves 3 and 4 of Fig. 15). We should expect that ions of the type  $Al^{3+}$  appearing in the solution due to dissolution of the fuel elements should

We have analyzed experimental data on the corrosive activity of fuel element solvents with respect to structural materials, using modern ideas on the dependence of the corrosion rate of metals and alloys on the potential; the following general conclusions were reached:

1. The acceleration of the corrosion of 18-8 steels in boiling (8-14 M)  $\text{HNO}_3$  solutions is connected with the disturbance in their passive state and dissolution according to a superpassivation mechanism. The corrosion of steels in boiling 10-14 M  $\text{HNO}_3$  solutions proceeds with preferential cathodic control. The possibility has been established of a sharp increase in the corrosion rate of steels in dilute  $\text{HNO}_3$  solutions when there is contact with electronegative metals.

2. Monel metal, the most corrosion-resistant structural metal in HF solutions, breaks up in the vapor phase at rates which are an order higher than these inside the solution. This phenomenon is due to the fact that the corrosion of monel metal proceeds with oxygen depolarization with preferential cathodic control. The corrosion of monel metal is accompanied by cracking, having a specific character.

3. Small additions of fluorides to  $\text{HNO}_3$  solutions sharply reduce the corrosion resistance of stainless steels. The degree of corrosiveness of fluoride additions is a function of the hydrogen ion concentration and appears over a wide region of potentials. The catalytic accelerating action of fluoride additions on the corrosion of stainless steels in  $\text{HNO}_3$  solutions amounts to the facilitation of the anodic process due to dissolution of the passivating films by hydrofluoric acid. We have shown that the retardation of the corrosion of steels by  $\text{Al}^{3+}$  ions is due to a reduction in the concentration of free HF, due to the fluorine ions being combined into stable complex compounds.

4. We have shown the possibility of reducing the rate of corrosion of Kh23N27M3D3T steel in boiling  $\text{H}_2\text{SO}_4$  solutions by cathodic protection and the introduction of additions of oxidizing agents to the solution, displacing the potential of the steel to the region of the stable passive state.

#### LITERATURE CITED

1. F. Culler and R. Blanco, Report No. 1930 presented by the USA to the International Conference on the Peaceful Uses of Atomic Energy, Geneva (1955).
2. K. F. Bonhoeffer, In: Transactions of the Fourth Conference on Electrochemistry [in Russian], Moscow, Izd. AN SSSR, p. 579 (1959).
3. S. Edeleanu, Nature, 173, 739 (1954).
4. Ya. M. Kolotyrkin, N. Ya. Buné, and V. M. Knyazheva, In: Transactions of the Fourth Conference on Electrochemistry [in Russian], Moscow, Izd. AN SSSR, p. 594 (1959).
5. A. M. Sukhotin, In: Transactions of the Fourth Conference on Electrochemistry [in Russian], Moscow, Izd. AN SSSR, p. 621 (1959).
6. Chemical Processes and Equipment, Reports of the United States Atomic Energy Commission [Russian translation], Moscow, Izd. inostr. lit. (1956).
7. J. Bünger, Werkstoffe und Korrosion, 9, 747 (1958).
8. J. Truman, J. Appl. Chem., 4, 273 (1954).
9. A. B. McIntosh, Chem. and Ind., No. 22, 687 (1957).
10. W. Walker, Werkstoff und Korrosion, 10, 113 (1959); 11, 563 (1960).
11. M. M. Kurtepov and G. V. Akimov, Dokl. AN SSSR, 87, 93; 795; 625 (1952).
12. M. M. Kurtepov and A. S. Gryaznova, Dokl. AN SSSR, 135, 899 (1960).
13. K. Vetter, Z. phys. Chem., 194, 199 (1950).
14. A. M. Sukhotin, Zh. neorgan. khim., No. 8, 1277 (1959).
15. G. V. Akimov, The Theory and Methods of Investigation into the Corrosion of Metals [in Russian], Moscow, Izd. AN SSSR (1945).
16. N. D. Tomashov, Theory of Corrosion and Protection of Metals [in Russian], Moscow, Izd. AN SSSR (1959).
17. E. N. Mirolyubov, M. M. Kurtepov, and N. D. Tomashov, Izv. AN SSSR, Otd. khim. nauk., No. 7, 1178 (1960).
18. N. D. Tomashov, M. M. Kurtepov, and E. N. Mirolyubov, Zh. fiz. khim., 32, 904 (1958).
19. E. N. Mirolyubov, M. M. Kurtepov, and N. D. Tomashov, Izv. AN SSSR, Otd. khim. nauk., No. 6, 1015 (1960).
20. E. N. Mirolyubov, M. M. Kurtepov, and N. D. Tomashov, Izv. AN SSSR, Otd. khim. nauk., No. 6, 1015 (1960).\*
21. B. Morton, Corrosion, 1, 228 (1945).
22. M. Schussler, Industr. and Engng. Chem., 47, 135 (1955).
23. H. Copson and G. Cheng, Corrosion, 12, 647 (1956).

\* [19] and [20] are identical and appear this way in the Russian [Publisher's note].



24. I. L. Rozenfel'd, Inhibitors of the Corrosion of Metals in Neutral Media [in Russian], Moscow, Izd. AN SSSR (1954).
25. Nucl. Sci. Abstrs., 13, 8609, 8632, 9842, 19983 (1959); 14, 4381, 4385, 5261, 9732 (1960).
26. I. Oknin, Zh. prikl. khim., 24, 167 (1951).
27. K. B. Yatsimirskii and V. P. Vasil'ev, Instability Constants of Complex Compounds [in Russian], Moscow, Izd. AN SSSR (1959).
28. E. V. Zotova, Stal', No. 6, 552 (1958).
29. V. V. Andreeva and T. P. Stepanova, Investigations into Stainless Steels [in Russian], Moscow, Izd. AN SSSR, p. 92 (1957).

---

All abbreviations of periodicals in the above bibliography are letter-by-letter transliterations of the abbreviations as given in the original Russian journal. *Some or all of this periodical literature may well be available in English translation.* A complete list of the cover-to-cover English translations appears at the back of this issue.

---

RADIATION DOSIMETERS BASED ON THERMOLUMINESCENCE  
MEASUREMENTS IN ALUMINUM PHOSPHATE GLASS (IKS DOSIMETERS)

I. A. Bochvar, A. A. Vasil'eva, I. B. Keirim-Markus,  
T. I. Prosina, Z. M. Syrinskaya, and V. V. Yakubik

Translated from *Atomnaya Énergiya*, Vol. 15, No. 1,  
pp. 48-52, July, 1963  
Original article submitted May 19, 1962

Glass dosimeters useful in beta-gamma dosimetry, slow neutron dosimetry, and the dosimetry of high-energy charged particles in the  $0.02$  to  $(1-2) \cdot 10^6$  rad range have been developed. The dosimeters are capable of storing and retaining information for an unusually long interval (as long as a month in a  $150^\circ\text{C}$  environment). These glasses are not excited by daylight, but daylight does exert a deexcitation effect: 26 to 38% of the stored light sum is dissipated by deexcitation in a period of 40 days.

The effective atomic number of the optimum glass recipes is 11 to 13. A filter of 0.6 mm Sn + 0.5 mm Al helps counteract the "hardness variation" in the range from 40 keV on higher, within an error of  $\pm 20\%$ . The glass dosimeters are usable repeatably.

Suggestions have been made on repeated occasions to take advantage of the thermoluminescence of crystal phosphors in dosimetry (such phosphors as  $\text{CaSO}_4\text{-Mn}$  [1];  $\text{CaSO}_4\text{-Sm}$  [2];  $\text{CaF}_2\text{-Mn}$ , LiF [3] have been recommended). The phenomenon of radiophotoluminescence [4] and browning of glass in response to a radiation exposure [5] are used to advantage in glass dosimeters.

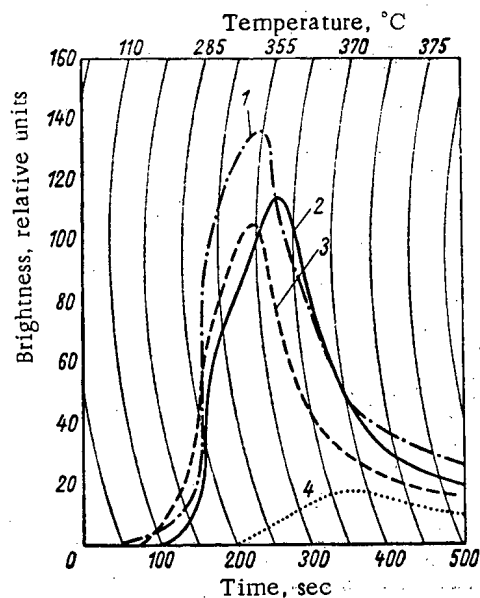


Fig. 1. Thermal deexcitation curves for  $7 \times 30 \times 30$  mm glass specimens exposed to  $0.1 \text{ r Co}^{60}$  gamma radiation: 1)  $5^{0-26}$  glass; 2)  $34^{0-3}$  glass; 3)  $2^{0-3}$  glass; 4) emission by heating unit.

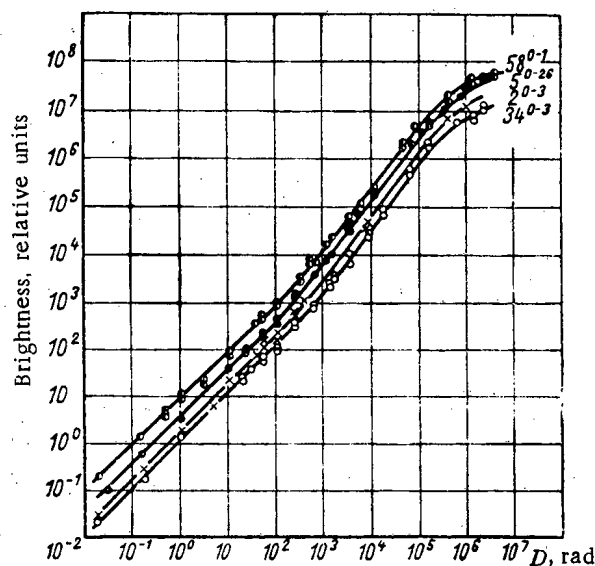


Fig. 2. Gamma dosage dependence of peak thermo-luminescent brightness of various glasses ( $\text{Co}^{60}$  gammas).

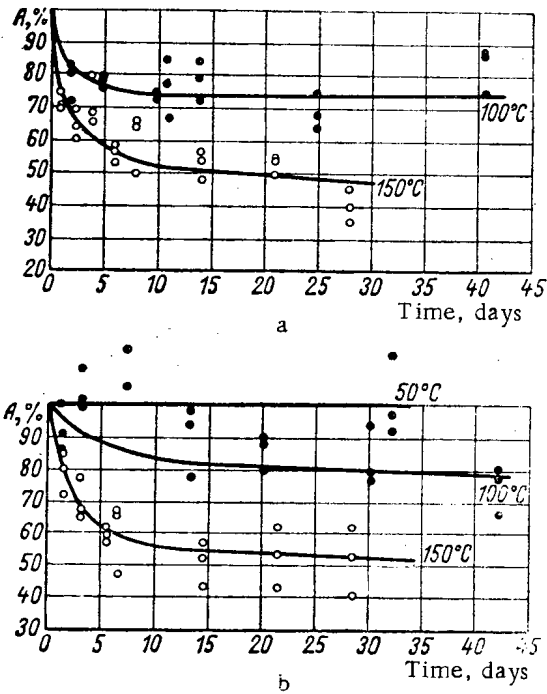


Fig. 3. Variation in stored light sum (A) as a function of shelf time [a)  $5^{0-26}$  glass; b)  $34^{0-3}$  glass].

This paper describes thermoluminescent dosimeters made of aluminum phosphate glass [6]. The method applied is based on the fact that the energy of the ionizing radiations absorbed by the glass is stored in the glass in the form of a luminescence light sum, which is reemitted when the glass is heated, and may be recorded. Glass compositions studied included:  $R_xO \cdot P_2O_5 - Al_2O_3 \cdot 3P_2O_5$ , where  $R_xO$  is one of the oxides of Li, Na, K, Rb, Cs, Be, Mg, Ca, Zn, Sr, Cd, Ba, or Pb. Multicomponent glasses containing oxides of two or more elements belonging to groups I and II in the periodic table, as well as  $SiO_2$ , are also being studied. Activators in use are Cr, Mn, Fe, Co, Ni, Cu, Ag, Sn, Sb, Ce, Pr, Nd, Sm, Pb, Bi, and U. Optimum compositions activated by  $MnO_2$  (0.1 wt. %) were selected. These are glasses made with partial utilization of raw materials in the form of sulfates:  $5^{0-26} - MgO \cdot P_2O_5 - Al_2O_3 \cdot 3P_2O_5$ ;  $34^{0-3} - SrO \cdot P_2O_5 - Al_2O_3 \cdot 3P_2O_5$ ;  $2^{0-3} - Li_2O \cdot P_2O_5 - Al_2O_3 \cdot 3P_2O_5$ ; and  $58^{0-1} - SrO \cdot P_2O_5 - SiO_2 \cdot P_2O_5 - 2(Al_2O_3 \cdot 3P_2O_5)$ . Wafers  $4 \times 15 \times 15$  mm and  $7 \times 30 \times 30$  mm were fabricated for the dosimeters. One square side of the wafers was polished, and the remaining were given a matte finish. The thermoluminescent emission was measured in a special heating unit [7] by means of a FÉU-29 photomultiplier tube; the thermal deexcitation curves were measured with an automatic recorder. Inspection of Fig. 1 immediately reveals the fact that heating took place at an uneven rate as dc current was passed through the heater. The temperature emission of the furnace, which governs the sensitivity limit, depends on the current.

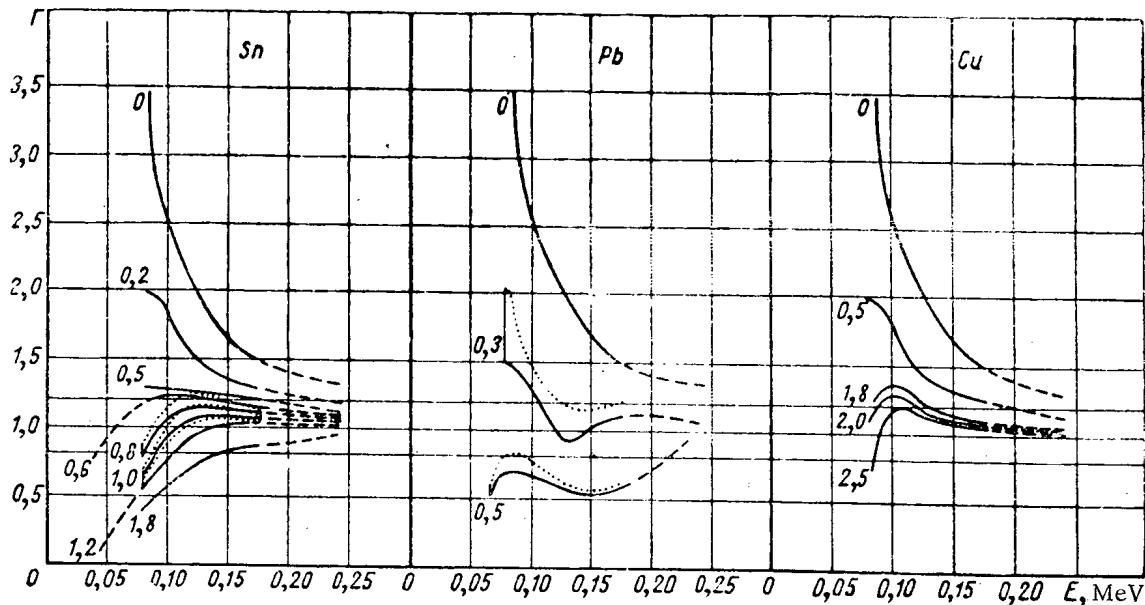


Fig. 4. Hardness variation of gamma radiation ( $\Gamma$ ) for specimens of  $5^{0-26}$  glass 4 mm thick (figures on curves indicate filter thickness, in mm): —) filter with 0.5 mm aluminum substrate; ..... ) unbacked filter.

The emission of the glasses is in the orange region, and is apparently due to the  $Mn^{2+}$  ion in a position with coordination number 6 [8]. The energy yield of the light sum amounts to 2-5% in the glasses. As we see from Figs. 1 and 2, the  $7 \times 30 \times 30$  mm glass dosimeters are capable of recording doses from 0.02 to  $(1-2) \cdot 10^6$  rad. Hence, the

full range of measurement encompasses eight orders of magnitude. At doses upward of  $10^4$  rad, a pronounced coloration of the glasses is observed in pink and violet colors, and this enables us to determine even larger doses from the change in optical absorption. Special experiments using glass specimens of different thickness have succeeded in showing that thermoluminescence saturation at doses  $\sim 10^6$  rad is not due to increased thermoluminescent absorption in the glass as a result of browning of the glass.

By comparing our findings with the readings of ferrosulfate chemical dosimeters, we found that the amount of the light sum stored in the glasses is independent on the dose rate of  $\text{Co}^{60}$  gammas up to a level of 25 rad/sec, and independent of the dose rate of protons of  $\sim 500$  MeV energy up to 400 rad/sec (per pulse) [9].

The glass dosimeters are always ready for service and are capable of storing and retaining information for an unusually protracted time interval. As we see from Fig. 3, the glasses  $5^{0-26}$  and  $34^{0-3}$  are capable of measuring doses over a month or longer, with the introduction of appropriate corrections, even in a  $150^\circ\text{C}$  environment. In one of the experiments, dosimeters of this type were issued to personnel present for 122 days in a field of gamma radiation with little variation in dose rate. The dosimeter readings upon conclusion of the experiment averaged out at  $98.5 \pm 2.5\%$  of the true value. Tentative calculations reveal that the energy depth of electron traps in the glasses is about 2 eV, and that at ordinary temperatures the light sum in these should be retained for centuries.

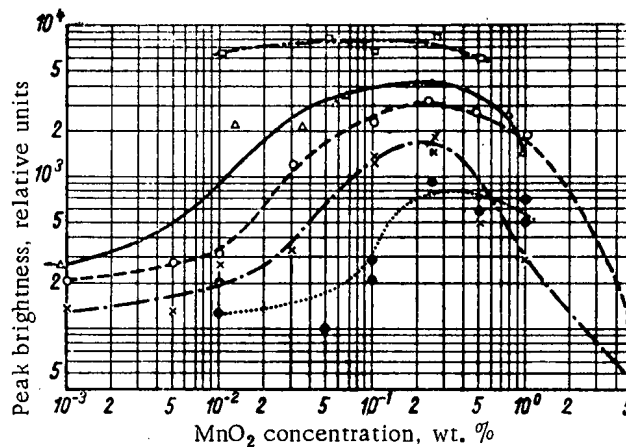


Fig. 5. Peak thermoluminescent brightness of MgO glasses as a function of  $\text{MnO}_2$  concentration: ... (●)  $\text{Al}_2\text{O}_3 \cdot 3\text{P}_2\text{O}_5$ ; --- (x)  $3(\text{Al}_2\text{O}_3 \cdot 3\text{P}_2\text{O}_5) - \text{MgO} \cdot \text{P}_2\text{O}_5$ ; --- (○)  $\text{Al}_2\text{O}_3 \cdot 3\text{P}_2\text{O}_5 - 3(\text{MgO} \cdot \text{P}_2\text{O}_5)$ ; — (Δ)  $5^{0-26}$ ; - · - · - (□)  $\text{Li}_2\text{O} \cdot \text{P}_2\text{O}_5 - \text{MgO} \cdot \text{P}_2\text{O}_5 - \text{SrO} \cdot \text{P}_2\text{O}_5 - \text{SiO}_2 \cdot \text{P}_2\text{O}_5 - 4(\text{Al}_2\text{O}_3 \cdot 3\text{P}_2\text{O}_5)$ .

The broad range of the measurements and the unlimited information storage time, combined with the mechanical and chemical stability, render thermoluminescent glasses ideal memory units.

The glasses remain virtually unaffected by daylight. To check the degrading effect of daylight, a batch of exposed glasses, of recipes  $5^{0-26}$ ,  $58^{0-1}$ , and  $34^{0-3}$ , were left out in the open over a 40 day period. A comparison of the peaks on the thermoluminescence degradation curves for the glasses exposed in the open and for glasses wrapped in black paper showed that the peaks on the curves were reduced by the daylight exposure by as much as 36, 38, and 26%, respectively, for the three types tested. The degrading effect of daylight is quite modest, as we see, but shielding against daylight would be required in the case of prolonged exposures.

The sensitivity of personnel glass dosimeters (IKS dosimeters) to various types of ionizing radiations has been investigated. The hardness variation observed in the recording of gamma radiation is determined, as we know, by the effective atomic number  $Z_{\text{eff}}$ , and also by the specimen thickness. Calculations of  $Z_{\text{eff}}$  for these glasses yielded values ranging from 11.8 for  $2^{0-3}$  glasses to 18.6 for  $34^{0-3}$  glass. As we see from the calculations, in glasses 4 mm thick and containing no strontium, the hardness variation does not exceed 350%. Experimental research has aided in the selection of a filter to counteract this hardness variation. For  $5^{0-26}$  glasses, a 0.6 mm Sn + 0.5 mm Al filter compensates for the hardness variation with an error of  $\pm 20\%$  in the 40 keV range and higher (Fig. 4).

IKS dosimeters and other types of dosimeters were exposed to a flux of 100 to 500 MeV protons at the synchrotron of the Dubna Joint Institute for Nuclear Research. It was found that the sensitivity of the glasses to a tissue dose of high-energy protons agrees, to within ~10% accuracy, with the sensitivity of the glasses to a dose of gamma rays, and the glasses are consequently pronounced suitable for use as dosimeters in mixed p- $\gamma$ -emission.

A comparison of the thermoluminescence degradation curves of glasses irradiated by thin Pu<sup>239</sup> applicators and Co<sup>60</sup> gamma photons aided in determining the  $\alpha/\beta$  ratio of the light sum yield, which came to 16-18% for the 5<sup>0-26</sup>, 34<sup>0-3</sup>, and 58<sup>0-1</sup> glasses, and to 3-7% for the 2<sup>0-3</sup> glasses and for other glasses containing Li<sub>2</sub>O. The relative sensitivity to products of the Li<sup>7</sup>(n,  $\alpha$ )T<sup>3</sup> reaction proved to be even higher. It was found that the relative sensitivity to thermal neutrons as compared to the sensitivity to gamma rays is proportional to the lithium content in the composition of the glasses. The energy yield of the light sum in response to bombarding by thermal neutrons is ~50% of the value obtained in response to a gamma exposure. Assuming the  $\alpha/\beta$  ratio not to be in excess of 7% in the case of 2.7 MeV alpha particles formed in a nuclear reaction, then the energy yield for tritons of roughly 3 MeV energy formed simultaneously (and consequently likewise for protons of ~1 MeV energy) will exceed 90% of the gamma yield. We may assume then, on the basis of already available data, that the dependence of IKS personnel dosimeter readings on linear energy losses of charged particles will be weaker than in the case of organic scintillators, but still weaker in organic crystals of types NaI (T1) and CsI (T1) [9].

The light sum stored by 2<sup>0-3</sup> glasses irradiated by thermal neutrons turns out to be greater by a factor of ten than when irradiated by the same tissue dose of gamma radiation (expressed in rems). Consequently, 2<sup>0-3</sup> glasses are attractive for use in determining the dose contribution of slow neutrons against a background of intense gamma radiation. Even more suitable for this application are the 3<sup>0-5</sup> glasses which contain 1.5 times more lithium. A simple calculation reveals that glasses containing Li<sub>2</sub>O in amounts of about 1 wt. % are capable of directly measuring a mixed dose of gammas and thermal neutrons. All of the glasses studied here are virtually insensitive to fast neutrons, as we see from calculations of absorbed dose and from direct measurements.

The optimum glass recipes are not critical. As we see from an example of MgO glasses (Fig. 5), the thermoluminescent brightness drops to one-half as the fraction of MgO in the basic composition of the glass varies by a factor of two, and as the MnO<sub>2</sub> concentration varies by over one order of magnitude.

Specimens of glass exhibit excellent reproducibility when made in quartz crucibles with stirring of the melt. Fifty dosimeters produced in a single laboratory-bench operation differed by not more than 15% in the calibration, and this is commensurate with the accuracy attainable in the measurements.

IKS personnel dosimeters can be used repeatedly. Measurements repeated 50 times with 5<sup>0-26</sup> and 34<sup>0-3</sup> glasses failed to reveal any changes in the thermoluminescence degradation curves. Several specimens of glass have been in service for over three years, and no deterioration of the calibration has been detected.

Some distinct glass compositions containing Li<sub>2</sub>O yielded poorly reproducible readings in repeated measurements, and this is apparently accounted for by the low softening point of those glasses. It is quite possible that irreversible ionic or chemical processes affecting the emission yield take place at an appreciable rate in the glasses even at the temperatures at which the thermoluminescence degradation curves were measured.

Five to seven minutes were spent in the laboratory measurements to plot the thermoluminescence degradation curves. At the present time, new heaters are being developed to aid in successfully shortening the measurement time to 2 min with no losses in sensitivity.

The broad range of measurable dose levels and the protracted retention of information make it possible to consider glass dosimeters for use in the practical solution of quite a few problems. The method is well suited to personnel dosimetry of  $\beta$ - $\gamma$ -radiation, slow neutrons, and high-energy charged particles with a weekly-quarterly exposure cycle. IKS personnel dosimeters may apparently be used to record a radiation dose obtained over the entire service life of the dosimeter, as well as for individual personnel dosimetry in emergency and overhaul or maintenance operations. They may prove useful as dosimetric monitors in x-ray therapy and in some other areas of applications of radiation effects, such as sterilization of potatoes, disinfection, etc. Thanks to its properties, the method is feasible as a tool of scientific experimentation in the study of dose fields under extreme conditions, i.e., very minute doses, including doses of background radiation, as well as for the study of a very wide range of doses under high temperature conditions, in a corrosive medium, etc.

## LITERATURE CITED

1. W. Kossel, U. Mayer, and H. Wolf, *Naturwissenschaften*, 41, 209 (1954); B. M. Nosenko, L. S. Revzin, and V. L. Yaskolko, *Zhur. tekhn. fiz.*, 26, 2046 (1956); V. A. Arkhangel'skaya, et al., *JAE*, 8, 559 (1960).
2. H. Peter, *Atomkernenergie*, 5, 453 (1960).
3. D. Patterson and H. Friedman, *J. Opt. Soc. America*, 47, 1136 (1957); R. Ginther and R. Kirk, *J. Electrochem. Soc.*, 104, 365 (1957).
4. J. Schulman, et al., *Nucleonics*, 11, 52 (1953).
5. J. Schulman, et al., *Nucleonics*, 13, 30 (1955); N. Kreidl and G. Blair, *Nucleonics*, 14, 56, 82 (1956); 17, 58 (1959).
6. I. B. Keirim-Markus, Z. M. Syritskaya, and V. V. Yakubik, *Steklo. Byull. Gos. inst. stekla*, No. 2 (111), 77 (1961); I. A. Bochvar, et al., *Ibid.*, No. 2 (1963).
7. I. A. Bochvar and I. B. Keirim-Markus, *Pribory i tekhnika éksperimenta*, No. 6, 139 (1961).
8. S. Linwood and N. Weyl, *J. Opt. Soc. America*, 32, 443 (1942).
9. *Radiation dosimetry*, Edited by Hine and Brownell, Academic Press, N.Y. (1956).

---

All abbreviations of periodicals in the above bibliography are letter-by-letter transliterations of the abbreviations as given in the original Russian journal. Some or all of this periodical literature may well be available in English translation. A complete list of the cover-to-cover English translations appears at the back of this issue.

---

MONITORING IONIZING RADIATIONS RESULTING  
FROM NITROGEN REACTIONS

M. T. Dmitriev

Translated from *Atomnaya Énergiya*, Vol. 15, No. 1,

pp. 52-59, July, 1963

Original article submitted October 30, 1961

Problems of monitoring ionizing radiations and neutrons from nitrogen reactions taking place on irradiation of air, nitrogen-oxygen mixtures, nitrogen oxides, or water containing dissolved air and during capture of neutrons by nitrogen nuclei are discussed. Nitrogen-oxygen and nitrogen oxides ionizing-radiation and thermal neutron monitors are proposed on the basis of the investigated radiation-chemical effects. The lower limit of measurement of radiation dosage is 1 rad, and that of an integral neutral flux is  $10^9$  neutrons/cm<sup>2</sup>. Use of the appropriate procedure makes it possible to reduce these limits. The upper limits of measurement of dosages and neutron fluxes by open-type monitors are virtually unrestricted. The method makes it possible to carry out dosimetric measurements from samples of air and water under natural conditions.

The literature contains fairly numerous examples of determination of average and high doses of ionizing radiations from various physicochemical processes taking place under the effect of radiation in phosphors, glasses, aqueous solutions of inorganic compounds, carbohydrates and other substances. Our method of monitoring ionizing radiations from various nitrogen reactions is included in this type of monitors. Nitrogen monitors make it possible to determine doses by  $\gamma$ -radiation, electrons, protons and other types of ionizing radiations (starting at 1 rad) and integral neutron fluxes (starting at  $10^9$  neutrons/cm<sup>2</sup>). The most essential difference between monitoring from nitrogen reactions and other chemical monitoring methods is the possibility of direct determination of the amounts of absorbed energy by means of air samples taken from radiation apparatus, industrial plant or the atmosphere, and samples of water from soil or lakes. Further, the monitor may be filled with, say, air; this is an undoubted advantage whether in the laboratory or in field work. Monitors based on nitrogen radiation reactions may also be employed in radiobiological investigations.

TABLE 1. Energy Yield of NO<sub>2</sub> Formation Reaction in Air at Atmospheric Pressure in Relation to the Type of Ionizing Radiation (from data in [1-5])

Radiation	Temp., °C	NO <sub>2</sub> yield, mol/100 eV
Gamma radiation	17.5	1.4
" "	30	1.45
" "	150	2.45
Electrons	15	1.35
"	45	1.5
"	65	1.6
"	145	2.4
Protons	30	1.5
Ions and electrons	25	1.4
Nuclear reaction radiation	30	1.55
The same	49	1.8
" "	140	2.5 *

\* From data in [6].

**Nitrogen-oxygen system.** In [1] I investigated the effect of ionizing radiations on nitrogen-oxygen mixtures, particularly air. It was found that the primary elemental process leading to active nitrogen reactions is ionization of the nitrogen molecule. Reaction of nitrogen with oxygen commences, and is accelerated, at electron energies corresponding to formation of molecular and atomic nitrogen ions. The reaction rate is proportional to the value of nitrogen ionization. The following reactions may consist either of direct chemical reaction between a nitrogen molecular ion and an oxygen molecule, or reaction of the dissociation products of a molecular ion (an atom and atomic ion) with oxygen. Furthermore, recombination and recharging of ions play a considerable role in the reaction. As a result of ionization processes and the subsequent radiation-chemical reactions, primarily NO, NO<sub>2</sub>, and N<sub>2</sub>O are formed. Other, unstable nitrogen oxides, which are converted to NO<sub>2</sub> during analysis, are also formed. If molecular oxygen remains in the irradiated mixture (which is nearly always the case) NO is converted to NO<sub>2</sub>. Therefore, the principal radiolysis products of air are NO<sub>2</sub> and N<sub>2</sub>O. Formation of NO<sub>2</sub>, the amount of which may be readily determined by simple methods, is of maximum interest.

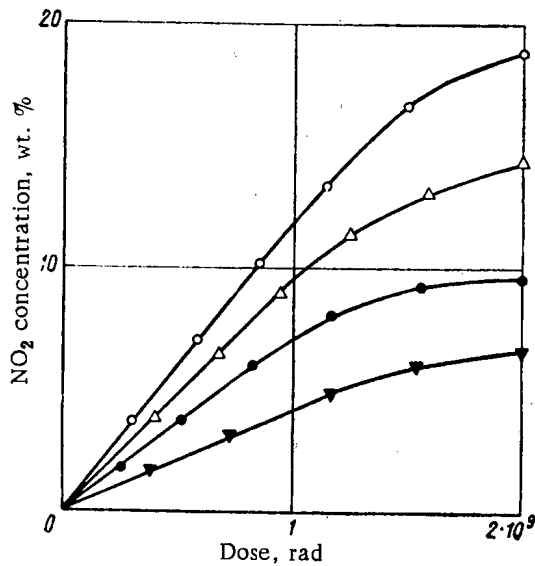


Fig. 1. Relation between NO<sub>2</sub> concentration and fast-electron and  $\gamma$ -radiation dose. Pressure 1 atm; temperature 20°C; composition of the mixture: ○) 50% N<sub>2</sub> + 50% O<sub>2</sub>; △) 70% N<sub>2</sub> + 30% O<sub>2</sub>; ●) air; ▼) 90% N<sub>2</sub> + 10% O<sub>2</sub>.

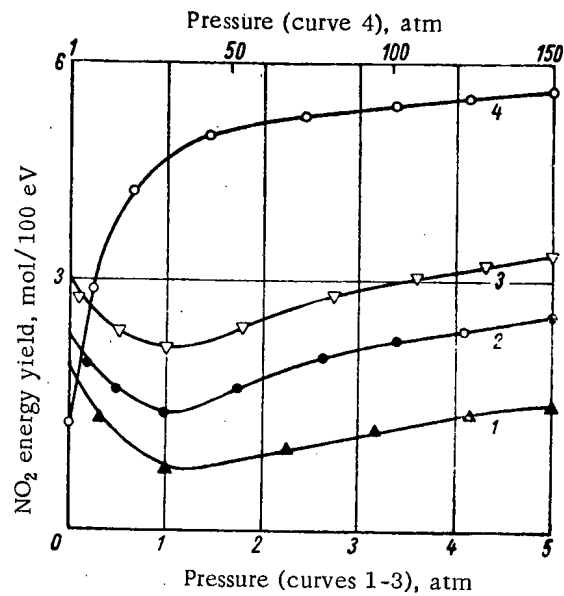


Fig. 2. Relation between the NO<sub>2</sub> energy yield and pressure. Temperature 20°C; composition of the mixture: 1) 90% N<sub>2</sub> + 10% O<sub>2</sub>; 2) air; 3) 50% N<sub>2</sub> + 50% O<sub>2</sub>; 4) air.

Table 1 gives the energy yields of NO<sub>2</sub> formation by the action of various ionizing radiations on air at atmospheric pressure. It may be seen that the energy yield of NO<sub>2</sub> formation is virtually independent of the type of ionizing radiation and therefore the ionization density; this is an undoubted advantage in monitoring a mixed radiation field. Approximately the same energy yields (related to the same temperature) are obtained from the action of electrons and  $\gamma$ -radiation and from irradiation of air by fission fragments [6]. Roughly the same results were also found for electric discharges in air [2, 3].

The values in Table 1 were obtained under different conditions and differing degrees of accuracy and can therefore only serve for a rough assessment.

Measurements were carried out to improve the accuracy of the NO<sub>2</sub> energy yields in air at atmospheric pressure under the effect of Co<sup>60</sup>  $\gamma$ -radiation and 0.2 MeV electrons. The NO<sub>2</sub> contents were determined by the spectrophotometric method, the absorbed irradiation energies were measured in a calorimeter with distilled water, described briefly in [4]. In particular, the following results (accuracy 1-3%) were obtained:

Temperature, °C	0	10	15	20	25	30
NO <sub>2</sub> molecule/100 eV	1.35	1.38	1.39	1.41	1.43	1.46

These values may be employed in radiation-monitoring measurements, irrespective of the type of ionizing radiation.



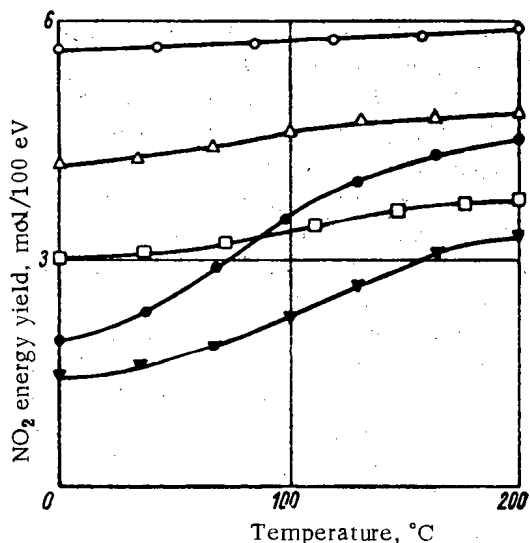


Fig. 3. Relation between the NO<sub>2</sub> energy yield and temperature for air. Pressure, atm: ○) 150; △) 10; ●) 0.1; □) 5; ▼) 1.

a mean energy of 32.5 eV necessary for formation of one ion pair in air). The following NO<sub>2</sub> concentrations formed in air at 760 mm Hg correspond to a dose of 1 rad: 0.64 · 10<sup>-8</sup> wt. % at 0°C, 0.66 · 10<sup>-8</sup> wt. % at 15°C, and 0.67 · 10<sup>-8</sup> wt. % at 20°C.

Apart from the absorbed radiation energy, the concentration of the NO<sub>2</sub> formed also depends on the composition of the mixture, temperature, and pressure. Figures 1-3 give data on the relation between the NO<sub>2</sub> concentration and these factors. When air samples taken at pressures other than atmospheric (e.g., at great heights) or at high temperatures are analyzed, appropriate corrections must be made for the relation between energy yield and these factors. Corrections must also be made if the monitor is filled with a nitrogen-oxygen mixture of different composition to air.

Figure 1 gives the relation between NO<sub>2</sub> concentration and the absorbed dose for mixtures of different composition. This shows that in the initial section, the NO<sub>2</sub> concentration is directly proportional to the dose up to ~1.5 · 10<sup>9</sup> rad:

$$[\text{NO}_2] = kE, \quad (1)$$

where [NO<sub>2</sub>] is the NO<sub>2</sub> concentration, wt. %; E is the absorbed dose, rad; k is the proportionality coefficient.

At 20°C and 1 atm the values of the coefficient k · 10<sup>9</sup> in relation to the mixture composition are as follows:

Air	5.12
90% N <sub>2</sub> + 10% O <sub>2</sub>	2.86
70% N <sub>2</sub> + 30% O <sub>2</sub>	6.72
50% N <sub>2</sub> + 50% O <sub>2</sub>	7.98
15% N <sub>2</sub> + 85% O <sub>2</sub>	4.08

According to [1, 4, 5], for other nitrogen-oxygen mixtures irradiated at 20°C at atmospheric pressure the coefficient k may be obtained from the equation

$$k = 32,0n(1 - n) \cdot 10^{-9}, \quad (2)$$

where n is the mole fraction of nitrogen in the gas mixture.

Equation (1) is not satisfied at electron doses higher than 1.5 · 10<sup>9</sup> rad, but calculations may still be made up to 2.5 · 10<sup>9</sup> rad from the relations given in Fig. 1. For electrons and γ-radiation, above 2.5 · 10<sup>9</sup> rad, the NO<sub>2</sub> concentration is independent of the value of E because a stationary state in which the decomposition rate of NO<sub>2</sub> is equal to its formation rate is established in the gas mixture.

It was noted above that the NO<sub>2</sub> formation reaction is directly related to ionization processes. A specific number of NO<sub>2</sub> molecules formed in this process corresponds to a particular number of the ions initially formed in air. Measurement of the concentration of ions formed in air is obviously only possible during the radiation process because most of the ions are neutralized as a result of recombination processes immediately after radiation has ceased. But the NO<sub>2</sub> molecules formed during ionization of air and subsequent reactions of the ions remain in the air for an indefinite period after radiation has ended. Therefore, the number of ions formed during radiation, but subsequently recombined, may be determined reliably from the concentration of the NO<sub>2</sub> method.

The action of the monitor based on radiation reactions of nitrogen ions and dissociation products of the latter in air is based on this effect. For a nitrogen-oxygen monitor of ionizing radiation (or merely of a sample of free air), radiation of 1 roentgen produces 9.15 · 10<sup>8</sup> molecules of NO<sub>2</sub> in 1 cm<sup>3</sup> of air (at 0°C and 760 mm Hg) (based on

TABLE 2. Values of the Coefficient  $k$  ( $\times 10^9$ ) in Relation to Pressure at 20°C

Gas mixture, %	Pressure, atm						
	0,1	0,5	1	10	20	100	150
Air	8,6	6,3	5,1	14,4	15,7	19,2	20,4
90N <sub>2</sub> +10 O <sub>2</sub>	4,8	3,5	2,9	11,7	14,6	17,9	18,9
50N <sub>2</sub> +50 O <sub>2</sub>	13,3	9,8	8,0	17,1	17,4	21,1	22,5
30N <sub>2</sub> +70 O <sub>2</sub>	11,2	8,3	6,7	16,4	16,7	20,5	21,7

TABLE 3. Values of  $k$  ( $\times 10^9$ ) for Different Air Pressures in Relation to Temperature

Air pressure, atm	Temperature, °C						
	0	20	30	70	100	150	200
1	4,9	5,1	5,3	6,0	6,9	9,6	11,9
0,1	7,7	8,6	8,9	10,6	12,8	17,2	20,0
5	10,0	10,4	10,5	10,8	11,1	12,0	12,8
10	14,1	14,4	14,7	14,9	15,4	16,2	16,8
150	20,2	20,4	20,5	20,8	21,0	21,3	21,5

Figure 3 gives the relation between NO<sub>2</sub> energy yield and temperature in the range 0-200°C. It may be seen that the yields increase with temperature, but with increasing pressure this increase is less marked. Table 3 gives some values of  $k$  in relation to temperature for air at different temperatures.

With an increase in temperature above 200°C the NO<sub>2</sub> energy yield falls, one of the causes being thermal decomposition of NO<sub>2</sub> to NO and oxygen. At the same time the energy yield of radiation decomposition for NO by electrons and  $\gamma$ -radiation is 7.1 times greater than for NO<sub>2</sub> [7]. This is due to a slight increase in the NO and NO<sub>2</sub> formation yield in air > 200°C. Further, it was found that NO molecules formed by irradiation of nitrogen-oxygen mixtures, and present in different excited states, transfer their excitation energy to the gas molecules in the form of kinetic energy and light radiation, and to other molecules during ion recombination and charge transfer processes. With a considerable increase in energy the excited molecules become unstable. Some of them decompose without ever reaching a normal state. The relative number of decomposed molecules depends on the temperature.

The following values of the NO<sub>2</sub> formation energy yield at high temperatures in air (atmospheric pressure) may be taken as correct to 5-10%

Temperature, °C	0	200	300	500	750
NO <sub>2</sub> molecules/100 eV	1.35	3.3	2.7	1.6	0.7

The N<sub>2</sub>O formation reaction may also be used for monitoring, but in this case the analytical procedure is somewhat more complicated. The N<sub>2</sub>O energy yield in air increases with pressure. The following results were obtained at 20°C:

Pressure, atm	1	5	10	25	50	100	150
N <sub>2</sub> O molecules/100 eV	0.62	1.2	1.8	2.1	2.9	3.1	3.2

As a radiation monitor N<sub>2</sub>O is the best form to employ when taking samples of free air because NO<sub>2</sub> is not sufficiently stable under natural conditions.

In liquid nitrogen-oxygen mixtures (at about -183°C) at a 1:1 N<sub>2</sub>:O<sub>2</sub> ratio, the NO<sub>2</sub> yield is 1.2 while that of N<sub>2</sub>O is 0.8 mol/100 eV (the values for liquid air are 1.1 and 0.7, respectively).

In [7] it was established that the NO<sub>2</sub> stationary concentration depends on the ionization density because the efficiency of NO<sub>2</sub> decomposition depends on the latter. The energy yield of NO<sub>2</sub> decomposition by fission fragments is several times less than for decomposition by electrons and  $\gamma$ -radiation. Therefore the stationary concentration of NO<sub>2</sub> by fission fragments is several times higher than for irradiation by electrons. In air the stationary concentration is 6 vol. % for the latter [1] and 20.3% for fission fragments [8]; in a 1:1 mixture these figures are 12% and 43.7%, respectively. From an analysis of the shape of the curve of NO<sub>2</sub> concentration versus the dose (Fig. 1), it may be concluded that in the case of fission fragments Eq. (1) will be satisfied up to doses of  $7 \cdot 10^9$  rad.

Figure 2 gives the relation between the NO<sub>2</sub> energy yield and pressure for mixtures of different composition. With an increase in pressure above 1 atm the NO<sub>2</sub> energy yield increases, but does not exceed 6 mol NO<sub>2</sub>/100 eV. The energy yield also increases to some extent if the pressure falls below 1 atm. The minimum values of the energy yield at a pressure slightly above 1 atm are related to the maximum of ion recombination efficiency [1]. Table 2 gives some values of the coefficient  $k$  in relation to pressure.

In addition to nitrogen oxides, ozone is formed in nitrogen-oxygen mixtures. The ozone yield in air at 20°C is about 3.5 mol/100 eV (~8 mol/100 eV in pure oxygen). In a liquid nitrogen-oxygen mixture (1:1) the ozone yield is ~3 mol/100 eV (in liquid oxygen ~5.5 mol/100 eV). The use of the ozone radiation formation reaction for monitoring is greatly complicated by the instability of ozone at high temperature, by the fact that ozone may decompose on metal surfaces and by other factors.

Under natural conditions, with free air sampling, ozone monitoring gives satisfactory results (accuracy up to 10%) with respect to absorbed energy. Formation of deposits greatly reduces the measurement accuracy.

In addition to ionizing radiation monitoring, determination of the ozone concentration in air allows one to find the absorbed energy of electric discharges. I employed this in my method for forecasting electrical storms of low probability, which is based on the fact that absorption of discharge energy in air (and therefore the appearance of high ozone concentrations) occurs mainly 2-3 hours before the storm commences, at the time of cumulus formation.

NO<sub>2</sub> formation in nitrogen-oxygen mixtures by ionizing radiations may also be used for measuring neutron fluxes. As a result of an N<sup>14</sup>(n, p)C<sup>14</sup> nuclear reaction, irradiation of the nitrogen-oxygen mixture by protons takes place simultaneously with the formation of radiocarbon. The intensity of proton irradiation can be measured from the NO<sub>2</sub> formation rate [1]. The thermal neutron flux may be determined by means of the following equation:

$$f = 5,75a \frac{vT}{nPG}, \quad (3)$$

where  $f$  is the neutron flux, neutron/cm<sup>2</sup>·sec;  $P$  is the gas pressure in the radiation monitor, mm Hg;  $T$  is the temperature, °K;  $G$  is the NO<sub>2</sub> energy yield at the given temperature and pressure, mol/100 eV;  $v$  is the NO<sub>2</sub> formation rate, mol/cm<sup>3</sup>·sec. The coefficient  $a$  (always < 1) depends on the degree of proton energy absorption in the radiation monitor. At  $P=1$  atm and a monitor diameter of 1 cm, the value of the coefficient is 0.78, while for a diameter of 2 cm it is 0.92.

In the case of simultaneous irradiation of the monitor by neutrons and other types of ionizing radiations ( $\gamma$ -quanta, electrons, etc.) the neutron flux is

$$f = 5,75 \cdot 10^{-2} a \frac{(100v - GI) T}{nPG}, \quad (4)$$

where  $I$  is the intensity of the corresponding ionizing radiation, eV/cm<sup>3</sup>·sec.

The significance of the intensity of the accompanying ionizing radiation may be eliminated in the case of measurement of a neutron flux by two monitors with different compositions, in which the energy yields are the same. For example, if the first monitor contains 80% N<sub>2</sub> + 20% O<sub>2</sub>, and the other one 20% N<sub>2</sub> + 80% O<sub>2</sub>, the neutron flux will be

$$f = 9,3a (v_1 - 0,925v_2) \frac{T}{PG}, \quad (5)$$

where  $v_1$  and  $v_2$  are the reaction rates in the first and second monitors, respectively.

In the case of irradiation of large masses of air, particularly in a free atmosphere, the hard  $\gamma$ -radiation emitted during an N<sup>14</sup>(n,  $\gamma$ )N<sup>15</sup> nuclear reaction (and competing with the radiocarbon formation reaction) is effectively absorbed. For free air sampling the thermal neutron flux and the NO<sub>2</sub> formation rate are related as follows (here  $a=1$  and  $n=0.8$ ):

$$f = 3,47 \frac{vT}{PG}. \quad (6)$$

When air is irradiated simultaneously by neutrons and other ionizing radiation in a free atmosphere the neutron flux is

$$f = 3,47 \cdot 10^{-2} \frac{(100v - GI) T}{PG}. \quad (7)$$

The NO<sub>2</sub> formation energy yields in a nitrogen-oxygen system, necessary for calculations by Eqs. (3)-(7), may be calculated from the values of  $k$  in Tables 2 and 3, employing the relationship

$$G = 2,76 \cdot 10^8 k. \quad (8)$$

Nitrogen oxides. In addition to nitrogen itself, the oxides ( $\text{NO}$ ,  $\text{N}_2\text{O}$ , and  $\text{NO}_2$ ) may be used for monitoring ionizing radiations from nitrogen reactions. The effect of such radiation on nitrogen oxides is described in detail in [7, 9].

When these oxides are irradiated by ionizing radiations they decompose into nitrogen and oxygen. Other oxides are also formed. The relative yield of each reaction product depends on the pressure, composition, and, in some cases, the ionization density.

The energy yield of the  $\text{N}_2\text{O}$  decomposition products at 1 atm and  $20^\circ\text{C}$  when  $\gamma$ -radiation is used is 11.4 mol  $\text{N}_2\text{O}/100$  eV. Values close to 11.6 mol/100 eV are obtained in the case of  $\alpha$ -particles, protons and fission fragments. The yield of  $\text{N}_2\text{O}$  decomposition products is therefore virtually independent of the ionization density. At  $20^\circ\text{C}$  the nitrogen yield is 9.2 mol/100 eV, while the oxygen and  $\text{N}_2\text{O}$  yields are 1.3 and 4.4 mol/100 eV, respectively. The efficiency of  $\text{N}_2\text{O}$  decomposition depends on the temperature. For example, with an increase in temperature from  $0^\circ$  to  $400^\circ\text{C}$  the yield of  $\text{N}_2\text{O}$  decomposition products is increased 1.9 times.

The yield of  $\text{NO}$  decomposition products depends to some extent on the ionization density. For  $\gamma$ -radiation and electrons the yield of decomposition products is 14.8 mol  $\text{NO}/100$  eV, while for fission fragments it is 9.5-13.8 mol  $\text{NO}/100$  eV [10]. The following yields are obtained when  $\text{NO}$  is subjected to  $\gamma$ -radiation at 1 atm and  $20^\circ\text{C}$ : nitrogen, 3.8;  $\text{N}_2\text{O}$ , 0.4; and  $\text{NO}_2$ , 7.2 mol/100 eV. Within a wide temperature range the  $\text{NO}$  decomposition efficiency is virtually independent of temperature which is a clear advantage of the nitrogen oxide monitor. Thus, with an increase in temperature from  $0^\circ$  to  $400^\circ\text{C}$  the yield of  $\text{NO}$  decomposition products decreases by only 10%, this decrease taking place mainly  $> 250^\circ\text{C}$  [7].

Nitrogen dioxide is the least suitable for use as a radiation monitor [7]. For  $\gamma$ -radiation the yield of decomposition products is 2.1 mol  $\text{NO}_2/100$  eV. The nitrogen, oxygen, and  $\text{N}_2\text{O}$  yields are 0.45, 1.8, and 0.6 mol/100 eV, respectively. With an increase in temperature from  $0^\circ$  to  $400^\circ\text{C}$  the yield of  $\text{NO}_2$  decomposition products is increased seven fold, while a change in pressure from 10 mm Hg to 1.5 atm reduces it by 38%. As was mentioned above, the energy yield of the  $\text{NO}_2$  decomposition products depends markedly on the ionization density and the irradiation intensity.

Aqueous solutions of nitrogen. Data on reactions of these solutions were given in [11]. Irradiation gives nitrate, nitrite and ammonia ions. The relative yields of these products depend on the pressure of the saturated gas, its composition, irradiation temperature and, in some cases, the irradiation intensity and ionization density. Radiation-chemical reactions in aqueous solutions of nitrogen or air may also be used for monitoring.

The concentration of combined nitrogen compounds is proportional to the dose up to a certain value of the absorbed energy. For example, in the case of saturation of water with air at atmospheric pressure and use of  $\gamma$ -radiation the following results were obtained at  $20^\circ\text{C}$ :

Absorbed dose, rad $\times 10^{-8}$	1.72	3.06	5.32	7.53	8.02	9.85	15.52
Nitrate and nitrite concentration, mol/cm <sup>3</sup> $\times 10^{-17}$	1.05	2.15	3.45	4.90	5.25	6.20	6.95

From this relation it follows that the concentration of the products is proportional to the absorbed dose up to  $1.2 \cdot 10^9$  rad. At  $20^\circ\text{C}$  and saturation of water with air at 1 atm the energy yield in the case of fast electrons is 0.032 atoms of combined nitrogen in the form of nitrate, and 0.021 and 0.085 atoms of nitrogen in the form of nitrite and ammonia, respectively.

The most suitable monitoring method is to employ the sum of the nitrate and nitrite concentrations because this is not greatly affected by various factors during irradiation of aqueous nitrogen solutions. The accuracy of dosimetric measurements from reactions of free nitrogen in aqueous solution is low (10-30%), but in some cases this method provides a reliable analysis of the origin of natural and waste waters and their degree of irradiation.

Analytical procedure. The monitors are quartz or molybdenum glass ampoules (volume  $1 \text{ cm}^3 - 10^3 \text{ cm}^3$ ) filled with air or mixtures of nitrogen and oxygen or nitrogen oxides. The minimum dose reliably determinable by nitrogen-oxygen monitors depends on the accuracy of the method of analyzing the monitors. The following methods were employed in this work.

Manometric analysis is based on a specific use of convective [12] and thermoelectric [13] manometers. The nitrogen oxides are separated by vacuum distillation [7]. The minimum amount of  $\text{NO}_2$  determinable by this method is  $\sim 10^{12}$  moles; for a monitor volume of  $1 \text{ cm}^3$  this corresponds to an absorbed dose of  $\sim 10^3$  rad.

Spectrophotometric analysis [4] allows determination of the  $\text{NO}_2$  concentration in the monitor itself or in air from absorption of light with wavelengths of 390-450  $\mu$ . For a monitor volume of  $1 \text{ cm}^3$  the lower limit corresponds to  $\sim 10^4 - 10^5$  rad. The apparatus consists of a light source, a cell through which air is passed, a monochromatic illuminator, photomultiplier, galvanometer, and blower.

In the case of chemical analysis [5]  $\text{NO}_2$  is dissolved in bidistillate, and the nitric acid content is determined from the reaction with phenoldisulfonic acid and ammonia, and the nitrous acid content from the reaction with  $\alpha$ -naphthylamine and sulfanilic acid. The colored solutions are measured in a colorimeter at wavelengths of 413-508  $\mu$ . The minimum amount of acid reliably determinable by this method is  $\sim 10^{-3}$  mg. The lower limit of dose determination in a  $1 \text{ cm}^3$  monitor is  $10^6$  rad.

In some cases chemical analysis may be replaced by a determination of the amounts of reaction products from the electrical conductivity of water added in required amounts to the monitor specifically for absorption of nitrogen oxides [1]. The dissolution kinetics of  $\text{NO}_2$  in water were investigated in [3]. The electrical conductivity of the solutions is proportional to the acid concentration. The lower limit of measurements in a  $1 \text{ cm}^3$  monitor is  $5 \cdot 10^6$  rad. A monitor with electrodes for measuring electrical conductivity is suitable for remote-controlled and continuous measurements (the same is true for a monitor with a spectrophotometer).

The lower limit of measurement of a dose by a nitrogen oxide monitor may be reduced several times by increasing the monitor volume from  $1 \text{ cm}^3$  to  $10^3 \text{ cm}^3$  or by increasing the amount of irradiated air when taking samples from the atmosphere. Enrichment of the sample with nitrogen oxide is carried out during irradiation by introducing an absorbent into the monitor or by passing the gas repeatedly through liquid-nitrogen cooled traps (or passing it through packed columns filled with alkali solutions or other  $\text{NO}_2$  absorbents). In such cases the lower limit of measurement of a dose may be readily reduced to 1 rad. This limit may also be attained by increasing the length of the cell in the spectrophotometric apparatus.

The upper limit of dose measurement, limited by exhaustion of one of the reagents in the monitor or by establishing of a stationary state, is  $\sim 10^9$  rad. The range of measurement of an absorbed dose by a nitrogen oxide monitor is therefore  $1 - 10^9$  rad. The integral neutron fluxes which may be measured by a nitrogen oxide monitor are  $10^9 - 10^{20}$  neutrons/ $\text{cm}^2$ .

The upper limit of dose and integral neutron flux measurement may be increased infinitely by using open type monitors in which the reaction products are absorbed continuously by an absorbent (or small amount of alkali solution) in the walls, and the gas (e.g., air) composition remains constant. The lower limit of dose measurement may be reduced to well below 1 rad by using strong absorbents at high air flow rates, and by improving the analytical procedure, e.g., by means of electron paramagnetic resonance or mass spectrometry.

Procedure with nitrogen oxide monitors is similar to that for nitrogen-oxygen monitors [14]. When a monitor with an aqueous solution of nitrogen is used (and when samples are taken from lakes and soils) the absorbed doses are determined by chemical analysis or electrical conductivity measurements.

#### LITERATURE CITED

1. M. T. Dmitriev, Dissertation (1959).
2. M. T. Dmitriev, Zh. fiz. khim., 32, 2418 (1958).
3. M. T. Dmitriev and E. I. Zolotarev, Chemistry and Technology of Nitrogen Fertilizers [in Russian], Moscow, Goskhimizdat, p. 182 (1961).
4. M. T. Dmitriev and S. Ya. Pshezhetskii, Zh. fiz. khim., 33, 463 (1959).
5. M. T. Dmitriev and S. Ya. Pshezhetskii, Zh. fiz. khim., 34, 880 (1960).
6. P. Harteck and S. Dondes, Nucleonics, 14, 22 (1956).
7. M. T. Dmitriev, L. V. Saradzhev, and M. A. Miniovich, Zh. prikl. khim., 33, 808 (1960).
8. P. Harteck and S. Dondes, J. Phys. Chem., 63, 956 (1959).
9. M. T. Dmitriev and L. V. Saradzhev, Zh. fiz. khim., 35, 727 (1961).
10. P. Harteck and S. Dondes, J. Chem. Phys., 27, 547 (1958).
11. M. T. Dmitriev and S. Ya. Pshezhetskii, Atomnaya Energiya, 8, 59 (1960).

12. M. T. Dmitriev, *Pribory i tekhnika éksperimenta*, 3, 148 (1959).
13. M. T. Dmitriev and E. I. Zolotarev, *Tr. Gos. n.-i. in-ta proektn. azotn. prom-ti*, 12, 342 (1961).
14. M. T. Dmitriev, *Zh. prikl. khim.*, 36, 3 (1963).

---

All abbreviations of periodicals in the above bibliography are letter-by-letter transliterations of the abbreviations as given in the original Russian journal. *Some or all of this periodical literature may well be available in English translation.* A complete list of the cover-to-cover English translations appears at the back of this issue.

---

## LETTERS TO THE EDITOR

OSCILLATIONS IN A SPATIALLY NONUNIFORM PLASMA  
IN A MAGNETIC FIELD

V. G. Davidovskii

Translated from *Atomnaya Énergiya*, Vol. 15, No. 1,

pp. 60-61, July, 1963

Original article submitted October 18, 1962

Stability of a magnetized, rarefied, spatially nonuniform plasma means, from the magnetohydrodynamic viewpoint, stability with respect to long-wave oscillations which could lead to rapid macroscopic escape of plasma from the system. However, magnetohydrodynamic stability of a plasma can turn out to be instability with respect to short-wave collisionless oscillations. Such oscillations, creating local nonuniformities in the field, lead to anomalous diffusion [1], i.e., to a slow escape of plasma from the system. The rate of the anomalous diffusion process is determined by wave amplitude and by the number of particles for which resonance with the waves is possible. It is natural to suppose that, qualitatively, the magnitude of the wave amplitude is determined by the wave increments. Consequently, in studying the anomalous diffusion process, it is important to know the wave increments as functions of the projection of their phase velocity on the magnetic field direction in all regions where the main quantity of particles is contained according to the particle velocity distribution function.

As has been shown [2], a spatially nonuniform, magnetized plasma is unstable with respect to short-wave potential oscillations for arbitrary values of  $d \ln T / d \ln n$ , where  $T$  is plasma temperature and  $n$  is density. In this sense, the instability mentioned is called "universal"; but potential plasma oscillations exist only for

$$\frac{\omega/k_z}{v_A} \ll 1$$

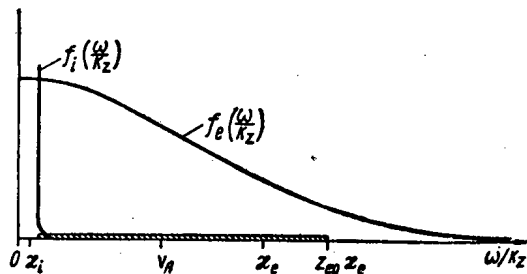
(here  $v_A$  is the Alfvén velocity). This means that, if  $v_A \ll v_e$ , the main portion of the electrons interacts with waves other than potential waves.

We shall derive a dispersion equation for the oscillations of a magnetized, rarefied, collisionless plasma with density and temperature gradients (directed along one axis) which is valid for the following conditions:

$$\frac{p^2}{H^2/8\pi} \ll 1; \quad \frac{\omega}{\omega_{Bi}} \ll 1.$$

where  $\omega$  is the frequency of the oscillation under investigation;  $\omega_{Bi}$  is the Larmor ion frequency.

We choose a coordinate system in which the  $z$  axis directed along the external magnetic field  $\mathbf{H}$ , and the  $x$  axis along the direction of the gradients. The plasma particle distribution function is chosen in the form which was used in [2]:



Phase velocity region for growing waves.

$$F = \left[ 1 + \left( x + \frac{v_y}{\omega_B} \right) \frac{d}{dx} \right] f(x); \quad (1)$$

$$f(x) = \left[ \frac{m}{2\pi T(x)} \right]^{3/2} n(x) \cdot e^{-\frac{mv^2}{2T(x)}}.$$

We consider a perturbation of the form  $\exp [i(k_y y + k_z z - \omega t)]$ , where  $k_y \gg k_z$  and, therefore, one can simply write  $\underline{k}$  in the following in place of  $k_y$ .

Using the method of integration along trajectories developed for a uniform plasma [3], it is easy to obtain  $\epsilon_{ik}$ , the dielectric susceptibility tensor, for a plasma with the distribution function (1). It has been shown that the dispersion equation,

for a perturbation of the form being considered, written out exactly up to terms in  $\frac{P^2}{H^2/8\pi}$  inclusive has the form

$$k_y^2 \epsilon_{yy} + k_z^2 \epsilon_{zz} - \frac{\omega^2}{c^2} \epsilon_{yy} \epsilon_{zz} = 0. \quad (2)$$

We introduce the following notation:

$$\begin{aligned} \kappa_i &= \sqrt{\frac{2T}{M}}; & \kappa_e &= \sqrt{\frac{2T}{m}}; \\ z_i &= \frac{\omega}{k_z \kappa_i}; & z_e &= \frac{\omega}{k_z \kappa_e}; & \theta &= \frac{k_y \kappa_i}{\omega_{Bi}}; \end{aligned}$$

$m$  is the electron mass;  $M$  is the ion mass;

$$\begin{aligned} Q &= \frac{k_y \kappa_i^2}{2\omega \omega_{Bi}} \cdot \frac{1}{n(x)} \cdot \frac{dn(x)}{dx}; \\ R &= \frac{k_y \kappa_i^2}{2\omega \omega_{Bi}} \cdot \frac{1}{T(x)} \cdot \frac{dT(x)}{dx}; \end{aligned} \quad (3)$$

$\varphi = e^{-\theta^2/2} \cdot I_0\left(\frac{\theta^2}{2}\right)$ ;  $\varphi'$  is the derivative of  $\varphi$  with respect to  $\theta$ ;  $I_0\left(\frac{\theta^2}{2}\right)$  is a Bessel function with imaginary argument;  $\omega_{0i}$  is the Langmuir ion frequency;

$$W(z) = \frac{i}{\pi} \int_{-\infty}^{\infty} \frac{e^{-t^2}}{z-t} dt.$$

Considering  $\frac{c^2}{v_A^2 \theta^2} \gg 1$ , we obtain the desired dispersion equation:

$$\begin{aligned} &2 - R(z_i^2 \varphi - z_e^2) - 2 \frac{\kappa_i^2}{v_A^2} \cdot \frac{z_i^2}{\theta^2} \left[ (1 - \varphi)(1 - Q) \right. \\ &+ \left. \varphi' \frac{\theta}{2} R \right] \left[ 1 + \varphi + Q(1 - \varphi) - R \left( \varphi' \frac{\theta}{2} + \right. \right. \\ &+ \left. \left. z_i^2 \varphi - z_e^2 \right) \right] + i \sqrt{\pi} \cdot \left\{ W(z_i) \cdot z_i \cdot \left[ \varphi(1 - Q) - \right. \right. \\ &- \left. \left. R \left( \varphi' \frac{\theta}{2} + z_i^2 \varphi - \frac{\varphi}{2} \right) \right] + W(z_e) z_e \cdot \right. \\ &\times \left[ 1 + Q + R \left( z_e^2 - \frac{1}{2} \right) \right] \left\{ 1 - 2 \frac{\kappa_i^2}{v_A^2} \cdot \frac{z_i^2}{\theta^2} \times \right. \\ &\times \left. \left[ 1 - \varphi - Q(1 - \varphi) + R \varphi' \frac{\theta}{2} \right] \right\} = 0. \end{aligned} \quad (4)$$

In the region  $\frac{\kappa_i^2 z_i^2}{v_A^2} = \frac{(\omega/k_z)^2}{v_A^2} \ll 1$ , and also within the limits  $\theta^2 \gg 1$ , Eq. (4) transforms into the equation for potential oscillations which was obtained by careful investigation [2]. In the region

$$\kappa_i \ll \frac{\omega}{k_z} \ll \kappa_e$$

the dispersion Eq. (4) agrees with the equation given without derivation in [4], and with the condition

$$v_A \ll \frac{\omega}{k_z} \ll \kappa_e$$

permits the existence of the following two types of oscillations:

$$\omega = Q_0 - \frac{\varphi' \frac{\theta}{2}}{1 - \varphi} R_0; \quad (5)$$



$$\omega = -Q_0 - \frac{i}{2} \sqrt{\pi \frac{m}{M} \kappa_i |k_z| Q_i^2 b}; \quad b = \frac{\partial \ln T}{\partial \ln n}. \quad (6)$$

However, as has been shown [5], this solution appears only for purely locally considered oscillations, and, in fact, it is therefore false.

In the region  $\frac{\omega}{k_z} \gg \kappa_e$ , using the asymptotic expansion of  $W(z)$  for  $z \gg 1$ , the dispersion Eq. (4) can be reduced to the form

$$\begin{aligned} & \left( z_e - Q_e + \frac{\Phi'}{1-\Phi} R_e \right) \cdot \left[ 1 + \frac{Q_e}{z_e} + \frac{R_e}{z_e} - \right. \\ & \left. - i \sqrt{\pi} z_e^{-2} e^{-z_e^2} (z_e + Q_e + R_e z_e^2) \right] = \\ & = - \frac{\theta^2}{\left( \frac{\kappa_e}{v_A} \right)^2} \cdot \left( z_e - Q_e + \frac{\theta}{2} \cdot \frac{\Phi'}{1-\Phi} R_e \right). \end{aligned} \quad (7)$$

where  $Q_e = \frac{Q\omega}{|k_z| \kappa_e}$ ;  $R_e = \frac{R\omega}{|k_z| \kappa_e}$ . Under the condition  $\left( \frac{\kappa_e}{v_A} \right)^2 \gg 1$  Eq. (7) in the region  $\frac{\omega}{k_z} \gg \kappa_e$  permits the existence of the following oscillations:

$$\omega = Q_0 - \frac{\Phi' \frac{\theta}{2} R_0}{1-\Phi} \quad (8)$$

[this oscillation coincides with that in (5)], and

$$\omega = -Q_0(1+b) - i2 \sqrt{\pi} |k_z| \kappa_e Q_e^6 b (1+b)^5 \cdot e^{-Q_e^2(1+b)^2} \quad (9)$$

(this oscillation grows when the condition  $-1 < b < 0$  is satisfied).

The qualitative region where the increment of  $\nu > 0$  is indicated in the figure in which the velocity distribution functions of the ions and the electrons are shown for the purposes of comparison. It is clear that only an exponentially small portion of the ions fall into resonance with the developing oscillations whereas a considerable fraction of the electrons can do so.

The author thanks R. Z. Sagdeev for advice and V. N. Oraevskii for helpful discussions.

#### LITERATURE CITED

1. A. A. Vedenov, *Atomnaya Énergiya*, **13**, 5 (1962).
2. A. A. Galeev, V. N. Oraevskii, and R. Z. Sagdeev, *Zh. Éksperim. i teor. fiz.*, **44**, No. 3 (1963).
3. V. D. Shafranov, *Plasma Physics and the Problem of Controlled Thermonuclear Reactions* [in Russian], Vol. 4, Moscow, Izd-vo AN SSSR, p. 416 (1958).
4. A. B. Mikhailovskii and L. I. Radakov, *Zh. Éksperim. i teor. fiz.*, **44**, No. 3 (1963).
5. A. A. Galeev, *idem*, No. 6.

All abbreviations of periodicals in the above bibliography are letter-by-letter transliterations of the abbreviations as given in the original Russian journal. Some or all of this periodical literature may well be available in English translation. A complete list of the cover-to-cover English translations appears at the back of this issue.

## NEW WAYS OF INCREASING THE EFFICIENCY OF THE MICROTRON

K. A. Belovintsev, A. Ya. Belyak, V. I. Gridasov,  
and P. A. Cherenkov

Translated from Atomnaya Énergiya, Vol. 15, No. 1,  
p. 62, July, 1963

Original article submitted October 25, 1962

The efficiency  $\eta$  of the microtron may be defined as the ratio of the useful power  $P_n$  required to accelerate the resonance electrons, to the minimum high frequency generator power  $P_g$  required to give stable operation of the acclerator under a given set of conditions. The expression for  $\eta$  may be written in the explicit form

$$\eta = \frac{P_n}{P_g} \approx \frac{nN\Delta E}{P_l + P_r + \frac{n\Delta E}{k} + n\Delta E(N-1)} \quad (1)$$

where  $n$  is the number of electrons accelerated per unit of time,  $N$  is the number of orbits,  $\Delta E$  is the energy added per revolution,  $P_l$  is the power loss in the waveguide,  $P_r$  is the ohmic loss in the resonator walls and  $k$  is the capture coefficient, defined as the ratio of the number of electrons in the beam to the number of electrons injected.

In microtrons of low energy of the order of 6 MeV ( $N=12$ ) the values of  $\eta$  that have been achieved so far do not exceed 7%, which is due, first, to taking out a considerable fraction of the power through the stabilizing water load [ $P_l \approx (0.5-0.6) P_g$ ] (see for example [1]), and, second, to the low value of  $k \approx 3\%$ .

To reduce the value of  $P_l$  and simplify the construction of the waveguide circuit of the accelerator in the microtron of the Photomeson Laboratory of the P. N. Lebedev Physics Institute, Academy of Sciences, USSR, a ferrite valve [2] was used as a matching and decoupling element between the magnetron generator and the accelerating resonator instead of the usual system with a water load and a phase shifter. This modification of the waveguide circuit of the microtron made it possible to increase the efficiency by a factor of about two (here  $P_l \approx 0.25 P_g$ ), and decoupling the magnetron generator from the load appreciably increased the stability of operation of the high frequency circuit as a whole.

Reducing the length of the waveguide circuit and the number of transition couplings also permitted complete evacuation of the waveguide system, in this way greatly increasing the breakdown strength. On the other hand, since the ferrite valve is simultaneously performing the functions of matching element, attenuator, and phase shifter, tuning and control of the microtron was made considerably simpler and easier, and, in addition the stability of operation was improved.

Further increase in efficiency of the microtron, as follows from Eq. (1), may be made by increasing  $k$ , which may be done by applying a positive bias to the cathode of the microtron injector. This reduces the width of the phase region of the emission current, and, accordingly, reduces the resonator load, while the width of the operating range of the initial phases remains unchanged.

In our experiments, the positive bias was applied to the cathode automatically by charging the mounting capacity of the cathode heater circuit with the emission current. The amount of bias may be adjusted smoothly by changing the internal resistance of a high voltage triode connected between the cathode and ground, i.e., by changing the leakage resistance.

Experiments have show that to a first approximation,  $k$  is a linear function of the positive bias value, with the proportionality constant depending on the dimensions of the injecting opening in the resonator and the position of the cathode.

As a result of using the above method, the capture coefficient could be increased by as much as  $\sim 10\%$ , for positive biases of  $\sim 2-3$  kV. The high frequency power thus set free may be used to accelerate an additional number of electrons.

Using these methods on the microtron at the Physics Institute, Academy of Sciences, USSR has made it possible to increase the accelerated electron current to ~110 mA in the pulse at an energy of 6.5 MeV.

It should be noted in conclusion that making any further increase in the maximum current of the microtron by means of the above methods means developing new cathode designs, since even at the currents that have been achieved there is already intense evaporation of the cathode material as a result of overheating.

LITERATURE CITED

1. S. P. Kapitsa, V. P. Bykov, and V. N. Melekhin, *Zh. Ékspserim. i teor. fiz.*, 41, 368 (1961).
2. K. A. Belovintsev, et al., *Atomnaya Énergiya*, 14, 359 (1963).

---

All abbreviations of periodicals in the above bibliography are letter-by-letter transliterations of the abbreviations as given in the original Russian journal. *Some or all of this periodical literature may well be available in English translation.* A complete list of the cover-to-cover English translations appears at the back of this issue.

---

## FAST NEUTRON POLARIZATION APPARATUS

N. V. Alekseev, U. R. Arifkhanov, N. A. Vlasov,  
V. V. Davydov, and L. N. Samoïlov

Translated from *Atomnaya Énergiya*, Vol. 15, No. 1,  
pp. 62-64, July, 1963

Original article submitted March 25, 1963

Investigating the polarization of nucleons and light nuclei in scattering and in nuclear reactions is of great interest both for finding the spin dependence of the nuclear forces, and for finding the spins of nuclei in different states. Methods for investigating the polarization of medium energy neutrons are still in the development stage, and are being developed in many nuclear physics laboratories. Systematic studies on polarized fast neutrons have so far only been made in the quite narrow energy range of 0.3-3 MeV [1]. In the Lenin Order Cyclotron Laboratory of the I. V. Kurchatov Atomic Energy Institute, studies are being proposed on polarized neutrons in the energy range 5-40 MeV. The present paper gives a description of the apparatus built for this work, and the results of measuring the polarization of the neutrons from the  $T(p, n)He^3$  reaction, carried out in this laboratory.

Figure 1 shows an over-all diagram of the equipment. In analyzing the polarization  $P$  of the neutrons, use was made of scattering by  $He^4$  at an angle of  $123^\circ$ . From the existing results, of an analysis of the nucleons scattered by  $He^4$  [2], strong asymmetry is to be expected in the scattering in this direction over a wide range of neutron energies. Gaseous  $He^4$ , containing 3-5% xenon, fills a spherical or cylindrical chamber with a glass window on one side. The helium chamber is the scintillator. The light flashes from the recoil  $\alpha$ -particles are detected by an FÉU-36 photomultiplier. The gas pressure in the chamber is about 100 atm. The scattered neutrons are detected by scintillation counters consisting of  $70 \times 100$  mm cylindrical samples of activated polished styrene and an FÉU-36. The helium chamber and the neutron counters are connected into a fast-slow coincidence circuit, which makes it possible to distinguish the desired cases of  $n-\alpha$  scattering from the different backgrounds, and at the same time use multichannel amplitude analyzers to measure the spectra of the recoil  $\alpha$ -particles selected by the coincidence circuit. Setting up two counters permits simultaneous detection of the scattering intensity "left" and "right".

To eliminate the inevitable errors in experiments of this type, coming from geometrical asymmetry in the mounting, a scheme was used which made it possible to produce  $90^\circ$  rotation in the spin of the polarized neutrons on the way from the cyclotron target to the helium chamber. The rotation was effected by means of a solenoid which produced a longitudinal magnetic field in the path of the neutrons. The plane of scattering of the neutrons makes an angle of  $90^\circ$  with the plane of the reaction. Changing the direction of the scattering from "left" to "right" or the other way around is accomplished by changing the direction of the current in the solenoid. This method was first proposed by Hillman [3].

The solenoid has 1000 turns, and is made up of 50 sections. The tube in the solenoid is made of copper, cooled by a stream of water. The 50 sections are connected in parallel in the cooling scheme. The total length of winding in the coil of the solenoid is 71 cm. The length of the solenoid with its external soft steel shield is 80 cm, and the inside diameter is 10 cm. For a current of 500 A, the field intensity in the center of the solenoid is 9.3 kOe, while the line integral is  $\int H dl = 6.62 \cdot 10^5$  Oe  $\cdot$  cm, which is sufficient to produce  $90^\circ$  rotation in the spin of a 30 MeV neutron. The resistance of the solenoid winding is  $0.82 \Omega$ .

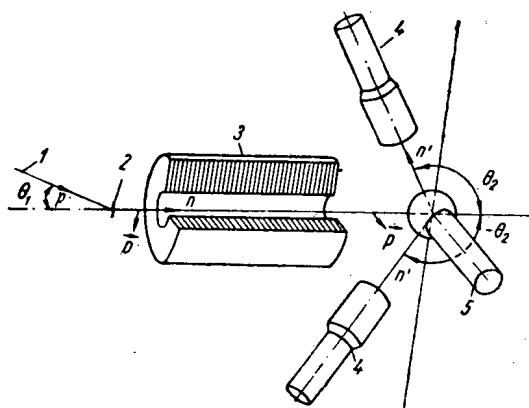


Fig. 1. Diagram of equipment: 1) cyclotron beam; 2) target (T); 3) solenoid; 4) neutron counter; 5) helium scatterer.

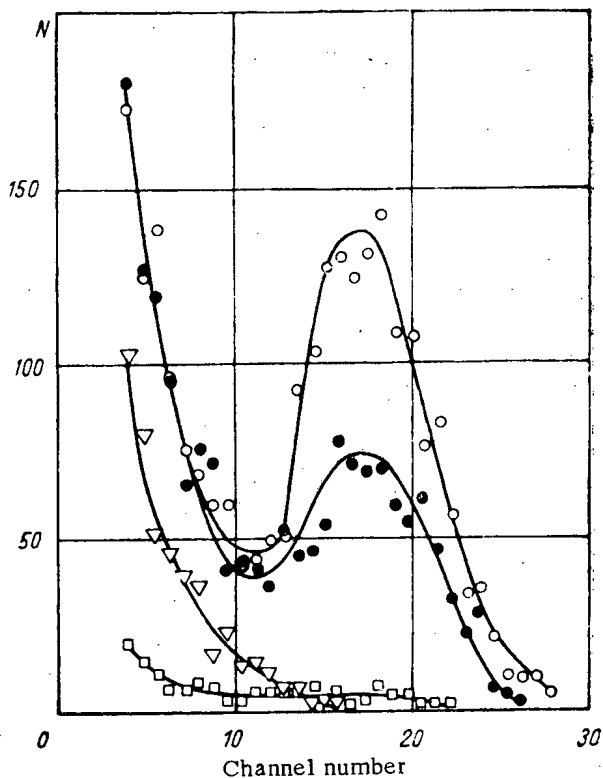


Fig. 2. Spectra of recoil  $\alpha$ -particles in helium chamber, detected in coincidence with the neutron counter, for different directions of the current in the solenoid:  $\circ$ ,  $\bullet$ ) number of counts for current "right" and "left," respectively;  $\nabla$ ) background;  $\square$ ) chance coincidence.

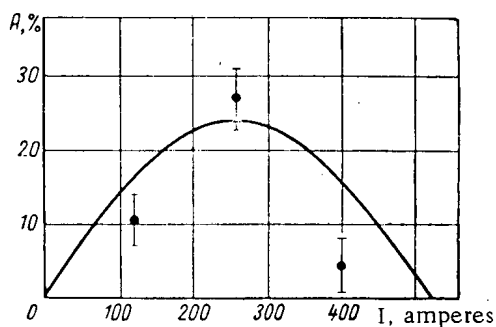


Fig. 3. Asymmetry as a function of solenoid current.

This value is in satisfactory agreement with the previous results [4, 5], and gives a more accurate value. Further, it shows that the apparatus is working properly as a neutron polarization analyzer, and that it is suitable for further measurements.

A more detailed description of the apparatus is given in a preprint of the I. V. Kurchatov Atomic Energy Institute.

\* The definition of the sign of the polarization is taken in accordance with the Basel convention.

Using this equipment, measurements were made of the magnitude and sign of the polarization of the neutrons from the  $T(p, n)He^3$  reaction with  $E_p = 10.5$  MeV at an angle of  $40^\circ$  in the laboratory coordinate systems. From measurements made by the reverse reaction method [4], and confirmed at the University of Wisconsin [5], it was found that under these conditions, it was possible to get neutrons with a degree of polarization of about 30%.

Figure 2 shows the spectra of the pulses from the  $\alpha$ -particles detected by the helium chamber, and in coincidence with the neutron counter pulses for the two directions of the magnetic field. In the range of the spectrum corresponding to the energy of the recoil  $\alpha$ -particles from the neutrons from the  $T(p, n)He^3$  reaction, the intensities of the spectra for the two directions of the field are appreciably different, which was to be expected for polarized neutrons with different directions of the solenoid field. The measurements were made both right and left of the proton beam at an angle of  $40^\circ$ . Here, as was assumed, the direction of the solenoid current corresponding to the more intense  $\alpha$ -particle spectrum changed sign, while the same amount of asymmetry was maintained within the limits of accuracy of the measurement. The current in the solenoid,  $I_0$ , corresponding to rotating the neutron spin  $90^\circ$ , is 260 A in this case. As a check, measurements were made at the points 120 and 400 A. The amount of asymmetry observed,  $A$ , is here less (Fig. 3), and within the limits of experimental accuracy followed the expected law

$$A = A_0 \sin \frac{\pi}{2} \cdot \frac{I}{I_0}.$$

The mean asymmetry,  $A_0$ , found as a result of the measurements is  $(27.4 \pm 3.9)\%$ . To obtain the value of the polarization, use may be made of the analyzing ability of the helium analyzer, given in [2]. Averaging over the range of scattering angles for the geometric conditions of the experiment (helium chamber diameter 11 cm, neutron counter diameter 7 cm, distance between them 40 cm) gives the value 0.96 for the analyzer asymmetry. For the polarization of neutrons from the  $T(p, n)He^3$  reaction at  $E_p = 10.5$  MeV at an angle of  $\theta_1 = 40^\circ$ , the value is  $P = (-28.6 \pm 4.1)\%$ .\*

LITERATURE CITED

1. H. Barschall, Proceedings of the International Symposium on Polarization Phenomena of Nucleous, Basel, p. 227 (1961).
2. I. I. Levintov, A. V. Miller, and V. N. Shamshev, Zh. Ėksperim. i teor. fiz., 32, 274 (1957).
3. P. Hillman, G. Stafford, and C. Whitehead, Nuovo Cimento, IV, 67 (1956).
4. K. P. Artemov, N. A. Vlasov, and L. N. Samoïlov, Zh. Ėksperim. i teor. fiz., 37, 1184 (1959).
5. R. L. Walter, et al., Nucl. Phys., 30, 292 (1962).

---

All abbreviations of periodicals in the above bibliography are letter-by-letter transliterations of the abbreviations as given in the original Russian journal. *Some or all of this periodical literature may well be available in English translation.* A complete list of the cover-to-cover English translations appears at the back of this issue.

---

THE NUMBER OF PROMPT NEUTRONS AND THE KINETIC ENERGY  
OF FRAGMENTS DURING LOW-ENERGY FISSION OF  $U^{235}$

Yu. A. Blyumkina, I. I. Bondarenko, V. F. Kuznetsov,  
V. G. Nesterov, V. N. Okolovich, and G. N. Smirenkin

Translated from *Atomnaya Énergiya*, Vol. 15, No. 1,  
pp. 64-66, July, 1963

Original article submitted August 4, 1962

Several papers [1-3] have been published recently on deviations of the energy relation of the mean number of prompt neutrons  $\bar{\nu}$  and of the mean kinetic energy of fission fragments  $\bar{E}_k$  from hitherto accepted ideas on these fission characteristics. Such ideas are based on Fowler's hypothesis that  $\bar{E}_k$  is unrelated to the excitation energy of the nucleus undergoing fission, and on the resultant assumption that  $\bar{\nu}$  increases linearly with increasing energy of the neutrons  $E_n$  causing fission [4]. It is known that these laws are correct at fairly high  $E_n$  [2, 5]. But at low  $E_n$ , when the excitation energy in the saddle point of the nucleus  $E^*$  is of the order of the distance between the fission channels 0.7-0.8 MeV [6], hitherto unconsidered effects may occur due to the discreteness of their spectrum.

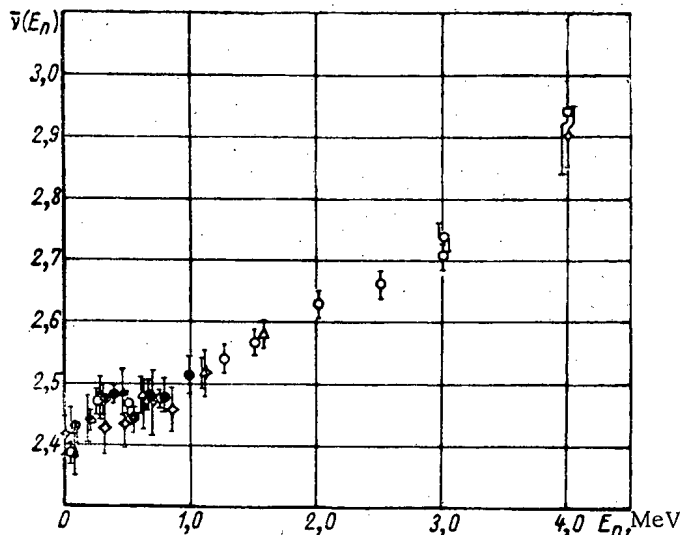


Fig. 1. Energy relation between  $\bar{\nu}$  and  $E_n$ . The data are taken from the following sources: ●, ▲) obtained with a scintillation detector and thorium chamber, respectively (our work); ○) [3]; ▽) [10]; △) [11]; ◇) [12]; □) [13].

The first theories on the behavior of the relation between  $\bar{\nu}$  and  $\bar{E}_k$  and  $E_n$  taking into account the discrete spectrum of the channels were put forward by V. N. Andreev [7], who forecast the deviation of the energy relation  $\bar{\nu}(E_n)$  from linear increase.

Our aim was to make a more thorough investigation of possible irregularities in this relation. In addition to its considerable practical importance, an experimental investigation of the energy relation of  $\bar{\nu}$  and  $\bar{E}_k$  may assist in understanding the nature of fission channels and the distribution mechanism of the energy produced.

Using a  $U^{235}$  target nucleus, we investigated the energy relations  $\bar{\nu}(E_n)$  for  $E_n = 0-1.0$  MeV and  $\bar{E}_k(E_n)$  for  $E_n = 0-2.5$  MeV. The measurements were made in an electrostatic generator, using a  $T(p, n)$  reaction.

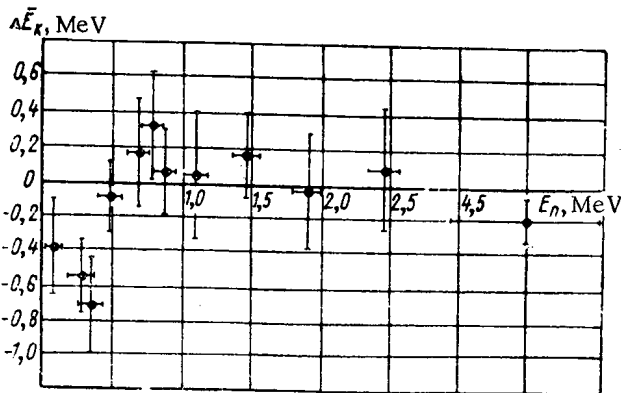


Fig. 2. Relation between the difference  $\Delta E_k$  of mean kinetic energies during fission of  $U^{235}$  by thermal neutrons, on the one hand, and the energy of the fission neutrons on the other.

The value of  $\bar{\nu}$  was determined in two stages: first we determined the relative course of the relation  $\bar{\nu}(E_n)$  and then calibrated the relations obtained against the value of  $\bar{\nu}_T$  for hot neutron fission. The relative course was measured by recording the neutrons emitted by  $U^{235}$  disks (thickness 3 mm and diameter 30 mm) by means of threshold detectors: a stilbene scintillation counter with discrimination of  $\gamma$ -rays with respect to luminescence time, and a multilayer thorium fission chamber (two different experiments). The relative number of fissions in the disk was determined by counting the fragments in the  $U^{235}$  layer close to both sides of the disk. The ratio of the counts of the neutron detector to those of the fission chamber with  $U^{235}$  layers served as the  $\bar{\nu}$ -proportional monitor.

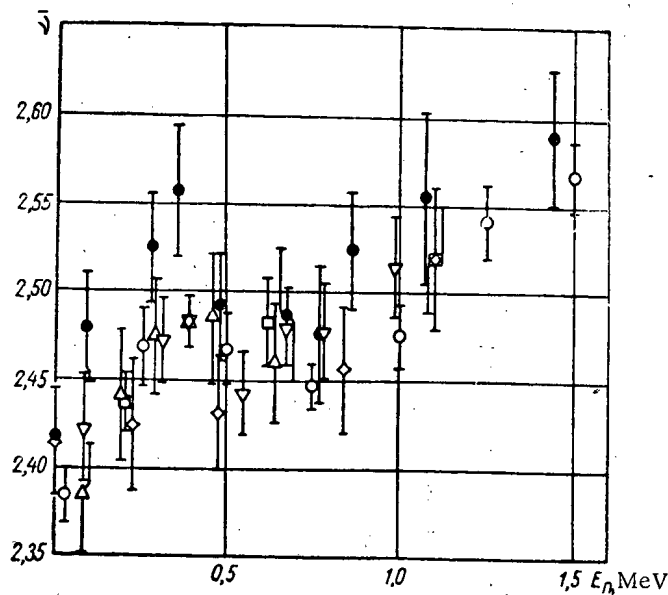


Fig. 3. Agreement between the results of measurements of  $\bar{E}_k$  and  $\bar{\nu}$ . ●) Values of  $\bar{\nu}$  calculated from  $\Delta \bar{E}_k$  data in accordance with the balance equation; ▽, Δ) data obtained with a scintillation detector and a thorium fission chamber (our work); ○, □, ◇) data from [3, 11, 12].

As a result of the measurements, slight corrections were made to compensate a number of effects influencing the proportionality coefficient between the measured ratios and  $\bar{\nu}$  (angular anisotropy of the separation of fragments [8], increase in the fission neutron energy with increasing excitation energy of the fragments [9], neutron multiplication in the disk). For calibration, consisting in comparison of  $\bar{\nu}$  (for a reference energy  $E_n = 0.39$  MeV) with  $\bar{\nu}_T = 2.42$ , we used the accepted method of recording the coincidences between the fission chamber and a  $BF_3$  counter lump in paraffin. Figure 1 gives the final results and a comparison of these with data of other investigators. But direct comparison of all known experimental data so as to establish the direct relation between  $\bar{\nu}$  and  $E_n$  is impossible because most of the data are from reviews which refer to unpublished information; further, in many cases they are based on unknown calibration methods and on differing and redundant standard values of  $\bar{\nu}$ . Therefore, Fig. 1 gives only those data [4, 10-12] determined on monoenergy neutrons in the form of the ratio  $\bar{\nu}(E_n)/\bar{\nu}(E_T)$ , and the results of recent very detailed measurements of  $\bar{\nu}$  by Moat, et al.[3].



The relation between the mean kinetic energy of fission fragments  $\bar{E}_k$  and  $E_n$  was determined by means of an ionization chamber with a grid by measuring the ratio  $\bar{E}_k(E_n)/\bar{E}_k^T$ , where  $\bar{E}_k^T = 166$  MeV is the mean kinetic energy of fragments obtained by thermal neutron fission. This method was described in detail in [2]. Figure 2 gives the results of measurements in the form of the difference  $\Delta\bar{E}_k = \bar{E}_k(E_n) - \bar{E}_k^T$ .

From Figs. 1 and 2 it may be seen that the experimental values of  $\bar{\nu}$  and  $\bar{E}_k$  measure much the same parameter. An attempt may be made to represent the correlation between these data quantitatively by employing the equation for the balance of the energy produced during fission. Assuming that the distribution of the fragment masses and charges and the energy removed by  $\gamma$ -rays are independent of the fission neutron energy, we obtain

$$E_n = \Delta\bar{E}_k + a\Delta\bar{\nu},$$

where  $\Delta\bar{E}_k$  and  $\Delta\bar{\nu}$  are the changes in  $\bar{E}_k$  and  $\bar{\nu}$  in comparison with the values of  $\bar{E}_k^T$  and  $\bar{\nu}$  ( $E_T$ ) for thermal neutron fission. The parameter  $a$  virtually agrees with the reciprocal

$$\frac{d\bar{\nu}}{dE_n} \approx 0,13 \text{ MeV}^{-1},$$

which characterizes the linear increase in  $\bar{\nu}$  with increasing  $E_n$  in the region of fairly high excitation energies.

Figure 3 gives a comparison of the values of

$$\bar{\nu}' = \bar{\nu}_r + \frac{d\bar{\nu}}{dE_n} \times (E_n - \Delta\bar{E}_k),$$

calculated from  $\Delta\bar{E}_k$  data by the above-mentioned ratio, with the results of direct measurements of  $\bar{\nu}$  in the  $E_n$  range from 0 to 1.5 MeV (of most interest to us). From these data it follows that the character of the energy relation of the values of  $\bar{\nu}$  and  $\bar{\nu}'$ , measured here and in [3], is the same and shows a characteristic convexity in the region  $0 < E_n < 0.5$  MeV, whereas the results of Diven and Hopkins [12] have the opposite tendency. Further, within the limits of experimental error and the accepted value of the parameter

$$a \approx \left( \frac{d\bar{\nu}}{dE_n} \right)^{-1}$$

our data for  $\bar{\nu}$  and the results of relative measurements of  $\bar{E}_k$  agree quantitatively with one another. This indicates that the change in fragments mass distribution also takes place in this region of  $E_n$  and within very narrow limits, corresponding to the accuracy of the check of the balance of the energy produced ( $\sim 0.3$  MeV).

Our main object was to find deviations from Fowler's hypothesis at  $E_n < 1$  MeV. At higher energies this hypothesis is satisfied up to  $E_n \approx 5$  MeV to an accuracy of 0.2-0.3 MeV. This trend must evidently be attributed to the fact that at low energies fission takes place via a few channels (the individual properties of the latter coming into play during this process), whereas at high energies a fairly large number of channels are involved; therefore, an effect which is averaged out over the channels as a whole is observed in the experiment. In particular, the experimental results indicate different kinetic energies of the fragments and a corresponding difference in  $\bar{\nu}$  in the case of s- and p-neutron fission, i.e., for fission via channels of different symmetry.

L. N. Usaev has made a number of suggestions based on a specific model of fission channels; these make it possible to interpret the behavior of  $\bar{\nu}$  and  $\bar{E}_k$ , but are outside the scope of this paper. We will merely mention that, according to his interpretation, as one passes from s-neutron to p-neutron fission of a  $U^{233} (5/2)^+$  target nucleus the kinetic energy of the fragments must increase by roughly the same amount by which it falls in the case of  $U^{235} (7/2)^-$ . Our preliminary results obtained from  $\bar{E}_k$  measurements for  $U^{233}$  agree with this prediction.

We wish to express our thanks to A. I. Leipunskii for his constant interest in this work, to L. N. Usaev and V. N. Andreev for discussing the experimental results, and to V. I. Bol'shov, L. D. Gordeeva, and L. I. Prokhorova for helping in the work and the measurements.

#### LITERATURE CITED

1. I. I. Bondarenko, Physics of Fast and Intermediate Reactors, Proc. of a Seminar, Vienna (1961); V. III. Vienna, p. 450 (1962); *Atomnaya Énergiya*, 12, 461 (1962).
2. V. N. Okolovich, G. N. Smirenkin, and I. I. Bondarenko, *Atomnaya Énergiya*, 12, 461 (1962).

3. A. Moat, D. Mather, and P. Fieldhouse, *Physics of Fast and Intermediate Reactors*, Proc. of a Seminar, Vienna, (1961); V. I. Vienna, p. 139 (1962).
4. R. Leachman, *Phys. Rev.*, 101, 1005 (1956).
5. I. I. Bondarenko, *Proceedings of the Second International Conference on the Peaceful Uses of Atomic Energy*, Geneva (1958); *Reports of Soviet Scientists [in Russian]*, 1, Moscow, Atomizdat, p. 438 (1958).
6. J. Northrop, et al., *Phys. Rev.*, 115, 1277 (1959).
7. V. N. Andreev, *Abstract of Report to the Conference on Nuclear Fission [in Russian]*, Leningrad, Izd-vo AN SSSR (1961).
8. V. G. Nesterov, G. N. Smirenkin, and I. I. Bondarenko, *Atomnaya Énergiya*, 11, 249 (1961).
9. G. N. Smirenkin, *Zh. éssperim. i teor. fiz.*, 37, 1822 (1959).
10. R. Leachman, *Proceedings of the Second International Conference on the Peaceful Uses of Atomic Energy*, Geneva (1958); *Selected Reports on Foreign Scientists [Russian translation]*, 2, Moscow, Atomizdat, p. 342 (1959).
11. D. Butler, et al., *Physics of Fast and Intermediate Reactors*, Proc. of a Seminar, Vienna (1961); V. I. Vienna, p. 125 (1962).
12. B. Diven and J. Hopkins, *Physics of Fast and Intermediate Reactors*, Proc. of a Seminar, Vienna (1961); V. I. Vienna, p. 149 (1962).
13. G. N. Smirenkin, et al., *Atomnaya Énergiya*, 4, 188 (1958).

---

All abbreviations of periodicals in the above bibliography are letter-by-letter transliterations of the abbreviations as given in the original Russian journal. *Some or all of this periodical literature may well be available in English translation.* A complete list of the cover-to-cover English translations appears at the back of this issue.

---

THE OPTIMUM CONDITION FOR BIOLOGICAL SHIELDING  
AGAINST A NUMBER OF RADIATION SOURCES

G. A. Lisochkin

Translated from Atomnaya Énergiya, Vol. 15, No. 1,  
pp. 67-68, July, 1963  
Original article submitted January 23, 1963

In many practical cases biological shielding must attenuate the radiation from several sources. In view of this, we may consider the problem of optimizing the fractional contributions made by the different sources to the total dose rate. The optimum fractional contribution in this case should be taken to be the one for which the total dose rate is a minimum when the total weight of the shielding is fixed.

As our simplest example, let us define the optimum condition for the case when the dose rate at a given point depends on the radiation from two sources, each of which is separately shielded, that is, when changing the dimensions of the shield of one source does not affect the dose rate from the other source. (The method used in this discussion may equally well be used to determine the optimum biological shielding for any number of sources.)

The variation of the shielding weight  $q$  that changes the dose rate from one source by a factor of  $e$  is represented by

$$q = \rho L S, \quad (1)$$

where  $\rho$  is the density of the shielding material,  $L$  is the relaxation length of the radiation, and  $S$  is the surface area of the shielding for which the thickness is varied.

Thus, the relationship between the dose rate  $f$  from one source and the change  $x$  in shielding weight can be expressed as follows:

$$f = p e^{-x/q}, \quad (2)$$

where  $q$  is the above defined weight characteristic for the shielding material;  $p$  is the dose rate from a given source for some variant of the shielding. Then the total dose rate from the two sources is

$$P = p_1 e^{-x_1/q_1} + p_2 e^{-x_2/q_2}. \quad (3)$$

We must determine the minimum of the dose rate, that is, of the function  $P(x_1, x_2)$  for a fixed shielding weight:

$$\varphi = x_1 + x_2 = 0.$$

The given problem of finding the relative extremum may be solved by the method of Lagrangian multipliers. The extremum condition is

$$\left. \begin{aligned} \frac{\partial P}{\partial x_1} + \lambda \frac{\partial \varphi}{\partial x_1} &= 0; \\ \frac{\partial P}{\partial x_2} + \lambda \frac{\partial \varphi}{\partial x_2} &= 0; \\ x_1 + x_2 &= 0, \end{aligned} \right\} \quad (4)$$

where  $\lambda$  is an arbitrary Lagrangian multiplier.

Performing the necessary differentiation and solving the system of equations for the unknowns, we find

$$x_1 = -x_2 = \frac{\ln \left( \frac{p_1 q_2}{p_2 q_1} \right)}{q_1 + q_2} q_1 q_2. \quad (5)$$

It follows from this that at the optimum point the dose rate from the given source  $p_1^0$  and the corresponding weight characteristic  $q_1$  are related by the following equation (which can easily be extended to a larger number of sources):

$$\frac{p_1^0}{q_1} = \frac{p_2^0}{q_2} = \dots = \frac{p_n^0}{q_n} \quad (6)$$

In determining those fractional contributions made by the different sources which correspond to a minimum of the shielding weight for a fixed total dose rate, the extremum condition obtained by using the Lagrangian multiplier method will be expressible by a system similar to the system (4), the only difference being that the functions  $\varphi$  and  $P$  are interchanged and the last equation is replaced by the condition that  $P$  remains constant.

It is readily shown that the new system has the same solution as (4) and both formulations of the optimum condition are equivalent; this also follows from self-evident considerations.

Another problem of practical importance is the determination of the extremum condition for two geometrically coincident sources which emit different types of radiation (for example, neutrons and gamma quanta) and a combined shield consisting generally of two components each of which is more effective for one of the types of radiation. Such components may be, for example, water and lead. A variation in the thickness of the component designed to attenuate one type of radiation produces a change in the dose rate from the other. In this case the equation similar to (3) and showing the variation of the dose rate as a function of the shielding weight will be of the form

$$P = p_1 e^{-\left(\frac{x_1}{q_{11}} + \frac{x_2}{q_{12}}\right)} + p_2 e^{-\left(\frac{x_1}{q_{21}} + \frac{x_2}{q_{22}}\right)}, \quad (7)$$

where  $p_1$  and  $p_2$  are the dose rates of the two types of radiation behind the shield in the original (nonoptimal) case;  $x_1$  and  $x_2$  are the changes in the weight of the shielding components, each of which is more effective for a given type of radiation;  $q_{11}$ ,  $q_{12}$ , and  $q_{22}$ , are the weight characteristics of each of the shielding components for a given form of radiation, defined as in (1).

We shall seek an extremum condition for formula (7) which fulfills the auxiliary requirement

$$\varphi = x_1 + x_2 = 0.$$

After differentiating and performing the necessary transformations on the system (4), we obtain the equation

$$p_1^0 \left( \frac{1}{q_{11}} - \frac{1}{q_{12}} \right) = p_2^0 \left( \frac{1}{q_{22}} - \frac{1}{q_{21}} \right), \quad (8)$$

which makes it possible to determine that relationship between the intensities of different types of radiation which corresponds to the minimum total dose rate for a fixed shielding weight.

As an example, let us find the optimum relationship between the dose rate from neutrons (first source) and 7-MeV gamma quanta (second source). We shall assume, in accordance with common practice, that water is used as shielding against the first source and lead against the second. Since the shielding thickness in this case can be corrected chiefly by means of the outer layers, situated at an approximately equal distance from the radiation source, we have reasonable justification for considering the areas  $S_1$  and  $S_2$  equal. From the structure of formula (8) it is readily seen that the area of the shielding section  $S$  may then be taken equal to unity.

Using the appropriate data on removal cross sections for fast neutrons and attenuation coefficients for gamma quanta for 7-MeV gamma quanta, we find by formula (1)

$$q_{11} = 10 \text{ g}; \quad q_{12} = 104 \text{ g}; \quad q_{22} = 22,2 \text{ g}; \quad q_{21} = 39 \text{ g}.$$

In this case, from Eq. (8), we can readily find

$$\frac{p_1^0}{p_1^0 + p_2^0} = 0,17. \quad (9)$$

The above example shows that for a minimum shielding weight the dose rate from the neutrons should be of the order of 15-20% of the total dose rate of penetrating radiation.

Since the removal cross section for fast neutrons was used in the calculation, it is assumed that the shielding satisfies the conditions for which that quantity may properly be used.

In the present problem the use of the attenuation coefficient for a narrow beam of gamma rays is allowable, since in correcting the shielding thickness near the optimum value we may neglect, for practical purposes, the variation in the build-up factor found for the total shielding thickness.

Another characteristic example of the use of the above formulas may be found in the problem of the optimal contribution made by different gamma ray sources at a nuclear power installation to the total dose of penetrating radiation. Among such sources we may mention the gamma radiation of the active zone, the capture gamma radiation of the iron-water structure of the biological shielding, the gamma radiation of the activated water, etc. In all of these cases the radiation intensity outside the shielding depends chiefly on the hard component (about 7 MeV) of the gamma ray spectrum.

Since the above sources are situated within the biological shielding at different distances from the surface, in most cases it is possible to make individual changes in the contribution of each of them to the total dose rate outside the shielding. Formula (6) may be used in this connection. If the optimum condition (6) is satisfied by correcting the same shielding material (for example, lead), then the quantity  $\rho L$  has the same value for all gamma radiation sources. In this case Eq. (6) yields

$$\frac{P_1^0}{S_1} = \frac{P_2^0}{S_2} = \dots \quad (10)$$

In particular, in the plane case we should ensure that each of the main gamma radiation sources of a nuclear power installation makes an equal contribution to the total dose rate of penetrating radiation.

In addition to the above problems, which are most frequently encountered in shielding design practice, the above optimization method may also be extended to other individual cases.

In conclusion, the author considers it his pleasant duty to express his sincere thanks to D. L. Broder for the interest he has shown in the work.

THE STRUCTURE OF THE GAMMA RADIATION FIELD FROM AN ISOTROPIC  
POINT SOURCE IN ALUMINUM WITH BARRIER GEOMETRY

V. A. Vorob'ev

Translated from *Atomnaya Énergiya*, Vol. 15, No. 1,  
pp. 68-70, July, 1963

Original article submitted July 6, 1962

In recent years there have been a number of published experimental and theoretical studies investigating the structure of the gamma radiation field of local sources in barrier geometry [1, 2]. For the most part, detailed studies of the differential spectral-angular distribution of gamma quanta have been made only for points in the boundary plane, at the foot of the normal from the source center [3, 4]. To solve the numerous problems of applied radio-metry (geophysical prospecting, shielding from ionizing radiation, etc.), we must know the structure of the gamma radiation field under conditions of barrier geometry in an absorbing medium.

In the present study we consider the gamma radiation field formed by an isotropic point source (with quantum energies  $E_0 = 0.661, 1.0, 1.38, \text{ and } 2.62$  MeV) situated in a semiinfinite absorber (aluminum) at depths  $H$  equal to 0, 0.5, 1, and 2 mean free paths of the primary radiation. The majority of the gamma quanta will be emitted through a small element of surface whose dimensions, because of the absorption in the scattering material (aluminum), do not exceed 2-3 mean free paths, that is, some tens of centimeters. For that reason, at distances greater than 1-2 m (the most commonly encountered case) this surface element may be regarded as a point and the radiation emitted through it may be characterized solely by the gamma quanta energy  $E$  and the azimuth angle  $\theta$  measured from the normal to the surface of the scattering material.

The Monte Carlo method [5] was used to determine the spectral-angular distribution of the gamma radiation emitted through the boundary surface.

For convenience in calculation the coefficients of interaction with the medium, taken from [6], were approximated by polynomials with an accuracy no worse than 10%.

The pseudo-random numbers were generated by an electronic calculator using a specially selected program.

Each gamma quantum was tracked until it left the medium or its energy fell below 0.03 MeV.

The investigation showed that the contribution which the scattered radiation from deep layers made to the total energy intensity decreased exponentially and became negligible for  $H > 2$ .

Consequently, for economy of computer time the gamma quanta originating from a depth of more than two mean free paths were assumed to have been absorbed and were left out of consideration.

In the matrix of final results the graduation in angular values was taken through  $15^\circ$ . In energy graduation the first intervals were taken at 0.03-0.05 and 0.05-0.10 MeV, and thereafter 0.1 MeV intervals were used, apart from the case  $E_0 = 2.62$  MeV, where, starting with  $E = 0.5$  MeV, the interval width was taken as 0.25 MeV.

#### Results of the Albedo Calculations

Figures 1a and 1b show the curves of the spectral-angular distribution of the intensity of the reflected gamma radiation  $I(E_0, E, \theta) = EN(E_0, E, \theta)$  for  $E_0$  equal to 1.0 and 2.62 MeV, normalized to primary radiation fluxes of unity.

From an analysis of the calculation results the following conclusions can be drawn:

1. All the energy distributions for the gamma radiation have a maximum (peak) at  $E \approx 0.25$  MeV, with an amplitude which decreases almost linearly with the angle of inclination  $\theta$ , with a slight dip (about 20 units) at  $\theta \approx 40^\circ$ . As  $E_0$  varies, the relative contribution made by the peak to the albedo and its absolute value vary almost linearly.\*

\*Calculations in which the reflection from the upper half-space (homogeneous medium) was taken into consideration indicate that because there is multiple albedo, contributing chiefly in the soft region of the spectrum, the position of the peak is displaced to  $E \approx 0.1$  MeV, in accordance with the data obtained by the method of moments [7].

As the angle  $\theta$  increases, harder quanta appear in the reflected radiation, so that a second maximum (peak) is formed, primarily caused by the singly scattered quanta and having an amplitude practically independent of  $\theta$ . The upper energy limit of the peak corresponds to the maximum possible energy of singly scattered gamma quanta in that direction.

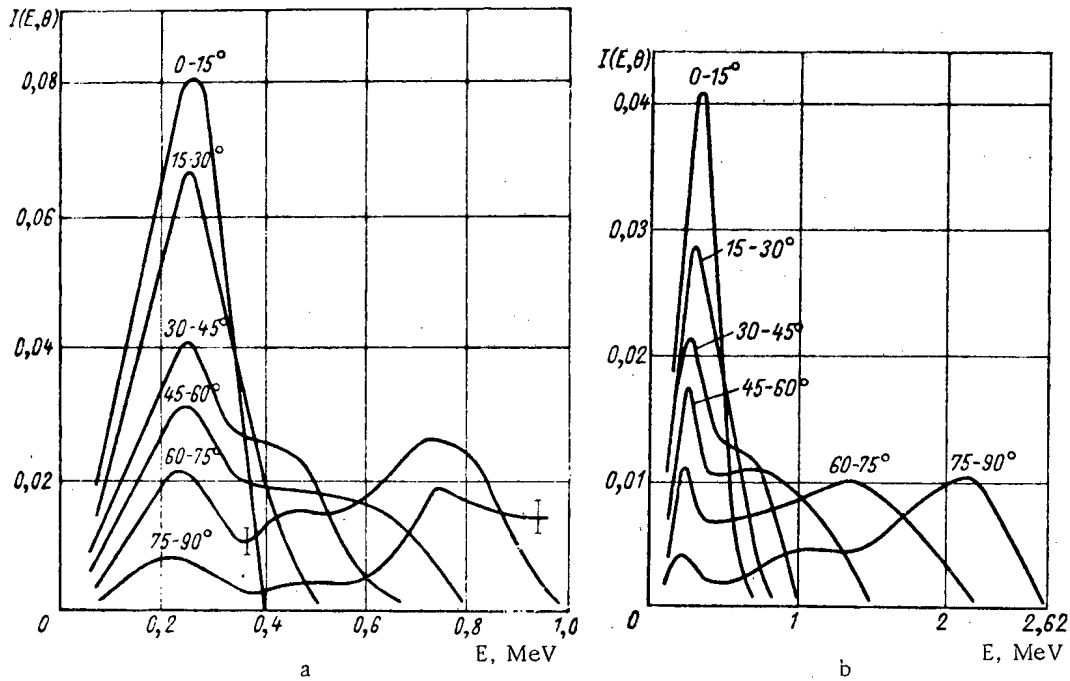


Fig. 1. Spectral-angular distribution of the intensity of reflected gamma radiation from an isotropic point source, with  $E_0$  equal to: a) 1 MeV; b) 2.62 MeV.

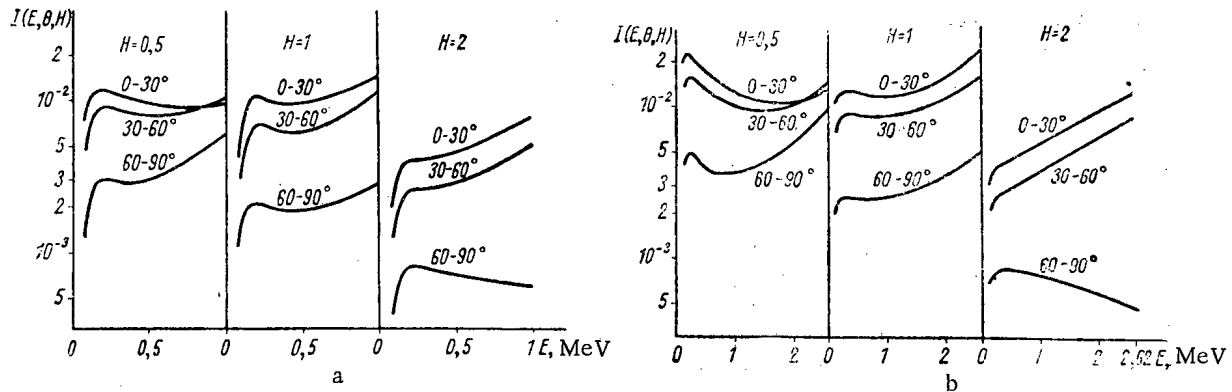


Fig. 2. Spectral-angular distribution of gamma radiation from an isotropic point source with  $E_0 = 1$  MeV (a) and 2.62 MeV (b), situated at a depth of 0.5, 1, or 2 mean free paths.

2. We calculated the mean energies of reflected gamma quanta as a function of the observation angle  $\theta$ , as well as the mean energies of the total albedo for each  $E_0$ , that is, the quantities

$$E(E_0, \theta) = \frac{\int I(E_0, E, \theta) dE}{\int N(E_0, E, \theta) dE} = \frac{I(E_0, \theta)}{N(E_0, \theta)}$$

and

$$E(E_0) = \frac{2\pi \int I(E_0, \theta) \sin \theta d\theta}{2\pi \int N(E_0, \theta) \sin \theta d\theta} = \frac{I(E_0)}{N(E_0)}$$

$\bar{E}(E_0, \theta)$  increases with increasing  $\theta$ , and the rate of increase is greatest for  $\theta > 60^\circ$ . For albedo in the vertical direction, that is, for  $\theta \approx 0^\circ$ ,  $\bar{E}(E_0, \theta) \approx 0.2 E_0^{0.2}$ , and for  $\theta > 75^\circ$ ,  $\bar{E}(E_0, \theta) \approx 0.5 E_0^{0.75}$ .

As shown by the calculations,  $\bar{E}(E_0) = 0.30 \sqrt{E_0}$ , with an accuracy of the order of several percent.

3. The angular distribution of the total number of reflected gamma quanta per unit solid angle  $N(E_0, \theta)$  depends only slightly on the primary energy, and for observation angles  $\theta < 70^\circ$ , it may be described with an accuracy of about 15% by the function

$$ae^{-\frac{\theta}{75}}$$

The angular distribution of the energy flux per unit solid angle  $I(E_0, \theta)$  for  $\theta < 70^\circ$  at  $E_0 > 2$  MeV is close to the isotropic distribution (with a slight drop of about 15% in the region  $\theta \sim 45^\circ$ ) and tends to a cosinusoidal distribution as the primary energy decreases.

4. The total albedo with respect to the number of particles in the observed interval of primary energies may be approximated by the function  $R_N(E_0) = 0.41 \cdot E_0^{-0.2}$ , and the energy albedo by  $R_E(E_0) = 0.12 \cdot E_0^{-0.75}$ . The resulting values agree to within less than 10% with the results of [1].

#### Point-Source Gamma Radiation Passing Through a Layer

Figure 2 shows the curves of the spectral-angular distribution of the gamma quantum intensity  $I(E_0, E, \theta, H)$  of an isotropic point source with  $E_0 = 1$  MeV and 2.62 MeV, placed at a depth of 0.5, 1, or 2 mean free paths. The curves are normalized to unit source intensity.

From an analysis of similar curves for the set of primary energies and depths we draw the following conclusions:

1. In contrast to the energy distribution of gamma radiation in a homogeneous medium, the spectrum of quanta passing through a layer thicker than one mean free path has practically no peak in the soft region.
2. The mean energies of scattered gamma quanta  $\bar{E}(E_0, \theta, H)$  for depths  $H \leq 0.7$  increase with increasing angle  $\theta$ , reaching a value of about  $0.5 E_0$ .

For large absorber thicknesses the quantity  $\bar{E}(E_0, \theta, H)$  varies comparatively little (about 30%) and assumes maximum values of the order of  $0.4 E_0$  for angles  $40^\circ \leq \theta \leq 60^\circ$ .

3. The angular dependence of the number of scattered quanta per unit solid angle depends only slightly on the primary energy, and for  $H \geq 0.5$  it may be described, with an accuracy of about 20%, by a linear function of  $H$  and  $\theta$ . In particular, if  $E_0 = 1$  MeV, for a source with unit activity

$$N(E_0, \theta, H) = \frac{0.27 - 0.1 H}{1 - \frac{\theta}{90}}$$

The angular characteristic of the energy flux for scattered quanta  $I(E_0, \theta, H)$  for  $H = 0.5$  is approximately cosinusoidal. As  $H$  increases, the directionality increases somewhat.

4. The total intensity, both for the number of emitted scattered quanta  $N(E_0, H)$  and for their energy  $I(E_0, H)$ , reaches a maximum if the source is located in the absorber at a depth of  $H \approx 1/3$  from the boundary surface.

5. The ratios of  $N(E_0, H)$  and  $I(E_0, H)$  to the primary radiation intensities are of the nature of integral build-up factors  $B_N(E_0, H) - 1$  and  $B_E(E_0, H) - 1$ ; in the depth and energy intervals under consideration they may be approximated, with an accuracy of about 10-15%, by the functions

$$\begin{aligned} B_N(E_0, H) - 1 &= R_N(E_0) + 2.95 \cdot E_0^{-0.42} H, \\ B_E(E_0, H) - 1 &= R_E(E_0) + 1.08 \cdot E_0^{-0.57} H, \end{aligned}$$

where  $R(E_0)$  is the albedo for the corresponding primary radiation.

In conclusion, the author expresses his gratitude to R. M. Kigan for his appraisal of the results obtained, as well as Z. D. Dobrokhovova and E. N. Goryanina for their help with the calculations.



LITERATURE CITED

1. M. Berger and D. Raso, *Radiation Res.*, 12, 20 (1960).
2. M. Berger, *J. Appl. Phys.*, 28, 1052 (1957).
3. Yu. A. Kazanskii, *Atomnaya Énergiya*, 8, 432 (1960).
4. G. Whyte, *Canad. J. Phys.*, 33, 96 (1955).
5. M. Berger, *J. Res. Nat. Bur. Standards*, 55, 343 (1955).
6. C. Davisson and R. Evans, *Rev. Mod. Phys.*, 24, 79 (1952).
7. H. Goldstein and I. Wilkins, *Calculation of Penetration of Gamma Rays*, NYO-3075 (1954).

THE RATIO OF THE THERMAL NEUTRON FLUX IN WATER  
TO THE POWER OF A POINT SOURCE

E. A. Garusov and Yu. V. Petrov

Translated from Atomnaya Énergiya, Vol. 15, No. 1,

p. 71, July, 1963

Original article submitted October 13, 1962

The value of the parameter  $\Phi_t/W$  (the ratio of thermal neutron flux to reactor power) for research reactors was given in [1]. The same report contained a calculation in the age-theory approximation of the maximum value  $\Phi_t/W$  for a point source with no self-absorption in an infinite medium consisting of a number of substances. The calculations showed that among all the moderators available for practical reactor use, ordinary water yields the maximum value of  $\Phi_t/W$ . However, as is known, the age-theory approximation cannot be satisfactorily applied to water. On the other hand, the three-group theory gives much larger values than the age-theory approximation. It is therefore of interest to find the value of  $\Phi_t/W$  directly from experimental data. Reference [2] gives measurements for the distribution of a flux of neutrons with energy  $E=1.46$  eV in water from a  $U^{235}$  point fission source. On the basis of experimental data the maximum ratio of thermal neutron flux to power was calculated. The age-theory approximation was used for the moderation of neutrons from 1.46 eV to thermal energies. The age value of  $\Delta\tau = 1$  cm<sup>2</sup> was taken from [3]. A variation of  $\pm 50\%$  in  $\Delta\tau$  introduces a correction of not more than 5% into  $\Phi_t/W$ .

The diffusion length of the thermal neutrons was taken to be 2.73 cm and the diffusion coefficient 0.165 cm. The space integral of the experimental curve was normalized with respect to the total number of fast neutrons from  $U^{235}$  fission.

The error in  $\Phi_t/W$ , caused primarily by the experimental error, was  $\pm 25\%$ . The values for  $\Phi_t/W \cdot 10^{-13}$  (1/cm<sup>2</sup> · sec · mW) obtained by the age-theory approximation, by the three-group theory, and experimentally were 38,\* 100, and  $80 \pm 20$ , respectively.

The authors express their gratitude to A. N. Erykalov for his critique of the results.

LITERATURE CITED

1. S. M. Feinberg, et al., Proceedings of the Second International Conference on the Peaceful Uses of Atomic Energy [Russian translation], Reports of Soviet Scientists, Vol. 2, Moscow, Atomizdat, p. 334 (1958).
2. L. N. Yurova, A. A. Polyakov, and A. A. Ignatov, Atomnaya énergiya, 12, 151 (1962).
3. L. M. Barkov and K. I. Mukhin, Atomnaya énergiya, No. 3, 31 (1956); L. M. Barkov, V. K. Makar'in, and K. I. Mukhin, Ibid., p. 33.

\* The age value to thermal energies was taken to be 28.3 cm<sup>2</sup>.

THE EFFECTIVENESS OF A SYSTEM OF ABSORBER RODS ARBITRARILY  
DISTRIBUTED IN A REFLECTED REACTOR

V. I. Nosov

Translated from Atomnaya Énergiya, Vol. 15, No. 1,  
pp. 71-74, July, 1963  
Original article submitted October 15, 1962

In previous studies [1-3] we found the critical conditions and neutron flux distributions for a homogeneous thermal-neutron reactor with a system of absorber rods distributed at equal intervals in a ring in the active zone or the radial reflector.

In the present study we use a two-group approximation to generalize the case to arbitrarily distributed rods fully inserted into the reactor.

System of Rods in the Reflector of the Reactor. In a cylindrical reactor with a system of rods placed in an arbitrary manner in a radial reflector, the solution in matrix form for the fast neutron flux  $\varphi_1$  and the thermal neutron flux  $\varphi_2$  will be

$$\varphi^I = \begin{bmatrix} \varphi_1^I \\ \varphi_2^I \end{bmatrix} = \begin{bmatrix} S_1 & S_2 \\ 1 & 1 \end{bmatrix} \begin{bmatrix} L^I \\ M^I \end{bmatrix}; \quad \varphi^{II} \equiv \begin{bmatrix} \varphi_1^{II} \\ \varphi_2^{II} \end{bmatrix} = \begin{bmatrix} S_3 & 0 \\ 1 & 1 \end{bmatrix} \begin{bmatrix} L^{II} \\ M^{II} \end{bmatrix}, \quad (1)$$

where

$$\begin{bmatrix} L^I \\ M^I \end{bmatrix} = \sum_{n=0}^{\infty} \begin{bmatrix} J_n(\kappa r) & 0 \\ 0 & I_n(\beta r) \end{bmatrix} \begin{bmatrix} A_{1n} \cos n\varphi + E_{1n} \sin n\varphi \\ A_{2n} \cos n\varphi + E_{2n} \sin n\varphi \end{bmatrix};$$

$$\begin{bmatrix} L^{II} \\ M^{II} \end{bmatrix} = \sum_{n=0}^{\infty} \begin{bmatrix} I_n(\nu r) (C_{2n} \cos n\varphi + F_{2n} \sin n\varphi) + K_n(\nu r) (D_{2n} \cos n\varphi + H_{2n} \sin n\varphi) \\ I_n(\mu r) (C_{1n} \cos n\varphi + F_{1n} \sin n\varphi) + K_n(\mu r) (D_{1n} \cos n\varphi + H_{1n} \sin n\varphi) \end{bmatrix} +$$

$$+ \sum_{m=0}^{\infty} \sum_{i=1}^N \begin{bmatrix} K_m(\nu \rho_i) & 0 \\ 0 & K_m(\mu \rho_i) \end{bmatrix} \begin{bmatrix} B_{2mi} \cos m\omega_i + P_{2mi} \sin m\omega_i \\ B_{1mi} \cos m\omega_i + P_{1mi} \sin m\omega_i \end{bmatrix}. \quad (2)$$

Here  $N$  is the number of rods;  $i$  is the index number of the rod;  $\underline{r}$  is the distance from the center of the reactor to some arbitrary point  $P$ ;  $\rho_i$  is the distance from the center of rod number  $i$  to some point  $P$ ;  $\varphi$  and  $\omega_i$  are the corresponding azimuth angles (see diagram);  $S_1, S_2, S_3$  are coupling coefficients;  $I, II$  are the indices of the active zone and the reflector, respectively.\*

From the fast neutron flux continuity condition and flux density at the boundary between the active zone and the reflector

$$\left( \varphi_1^I = \varphi_1^{II}; \quad \frac{d\varphi_1^I}{dr} = \gamma_2 \frac{d\varphi_1^{II}}{dr} \right)$$

we obtain:

$$\left. \begin{aligned} (A_{2n}, E_{2n}) &= (A_{1n}, E_{1n}) \varphi_n - \sum_{m=0}^{\infty} \sum_{i=1}^N [B_{2mi} \Phi_{nm}(\cos n\varphi_i) \mp P_{2mi} \bar{\Psi}_{nm}(\sin n\varphi_i, \cos n\varphi_i)], \\ (C_{2n}, F_{2n}) &= (A_{1n}, E_{1n}) \varphi_n + \sum_{m=0}^{\infty} \sum_{i=1}^N [B_{2mi} \chi_{nm}(\cos n\varphi_i, \sin n\varphi_i) \mp P_{2mi} \bar{\chi}_{nm}(\sin n\varphi_i, \cos n\varphi_i)]. \end{aligned} \right\} \quad (3)$$

\* For the rest of the notation, see [1].

Here the functions  $f_n, \varphi_n, \Phi_{nm}, \chi_{nm}$  will have the same form as the corresponding functions  $f_n, \dots, \chi_{nm}$  in [1], if we take  $\gamma_1 = 1$  in those functions;  $\bar{\Phi}_{nm}$  is written like  $\Phi_{nm}$  if, instead of the functions  $r_{nm}$  and  $v_{nm}$  appearing in the expression for  $\Phi_{nm}$ , we introduce their value with a bar:

$$\begin{aligned} \bar{r}_{nm} &= I_{n-m}(vR_i) - I_{n+m}(vR_i), \\ \bar{v}_{nm} &= K_{n-m}(vR_i) - K_{n+m}(vR_i); \end{aligned}$$

$\bar{\chi}_{nm}$  is written in the same way as  $\chi_{nm}$  if, in the expression for  $\chi_{nm}$ , the values of  $r_{nm}, v_{nm}, \Phi_{nm}$  are taken equal to  $\bar{r}_{nm}, \bar{v}_{nm},$  and  $\bar{\Phi}_{nm}$ , respectively.

It should be noted that, since we are considering a system of arbitrarily distributed rods, the index  $nN$  in the Bessel function of [1] should be replaced everywhere by  $n$ , and  $R_c$  and replaced by  $R_i$ . In obtaining Eqs. (3) we used the addition theorem for  $K_m(\nu, \mu\rho_i)$  and the relationships for the constants  $D_{1n}, D_{2n}$  and  $H_{1n}, H_{2n}$  which are obtained from the boundary values for  $\varphi_1$  and  $\varphi_2$  at the reactor surface ( $\varphi_1 = \varphi_2 = 0$  for  $r = R_{eq}$ ):

$$\begin{aligned} (D_{2n}, H_{2n}) &= -(C_{2n}, F_{2n}) \frac{I_n(vR_{eq})}{K_n(vR_{eq})} - \sum_{m=0}^{\infty} \sum_{i=1}^N \frac{\delta_n}{2} [B_{2mi} r_{nm} (\cos n\varphi_i, \sin n\varphi_i) \mp P_{2mi} \bar{r}_{nm} (\sin n\varphi_i, \cos n\varphi_i)]; \\ (D_{1n}, H_{1n}) &= -(C_{1n}, F_{1n}) \frac{I_n(\mu R_{eq})}{K_n(\mu R_{eq})} - \sum_{m=0}^{\infty} \sum_{i=1}^N \frac{\delta_n}{2} [B_{1mi} b_{nm} (\cos n\varphi_i, \sin n\varphi_i) \mp P_{1mi} \bar{b}_{nm} (\sin n\varphi_i, \cos n\varphi_i)], \end{aligned}$$

where  $\delta_n = 1$  for  $n=0$ ;  $\delta_n = 2$  for  $n \geq 1$ ;  $b_{nm} = I_{n-m}(\mu R_i) - I_{n+m}(\mu R_i)$ .

From the thermal neutron flux continuity condition and flux density at the boundary between the active zone and the reflector

$$\left( \varphi_2^I = \varphi_2^{II}, \quad \frac{d\varphi_2^I}{dr} = \gamma_0 \frac{d\varphi_2^{II}}{dr} \right)$$

it follows that

$$\left. \begin{aligned} (C_{1n}, F_{1n}) &= \sum_{m=0}^{\infty} \sum_{i=1}^N [(B_{1mi} Q_{nm} + B_{2mi} \Delta_{nm}) (\cos n\varphi_i, \sin n\varphi_i) \mp (P_{1mi} \bar{Q}_{nm} + P_{2mi} \bar{\Delta}_{nm}) (\sin n\varphi_i, \cos n\varphi_i)]; \\ (A_{1n}, E_{1n}) &= \sum_{m=0}^{\infty} \sum_{i=1}^N [(B_{1mi} R_{nm} + B_{2mi} T_{nm}) (\cos n\varphi_i, \sin n\varphi_i) \mp (P_{1mi} \bar{R}_{nm} + P_{2mi} \bar{T}_{nm}) (\sin n\varphi_i, \cos n\varphi_i)]. \end{aligned} \right\} (4)$$

Here the functions  $Q_{nm}, R_{nm}$  are of the same form as the corresponding functions in [1];  $\bar{Q}_{nm}, \bar{R}_{nm}$  are written in the same way as  $Q_{nm}, R_{nm}$  if instead of the functions  $b_{nm}, a_{nm}$  we write their value with a bar:  $\bar{b}_{nm}$  and  $\bar{a}_{nm} = K_{n-m}(\mu R_i) - K_{n+m}(\mu R_i)$ ;  $\bar{\Delta}_{nm}, \bar{T}_{nm}$  are written in the same way as  $\Delta_{nm}, T_{nm}$  if instead of  $\chi_{nm}, \Phi_{nm}, r_{nm}, v_{nm}$  and  $\Delta_{nm}$  we introduce the corresponding functions  $\bar{\chi}_{nm}, \dots, \bar{\Delta}_{nm}$ .

If we use the boundary conditions for  $\varphi_1^{II}$  and  $\varphi_2^{II}$  at each of the absorber rods and the corresponding addition theorems for Bessel functions for  $\rho_i < R_i, \rho_i < \rho_{is}$  ( $\rho_i \approx a_i$ ), after some transformations we obtain the following equations:

$$\begin{aligned} & \sum_{i=1}^N \sum_{k=0}^{\infty} \sum_{m=0}^{\infty} \sum_{n=0}^{\infty} \{ [B_{1mi} (g_{1ki} H_{nmki} + g_{2ki}^{Y_i} q_{nmki}) + \\ & + \delta_{mk} \delta_{is} L_{1ki} + g_{1ki} \delta_{si} \Lambda_{1mki}) + B_{2mi} (g_{1ki} \omega_{nmki} + \\ & + g_{2ki}^{Y_i} \pi_{nmki} + \delta_{mk} \delta_{is} L_{2ki} + g_{2ki}^{Y_i} \delta_{si} \Lambda_{2mki}) + \\ & + \delta_{si} (g_{1ki} P_{1mi} \Omega_{1mki} + g_{2ki}^{Y_i} P_{2mi} \Omega_{2mki})] \cos k\omega_i + \\ & + [P_{1mi} (g_{1ki} \bar{H}_{nmki} + g_{2ki}^{Y_i} \bar{q}_{nmki} + \delta_{mk} \delta_{is} L_{1ki} + \\ & + \delta_{si} g_{1ki} \bar{\Omega}_{1mki}) + \delta_{si} (g_{1ki} B_{1mi} \bar{\Lambda}_{1mki} + g_{2ki}^{Y_i} B_{2mi} \bar{\Lambda}_{2mki}) + \\ & + P_{2mi} (g_{1ki} \bar{\omega}_{nmki} + g_{2ki}^{Y_i} \bar{\pi}_{nmki} + \delta_{mk} \delta_{is} L_{2ki} + \\ & + g_{2ki}^{Y_i} \delta_{si} \bar{\Omega}_{2mki})] \sin k\omega_i \} = 0, \end{aligned} \quad (5)$$

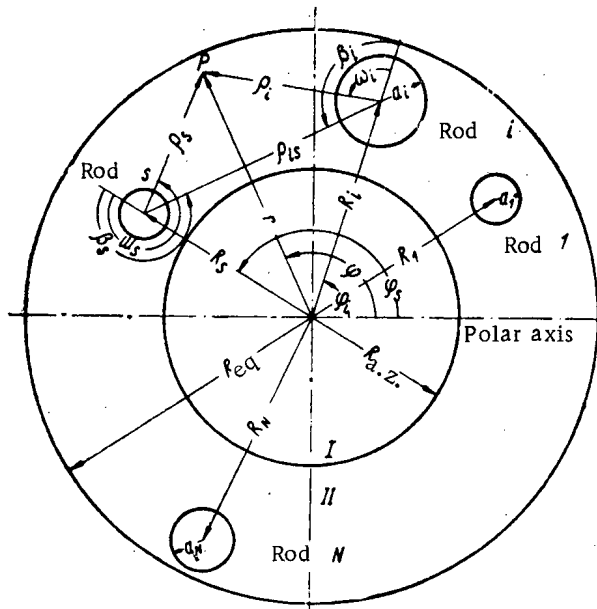


Diagram showing the distribution of the rods in the reflector of the reactor.

$$\sum_{i=1}^N \sum_{h=0}^{\infty} \sum_{m=0}^{\infty} \sum_{n=0}^{\infty} \{ [B_{1mi} g_{2ki}^{d_i} \bar{q}_{nmki} + B_{2mi} (g_{2ki}^{d_i} \bar{\pi}_{nmki} + \delta_{mh} \delta_{is} L_{2ki}^{d_i} + \delta_{si} g_{2ki}^{d_i} \bar{\Lambda}_{2mki}) + P_{2mi} \delta_{si} g_{2ki}^{d_i} \bar{\Omega}_{2mki}] \cos k\omega_i + [P_{1mi} s_{2ki}^{d_i} \bar{q}_{nmki} + P_{2mi} (g_{2ki}^{d_i} \bar{\pi}_{nmki} + \delta_{mh} \delta_{is} L_{2ki}^{d_i} + \delta_{si} g_{2ki}^{d_i} \bar{\Omega}_{2mki}) + B_{2mi} \delta_{si} g_{2ki}^{d_i} \bar{\Lambda}_{2mki}] \sin k\omega_i \} = 0.$$

Here the functions  $H_{nmki}$ ,  $q_{nmki}$ ,  $\omega_{nmki}$ , and  $\pi_{nmki}$  are of the same form as the corresponding functions  $H_{nmk}$ , ...,  $\pi_{nmk}$  in [1] ( $R_c$  is everywhere taken equal to  $R_i$ ); the functions  $\bar{H}_{nmki}$ ,  $\bar{q}_{nmki}$ ,  $\bar{\omega}_{nmki}$ , and  $\bar{\pi}_{nmki}$  are written like  $H_{nmki}$ , ...,  $\pi_{nmki}$  if instead of the functions  $b_{nk}$ ,  $b_{nm}$ ,  $Q_{nm}$ ,  $R_{nm}$ ,  $\Delta_{nm}$ ,  $T_{nm}$ ,  $\chi_{nm}$ ,  $r_{nk}$ ,  $r_{nm}$ , and  $v_{nk}$  we use the corresponding value with a bar; the functions  $g_{1ki}$ ,  $g_{2ki}$ ,  $\gamma_i$ ,  $d_i$ ,  $L_{1ki}$ ,  $L_{2ki}$ ,  $\gamma_i$ ,  $d_i$  are expressed like the functions  $g_{1k}$ ,  $g_{2k}$ ,  $\gamma^d$ ,  $L_{1k}$ ,  $L_{2k}$ ,  $\gamma^d$  in [1] if the values of  $a$ ,  $\gamma$ , and  $d$  in the latter are taken equal to  $a_i$ ,  $\gamma_i$ , and  $d_i$ , respectively;  $\delta_{is} = 1$  for  $s = i$ ;  $\delta_{is} = 0$  for  $s \neq i$ ;  $\delta_{si} = 0$  for  $s = i$  and  $\delta_{si} = 1$  for  $s \neq i$ ;  $\delta_{mk} = 1$  for  $m = k$  and  $\delta_{mk} = 0$  for  $m \neq k$  [at the surface of the rods the boundary conditions were given in the form

$$(d\varphi_1^{II}/dQ_i) (\varphi_1^{II})^{-1} = \frac{1}{a_i} \Big|_{Q_i=a}$$

and

$$(d\varphi_2^{II}/dQ_i) (\varphi_2^{II})^{-1} = \frac{1}{\gamma_i} \Big|_{Q_i=a_i}.$$

The functions  $\Lambda_{1mki}$ ,  $\bar{\Lambda}_{1mki}$ ,  $\Omega_{1mki}$ , and  $\bar{\Omega}_{1mki}$ , are found from the formulas

$$\begin{aligned} \Lambda_{1mki} &= \frac{\epsilon_k}{2} [K_{m+k} (\mu Q_{is}) \cos (m\beta_s + k\beta_i) + \\ &\quad + K_{m-k} (\mu Q_{is}) \cos (m\beta_s - k\beta_i)]; \\ \bar{\Lambda}_{1mki} &= \frac{\epsilon_k}{2} [K_{m+k} (\mu Q_{is}) \sin (m\beta_s + k\beta_i) - \\ &\quad - K_{m-k} (\mu Q_{is}) \sin (m\beta_s - k\beta_i)]; \\ \Omega_{1mki} &= \frac{\epsilon_k}{2} [K_{m+k} (\mu Q_{is}) \sin (m\beta_s + \\ &\quad + k\beta_i) + K_{m-k} (\mu Q_{is}) \sin (m\beta_s - k\beta_i)]; \\ \bar{\Omega}_{1mki} &= [-K_{m+k} (\mu Q_{is}) \cos (m\beta_s + k\beta_i) + \\ &\quad + K_{m-k} (\mu Q_{is}) \cos (m\beta_s - k\beta_i)]. \end{aligned}$$

The functions  $\Lambda_{2mki}$ ,  $\bar{\Lambda}_{2mki}$ ,  $\Omega_{2mki}$ , and  $\bar{\Omega}_{2mki}$  are written in the same way, but  $\nu$  is used instead of  $\mu$ .

In deriving Eqs. (5) it was assumed that  $d_i$  and  $\gamma_i$  were independent of angle. From Eqs. (5) we can find the criticality condition for the present problem if we restrict ourselves to a  $k$ -th order approximation; we obtain a system of  $2N(2k+1)$  linear homogeneous algebraic equations, the vanishing of whose determinant is the criticality condition for the problem under study. The effectiveness of the rod system will be characterized by the difference  $K_{eff}$  between the cases with and without absorber rods in the reactor. In most of cases encountered in practice we can restrict ourselves to a zero-order approximation ( $k=0$ ), and its is only for large absorber diameters that we must use one more term of the expansion in  $k$  [2]. If the rods are placed at equal intervals along the circumference of a circle, this solution becomes the solution obtained in [1]. In this case, in Eqs. (5) the constants  $P_{1mi}$ ,  $P_{2mi}$  should be taken equal to zero, since the problem becomes symmetric with respect to  $\varphi$  and  $\omega_i$  (if the angles are counted

from the polar axis passing through the center of the reactor and the center of any rod). The functions  $\bar{A}_{1mki}$ ,  $\bar{A}_{2mki}$ , as well as  $E_{1n}$ ,  $E_{2n}$ ,  $F_{1n}$ ,  $F_{2n}$ ,  $H_{1n}$ , and  $H_{2n}$  in Eqs. (1), (2) vanish for the same reason.

The problem is solved in a similar manner for an arbitrary distribution of the system of absorber rods in the active zone of a reactor with a reflector (lack of space prevents us from stating the solution).

The authors thanks N. N. Ponomarev-Stepnoi for his valuable advice and assistance in developing methods of calculating the efficiency of control units in a reactor with a reflector.

#### LITERATURE CITED

1. V. I. Nosov, *Atomnaya énergiya*, 9, 262 (1960).
2. V. I. Nosov, *Atomnaya énergiya*, 10, 269 (1961).
3. V. I. Nosov, *Atomnaya énergiya*, 12, 326 (1962).
4. G. N. Watson, *Theory of Bessel Functions* [Russian translation], Moscow, Izd-vo inostr. lit. (1949).

## FREQUENCY ANALYSIS IN A SYSTEM WHICH INCLUDES A RUNAWAY REACTOR

A. R. Mirzoyan and I. N. Briker

Translated from Atomnaya Energiya, Vol. 15, No. 1,

pp. 74-76, July, 1963

Original article submitted October 2, 1962

The frequency analysis of feedback systems which include a reactor requires a knowledge of the transfer function of the kinetic reactor. When the reactor operates at a constant power level, this function is known [1]. However, the transfer function given in [1] cannot be used for the frequency analysis of runaway reactor operation.

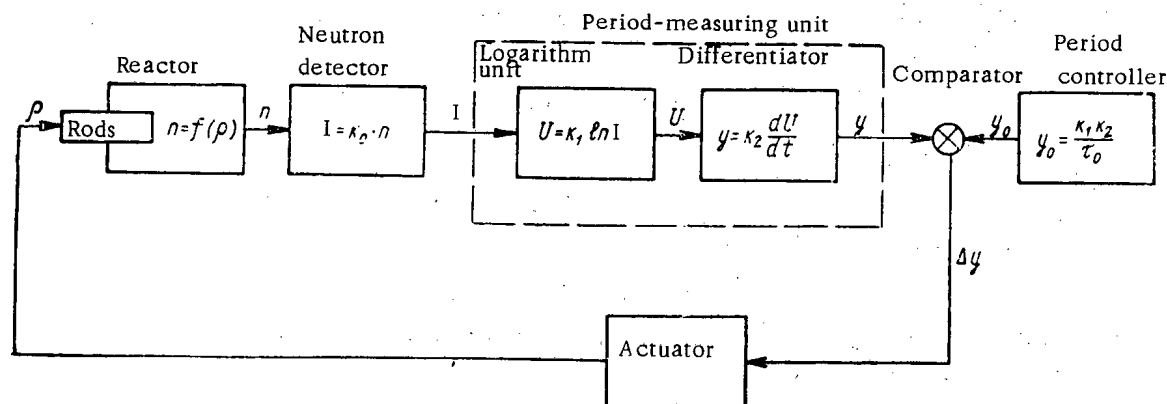


Fig. 1. Automatic control system for maintaining constant period.

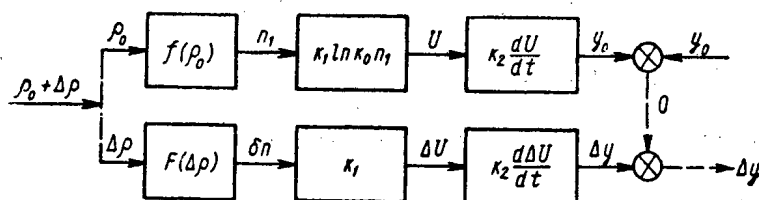


Fig. 2. Functional schematic describing the process of period control.

An attempt was made in [2] to obtain the transfer function for a runaway reactor. Because of the "algebraic" difficulties, however, it was not obtained in Laplace transform expressions in [2]; only a harmonic analysis of a runaway reactor was given.

In the present study we derive such a transfer function in explicit form and give a block diagram for a period control circuit. This enables us to analyze automatic reactor start-up systems by frequency methods.

Let us consider the case of runaway in a reactor with a period  $\tau_0$ . If the runaway proceeds ideally, the steady-state neutron flux will change exponentially  $n_1(t) = n_0 e^{t/\tau_0}$  (where  $n_0$  is the initial neutron flux level). The excess reactivity  $\rho_0$  corresponding to this process remains constant. However, in controlling the runaway the period  $\tau$  deviates from the given value  $\tau_0$ . This deviation is caused by the oscillation of the excess reactivity  $\rho$  about  $\rho_0$ . We will therefore have, superimposed on the steady-state exponential function, neutron flux oscillations caused by the control reactivity:  $\Delta\rho(t) = \rho(t) - \rho_0$ .

Let us consider the relative deviation of the neutron flux

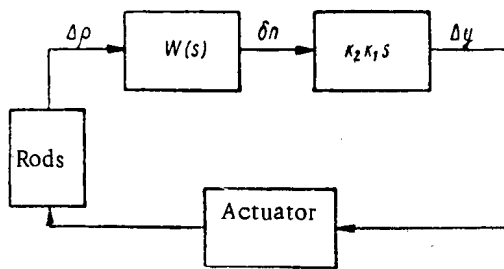


Fig. 3. Linearized block diagram for automatic control to maintain constant period.

$$\left. \begin{aligned} \delta n(t) &= \frac{n(t) - n_1(t)}{n_1(t)} \\ n(t) &= n_1(t) [1 + \delta n(t)], \end{aligned} \right\} \quad (1)$$

or

where  $n(t)$  is the instantaneous value of the neutron flux. We shall assume that  $\delta n(t)$  is small; that is,  $|\delta n(t)| \ll 1$ , which will be true if there is feedback.

Derivation of the Transfer Function for a Runaway Reactor. Let us consider the equations of a kinetic reactor:

$$\frac{dn}{dt} = \frac{\rho - \beta}{l} n + \sum_{i=1}^m \lambda_i C_i, \quad (2)$$

$$\frac{dC_i}{dt} = -\lambda_i C_i + \frac{\beta_i}{l} n. \quad (3)$$

Let  $\rho$  be the excess reactivity. Then for small deviations about the equilibrium state we may express  $\rho$  as the sum of two components—a stationary  $\rho_0$  and an oscillating component  $\Delta\rho$ :

$$\rho(t) = \rho_0 + \Delta\rho(t). \quad (4)$$

For  $\rho(t) = \rho_0$  Eqs. (2) and (3) give the equilibrium solutions

$$n(t) = n_1(t), \quad C(t) = C_1(t).$$

Introducing the deviation from this solution, that is,

$$n = n_1(1 + \delta n), \quad C = C_1 + \Delta C, \quad (5)$$

and substituting (4) and (5) into the kinetics equations, we obtain equations for the deviations. Applying the Laplace transform to these and eliminating  $\Delta C_i$ , we obtain

$$\begin{aligned} \left[ P - \frac{\rho_0}{l} + \sum_{i=1}^m \frac{\beta_i P}{l(P + \lambda_i)} \right] L(n_1 \delta n) = \\ = L\left(\frac{n_1 \Delta\rho}{l}\right) + L\left(\frac{n_1 \Delta\rho \delta n}{l}\right), \end{aligned} \quad (6)$$

where  $L$  is the Laplace transform sign and  $P$  is the Laplace operator.

In Eq. (6) the term  $L\left(\frac{n_1 \Delta\rho \delta n}{l}\right)$  may be neglected if  $|\delta n| \ll 1$ .

Using the formula  $n_1 = n_0 e^{t/\tau_0}$ , we consider one of the products under the  $L$  sign:

$$L[n_1 \varphi(t)] = n_0 L[e^{t/\tau_0} \varphi(t)].$$

Using the displacement theorem [3], we may write

$$n_0 L[e^{t/\tau_0} \varphi(t)] = n_0 \varphi\left(P - \frac{1}{\tau_0}\right). \quad (7)$$

Applying (7) to Eq. (6), we find

$$\frac{\delta n\left(P - \frac{1}{\tau_0}\right)}{\Delta\rho\left(P - \frac{1}{\tau_0}\right)} = \frac{1}{l \left[ P - \frac{\rho_0}{l} + \sum_{i=1}^m \frac{\beta_i P}{l(P + \lambda_i)} \right]}. \quad (8)$$

If we now replace  $P - 1/\tau_0$  by  $s$  and apply the "inverse hour" formula [4]

$$\rho_0 = \frac{l}{\tau_0} + \sum_{i=1}^m \frac{\beta_i}{1 + \lambda_i \tau_0}, \quad (9)$$



we obtain the transfer function for a runaway reactor

$$W(s) = \frac{\delta n(s)}{\Delta Q(s)} = \frac{1}{s \left[ l + \sum_{i=1}^m \frac{\beta_i \lambda_i}{\left( s + \frac{1}{\tau_0} + \lambda_i \right) \left( \frac{1}{\tau_0} + \lambda_i \right)} \right]} \quad (10)$$

where  $s$  is the Laplace operator.

It readily is seen that as  $\tau_0 \rightarrow \infty$  we obtain the transfer function of the reactor at constant power level [1].

It should be noted that Zadeh's method [5], applicable to the analysis of linear systems with variable parameters, gives the same result.

Block Diagram for Automatic Start-up. Figure 1 shows the block diagram for stabilizing the reactor period. The signal at the input of the period-measuring unit is proportional to the inverse period  $y = k_1 \cdot k_2 / \tau$ . The output of the comparator is the difference

$$\Delta y = \frac{k_1 \cdot k_2}{\tau} - \frac{k_1 \cdot k_2}{\tau_0} \approx - \frac{k_1 \cdot k_2}{\tau_0^2} \Delta \tau,$$

which is transmitted to the actuator which controls the reactivity.

In accordance with the results obtained in the preceding section, the equation  $n(t) = f(\rho)$  may be written as follows:

$$\begin{aligned} n(t) &= n_1(t) + n_1(t) \delta n(t) = f(\rho_0 + \Delta \rho) = \\ &= f(\rho_0) + F(\Delta \rho) + O(\delta n). \end{aligned}$$

If we note, in addition, that (see Fig. 1)

$$U = k_1 \ln [k_0 n_1 (1 + \delta n)] \approx k_1 \ln k_0 n_1 + k_1 \delta n = U + \Delta U, \quad (11)$$

we can represent the forward loop by the functional schematic shown in Fig. 2.

If we consider control by means of deviations and take account of (10) and (11), we can use the block diagram of Fig. 3, to which the familiar methods of frequency analysis can be applied.

On the basis of the good agreement between the results of the frequency analysis and those obtained by non-linear simulation, we may state that an automatic start-up system may be analyzed by the method proposed here, without resorting to simulation.

#### LITERATURE CITED

1. M. Schultz, Control of Nuclear Reactors and Power Plants [Russian translation], Moscow, Izd-vo inostr. lit. (1957).
2. P. Potter, J. Nucl. Energy, 6, 291 (1958).
3. M. A. Lavrent'ev and V. V. Shabat, Methods of the Theory of Functions of Complex Variable [in Russian], Moscow, Fizmatgiz (1958).
4. S. Glasstone and M. Edlund, Elements of Nuclear Reactor Theory [Russian translation], Moscow, Izd-vo inostr. lit. (1954).
5. L. Zadeh, Proc. I. R. E., 38, 291 (1950).

# CALCULATION OF THE TEMPERATURE OF REGENERATIVE PREHEATING OF WATER IN TWO-CIRCUIT ATOMIC POWER PLANTS

D. Grecov

Rumanian-Soviet Scientific Institute of the Rumanian Academy of Sciences, Bucharest

Translated from Atomnaya Énergiya, Vol. 15, No. 1,

pp. 76-77, July, 1963

Original article submitted April 12, 1962

In thermodynamic systems of two-circuit atomic power plants [1] it is important to select correctly the end temperature  $t_a$  of regenerative preheating of the feed water because such systems have specific characteristics. In particular, in these plants a change in  $t_a$  leads to a change in the steam or heat-transfer agent parameters.

The optimum value  $t_a^{opt}$  also depends on the type of thermodynamic cycle: the problem is made considerably more difficult in the case of a cycle involving two pressures.

For determining  $t_a^{opt}$ , it is assumed that the thermal capacity of the nuclear reactor is constant. We may then describe the two cases encountered when planning atomic power plants:

1) the steam pressure in the thermodynamic cycle is constant. In this case it is assumed that the change in  $t_a$  corresponds to the change in temperature of the heat-transfer agent at the reactor inlet (according to the graph  $t-Q$ );

2) the temperatures of the heat-transfer agent at the reactor inlet  $t_1$  and outlet  $t_2$  (in °C) do not change, but a change in  $t_a$  leads to a change in the live steam pressure according to the graph  $t-Q$  [4].

The first case is encountered in practice when the pressure and steam temperature are given and it is required to find what the value of the parameter  $t_a$  will be if maximum efficiency (net) of the atomic power plant is guaranteed.

The other case is often found in calculations of atomic power plant systems when it is assumed that optimum values for  $t_1$  and  $t_2$  are obtained from preliminary calculations, while the determination of the value of  $t_a^{opt}$  amounts to a more accurate definition of the parameters providing maximum efficiency of the plant.

For a more accurate determination of the effect of different parameters on the choice of the optimum feed water temperature, in the first case we will base the calculations on the equation for the net efficiency of an atomic power plant [1]:

$$\eta_i = \left( \eta_t \eta_{0i} - \frac{B}{c_p^3 (t_2 - t_1)^3 \gamma_n \gamma_1} \right) \eta_{ga}, \quad (1)$$

where  $\eta_t$  is the thermodynamic efficiency of the plant;  $\eta_{0i}$  is the relative internal efficiency of the turbine;  $c_p$  is the average specific thermal capacity of the heat carrier, kcal/kg, °C;  $\gamma_n$  is the average specific gravity of the heat-transfer agent in the active zone of the reactor, kg/m<sup>3</sup>;  $\gamma_1$  is the specific gravity of the heat-transfer agent on entering the pumps (compressor), kg/m<sup>3</sup>;  $\eta_{ga}$  is the efficiency of the steam generator; the value of B depends on the geometry of the active zone, the heat-emitting elements of the reactor, the parameters and type of the heat-transfer agent [1]:

$$B = \frac{\zeta}{2g\eta_p} \cdot \frac{Q_T^2}{S_T^2} \cdot \frac{1}{427}, \quad (2)$$

where  $\zeta$  is the resistance coefficient of the first circuit;  $\eta_p$  is the efficiency of the primary circuit pumps;  $Q_T$  is the thermal capacity of the reactor, kcal/hour;  $S_T$  is the through cross section of the heat-transfer agent in the active zone, m<sup>2</sup>.

The approximate value of  $\eta_t$  from Eq. (1) may be expressed in the form [2]

$$\eta_t = 1 - \frac{T_C (\Delta S_0 - \Delta S_p)}{i_0 - \bar{t}_a}, \quad (3)$$

where  $T_C$  is the steam temperature in the condenser, °K;  $\Delta S_0$  is the increase in entropy of the working body from the condenser to the steam generator outlet, kcal/kg °C;  $i_0$  is the enthalpy of the steam at this outlet, kcal/kg;  $\bar{t}_a$  is the final enthalpy of the feed water preheating;  $\Delta S_p$  is the decrease in entropy of the steam emitted as a result of the regenerative bleedings for preheating the feed water, kcal/kg °C, expressed in the form [2]

$$\Delta S_p = Z c_{pa} \left[ 1 - \left( \frac{T_C}{T_a} \right)^{1/Z} \right], \quad (4)$$

where  $Z$  is the number of regenerative preheaters;  $c_{pa}$  is the average specific thermal capacity of the feed water, kcal/kg °C.

The value of  $t_a^{\text{opt}}$  is determined by the equation

$$\frac{\partial \eta_i}{\partial t_a} = 0. \quad (5)$$

According to the  $t$ - $Q$  graph, in a case where the initial steam pressure  $p_0 = \text{const}$  a change in  $t_a$  leads to a corresponding change in  $t_1$ . Assuming that the change in  $t_1$  in the steam generator is linear, we may write

$$\frac{t_2 - t_1}{i_0 - \bar{t}_a} = \text{const} = C_1. \quad (6)$$

Since the value of  $t_2$  is preset from the conditions of the thermostability of the active-zone materials (it can be shown that  $t_1$  has a relatively slight effect on the temperature field in the active zone when  $Q = \text{const}$  [1, 3]), and  $i_0 = \text{const}$ , we obtain

$$\frac{\partial t_1}{\partial t_a} = C_1,$$

where  $C_1$  is a constant defined by Eq. (6).

Employing Eq. (5) for determining  $t_a$ , we obtain a transcendental equation which may be solved by selecting

$$\left( \frac{T_C}{T_a} \right)^{\frac{Z+1}{Z}} - (1 - \eta_t) - \frac{3BC_1(i_0 - t_a)}{(t_2 - t_1)^4 \eta_{0i} c_p^3 \gamma_n \gamma_1} = 0. \quad (7)$$

Equation (7) may be simplified:

$$T_a^{\text{opt}} = \frac{T_C}{(1 - \eta_t + U)^{Z/Z+1}} \text{ °K}. \quad (8)$$

Since the value of  $\eta_t$  changes very little with a change in  $T_a$  in the optimum zone, the equation for  $U$  becomes

$$U = \frac{3\xi Q_T^2 C_1}{2g \eta_p c_p^3 \gamma_n \gamma_1 (t_2 - t_1)^4 S_T^2} \frac{i_{0T} \bar{t}_a}{\eta_{0i}} \frac{1}{427}.$$

where  $\xi$  is the derived value of the hydrodynamic resistance coefficient of the primary circuit (active zone, steam generator, piping system).

Equation (8) corresponds to the optimum equation in [2] for theoretical regenerative systems, but has the additional term  $U$  in the denominator, which leads to a considerable reduction in the value of  $t_a^{\text{opt}}$ .  $U$  depends on the value of  $c_p^3 \gamma_n \gamma_1$ , i.e., the physical properties of the heat-transfer agent, the cross section  $S_T$ , the thermal capacity of the reactor  $Q_T$  and the temperature difference  $t_2 - t_1$ , corresponding to  $t_a$  in the zone of maximum net efficiency  $\eta_i$ .

In general, the lesser the power expended on transferring the heat carrier the greater will be the value of  $t_a^{\text{opt}}$ ; in the end, it will be equal to the optimum temperature for the initial steam parameters  $p_0$  and  $t_0$  of conventional power plants.

It must be mentioned that for two-circuit atomic power plants the effect of the initial steam parameters on the value of  $t_a^{\text{opt}}$  has specific characteristics.

Whereas an increase in  $p_0$  in conventional power plants leads to a rapid increase in  $t_a^{\text{opt}}$ , in atomic power plants covered by case 1 in this paper it leads to a reduction in the latter. This is due to the fact that, together with the increase in  $p_0$ , there is an increase in the power required for transferring the heat carrier, due to the decrease in temperature difference  $t_2 - t_1$ . [In Eq. (8) an increase in  $p_0$  leads to an increase in  $U$  because the temperature difference  $t_2 - t_1$  decreases for the same value of  $t_a$ .]

Case 2, where  $t_1$  and  $t_2$  are constant, was considered in [1], from which it follows that the equation for calculating the optimum temperature of water preheating has the form

$$\eta_a^{\text{opt}} = \frac{T_c}{[aT_c + (1-\chi)(1-\eta_t)]^{Z/Z+1}} \text{ } ^\circ\text{K}, \quad (9)$$

where

$$a \approx \frac{\Delta S_0}{\Delta t_a} \text{ and } \chi \approx \frac{\Delta i_0}{\Delta t_a}$$

are the changes in the initial entropy and initial enthalpy of steam respectively with a change in  $t_a$  by  $1^\circ\text{C}$ .

It should be noted that in case 2 a change in  $t_a$  leads to a change in  $p_0$ .

An increase in  $t_a$  leads to a change in steam pressure, which leads in turn to an increase in efficiency as a result of the increase in preheating temperature  $t_a$ , and the number of preheaters  $Z$  will be reduced because of the reduction in  $p_0$ . It may be shown that the effect of temperature on  $p_0$  is more marked with an increase in  $t_2 - t_1$ .

The absolute values of  $a$  and  $\chi$  in Eq. (9) will evidently be higher the greater the difference  $t_2 - t_1$ , and the optimum value of the parameter will be less in this case.

It must be emphasized that this analysis is only correct for a cycle with one pressure; for a cycle with two or more pressures the problem of determining the optimum preheating temperature is more complicated and requires a particular approach.

#### LITERATURE CITED

1. D. Grecov, Rev. electrotechn. et energetique, V, No. 2, 423 (1960).
2. D. D. Kalafati, Fundamentals of the Theory of Regenerative Cycles of High-Pressure Steam Power Plants [in Russian], Moscow, Trudy MÉI, No. XI (1953).
3. D. D. Kalafati, Teploenergetika, 4, 74 (1960).
4. M. Chambadale, Rev. gen. electr., 67, No. 6, 332 (1958).

AN INVESTIGATION OF CRITICAL HEAT FLUXES DURING FORCED MOVEMENT  
OF MONOISOPROPYL DIPHENYL HEATED BELOW THE SATURATION TEMPERATURE

G. N. Karavaev, A. D. Leongardt, and Yu. P. Shlykov

Translated from *Atomnaya Énergiya*, Vol. 15, No. 1,

pp. 77-79, July, 1963

Original article submitted October 23, 1962

There has recently been an intensive investigation of the use of organic heat-transfer agents for nuclear power plants.

The advantages of employing organic liquids for these purposes are well known and will not be discussed here. The organic liquids most closely investigated at the moment are various polyphenyls (diphenyl, isopropyl diphenyl, terphenyl, etc.).

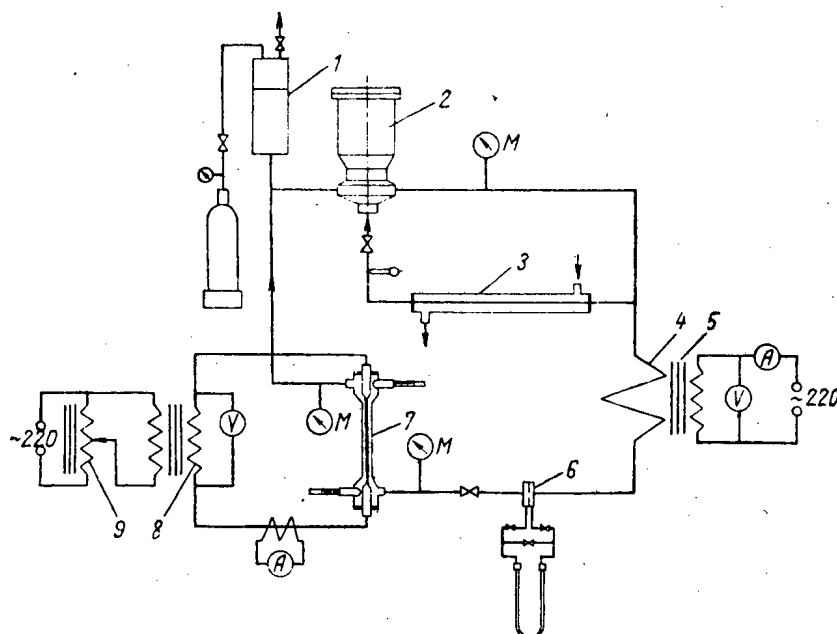


Fig. 1. Diagram of the experimental apparatus: 1) compensation tank; 2) circulation pump; 3) cooler; 4) heater; 5) transformer of the heater; 6) flow-meter diaphragm; 7) working area; 8) transformer of the working area; 9) autotransformer.

The density of heat fluxes in reactors is very high; therefore, even under conditions of heat transfer to a non-boiling liquid, with fairly considerable variations in the reactor capacity and a change in the pressure of the liquid or of the geometry of the heat-transfer surfaces the temperature of the walls of the heat emitting elements may sometimes exceed the saturation temperature. Film boiling (critical region of heat removal) may occur. Therefore, to establish reliable thermal conditions for a reactor. Data on the critical thermal loads for the corresponding heat-transfer agent are necessary.

Absence of reliable generalized relations for determining critical heat fluxes during forced flow of different liquids requires experimental data. Our aim was to investigate the critical region of heat removal during forced flow of monoisopropyl diphenyl (MIPD), below the saturation temperature, in a channel.

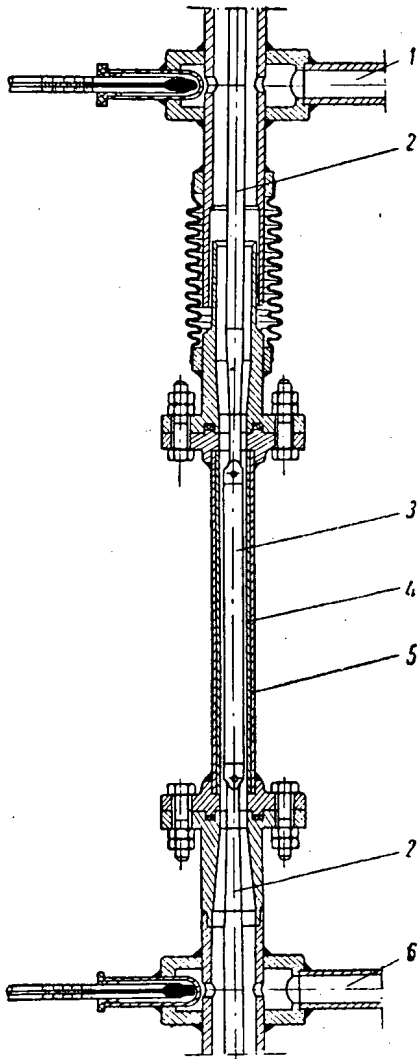


Fig. 2. Working area: 1) heat-transfer agent outlet; 2) current conducting rods; 3) working element (plate); 4) ceramic insert; 5) working area pipe; 6) heat-transfer agent inlet.

The design of the working area is shown in Fig. 2. The working element was a plate of 1Kh18N9T stainless steel to which current conducting rods were welded; it was installed in a tube with a ceramic insert and was centered in two mutually perpendicular directions. The working element was heated by an alternating current from transformer 8 (see Fig. 1), incorporated in the circuit via regulating autotransformer 9. Transformer 5, whose secondary winding consisted of twelve coils of the loop pipeline, served for preheating the liquid in the loop. The flow rate of the heat-transfer agent was determined by diaphragm 6, calibrated against water.

The experiments were carried out on plates of width 6 and 8 mm, thickness 0.2 mm and length 125 mm. The diameter of the ceramic inserts was 8 and 10 mm, respectively.

In most experiments the critical thermal load was obtained by a slow increase in the electric power through the working element at constant pressure, temperature and velocity of MIPD at the working area outlet, and was recorded from instrument readings at the time of plate overheating. In some experiments the critical load was obtained by a gradual reduction in underheating of the liquid to the saturation temperature. Burning out of the experimental element when the critical region of heat transfer was approached took place at the liquid outlet.

The critical thermal load varied from  $3.7 \cdot 10^6$  to  $4.8 \cdot 10^6$  kcal/m<sup>2</sup>·h when the speed of the liquid was 6.3 m/sec and the value of underheating 124-190°C; it was between  $2.7 \cdot 10^6$  and  $3.6 \cdot 10^6$  when the speed of the liquid was 4.24 m/sec and the underheating 120-195°C. The accuracy of a critical load determination was 4.5%.

Figure 3 gives the results of experiments at these two speeds. From the results, it may be concluded that the critical heat fluxes for MIPD are a linear function of the underheating, as was previously established for other liquids.

The apparatus shown in Fig. 1 was set up for experimental determination of the critical thermal loads; it consisted of a closed circulation loop, in which a centrifugal pump (without a gasket) and electric heater were connected in series, and a working area. To cool the pump bearings and control the temperature in the loop, some of the heat-transfer agent was passed from the pressure main of the pump to the bearing unit of the latter via a cooler. The pressure in the loop was created by means of an expansion tank, to which nitrogen was fed from a cylinder. All components and pipelines in contact with MIPD were made of steel 1Kh18N9T.

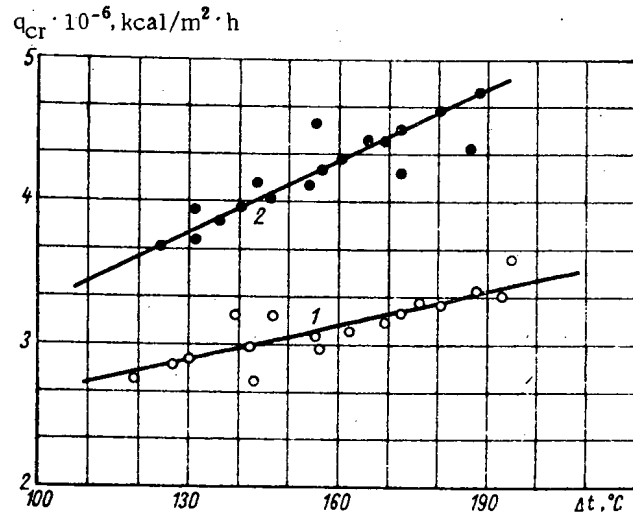


Fig. 3. Relation between the critical thermal load and underheating of the liquid for two circulation rates (1, 2—circulation rate 4.24 and 6.27 m/sec, respectively).

The fact that the experimental points for different pressures (3-6 abs atm) lie fairly close to a straight line indicates that within this range of variation the pressure has little effect on the critical thermal load. A comparison showed that the experimental data do not agree with some of the criterial relations proposed for determining critical heat fluxes [1-3].

LITERATURE CITED

1. S. S. Kutateladze, Heat Transfer During Condensation and Boiling [in Russian], Moscow, Mashgiz (1952).
2. A. A. Ivashkevich, Atomnaya Energiya, 8, 51 (1960).
3. B. A. Zenkevich, Atomnaya Energiya, 6, 169 (1959).

## DETERMINATION OF THE PERMEABILITY OF PIPE WALLS WITH RESPECT TO HELIUM

I. S. Lupakov, Yu. S. Kuz'michev, and Yu. V. Zakharov

Translated from *Atomnaya Énergiya*, Vol. 15, No. 1,

pp. 79-80, July, 1963

Original article submitted August, 18, 1962

The use of helium as a heat-transfer agent in high-temperature and high-pressure installations involves considerable difficulties because leaks may occur via the walls of vessels and pipes or welds.

Helium may leak through microdefects of welds of the metal itself or as a result of diffusion through the walls of pipes or vessels.

Information on diffusion of inert gases through metals is very contradictory. Some investigators [1, 2] state that inert gases do not diffuse through metals at all, while others [3, 6] give experimentally determined coefficients of diffusion of inert gases through various metals. In their experiments the inert gas was introduced into the metal by ionic bombardment or dissolution of radioactive isotrops (decomposition of the latter giving inert gases).

Diffusion of helium introduced by such methods only confirms the possibility of helium diffusion from the gas phase. There are no direct experimental proofs of this in the literature.

To investigate the permeability of the walls of tubular metal samples with respect to helium, an apparatus (Fig. 1) was therefore developed; it consisted of a vacuum furnace containing the sample, a PTI-4A leak detector and systems for pumping and feeding helium to the sample.

The vacuum furnace consisted of cylindrical chamber 2 (volume 7.5 liters) containing tubular furnace 3, made from alundum cylinders 1, with Fecraloy-type spiral 4. One end of the chamber was hermetically sealed, the other end had a detachable cover 15 with a rubber seal. A flanged sleeve 14 was welded to the cover. The sample investigated 10 (a tube with a hermetically sealed end) was fixed to this flange. On the other side of the pipe was a flange with a connecting pipe. The maximum diameter of the tube was 35 mm and the length 600 mm. Pipe 11 was led into the connecting pipe of the sample; helium was fed to the latter via 11 from a cylinder with two valves 9 and 12 (allowing exact control of flow) and gauge 13 for measuring the helium pressure in the sample.

Valve 12 served for feed and control of helium pressure in the sample; the high-pressure system was connected to the atmosphere by valve 9. The vacuum furnace was evacuated by backing pump 6 and diffusion pump 7. The vacuum furnace was cut off from the evacuation system, connected to leak detector 5, by valve 8. During the investigations the vacuum in the chamber was measured by an LM-2 tube with a VIT-1 instrument; the temperature of the sample was measured by two chromel-alumel thermocouples.

The temperature fall was measured on all samples before determining the permeability in order to determine the surface of the sample heated to the pre-set temperatures. The temperature fall over the length of the tube was measured at eight points by the chromel-alumel thermocouples and a portable potentiometer.

To check that defects were absent, all the tubes were subjected to hydraulic tests (pressure of the water

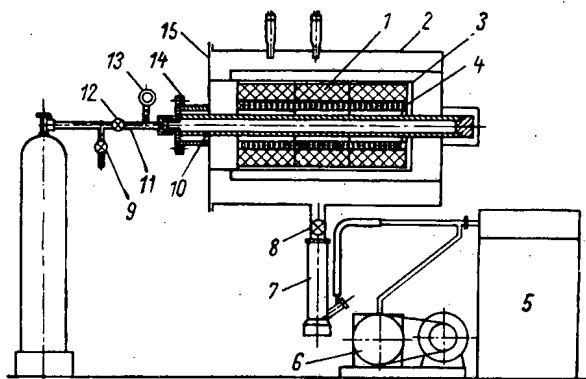


Fig. 1. Diagram of the apparatus for determining helium permeability.



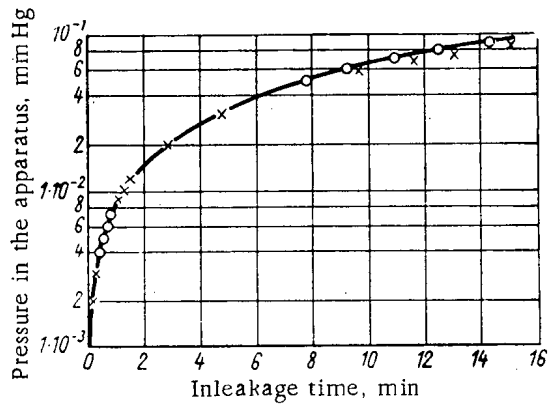


Fig. 2. Inleakage curve of the vacuum system: O) no helium in the investigated tube; X) investigated tube filled with helium.

Under stable conditions such measurement is perfectly justified because in this case the amount of helium in the mass spectrometer chamber at any time is proportional to the amount of helium in the vacuum furnace chamber.

The qualitative relationship between permeability, time and stress in the tube walls may be assessed from the results obtained in this way.

The quantitative relationship between temperature, pressure and stress in the walls was investigated in the same apparatus.

After the temperature, vacuum and helium pressure in the investigated sample had been stabilized, the pumping system was cut off from the vacuum chamber by valve 8 (see Fig. 1) (during this process the leak detector was also cut off from the system) and the inleakage of gas in the vacuum chamber was measured by means of tube LT-2 and the VIT-1 instrument. The inleakage time was measured by a stopwatch. The measurements were made with and without helium in the tube. The inleakage as a result of permeation of helium via the metal may be determined from the inleakage differences in the two cases.

For higher accuracy of measurements it was necessary that the initial vacuum was the same in both cases before the measurements were begun. It must be borne in mind that the smaller the inleakage as a result of gas emission from the walls of the chamber and components in the latter the smaller the value of the permeability determinable by this method. It may be shown that for the conditions of our vacuum system the minimum permeability determinable in this way is  $\sim 10^{-9}$  liter/cm<sup>2</sup>·sec.

In fact, the helium permeability may be expressed by the relation

$$Q = \frac{\Delta p v}{760 t S},$$

where  $\Delta p$  is the pressure change in the system as a result of helium permeability, mm Hg;  $v$  is the volume of the vacuum chamber (7.5 liters);  $S$  is the sample surface heated to the preset temperature (300 cm<sup>2</sup>); and  $t$  is the time in which the pressure in the chamber changes by a value  $\Delta p$  as a result of helium permeability.

From the inleakage curve (Fig. 2) for our system it may be seen that in 75 sec  $\Delta p$  as a result of helium permeability must be not less than  $2 \cdot 10^{-3}$  mm Hg because the scatter of the points on the curve in this region is  $1 \cdot 10^{-3}$  mm Hg.

Substituting these values we obtain  $Q = 0.9 \cdot 10^{-9}$  liter/sec·cm<sup>2</sup>.

Samples of austenitic stainless steel (two marks) and a nickel-based alloy were tested in this apparatus. It was found that at temperatures  $> 600^\circ\text{C}$  and pressures  $> 60$  atm, helium passes through the walls of tubular samples, the permeability being less than  $1 \cdot 10^{-9}$  liter/cm<sup>2</sup>·sec.

up to 150 atm) before they were placed in the furnace. Further, the tightness of the welds and integrity of the tubes were checked by means of a leak detector at an excess helium pressure within the tube up to 100 atm and a vacuum of  $10^{-5}$  mm Hg outside the tube. These tests on the tubes at room temperature before and after determining the permeability were necessary to check absence of defects.

After the tube had been placed in the furnace it was evacuated to  $\sim 1 \cdot 10^{-5}$  mm Hg. The leak detector was made ready at the same time.

When the sample had reached the preset temperature, helium was fed to the tube, the stresses in the walls being varied by adjusting the pressure of the gas. After stable condition had been established, the amount of helium penetrating into the chamber from the sample was measured (in relative units) by the leak detector from the readings of an external instrument.

LITERATURE CITED

1. C. J. Smithells, Gases and Metals [Russian translation], Moscow, Metallurgizdat (1940).
2. R. Berrer, Diffusion in Solids [Russian translation], Moscow, Izd-vo inostr. lit. (1948).
3. A. M. Rodin and V. V. Surenyants, Fizika metallov i metallovedenie, 10, No. 2 (1960).
4. A. Le Clair and A. Rowe, Rev. met., 52, 94 (1955).
5. K. Zimen and L. Dahl, Z. Naturforsch., 12a, No. 2, 167 (1957).
6. F. Norton and C. Tucker, J. Nucl. Materials, 2, No. 4 (1960).

## THE FLUORINATION OF URANIUM SULFATE BY CHLORINE TRIFLUORIDE

N. S. Nikolaev and Yu. D. Shishkov

Translated from *Atomnaya Énergiya*, Vol. 15, No. 1,

p. 81, July, 1963

Original article submitted November 1, 1962

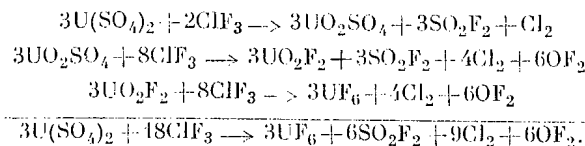
Chlorine trifluoride is used in fluorination processes instead of free fluorine [1]. Numerous syntheses have been described for fluorides of various metals, including the hexafluorides of molybdenum, tungsten, and uranium [2, 3]. Uranium tetrafluoride [4], uranyl fluoride [5], and other uranium compounds have been suggested as the starting compounds for the production of uranium hexafluoride.

## The Fluorination of Uranium Sulfate by Gaseous Chlorine Trifluoride

Temp. of fluorination, °C	Chemical composition of residue, %				Comp. of residue w. r. t. compounds, %			Yield of uranium as hexafluoride, %
	tetravalent uranium	hexavalent uranium	sulfate ion	fluorine	U(SO <sub>4</sub> ) <sub>2</sub>	UO <sub>2</sub> SO <sub>4</sub>	UO <sub>2</sub> F <sub>2</sub>	
18	46,10	12,67	37,66	1,80	83,20	2,20	14,60	9,49
50	38,71	21,71	34,28	2,30	70,60	11,50	18,55	21,67
100	30,92	31,44	30,33	3,00	56,00	20,00	24,00	41,00
150	25,80	38,05	28,33	3,00	46,39	29,44	24,13	58,73
200	10,00	56,00	23,00	3,00	18,00	57,00	24,50	75,60
250	3,00	64,60	20,40	3,60	5,30	68,00	26,70	81,30
300	--	74,43	15,70	5,00	--	62,00	38,00	90,74

The present work deals with the fluorination of uranium sulfate by gaseous chlorine trifluoride. The experiments were conducted in a horizontal cylindrical nickel reactor. The material to be fluorinated was placed in the reactor in a nickel boat. The volatile products which were formed during the reaction were frozen out in a condensation system consisting of copper and quartz traps.

The method consisted of the action of ClF<sub>3</sub> on 10 g of U(SO<sub>4</sub>)<sub>2</sub> for an hour at various temperatures. We studied the composition of the solid phase and the yield of the reaction with respect to UF<sub>6</sub>. Chemical and x-ray structural methods of analysis were used to determine the composition of the solid phase. The results of the experiments are shown in the table. It can be seen from the data that with increase in temperature the predominating component of the residue becomes UO<sub>2</sub>SO<sub>4</sub> instead of the original U(SO<sub>4</sub>)<sub>2</sub>. With increase in temperature the UO<sub>2</sub>F<sub>2</sub> content also increases and at 300°C the residue is UO<sub>2</sub>SO<sub>4</sub> with a content of UO<sub>2</sub>F<sub>2</sub> corresponding to the equilibrium state of both components. The formation of uranium hexafluoride is probably the result of fluorination of UO<sub>2</sub>F<sub>2</sub>. The fluorination of uranium sulfate can be represented in the following way:



## LITERATURE CITED

1. S. Simons, R. Bond, and R. McArthur, *J. Amer. Chem. Soc.*, **62**, 3477 (1940).
2. N. P. Galkin, et al., *Chemistry and Technology of Fluorine Compounds of Uranium* [in Russian], Moscow, Atomizdat (1961).
3. H. Leach, *Chem. and Ind.*, **5**, 242 (1960).
4. V. Labaton, *J. Inorg. and Nucl. Chem.*, **10**, 86 (1959).
5. S. Ellis and C. Forrest, *J. Inorg. and Nucl. Chem.*, **16**, 150 (1960).

## NEWS OF SCIENCE AND TECHNOLOGY

## XIII ALL-UNION CONFERENCE ON NUCLEAR SPECTROSCOPY

V. P. Rudakov

Translated from *Atomnaya Énergiya*, Vol. 15, No. 1,  
p. 82, July, 1963

The XIII All-Union Conference on Nuclear Spectroscopy convened in Kiev, January 25 to February 2, 1963. About 500 scientific workers from various research organizations throughout the nation, as well as scientists visiting from other socialist countries, participated in the deliberations.

A. B. Migdal and I. S. Shapiro delivered reports on new trends in the development of the theory of the nucleus and the theory of nuclear reactions.

The report delivered by A. G. Migdal dealt with a new approach to the study of the nucleus. Since the nucleus constitutes a system of many particles with some degree of interaction between them, a precise microscopic calculation of such a system is impossible. For the same reasons, the inquiry may not be restricted to various degrees of approximation in perturbation theory. The only way to attain quantitative relations between the various quantities characterizing the nucleus will be found in the phenomenological approach, i.e., by introducing empirically determined constants into the theory. The method resides in selecting some set of diagrams varying substantially in the energy and momentum region of interest, and in expressing their functional interrelationship by means of various constants not determined by theoretical prediction, in a manner similar to that followed in the theory of strong interactions between elementary particles where the observable mass and charge values are introduced into the dispersion relations. This way of approaching systems of strongly interacting particles was employed by Landau in the theory of the Fermi liquid. Carrying through a program of this type for the nucleus requires taking into account particles of two types, the finite dimensions of the system, and the effect of pair correlation. Among the first results obtained in this direction, we may note an estimate of the effective mass of quasi-particles in the nucleus, and an equation enabling researchers to find the probabilities of electromagnetic transitions in nuclei.

I. S. Shapiro gave an account of the dispersion theory of direct processes which he developed. In this theory, the amplitude of a nuclear reaction is approached as the sum of the amplitudes of the discrete processes, with some Feynmann diagram corresponding to each of these processes. For example, the Butler stripping process has a pole diagram, and more complicated direct processes such as knock-on reactions have a variety of triangular diagrams. The theory establishes the dependence of the contribution of various diagrams to the amplitude (distance of a singular point on the diagram with respect to the momentum transferred) on the physical region, value of the vertex parts of the diagram, and makes it possible to predict, in some cases, the role of a given process. For example, using dispersion theory as a starting point, I. S. Shapiro and S. F. Timashev succeeded in demonstrating that it is not the mechanism of the binary stripping process, the elementary theory behind which was given by Nunes, which predominates in the  $B^{10}(t, p)B^{12}$  reaction, but some other process. The angular distribution of protons in this reaction, differing markedly from that predicted by Nunes, is in excellent accord with the computations reported by Shapiro and Timashev.

Several review papers were presented to the conference. A. S. Davydov dealt with the present status of the theory of the excited states of odd nuclei. A paper presented by O. F. Nemets dealt with the use of deuteron-induced nuclear reactions in nuclear spectroscopy. A paper by B. S. Dzhelepov touched on various possible techniques for measuring the quadrupole moments of nuclei in excited states. I. V. Éstulin rendered an account on research on circular polarization of gamma photons accompanying beta decay.

Most of the time of the conference was spent in delivering original papers. Theoretical papers were primarily devoted to aspects of the theory of light and deformed nuclei. The experimental research papers may be divided into three general groups: research on the beta and gamma ray spectra of different nuclei, research on nuclear reactions with emphasis on stripping reactions, and research on Coulomb excitation of nuclei. Special sessions were also devoted to the technique of nuclear spectroscopy and to semiconductor radiation detectors.

The proceedings of the conference will be published in full in the periodical *Izvestiya Akad. Nauk SSSR*.

GEOCHEMICAL CONFERENCE DEDICATED TO THE CENTENNIAL

OF V. I. VERNADSKII

A. I. Tugarinov

Translated from *Atomnaya Énergiya*, Vol. 15, No. 1,  
pp. 82-84, July, 1963

A geochemical conference on the theme "Chemistry of the earth's crust," devoted to the centennial of the birth of the prominent Russian scientists, one of the founders of the science of geochemistry, Vladimir Ivanovich Vernadskii, was held at the House of Scientists (*Dom Uchenykh*) in Moscow, in March, 1963.

The enormous range of scientific interests, the exclusive exceptional ability to encompass a broad scope of natural phenomena and to refract his encyclopedic fund of knowledge in the form of bold empirical inferences, placed Vladimir Ivanovich Vernadskii at the head of the Soviet school of geochemists which he founded, and won universal recognition for the geochemical concepts of V. I. Vernadskii throughout the world.

Vladimir Ivanovich was one of the first scientists who found the ability, soon after the discovery of phenomena associated with radioactivity, to prophetically evaluate the significance of this new realm of knowledge. "The time is not far off," Vladimir Ivanovich wrote back in 1922, "when man will have atomic energy in his hands, such a source of power as will afford him the possibility of constructing his life as he wishes... Will man be able to exploit this force, to use it for good and not for self-destruction? Has man grown up to the point of knowing how to use this force which science must inevitably yield to his hands?"

As early as the second decade of this century, V. I. Vernadskii posed the question of developing a raw materials base of radioactive elements, and took active steps in the study of deposits of radioactive elements, by way of organizing several special expeditions and personally taking part in them. The resume compiled over the years 1910 to 1914 by V. I. Vernadskii on the abundance of radioactive minerals in Russia received its due acknowledgment only in the forties, when the problem of the supply of nuclear raw materials was resolved in the USSR.

In his program work "Outlines of geochemistry" [*Ocherki geokhimii*] published in 1924, V. I. Vernadskii for the first time laid bare the dominant features of uranium and thorium geochemistry, and his findings have been brilliantly confirmed by subsequent research. For example, Vladimir Ivanovich even in those years pointed out the intimate relationship linking natural uranium concentrations and organic matter. He emphasized the common geochemical fate of thorium and uranium in magmatic processes, and the separation of those elements in hydrothermal and surface migration phenomena. His formulation of the laws governing the dispersion of the elements, in particular of uranium, harks back to the same period.

V. I. Vernadskii was a zealous partisan of the idea of conducting research in the fields of radioactive heat, geochemistry of isotopes, assimilation of radioactive techniques in measurement of absolute geological time and of the age of rocks. "The introduction of this new time standard," he wrote, "ranging in the millions of years instead of the arbitrary-subdivisions of the geological stratigraphic time scale may be compared uniquely to the heroic age in the history of geology—to the creation 100 years ago of the basic stratigraphic approach in geology."

It could be boldly stated that the name of V. I. Vernadskii is linked to the founding of such presently acknowledged sciences as radiogeology and nuclear geochemistry. The enormous amount of interest now placed on this centennial by the scientific community of the entire world hardly requires any explanation in that light. It suffices to say that the Soviet scientists were not alone at the centennial conference, being accompanied by such distinguished foreign scientists as J. Orsel (France), one of V. I. Vernadskii's disciples, M. Roubeau (France), E. Szadecky-Kardos (Hungary), V. Ianovit (Rumania), K. Wedepohl (West Germany), E. Kautsch (East Germany), H. Todt (Canada), R. Russell (Canada), D. Kalp (USA), T. Lowering (USA), K. Sugowara (Japan), and others.

The conference set at its aim an elucidation of the present status of geochemical knowledge, extension of that knowledge along the lines first formulated by V. I. Vernadskii. The problems of biogeochemistry, representing an independent and enormous domain of science to which V. I. Vernadskii made a tremendous contribution in his time, were not touched upon at this conference, since these questions will be the subject of some special sessions scheduled for late 1963.

The brunt of the conference's attention centered on aspects of research into geological processes by isotope geochemistry techniques; experimental investigations of matter at elevated temperatures and pressures provide some interpretation of phenomena occurring at significant depths; and the geochemistry of individual elements in magmatogenic and sedimentary processes. A total of 52 papers were read.

Of unusual interest were reports on experimental attempts at melting out from chondrites (by way of simulating the earth's mantle) matter similar to the basalts, i.e., to the earth's crust, in its composition (A. A. Yaroshevskii, A. P. Vinogradov). The zone melting principle resides primarily in the fact that, as a heat wave (a temperature peak exceeding the melting point of the rock) moves slowly down a column of the material under study, the low-melting and volatile components are displaced in unison with the heat wave in the direction of wave motion. The high-melting fraction of the melt remains behind the wave front, as a result, with the low-melting components, including compounds of the radioactive elements, accumulate in the forward zone. This process conforms in some degree to the probable mechanism behind the differentiation of the earth's matter by radioactive heat generated in the depths of the earth's mantle.

A similar effect is presently invoked to account for the formation of rhythmically stratified intrusive alkali blocks of Lovozero pluton (V. P. Volkov, L. N. Kogarko).

The audience listened with rapt interest to a report delivered by W. Fife (USA) on the properties of transition metal ions and the dependence of those properties of the crystal field of minerals.

Several papers dealt with the geochemistry of isotopes and the problem of measuring geological (absolute) age.

D. Kalp formulated the conditions governing the applicability of various techniques of absolute age measurement to rocks of different origin. In particular, he pointed out the slight error introduced by weathering in measurements of argon-potassium age by the biotite method. Even with 50% potassium losses, the biotite usually yields an undistorted age value, since the potassium losses are paralleled by argon losses. On the other hand, an experimental study of cation exchange phenomena (processing of micas with calcium chloride and magnesium chloride solutions) demonstrated a considerable removal of strontium from the minerals, leading in the process to a pronounced decline in age values obtained by the strontium rubidium ratio. Micas subjected to ground-water action may, therefore, be measured successfully by the argon-potassium method, but the strontium method will prove to be far less suitable in that application. At the same time, measurements by the argon method on the age of rocks which have experienced considerable submergence actually fail to provide useful information on their primary age, or even on the age of the metamorphic changes. The values thereby obtained indicate the time when these rocks were brought up to the earth's surface and the removal of argon in response to heating by the temperature gradient established at great depths came to a halt. These data are sufficient to illustrate the extremely sharp bounds of applicability of both the argon and the strontium methods in absolute age measurements of rocks.

The lead-uranium-thorium method remains, as before, the most reliable one, despite its many limitations. For example, in his systematization of worldwide data on the subject, including Soviet data, Kalp pointed out that most uraniferous minerals should not be regarded as strictly closed systems, since a loss of radiogenic lead is typical of most such minerals. As an example, the uraninites selectively lose  $Pb^{208}$  through the special position of thorium in its structure, as a rule. The age determined by the  $Pb^{208}/Th^{232}$  ratio therefore generally comes out lower than the true age. Zircons lose their radiogenic lead to a rate directly proportional to their uranium content. The most reliable age value for that mineral species is, then, the value obtained by the  $Pb^{207}/Pb^{206}$  ratio.

É. K. Gerling cited exceptionally intriguing data on the age of ancient rocks older than 5 billion years, based on age measurements of pyroxenes in ancient gneisses and ultrabasic igneous rocks of the Kola peninsula; he used the argon-potassium method. Because of the exceptional stability of argon in the lattice structure of the pyroxenes and its insignificant concentration, ascribed to the low potassium content, these minerals appear as relics of the most ancient rocks in the earth's crust.

G. A. Kazakov reported the results of experimental studies on glauconite, which resulted in the reliable use of this mineral in measurements of the ages of sediments. A correlation of the Riphean-Sinian deposits throughout the entire territories of the USSR and the Chinese Peoples Republic was successfully completed with the aid of this method. The most ancient Riphean-Sinian formations, 1350 to 1500 million years old, were discovered in the Urals and in the Western Aldan region. On the basis of absolute age measurements, the Riphean is currently seen as subdivided into three formations characterized by distinct types of blue-green algae. Differences in the tectonic regimes of the regions in the Lower and Upper Riphean are acknowledged.

R. Russell, who has made a study of the variation in the isotope composition of lead exemplified by six large ore provinces (among which are Broken Hill, Sudberry), showed that lead found in ore may be regarded as a mixture of leads of different origins. In most cases, they constitute a mixture of two types of lead appearing in contrasting geological settings: in rocks with different proportions of lead, uranium, and thorium, and in rocks of different age. A statistically large number of measurements makes it possible to compute the isotopic composition of lead belonging to each such type included in a given mixture, and to establish in the specific case the age of the stratum in which the given lead was formed, the time it became detached from the host rock, and the uranium/thorium ratio in any such pay strata. Russell produced convincing examples of agreement between the data which he predicted on the basis of analyses of the isotopic composition of lead and data obtained by direct measurements of the uranium and thorium content in the original rocks, and their age. For instance, the earlier mineralization of the Broken Hill deposit is dated at 1600 to 1700 million years ago. A later mineralization dated at 500-530 million years ago is noted at the same deposit. Corresponding to this later stage is a lead mineralization which differs sharply in its isotope composition from the primary ores in the deposit. The later mineralization consists of a mixture of two leads: an earlier lead belonging to the primary ores in the deposit, and admixtures of lead separated out, as calculations demonstrate, from the host rock 510 to 80 million years ago. The  $Pb^{208}/Pb^{206}$  ratio in this admixture is indicative of the original thorium/lead ratio ranging from 3.8 to 6.7 in the host rock. A large number of thorium and uranium determinations in the rock yielded the same fluctuations in the thorium/uranium ratio. Russell's report was particularly remarkable in its added emphasis on the "terrestrial" origin of the ore-bed lead, placing its origin not at some unknown and impenetrable depths, but right in the rocks of the earth's crust.

H. Todt sketched out a convincing picture of the dependence of fractionation of sulfur isotopes on the rate at which life developed in the submerged-shelf seas at a certain geological epoch, and on vulcanization periods. V.A. Grinenko demonstrated the possibility of using isotope ratios of sulfur and sediments to find the degree of aeration of ancient sedimentation basins.

M. Roubeau reviewed the experience acquired in the use of a quantummeter at the Nancy research center, in order to obtain mass high-precision determination of elements in rocks. This experience points to the exceptional promise of this technique as a geochemical research tool. D. Shaw (Canada) likewise drew attention to the importance of mass high-precision measurements of the distribution of impurity elements, citing as an illustration examples of studies of the distribution of dispersed elements in apatite, to probe the genesis of that mineral. The same thought ran like a red thread through a paper by R. Coulomb (France), who gave an account of the setting up of geochemical research and experimentation at the French nuclear research center.

The last days of the conference heard reports devoted to the geochemistry of sediment formation and endogenic ore formation (A. B. Ronov, A. Migdisov, A. I. Tugarinov, V. L. Barsukov, A. A. Beus, E. Kautsch, and K. Wedepohl); these reports showed what enormous significance sedimentation processes have as one of the major factors in the differentiation of the earth's matter, in several cases predetermining the appearance of geochemical provinces.

The conference attracted a large number of participants, with the attendance surpassing 1000 persons on some days.

## NEW TRENDS IN RESEARCH AND APPLICATIONS FOR RARE EARTHS

L. Polyakov

Translated from *Atomnaya Énergiya*, Vol. 15, No. 1,  
pp. 84-86, July, 1963

A conference on new trends in the applications of rare-earth elements and research on those metals was held in Moscow in March, 1963 at the A. A. Baikov Institute of Metallurgy. The reports reviewed and discussed methods for winning and purifying rare-earth metals, studying phase diagrams, research on the electrical, magnetic, and semiconducting properties of the rare earths, studies of their crystal structures, and applications of rare earths in the production of alloys and steelmaking.

At the present time, the rare earths, with their unique and special properties, are winning ever increasing favor in applications in the most disparate branches of science and industry. The promise held forth in the utilization of the rare earths is most apparent in the metallurgical industry, in the production of various steels and alloys, inasmuch as alloying of steels, cast irons, and alloys with rare-earth elements enhances the properties of these industrial metals considerably. The rare-earth metals may likewise find broad areas of applications in nuclear power. Samarium, europium, gadolinium have large absorption cross sections for thermal neutrons, so that these metals and their compounds may be employed with success as materials for reactor control rods. Yttrium, which does not interact with fused uranium and which presents a relatively small absorption cross section to thermal neutrons, can be employed as a structural material for fuel-element cladding. Rare earths find a multiplicity of applications in electronic design, in radio engineering, in the silicate industry, etc., both the metals and their compounds figuring prominently. A successful exploitation of the properties of rare earths calls for a study of their internal structure, their phase diagrams, and their various properties (electrical, magnetic, semiconducting). Lanthanum and cerium are diamagnetic, neodymium, thulium and other earths are paramagnetic, while gadolinium, terbium, dysprosium are ferromagnetic, but only gadolinium possesses ferromagnetic properties at room temperatures in the case of the other earths.  $\gamma$ -cerium,  $\alpha$ -neodymium,  $\alpha$ -samarium, etc., are found to be antiferromagnetic in the low-temperature regions. Values of the mean atomic magnetic moment and the paramagnetic Curie point have been found for all the rare-earth metals and alloys studied in the temperature range from 77°C to 1400°C. Rare-earth alloys of types  $RCO_x$  and  $RFe_x$  (R standing for a rare earth element) exhibit the properties of ferromagnetic materials.

Rare-earth metals form high-melting compounds with boron, carbon, nitrogen, silicon, selenium, phosphorus, and other elements. For examples the refractory compounds  $ScB_4$  possesses a tetragonal structure, high electric resistivity (750 microhms/cm at 20°C), low coefficient of thermal expansion (equal to  $3 \cdot 10^{-6}$  in the 70 to 1000°C range of temperatures), great hardness ( $4200 \pm 325$  kg/mm<sup>2</sup>). The selenides of the rare earths (gadolinium selenide, lanthanum selenide) exhibit semiconductor properties. The sesquisulfides of the rare earths are p-type impurity semiconductors with a forbidden zone width 1.32-1.06 eV in the intrinsic conduction region. The monosulfides of the rare earths exhibit an electronic conduction of a metallic character. The thermoelectric figure of merit of the sesquisulfides of the rare earths is appreciably higher than in many known semiconducting materials. Findings obtained on studies of the various physicochemical, mechanical, and engineering properties of refractory rare-earth compounds indicate great promise for their exploitation in electronics, in semiconductor engineering, and in nuclear power applications.

Phosphors activated by rare-earth dopants are of significant interest.

The introduction of cerium into vanadium enhances the plastic properties of the latter, making it possible to roll vanadium cold with a total calcining of 95 to 99%, and with no intermediate anneals. Vanadium-gallium alloys exhibit superconducting properties. The introduction of trace amounts of ferrocium, combined with Si, Al, Ni, into LS74-3 brass brings about an improvement in the engineering properties of the brass.

The welding of 20GSYuT alloy wire, with alloying of both ferrocium in amounts of 0.3-1.5% and metallic cerium, lanthanum, has resulted in a metal seam stronger by a factor of 1.5 to 2 than the welded metal. Several papers dealt with research on the physicochemical properties of gadolinium, yttrium, and the interaction diagrams of these elements with various groups in the Mendeleev periodic table.

Some of the papers touched on applications of the rare earths as catalysts, conditions for wining rare-earth metals, etc.



Rare earths show a great affinity for oxygen, sulfur, phosphorus, arsenic, which drastically impair various properties desired in steels and alloys. Introduction of rare earths in small quantities in various steels, cast irons, and alloys consequently results in a significant improvement in the plastic, engineering, structural, corrosion-resistant, mechanical, and other properties of metals and alloys so treated.

In using rare earths (lanthanum, praseodymium, neodymium, cerium) in the process of deoxidation or killing of steels, refractory oxides form and are carried off in the slag. Using cerium to kill structural steels contributes to improvements in the quality of the ingot surface.

The engineering properties of steels, surface quality, corrosion-resistance properties, plasticity at hot rolling temperatures, all these are improved by the addition of 0.05 to 0.18% rare-earth metals to Kh18N12M2T and 1Kh18NTsG stainless steels, and by the addition of 0.08 to 0.12% rare-earth oxides.

Alloying of nickel-base KhN77TYu alloy by specific rare earths (Ce, La, Pr, Nd, Sm, mischmetal) effects a substantial lengthening of the long-term strength of the alloy, with enhanced resistance to creep flow at 700°C. Addition of lanthanum, cerium, neodymium, mischmetal in amounts up to 0.07% doubles the service life of the alloy under thermal cycling at 1200°C. The elements introduced simultaneously effect a vigorous deoxidation of the alloy, reducing the oxygen content by a factor of 2 to 6, modify the intragranular structure, and enhance the diffusion mobility of the alloying elements.

The introduction of rare-earth elements (cerium, lanthanum, neodymium, etc.) into iron, cobalt, nickel, in amounts corresponding to their solubility in those metals in solid solution (0.05-0.3%) refines the metals, comminutes the grain of the heat-worked metal, enhances the mechanical properties, and in some cases even brings about improvements in the electrical and magnetic properties.

The properties of such structural steels as 30KhGSA, 18KhNVA, 12Kh2N4A are markedly improved when rare-earth metals are added to them in the form of ferrocerium, in amounts of 0.1%; the dendritic structure is broken down, mechanical properties and the ability to take tempering treatment are improved, and the sulfur content is lowered.

Addition of 0.7 to 1.5 kg/ton ferrocerium in the melting of experimental batches of 34KhN1M and 40KhGS steels drastically improves the macrostructure of the ingot, and exerts a favorable effect in modifying the nature of the liquation of sulfur present. The introduction of rare-earth elements in amounts of 0.7 to 0.85 kg/ton improves the plasticity and resilience characteristics of 34KhN1M steel. Cerium exerts a modifying effect on the properties of pig iron in cast iron work. The greatest effect brought about by cerium modification is observed in pig irons of peritectic and hypereutectic compositions. The addition of ferrocerium to pig iron has a positive effect on the latter's mechanical and engineering properties.

Taking note of the achievements made in the field of the development of new techniques for purifying rare earths, producing single crystals, in investigations of many new physical properties, studies of phase diagrams, of alloy bases for steels, of alloys, the conference acknowledged the necessity of a further expansion of the scope of research work on phase diagrams, crystal structures, and on the thermodynamical, electrical, magnetic, semiconducting, piezoelectrical, ferroelectrical, and miscellaneous properties of the rare earths, to further broaden the use of the rare earths in the various branches of science and industry.

CONFERENCE ON NUCLEAR POWER DEVELOPMENT  
IN THE CZECHOSLOVAK SOCIALIST REPUBLIC

S. Medonos

Translated from *Atomnaya Energiya*, Vol. 15, No. 1,  
pp. 86-87, July, 1963

The II National Conference on engineering and costs aspects of nuclear power development in Czechoslovakia, organized by the nuclear power commission under the jurisdiction of the Central Council of the Czechoslovak Science and Engineering Society, met in Prague during October 1962. About 250 persons took part in the proceedings, with representatives of industrial enterprises, research institutes and design institutes, and also of advanced technical schools, prominent in attendance.

The major theme of the conference was the question to what extent and precisely in what manner nuclear energy might contribute, in the future years, to offsetting the deficit in the nation's fuel and energy budget. The reports and ensuing discussion attempted a summary of research and engineering work related to the design and fabrication of equipment for Czechoslovakia's first nuclear-fueled electric power station.

In the lead-off report by the Vice-Minister and Chairman of the State General Planning Commission Z. Pucek, a talk entitled "Prospects for the development of nuclear power in the CzSSR," mention was made of the difficulties impending in expansion of coal mining activities in the CzSSR in the future, this being the country's major energy source (the specific weight of coal in the total fuel needs of the nation amounts to near 90%). The conclusion of this introductory paper stressed the importance of costs aspects of nuclear power for a correct assessment of its tempo of development.

The second report to the conference was entitled: "Engineering and design problems in building the CzSSR first nuclear power station, and a survey of research work in the field of the physics and engineering of the KS-150 reactor." Reporter J. Hauer discussed the natural-uranium-fueled gas-cooled heavy-water power reactor modeled on Soviet designs [cf. A. I. Alikhanov, et al., *JAE*, 1, No. 1, 5 (1956)]. The main point of the paper was a detailed exposition of the design and production technology of the reactor pressure vessel. The vessel will apparently be the world's largest high-pressure vessel for power reactors at its date of completion (the design calls for a diameter of 5 meters, height of 20 meters, wall thickness 150 to 325 mm). Special equipment has been developed and fabricated to handle the forging, rolling, electroslag welding, assembly, machining, and heat treatment (this equipment includes welding machines, a large vertical turret lathe of special design, sectioned electric furnaces for heat treatment before and after welding, a special testing rig capable of developing 6000 to 8000 tons of force for studying brittle fracture of large parts, etc.). A model pressure vessel 5 meters in diameter and 10 meters long was built to facilitate a careful investigation of the optimum design and the internal stresses likely to arise in the vessel. In addition to the description of the principal reactor components, the report also included a general survey of research and experimental work on structural materials, on the fabrication technology and quality control methods employed in the production of individual reactor components.

A third paper, "Some aspects of the design, fabrication of equipment, and building of nuclear electric power stations," (delivered by C. Sklenicek) dealt with various subdivisions of the A-1 power station (steam generators, gas blowers and the ancillary equipment for the primary loop of the station, the turbogenerator, fixtures and ducting, control system). The introductory portion of the report considered the special features of nuclear power stations involving techniques to keep radioactive contamination from spreading, biological shielding, and operational safety measures. The concluding portion was given over to an analysis of some possibilities and ways to enhance the cost competitiveness of nuclear power stations.

In the concluding report delivered by J. Neumann, Chairman of the Czechoslovak Atomic Energy Commission ("Utilization of experience and survey of work concerning the A-1 nuclear power station, in other branches of the national economy of the CzSSR"), stress was placed on the significance of nuclear electric power generating stations in plans to provide Czechoslovakia with a sufficient amount of electric power in the future, and the contribution of scientific research to the precipitate rise in the technical level of the work of several metallurgical and machine tool plants throughout the country were mentioned.

The representatives of institutes and industrial plants who participated in the discussion gave accounts of their work and exchanged views which will undoubtedly bring a certain benefit, particularly in view of the work now lying ahead in the design and building of new nuclear electric power generating stations.

Technical films dealing with nuclear reactors (welding of the pressure vessel and assembly of fuel elements for the KS-150 reactor, reactor automatic control equipment) and the construction of the A-1 nuclear power station were shown to the participants at the conference. A trip was organized to the State Power Research Institute (in particular, to the laboratory on mechanical and aerodynamical testing of fuel elements).

The conference, which formed a definite part of a nation-wide discussion organized under the auspices of the Central Committee of the Communist Party of Czechoslovakia, demonstrated on the whole, in the area of prospects of the development of the socialist society in the CzSSR, that nuclear power can and must play a great future role in the country's power picture. However, a good deal of work stands before us in this endeavor.

The basic problems to be tackled in future work were outlined in resolution form at the conference:

a) speeding up the construction of the A-1 nuclear power station, to be the principal link on the road to technical assimilation of nuclear power techniques in the CzSSR, as well as constituting a distinct step in the program for building nuclear electric power generating stations;

b) proceeding ahead in work on the planned industrial nuclear power station A-2, and scheduling its construction during the coming Seven Year Plan (1964 to 1970);

c) developing a comprehensive nuclear power development plan wherein nuclear power is recognized as the only possible new power source for the CzSSR in the decade of the seventies;

d) acceleration of the discussion and completion of collaborative ties, coordination and delegating of work in the field of nuclear power between those countries adhering as members to the Council for Mutual Economic Aid.

In conclusion, the participants adopted a proposal to schedule a conference on heavy-water power reactors in the fall of 1963.

#### CONFERENCE OF THE PLASMA PHYSICS SECTION OF THE AMERICAN PHYSICAL SOCIETY

V. K.

Translated from *Atomnaya Énergiya*, Vol. 15, No. 1,  
pp. 87-88, July, 1963

The fourth conference on the plasma physics section of the American Physical Society met in Atlantic City (State of New Jersey) in late 1962. 400 physicists included guests from the United Kingdom, Canada, the Soviet Union, France, West Germany, Sweden, and Japan were in attendance, to hear about 200 papers and reports.

A wealth of new research findings probing in already familiar directions was reported to the conference delegates.

An intense research program is being conducted with the Princeton Stellarator C machine, with the object of studying the behavior of a plasma during and after completion of ohmic heating. The prominent dependence of the behavior of a plasma on current direction in the plasma with respect to the confining magnetic field drew the attention of experimenters during work with the stellarator coils disconnected. It is manifested in the difference in the amount of energy absorbed by the plasma, in the lifetime of the plasma, in the position of the plasma pinch in the chamber, and in the emission intensity of impurities. The best results are obtained when the current flowing through the plasma is in antiparallel direction to the confining magnetic field; the confinement time of the plasma in this case is 2.7 times longer than in the stellarator B-3. The difference described in the behavior of the plasma

is removable by means of a very weak field  $H_\phi$  (5 G on the axis  $H_Z = 35$  kG) established by four conductors lodged alongside the stellarator chamber above the coils of the confining field. This effect is contributed to appreciably when the stabilizing stellarator winding is turned on.

Measurements revealed that the principal radiation losses are due to oxygen (in the leading part of the ohmic heating pulse) and to carbon (in the trailing portion of the pulse).

A. Bishop, et al., measured radiation losses in the stellarator C in the region of the vacuum ultraviolet, and drew up the energy budget for various values of power supplied from outside. It was shown that the quantity of impurities present is not large (consisting of oxygen and carbon for the most part), since 80% of the energy emitted is accounted for by the helium line, with helium filling the chamber. If the supplied power does not exceed 100 kW (for a current below 4 kA), then the energy balance may be entirely accounted for by radiation. When the current is increased, the supplied power begins to exceed the measured radiated power. For example, at 6 kA current the measured radiated power did not exceed 50% of the supplied power. The temperature measured in these experiments relative to the intensity of the ionized oxygen line was not higher than 20 eV.

B. Stogyek, et al., found that superposition of a weak electric field  $\sim 0.01$  V/cm in a decaying cold plasma brought about a current density  $\sim 1$  A/cm formed for the most part by the small number of runaway electrons, while the current dropped by sharp discontinuities which are strictly correlated at an external electric field of 0.01 V/cm with noise bursts at the electron cyclotron and plasma frequencies, and with an increase in the emission of the  $H_\beta$  line.

In other experiments, a study was made of the dependence of plasma losses on the amount of ohmic heating current in the stellarator. It was found that the rate of particle losses is in excellent accord with the approximate ratio  $\sim H/T_e$ . For  $H > 25$  kG, a broad spread in the results is observed and the dependence on  $H$  becomes a weak dependence.

Measurements of the temperature of ions heated by means of ion cyclotron waves were carried out on the stellarator B-66, and showed that the peak ion temperature attains 250 eV, declining rapidly after the B4-generator is switched off (time constant  $\sim 20$   $\mu$ sec). The measurements were carried out by means of a diamagnetic loop and an ion energy analyzer.

Plasma instability was studied in the Table Top (the Livermore magnetic trap with mirrors). It was shown that channel instability arises solely within a specific range of plasma density values. When plasma is injected from a titanium source (W. Perkins) along the axis of the system, and is subsequently compressed by the fast magnetic field of the mirrors (compression time 80.35 and 16  $\mu$ sec), the fact was noted that the plasma pinch departed from the axis of the magnetic trap and began to rotate about that axis at an angular velocity  $\omega = 10^7$   $\text{sec}^{-1}$ . The principal field varied only very slowly (7500 and 460  $\mu$ sec).

In experiments on the interaction of a plasma obtained by means of a coaxial injector ( $v = 10^8$  cm/sec) and the magnetic field of a magnetic mirror ( $H = 25$  kG), reflection of the deuterium plasma from the mirror was observed (J. Marshall), accompanied by the emission of neutrons at an intensity  $5 \cdot 10^6$  neutrons/burst.

A. England used the method of electron cyclotron resonance in a resonator placed in a magnetic field of mirror configuration to obtain, under stationary conditions, a plasma of density  $\sim 10^{12}$  particles/cm<sup>3</sup> with hot electrons ( $T_e = 50$  keV) and cold ions. The neutron yield from the plasma was  $10^5$  neutrons/sec. Most of the neutrons had energies below 1 MeV.

B. Motley and associates studied, on Q machines, excitation, propagation, and collisionless absorption of ion acoustic oscillations in alkali plasmas. Ion-acoustic oscillations in the  $10^4$  to  $10^5$  Hz frequency range were excited and detected in a strongly ionized plasma of  $5 \cdot 10^{10}$  to  $5 \cdot 10^{11}$  density by means of a tungsten grid immersed in the plasma. The measured phase velocities showed no dispersion, and were 0.7 of the phase velocity predicted by theory for a collision-free isothermal plasma at  $T_e = 2300^\circ\text{K}$ . The attenuation length was independent of plasma density.

Measurements of the energy of protons leaving a 300-kilovolt plasma because of charge transfer during the time of plasma buildup were carried out on the DCX-1 machine, simultaneously with other experiments (measurements were carried out both in the stable state and during the decay of the plasma). It was shown that protons have an energy spectrum with a half-width of 20-60 keV. The fact was established that the half-width depends strongly on the injection current and on confinement time. The ion energy ranged from 100 to 300 keV. Intense radio-fre-

quency bursts were observed at 14 Mc frequency, corresponding to ion cyclotron oscillations. The duration of the bursts was  $\sim 2$  to 3 hundredths of a second, and the time between pulses 0.1 sec. At the initiation of a burst, the slow electrons move out through the mirrors; the positive potential of the plasma increases. At the end of a burst, the reverse electron current reduces the potential to the previous value. As the oscillations arise, there is also a related increase of fast proton losses through charge transfer. The suggestion was advanced that these irregular phenomena are related to the heating of the cold plasma in an ion cyclotron instability.

Three papers were devoted to plasma phenomena in solids. It was shown that a whole series of purely plasma effects such as the pinch effect, excitation of waves, etc., may be observed even in semiconductors.

Of special interest among the theoretical papers presented, we here single out contributions by D. Dowson and K. Smith, who made computer studies of the development of double-flow instabilities and anomalous resistivity in a collision-free plasma. They considered a model of a one-dimensional plasma consisting of a large number of charged infinite planar layers. The "plasma" was neutron on the average (1000 positive and 1000 negative particles per unit length). The mass of an "ion" was equal to 25 "electron" masses. The velocity distributions of the ions and electrons were Maxwellian, shifted by  $\Delta V$  with respect to each other. This problem simulates the behavior of a real plasma when a current is passed through the plasma. Theory predicts that, at sufficiently large  $\Delta V$  in the plasma, instability should ensue. However, a theoretical treatment of the nonlinear phase of the process of development of this instability would be extremely difficult. Dowson and Smith ran two cases on the computer:  $\Delta V = 0.6 \cdot V_{te}$  and  $\Delta V = 2.5 \cdot V_{te}$ , where  $V_{te}$  is the mean thermal velocity of the electrons. The value of the current flowing through the plasma remained fixed. The computations revealed that the velocity distribution of the electrons becomes smeared out at  $\Delta V = 2.5 \cdot V_{te}$  during a time  $t \sim 60/\omega_{pe}$  ( $\omega_{pe}$  being the plasma frequency) with an instability developing at the point (the mean energy of the electrons is approximately doubled), and that the growth of the oscillations comes to a halt later on. During the development of the instability, an anomalous resistivity  $R$  is observed for a current  $I_0$ , which may be computed as  $dW/dt = RI_0^2$ . These results confirm the qualitative inferences of the theory.

After the conference, the members of foreign delegations visited the physics laboratory at Princeton University, where they were familiarized with all the existing experimental facilities.

## STATUS OF THE URANIUM INDUSTRY IN THE CAPITALIST COUNTRIES AS OF 1962

V. D. Andreev

Translated from *Atomnaya Energiya*, Vol. 15, No. 1,  
pp. 88-91, July, 1963

During the years 1960 to 1962, uranium demands reached about 30,000 tons a year, 25 to 30% below the level prevailing in the years 1959 and 1960. As a result of the drop in demand, the curtailing of uranium ore mining operations and the drop in production of concentrates continued apace, with underutilization of production facilities a commonplace. According to estimates, 30,800 tons of  $U_3O_8$  were produced in 1962, 7% below the 1961 level. 1961 production fell 11% below the 1960 level.

The demand for uranium on the part of the nuclear power industry increased at a far slower rate than that anticipated. The discovery of large deposits of petroleum and gas, and the appreciable stepping up of production of fossil fuels liquidated the fuel deficit plaguing western Europe, and a sizable drop in specific capital investments and in the cost of electric power at conventional power stations imposed much more stringent requirements on nuclear power stations. (As an example, in order for the construction of nuclear power stations to be a profitable venture in the USA, the costs of electric power production at nuclear-fueled stations would have to be lowered not to 0.8 cents/kW-h, but the low figures of 0.6 or 0.65 cents/kW-h.) As a result, the power output of nuclear power stations in the capitalist countries will not exceed 10 million kW in 1967, as against 25 million kW envisaged back in 1957.

TABLE 1. Industrial Uranium Reserves in the Capitalist Countries

	Ore reserves, millions of tons	U <sub>3</sub> O <sub>8</sub> content in ore		Data at start of year
		%	Thous. of tons	
Total	—	—	900-920	1963
Union of South Africa	952.4	0.034	324	1959
Canada	273.1	0.121	252.2	1962
USA	60.7	0.28	170	1963
India	15.7	0.3	47	1960
Australia	—	0.1-0.3	25*	1962
France	—	0.1-0.3	21	1963
Gabon	20.0	0.5	6.0†	1963
Argentina	—	—	10.0	1962
Southwest Africa	3-5.0	0.22	7-10	1962
Spain	2.0	0.1-0.4	~4.0	1963
Italy	0.6	0.12	0.72‡	1962
Japan	3.0	0.05-0.2	1.5-6	1962
Switzerland	—	0.02-0.1	2.0	1963
Mexico	1.05	0.1-0.2	1-2	1963
West Germany	0.3	0.1-0.2	0.4	1962

\* 12.5 thousand tons from other data.  
† Only in ores containing 0.5% U<sub>3</sub>O<sub>8</sub>.  
‡ Data based solely on one deposit; geological reserves throughout the country estimated at 14,000 tons U<sub>3</sub>O<sub>8</sub>.

TABLE 2. Quantity of Fission Energy Contained in Atomic Ore Reserves in the USA, in 10<sup>18</sup> Kilocalories [8]\*

Cost, \$/kg	Energy in U <sup>235</sup>		Total energy content	
	Total	Including proved and probable reserves	Total	Including proved and probable reserves
U <sub>3</sub> O <sub>8</sub>				
0-22	0.1	0.04	12.6	5.544
22-26	0.756	0.043	10.08	6.048
66-220†	2.52	1.26	352.8	176.4
220-1100†	226.8	55.44	30,240.0	7,560.0
ThO <sub>2</sub>				
0-22	—	—	6.3‡	1.512‡
22-66	—	—	3.28‡	1.512‡
66-220†	—	—	554.4	176.4
220-1100†	—	—	47,880.0	15,876.0

\* Fission energy content computed on basis of assumption that all materials will be ultimately fissionable after being cycled through reactor cores. Losses incurred in recovery of spent nuclear fuel and other relatively small losses were ignored in the calculations.  
† In winning uranium and thorium from granite, and uranium from bituminous schists and phosphates.  
‡ Only incomplete data available.

TABLE 3. Mining of Uranium Ore in the Capitalist Countries, Millions of Tons [14-17]

Country	Mean U <sub>3</sub> O <sub>8</sub> content, %	1957	1960	1961	1962*
USA	0,25-0,27	3,0	7,2	7,3	6,3
Canada	0,4-0,15	6,0	10,0*	8,0*	6,6
Un. of S. Africa†	0,035	20,0	21,9	15,5	12,0
Australia*	0,2	0,2	0,8	0,9	0,8
France	0,2	...	0,9	0,8	0,8

\* Estimate.

† Processed at mills.

Some countries (India, Mexico, Argentina, the UAR, and others) are attempting to supply their own needs in the production of nuclear raw material, albeit in modest quantities.

Uranium needs in the USA and in Great Britain are supplied by deliveries meeting terms of contracts drawn up back in the mid-fifties. France, Sweden, and Japan are attempting to cover their atomic raw materials needs primarily by arranging their own domestic production, since uranium imports entail obligations which those countries tend to view as burdensome and unacceptable. All of this contributes to a deterioration in the position of the world's largest uranium exporters, Canada and the Union of South Africa.

TABLE 4. Uranium Production in Capitalist Countries in Tons U<sub>3</sub>O<sub>8</sub> [1, 3, 18-21]

Countries	1957	1960	1961	1962*
Total	21,700	37,000	33,000	30,800
USA	7,840	16,140	15,785	15,504
Canada	5,950	11,380	8,764	7,665
Union of South Africa	5,170	5,826	4,971	4,500
Australia	360	1,000	1,350	1,200
France†	296	984	1,187	1,060
Gabon	-	-	321	547
Malagasy Republic†	63	84	72	80
Portugal‡	-	-	1,492	450
Spain*	-	54	55	-
West Germany*	-	11	11	-
Argentina*	18	14	10	10
Italy**	1	8	-	-
Congo	1,500	1,080	-	-

\* Estimate.  
† Content of metallic uranium in concentrates.  
‡ USA imports; weight of uranium concentrates, not content of uranium oxide in concentrates. Coarse concentrates containing about 10% U<sub>3</sub>O<sub>8</sub>, to judge by cost figures, are produced in the country.  
\*\* Previous available estimates: 75 tons for 1960 and 130 tons for 1961 refer to planned production figures. Because of the overproduction and drop in world market prices, Italy has not arrived at industrial assimilation of its own deposits.

Changes in the raw materials base. The proved industrial reserves of uranium in the capitalist countries (see Table 1) has shrunk noticeably during the past three years. This is due to the contracted volume of geological prospecting activities for uranium and to the very large-scale mining operations in progress. During these years, over 100 million tons of ore containing from 110 to 115 thousand tons of U<sub>3</sub>O<sub>8</sub> were mined and processed.

About 50 million tons of ore were mined in Canada during the years 1958 to 1962, while no significant new deposits were discovered, the upshot being that industrial ore reserves ended up 20% less than in 1957 (the 1957 figure was computed at 342 million tons) [7].

The industrial reserves of uranium ore in the USA were likewise sharply revised downward, by as much as 25% over the years 1960 to 1962. According to USAEC estimates, industrial reserves of uranium in the USA will be cut

down to 90 thousand tons of  $U_3O_8$  by 1967. One of the factors behind this scaling down of prospecting and exploration work was the decision by the AEC to purchase ore, up to 1966, solely from deposits which were operational prior to 1958.

In an official USAEC report presented to the President in November, 1962, the total quantity of fission energy contained in the nuclear raw materials reserves in the USA were estimated at 79,290 billion kilocalories, which is many times in excess of the fossil fuel resources (Table 2).

Geological prospecting for uranium and exploration of deposits are continuing in western European countries (France, West Germany, Italy, Austria, Sweden), Asia (Japan, India, Pakistan), in Africa (United Arab Republic, Kenya, Tanganyika), Latin America (Argentina, Mexico, Peru).

TABLE 5. Uranium Ore Processing Mills

	In operation			Under construction or planned in 1962
	1960	1961	1962	
Total daily capacity, thousands of tons of ore	125	120	100	—
% capacity in use	88	80	70	—
Number of concerns involved	84	71	67	9*
USA	25	26	27	3
Union of South Africa	17	13	12	—
Canada	17	8	8	—
Australia	5	5	3	—
France	4	4	4	—
Gabon	—	1	1	—
Malagasy Republic	1	1	1	—
Spain	1	1	1	—
Portugal	1	1	1	—
West Germany†	1	1	1	—
Argentina‡	3	3	3	—
Italy†	1	1	1	—
Japan†	1	1	1	1
India†	1	1	1	1
Sweden†	1	1	—	1
Mexico‡	1	1	1	2
Brazil‡	1	1	1	1
Congo	1	—	—	—
Finland†	1	1	—	—
N. Rhodesia	1	—	—	—

\*Of which two have been completed.  
†Pilot plant.  
‡Experimental facility.

Recent data place the total (geological) reserves of uranium ore in France, Gabon, and the Malagasy Republic at 60,000 tons  $U_3O_8$ , and proved reserves at 21,000 tons in France proper and 6,000 tons in Gabon (Mounan) [3].

In Sweden, in the Norrocker district, bituminous schists with a higher uranium content than those at the Ranstad deposit were found in 1962, and a processing mill is being built to handle them [9].

Despite the intensified program of prospecting, no large uranium deposits were discovered in West Germany. The reserves at the Wöhlendorf (Bavaria) deposit were estimated at 100,000 tons with 200 tons  $U_3O_8$  content. The mean uranium content in the ore is comparatively high: 0.2%  $U_3O_8$ ; however, the depth at which the ore lies makes mine operations unprofitable [3]. The Waisenstadt (Bavaria) deposit contains 60 to 75 tons  $U_3O_8$ . The reserves at the



deposit in the Elweiler district, the only one presently being worked in West Germany, are estimated at 100 tons  $U_3O_8$  with a mean  $U_3O_8$  content in the ore of 0.1% [10]. The uranium reserves contained in the uraniferous anthracites of Upper Bavaria discovered in 1962 are estimated at several hundred tons. It is supposed that new zones of uranium content higher than that found in presently known deposits may be found in the coalfields of Upper Bavaria [11]. A uranium ore deposit was discovered in 1962 at Schwarzwalf in the Menzenswand district. The  $U_3O_8$  content found in an assay of 300 tons was very high: 1 to 1.4%. This indicates a vein type deposit whose reserves are probably modest, however [12].

Mexico's reserves of uranium have seen an appreciable increase. In mid-1962, the figure for total reserves of uranium ore stood at 0.4 million tons. An estimate at the year's end placed the level at 1.05 million tons [2, 13].

Several uranium deposits were discovered in India during 1962, particularly in the Kangra district in western Punjab [3].

News was published on the discovery of a promising uranium deposit in Peru in 1960, in the Vilcabamba district. However, operations would be unprofitable given the low market prices prevailing and the overproduction conditions [3].

On the basis of data on the number of mines in operation, their output and the production of concentrates, we may assume that mining of uranium ore underwent a curtailment during 1962 in the capitalist countries (Table 3). This curtailment in mining operations extended for the first time to all the major mining countries.

TABLE 6. USAEC Purchase Prices for Uranium Concentrates  
Dollars/kg  $U_3O_8$  [1, 24]

Suppliers	1959-1960	1960-1961	1961-1962
American	19.78	18.79	18.04
Canadian	24.49	24.00	21.89
Miscellaneous (Union of South Africa, Congo, Australia, Portugal)	26.42	25.92	25.26
Average prices	22.42	21.38	20.13

Mining of uranium ore in the USA was reduced 14% below the 1961 level. The  $U_3O_8$  content in mined ore was 15.3 thousand tons as against 17,000 tons the previous year, i.e., 10% lower, attesting to the increase in the mean  $U_3O_8$  content in the ore mined.

In 1962, by our estimate, the production of uranium concentrates dropped 2.2 thousand tons of  $U_3O_8$  as against 1961 (Table 4). The drop in Canada was greater (a 13% drop) as in the Union of South Africa (10%). The USA accounted for about 50% of the uranium production in the capitalist world during 1962.

Canada and the Union of South Africa, which boast the largest uranium ore reserves in the capitalist world, are being converted into virtually second-rank producers. This position is due to the fact that the USAEC, as the biggest consumer of uranium raw material, drastically cut purchases in other countries, thus shifting the center of gravity of its purchases onto American suppliers.

Production of uranium concentrates was cut first in France, by 11% compared to the 1961 figure. However, the amount of nuclear raw material at the disposal of the French Atomic Energy Commissariat increased by 27%. This is due to a marked increase in deliveries from Gabon, by a factor of eight over the 1961 figures.

The production of uranium concentrates in France, Gabon, and the Malagasy Republic will probably level off at 1960 tons of  $U_3O_8$  in the coming years [3, 20].

France, in striving to maintain its leading positions in the nuclear industry of the "Common Market" countries in the years to come, has begun an intensive development of its own raw materials base recently (a huge gas diffusion plant for production of enriched uranium, with a throughput as high as 1.5 thousand tons uranium metal annually, is now being built at Pierrelat).

1962 saw the curtailment of production hit Australia. The processing mill at Radium Hill and the Port Pirie plant, as well as a small plant in the northern section of the country, had been closed down. The contract for de-

livery of ore to the Joint Anglo-American Atomic Fuel Agency of uranium concentrates from the Rum Jungle plant had already expired. The closing of this plant was due to the liquidation of an entire industrial district based on the uranium mining operations. The government therefore decided to continue ore processing operations, warehousing the output.

As many as 22 plants, including 3 pilot plants (in Southern Rhodesia, Finland, and Sweden), closed down in the capitalist countries during 1960-1962, reducing the total production level by roughly 20% (Table 5).

Only one new plant went into operation during 1962, the Carbon County (Wyoming) operation in the USA, with a daily capacity of 180 tons of ore (450 tons according to data from another source). Two plants were built. The first, at Ranstad (Sweden) is to have a capacity of 140 tons  $U_3O_8$  and is scheduled to go into operation in 1965 [22], bituminous schists with 350 g/ton  $U_3O_8$  content will be processed; construction costs are estimated at \$28 million. As much as 800 thousand tons of ore will be mined yearly to supply the plant, and this will mean working the mine for 15 years. The concentrate will have the following composition (in percentages):  $U_3O_8$ -84;  $PO_4$ -0.014; Na-7.5; Fe-0.04; Mo-0.001;  $SO_4$ -0.1;  $CO_2$ -1.3 [22]. The second plant, located in India (in the Jaduguda district of the state of Bihar) is built for ~200 tons  $U_3O_8$  annual capacity; it is scheduled to go into operation in 1965 [23]. Plans call for expanding mining operations to 1000 tons daily in 1964, to meet the needs of the plant.

Construction of new plants is being planned in the USA (in the state of South Dakota, using as base operation of the large lignite field in the Bowman area), as well as several small operations in Japan, Brazil, and Mexico. However, because of the possibility of acquiring low-priced uranium on the market, it is hardly likely that all of these plans will be brought to fruition.

Price structure. As a result of the supply swamping the demand, the drop in ore mining costs and concentrate production costs, the shift to operation of the most profitable mines and plants, 1962 prices continued to decline (Table 6).

In 1960, an agreement was signed between Canada and Great Britain for the delivery of 10.9 thousand tons of  $U_3O_8$  to Great Britain over the 1963-1966 period, with the price averaged at 11.07 dollars/kg  $U_3O_8$ .

#### LITERATURE CITED

1. V. D. Andreev, JAE, 13, 293 (1962).
2. Metal Bulletin, No. 4763, 15 (1963).
3. Atomwirtschaft, VII, 618 (1962).
4. New York Times (September 23, 1962).
5. Metal Bulletin, No. 4743, 20 (1962).
6. Mining J., 258, 547 (1962).
7. J. Griffith, Canadian Mining J., 84, 97 (1963).
8. USAEC, Civilian Nuclear Power. A. Report to the President-1962, Washington (November 20, 1962), p. 23.
9. Mining J., 259, 153 (1962).
10. Glückauf, 97, 1028 (1961).
11. Industriekurier, p. 557 (Beilage) (September 5, 1962).
12. Atomwirtschaft, VII, 465 (1962).
13. Engng. and Mining J., 163, 180 (1962).
14. V. Andree, JAE, 11, 73 (1961).
15. Mineral Trade Notes, 55, 70-71 (1962).
16. American Metal Market (February 7, 1963).
17. Commissariat a l'energie atomique. Rapport Annuel, 1960, Paris (1961).
18. D. Baker and E. Tucker, Minerals Yearbook, 1961, Washington (1962).
19. Statistical Summary of the Mineral Industry, London (1962).
20. R. Bernick, Engng. and Mining J., 164, 117 (1963).
21. Northern Miner. (January 3, 1963).
22. Nuclear Power, 8, 54 (1963).
23. India News (May 4, 1962).
24. Appl. Atomics, No. 371, 7 (1962).

## USAEC DELEGATION VISITS THE SOVIET UNION

A. A.

Translated from *Atomnaya Energiya*, Vol. 15, No. 1,  
pp. 91-93, July, 1963

In response to the an invitation tendered by the chairman of the State Committee on the Uses of Atomic Energy of the USSR, a delegation of the US Atomic Energy Commission headed by AEC chairman Glenn T. Seaborg, made an official visit to the Soviet Union from May 19 to May 30 this year (1963). The delegation included the chairman of the AEC consultative committee, Manson Benedict, the AEC general manager A. Luedecke, the head of the international affairs board A. Wells, the director of the Argonne National Laboratory, A. Crewe, the president of the Association of Midwestern Universities, G. Tape, staff member A. Ghiorso of the Lawrence Radiation Laboratory, staff member A. Zucker of the Oak Ridge National Laboratory, and technical adviser to the AEC chairman A. Fritsch, assistant to the AEC chairman, C. King.



A. M. Petros'yants and Glenn T. Seaborg (left) after signing the Memorandum.

On the day following their arrival, the American delegates were welcomed by the chairman of the USSR State Committee on the Uses of Atomic Energy, A. M. Petros'yants. During their introductory chat, they discussed the agenda of the official visit and the text of a joint memorandum on collaboration in the field of the peaceful uses of atomic energy. On the same day, the American scientists visited Moscow State University, the Physics Institute of the USSR Academy of Sciences, and the Institute of Chemical Physics of the USSR Academy of Sciences. At Moscow State University, the guests inspected the auditory, the students dormitory quarters, and several laboratories, including the cosmic radiation laboratory.

On May 21, the delegation met with the president of the USSR Academy of Sciences, M. V. Keldysh.

At the Institute of Atomic Energy, which was visited on May 22, the guests were shown the linear electron accelerator, the cyclotron, the reactors, and several laboratories. Of the many thermonuclear machines there, the PR-5

facility, an adiabatic trap with combined magnetic field, with which Soviet physicists have recently achieved an enormous success by confining a plasma in the stable state for 10-15msec, was demonstrated. At the Institute, Dr. G. Seaborg delivered a lecture on the transuranium elements to the Soviet specialists present, and was heard with rapt interest.

On the following day, the American specialists traveled to Obninsk, to see the Physics and Power Engineering Institute there. There they were shown the World's First Nuclear Power Station, the BR-1 and BR-5 fast reactors, a portable nuclear power facility, and the sodium laboratory.

During their visit to the Nuclear Reactor Research Institute situated near Ul'yanovsk, the attention of the delegation was drawn to the operating reactor CM-2, the miniaturized nuclear organic-cooled power assembly, and a boiling-water reactor now under construction. The members of the American delegation voiced high praises for the CM-2 reactor.

On the next two days, the American scientists spent their time in Leningrad. At that point they were for the first time divided up into two teams: one headed up by G. Seaborg visited several laboratories of the Radium Institute, while the other team was received by specialists of the Physics and Engineering Institute of the USSR Academy of Sciences. In the evening, the entire delegation visited the Electrophysics Equipment Research Institute, where they were familiarized with the activities of the Institute, with its laboratories, and where they were shown a number of operating and partially completed thermonuclear and accelerator facilities, including the "Al'fa" toroidal thermonuclear machine, and a linear accelerator designed for medical research.

The members of the American delegation also stayed at the Physics and Engineering Institute in Kharkov, where they saw demonstrations of the linear accelerator for multiply-charged ions and the large 2 BeV linear electron accelerator.

On May 28, the delegation visited the Joint Institute for Nuclear Research at Dubna. Here the American specialists were informed on the latest work of the Nuclear Reactions Laboratory, where, as is generally known, a group of Soviet scientists recently scored a great success in synthesizing the new element 102, of mass number 256, on the multiply-charged ion cyclotron. The guests also inspected the pulsed fast reactor at the Dubna Institute.

On May 27 and 29, the American delegation paid visits to the construction site of the Novo-Voronezh nuclear power station and to the Serpukhovo 70 BeV proton accelerator.

On May 29, G. Seaborg was received in the Kremlin by the Chairman of the Presidium of the Supreme Soviet of the USSR, L. I. Brezhnev. A. M. Petros'yants took part in the discussion.

In the course of the visit, talks were conducted between the State Committee on the Peaceful Uses of Atomic Energy of the USSR and the US Atomic Energy Commission, concluding on May 21 with the signing of a Memorandum on collaboration in the field of the peaceful uses of atomic energy.

The Memorandum establishes an extensive program of scientific and technical exchanges with the purpose of developing and further expanding collaboration between the USSR and the USA in the field of the peaceful uses of atomic energy.

An understanding was arrived at on mutual visits of teams of specialists to promote the familiarization of colleagues of both countries with the status of scientific research in the following areas: nuclear power reactors including fast reactors and superheat reactors; plasma physics and controlled fusion; nuclear physics and the physics of high-energy particles; solid state physics; decontamination and burial of radioactive wastes; applications of labeled compounds in medicine, radioneurological research; design and operation of accelerators. The dates of the visits, their duration, and the composition of the delegates will be subject to further agreement in each specific case.

The Memorandum also provides for protracted transfers (for periods up to one year) of specialists on controlled thermonuclear fusion, reactor engineering, and high-energy particle physics in research laboratories, for the purpose of sharing practical experience and studying the operation of existing facilities and equipment.

Exchange of scientific information (books, papers, preprints) will be promoted, with lectures scheduled in those fields of scientific activity where exchanges of delegations occur. The Memorandum sets the amount of information to be exchanged and the information exchange periods. The Memorandum also provides for the simultaneous transmission of information intended for bilateral exchange through the International Atomic Energy Agency.

Two joint scientific conferences were decided upon. A conference will be held in the USSR on low-energy nuclear physics, and another in the USA on the decontamination, solidification, and burial of radioactive wastes.

Agreement was reached on exchange of scientific instruments. The conditions governing this exchange will be discussed further within the framework of the laws and export practices of the two countries.

The Memorandum envisages the possibility of taking supplementary measures to promote collaboration between the two countries and sets the dates for taking action and the procedure for extending the terms.

The text of the Memorandum was signed by the State Committee on the Uses of Atomic Energy of the USSR, represented by A. M. Petros'yants, and by the US Atomic Energy Commission, represented by Glenn T. Seaborg.

In summarizing the significance, effects, and benefits of their visit to the USSR, Glenn Seaborg and the members of the American delegation stated, at a press conference on May 30, that the delegation received a warm welcome. Our guests, Seaborg stated, were most hospitable and did everything possible to render our visit useful and profitable; we saw everything we set out to see. The view of the American scientists is that the Soviet Union has made tremendous strides in many areas of the peaceful uses of atomic energy. In these remarks, they of course include, for example, thermonuclear research, reactor design, and the study and production of transuranium elements, as well as other subjects.

## BRIEF COMMUNICATIONS

Translated from Atomnaya Énergiya, Vol. 15, No. 1,  
pp. 93-95, July, 1963

USSR. A coincidence scintillation spectrometer has been built at the Latvian nuclear reactor. This instrument is capable of recording several tens of thousands of gamma pulses resulting from neutrons bombarding atomic nuclei, in a fraction of a second. Physicists of Latvia and the other Baltic republics will be greatly aided by this new facility in their study of rare earths at the reactor.

USSR. Patent No. 146414 has been issued for a technique of producing sample radioactive gaseous sources with the special feature that a low-boiling radioactive liquid, the quantity and activity of which are already measured by conventional absolute techniques, is vaporized into a known sealed volume, in order to facilitate a wider use of relative methods of activity measurements.

The specific activity ( $a$ ) of the organic liquid labeled with a beta-active isotope is carefully determined when the proposed method is used. Several milligrams of this liquid are then collected in a tiny glass bead ampule crimped on the end, the ampule is sealed, and the amount ( $m$ ) of the material taken is determined before and after sampling by the difference in weight. The activity ( $A$ ) of the sample is determined from the relationship  $A = a \cdot m$ . The ampule is then placed in a suitable pressure-tight chamber and crushed inside. At this point the volume of the chamber must be sufficient to allow for complete evaporation of the radioactive liquid. After the sample of radioactive liquid has been evaporated, a gaseous radiation source results, with the activity precisely known and, once the volume of the chamber is known, we will have no trouble computing the activity contained in any part of the chamber.

USSR. A new method for separating potato tubers from stones and clumps of ground during harvesting operations involving the use of special machines has been developed at the All-Union Institute of Agricultural Mechanization. This method is based on the contrasting penetrability of gamma rays through potato tubers and through foreign matter. The potato tubers are sorted out on a turntable at the edge of which is positioned a circular conveyor with movable lift fingers. When the potato tubers come into the area being monitored, absorption of gamma radiation is minimal. But as soon as lumps of dirt or stones make their appearance, absorption rises steeply. Relays instantly feed a command to a reject mechanism, which proceeds to eject the foreign matter without delay into a special hopper.

USSR. A seminar was conducted at the Kadamjai mine (in Kirghizia) on applications of radioisotopes in mining. The seminar made a special point of the successful use of logging instruments incorporating gamma sources, in delineating the boundaries of rock and ore bodies, and in locating metal in rocks and assaying the metal percentage content in ore.

USSR. A seminar was conducted at Aktyubinsk at the chromium compounds plant, dealing with experience on the incorporation of radioisotope and nuclear radiation know-how into production. The seminar took special note of the use of instruments using radioactive sources in many process control applications.

USSR. Radioisotope instruments are currently in widespread use in the Donets region. Over 300 such instruments were in regular use at the beginning of 1963.

USSR. A radiological division was inaugurated at the P. Stradyniua clinical hospital in Riga (Latvia). Patients are accommodated in two-bed wards with specially designed shielding walls. During active cobalt therapy, contact with the medical staff is maintained by telephone; a closed-circuit television hook-up is being installed. The new radiological division boasts the latest in Soviet-manufactured gamma-therapeutic facilities.

USSR. An "Atoms for Peace" exhibit on wheels organized by the USSR State Committee on the Uses of Atomic Energy and the local Polytechnic Museum has been open to the public for some time in Vladivostok. In addition to the usual stands, the exhibit is demonstrating a sizable number of operational instruments and working mock-ups. A seminar was conducted during the exhibit for the benefit of laboratory staff members and workers in industrial establishments in the area.

IAEA. In April, a conference of experts on methods of assessing cost factors in nuclear power stations coupled into national power grids, and surveying the effect of nuclear power station operations on the performance and cost picture of conventional power stations coupled into the national power grid was held in Vienna. Eleven experts from 11 countries (Brazil, Great Britain, Hungary, India, Italy, USSR, USA, France, West Germany, Sweden, Japan) participated in the conference, along with 10 observers including two from Euratom and one from the UN European Economic Commission.

The conference placed the following points on its agenda:

1. differences between nuclear-fueled and fossil-fueled power stations operating in the same or different power systems (service life of station equipment, ability to respond to load and system variations, station off-duty time, cost structure of electric power at conventional and at nuclear power stations, effect of cost of fuel on the position of the power stations on the power system load diagram);
2. methods for comparing electric power costs at conventional and at nuclear power stations feeding power grids;
3. comparison of ultimate effects of hooking up a series of nuclear or conventional electric power stations into the power grid and changes wrought in the performance and cost picture of power stations already forming part of the grid;
4. cost evaluation of the role played by nuclear and conventional power stations in the power development programs of underdeveloped countries.

On the basis of the discussions conducted by these experts, and the materials presented by other experts to the IAEA secretariat, that body is commissioned to prepare a draft document on the economics of including nuclear electric power stations in national power utility systems, and this report will ultimately be published as an IAEA technical report.

IAEA. The International Atomic Energy Agency has decided to render assistance to member states in the field of outer space research, by organizing the collection and rapid delivery of newly fallen meteorites to laboratories for studies of their radioactivity. The General Director of IAEA has directed a request to all governments affiliated to IAEA to present a list of interested laboratories and to collaborate in the organization of delivery of new meteorites to the central organizations of the IAEA in Vienna, thus expediting a rapid distribution of meteoritic specimens to various laboratories.

East Germany. A research reactor with an Argonaut type annular core went critical at the Rossendorf Central Nuclear Physics Institute. The 10 kW-rated reactor was designed and built by scientists of the German Democratic Republic. Nuclear fuel is delivered by the Soviet Union.

Experience accumulated in five years of operating the German Democratic Republic's first research reactor, 2000 kW, was put to use in the design and construction of this pile. The function of the first reactor will now center primarily on isotope production, studies of solid state physics problems, and neutron physics research.

Poland. At the (Warsaw) State Institute of Hydrology and Meteorology, an isotopes applications laboratory has been commissioned.

The schedule of operations of the laboratory for the period ahead includes development of methods for spotting leaks in pipes and ducts (including water pipes) by means of sealed radiation sources, and investigation of ground water movement by tritium devices. Investigations of tritium content in natural waters, closely related to the above projects, are designed to establish the rate of turnover of deep-lying ground waters, and this will aid in determining the exploitable reserves of underground reservoirs.

Future projects include research on the rate of silt accumulation in riverbeds, harbor bottoms, water basins, dams and levees, and irrigation systems, and on the mechanisms responsible for silting.

## FROM THE EDITOR

In September 1961 the Committee on Standards, Measures, and Measuring Devices of the Council of Ministers of the USSR ratified GOST 9867-61, "International System of Units"; therefore, as of January 1, 1963 this is to be the preferred system of units in all branches of science, technology, and national economy, as well as in teaching.

Bearing in mind the importance of proper preparation for the introduction of the International System of Units into the national economy and for the proper explanation of the question of units in the scientific and technical literature, the editor presents in this issue a paper prepared and approved by the Committee on Standards, Measures, and Measuring Devices of the Council of Ministers of the USSR entitled, "The Introduction of an International System of Units in the USSR."

Approved by the Committee on Standards, Measures, and Measuring Devices of the Council of Ministers of the USSR

THE INTRODUCTION OF AN INTERNATIONAL  
SYSTEM OF UNITS IN THE USSR

Translated from Atomnaya Énergiya, Vol. 15, No. 1,  
pp. 96-98, July, 1963

The development of science and technology in recent years has raised the question of establishing more rigid requirements for the achievement of more uniform and precise measurements. These requirements have acquired increasing importance as the result of the widespread application of automation and computer controlled technology. In the latter the units used are among the most important elements of information and therefore the question of unification of the systems of units is of paramount importance.

In order to satisfy these requirements a rational system of units must be used to measure physical quantities.

In the USSR the following preferred systems of units have been approved as the government standards:

MKS system for the measurement of mechanical and acoustical quantities (GOST 7664-61 and GOST 8849-58) with the basic units meter, kilogram, and second, and 22 derived units (16 for mechanical and six for acoustical measurements);

MKSA system for the measurement of electric and magnetic quantities (GOST 8033-56) with the basic units meter, kilogram, second, and ampere, and 17 derived units;

MKSD system for the measurement of thermal quantities (GOST 8550-61) with the basic units meter, kilogram, second, and degree Kelvin,\* and 12 derived units;

MSC system for the measurement of light quantities (GOST 7932-56) with the basic units meter, second, and candle, and seven derived units.

Thus, as a whole, the indicated systems involve six basic units, which may be reproduced with the aid of governmental standards using the accepted principles for the determination of these units, and 58 derived units for the measurement of various physical quantities; the latter may be considered composite parts of a unified system of units.

In addition to the indicated systems, the existing government standards for the units of measurement also permit the use of the following systems:

CGS system for the measurement of mechanical, acoustical, electric, and magnetic quantities (GOST 7664-61, GOST 8849-58, and GOST 8033-56) with the basic units centimeter, gram, and second, and the associated derived units;

\*Provision is made for the use of two temperature scales: the thermodynamic temperature scale and the International practical temperature scale. The temperatures in each of these scales may be expressed in two ways - in degrees Kelvin or in degrees Celsius (centigrade).



MKGFS for the measurement of mechanical quantities (GOST 7664-61) with the basic units meter, kilogram-force, and second, and the associated derived units;

A series of mixed units for the measurement of mechanical, acoustical, thermal, and electrical quantities.

The use of the CGS, MKGFS, and mixed units is permitted because they are widely used in practice; however, it is recommended that the units of the MKS, MKSA, MKSD, and MSC systems be used.

The existence of many systems of units for the measurement of various physical quantities and also of a large number of widely used mixed units results in significant difficulties and inconveniences associated with the conversion of the numerical magnitudes of the measured quantities from one system of units to the other.

The pressing necessity arose for the establishment of a single, universal system of units to be used in all branches of science, technology, and national economy encompassing the measurement of mechanical, thermal, electric, magnetic, acoustic, and light magnitudes.

The most rational system of units to be used in the measurement of the various physical magnitudes is a system of units based on six basic units: the meter, kilogram, second, ampere, degree Kelvin, candle.

The preferred system of units in the USSR (six basic, 58 derived) contains all the necessary elements required for the formation of a single, universal system of units to be used for the measurement of the various physical quantities.

As the result of a detailed examination by and through the agreement of several international organizations, the International Metrological Organization, the International Standardization Organization (ISO), the International Union of Pure and Applied Physics (IUPAP), the International Commission on Electrical Engineering (ICEE), etc., the question of the unification of the systems of units was solved by the adoption of a single, universal international system of units based upon the six above-indicated units.

In October 1960 the Eleventh General Conference on Weights and Measures, held in Paris, adopted the International System of Units (SI) consisting of six basic units (meter, kilogram, second, ampere, degree Kelvin, candle), two additional units (radian, steradian), and the 27 most important derived units; this does not prevent the use of other derived units, which may be added later. All of the six indicated basic units, both supplementary units, and all of the 27 most important derived units coincide completely with the corresponding basic, supplementary, and derived units of the USSR government standards using the MKS, MKSA, MKSD, and MSC systems.

On September 18, 1961, GOST 9867-61, "International System of Units,"\* was ratified in the Soviet Union and put into effect as of January 1, 1963. It establishes the preferred use of this system of units in all branches of science, technology, national economy, and education. This standard does not provide for introduction of a preferential system of units for use in the USSR.

The basic merits of the SI consist of the following:

1. The unification of the units used in the various types of measurements.

The SI permits us to use a single common unit of measurement for each physical quantity encountered in the various branches of technology, e.g., the joule for all types of work and for the quantity of heat rather than the various units being used at present for this quantity (kilogram-force-meter, erg, calorie, watt-hour, etc.).

2. The system is universal.

The units of the SI cover all branches of science, technology, and national economy, they exclude the necessity of applying other units, and they represent, on the whole, a unified system common to all branches of measurement.

3. System coherence.

In all physical equations using derived units the coefficient of proportionality is always a dimensionless quantity equal to 1.

\*Reference to the system of units adopted at the Eleventh General Conference on Weights and Measures is indicated by the abbreviated designation for the system using the Latin letters SI (the first letters of the words *Système International*).

For example, in the equation for power

$$N = k(A/t),$$

where  $N$  is the power,  $A$  the work, and  $t$  the time, if we use the SI, in which the joule is the unit of work and the second is the unit of time, the unit of power is

$$1 \text{ watt} = 1 \text{ joule/1 second},$$

where  $k$ , the coefficient of proportionality, is a dimensionless number equal to 1.

The use of the SI units significantly simplifies the operations involved in solving equations, in calculations, and in the construction of graphs and nomograms since the necessity of using a significant number of conversion coefficients is eliminated.

4. The structure and interconnection of the SI significantly simplifies the study of the physical laws and the pedagogical process during the study of general and special scientific disciplines and also simplifies the derivation of the various formulas.

5. The principles involved in the design of the SI permit the development of new derived units as needed, and therefore the list of units of the system is open to further development.

Most of the units of the SI have already received wide practical application in the USSR (except for four or five of the 58 derived units included in the MKS, MKSA, MKSD, and MSC systems).

Let us consider the confusion existing at present regarding the term "weight," which customarily, and as far as the layman is concerned, is used to denote the characteristic mass (quantity of a substance) even though in mechanics it is used to denote the force of gravity. It is entirely obvious that measures must be taken to eliminate this confusion.

As we know, the weight  $W$  is equal to the product of the mass ( $m$ ) by the acceleration of free fall ( $g$ ).

Since the numerical value of  $g$  varies at different points on the earth the weight also varies, while the mass is independent of the location at which it is measured. In addition, the term "weight" is often used incorrectly for the characteristic mass.

In the SI the kilogram is the unit of mass while the unit of force (also the unit of weight) is the newton.

In all cases where we speak of a quantity of a substance, for example, when we speak of the amount of a metal or of other materials to be used in the manufacture of an article (machine tool, laboratory device, etc.), the mass must be given in kilograms (or grams, or integral or fractional parts of a gram).

In those cases where it is necessary to determine the lifting force or the weight-lifting force of a tap (fluid) or the load upon a foundation, etc., we must speak of the weight and express the weight in units of force, i.e., newtons (or integral or fractional parts of a newton).

The introduction into practical use of the newton as the unit of force rather than the kilogram-force, which is widely used at the present time, will facilitate the elimination of the indicated confusion and permit us to realize the advantages achieved as the result of the sharp differentiation between the units of mass (kilogram) and force (newton).

The introduction on January 1, 1963, of GOST 9867-61 does not mean that the use of all of the units of the CGS system, MKGFS system, and mixed units must cease immediately and that these units must be replaced by units of the SI in all branches of the nation's national economy.

The introduction into practical use of units of the SI which have not as yet received widespread use in the national economy must occur gradually over a number of years, which will vary for each unit, bearing in mind the region of application of the unit, the instruments used, economic considerations, and other factors. The introduction into practical use of the SI units should not involve special expenses and should enable us to continue using the existing measuring devices until the time that they normally wear out.

A small amount of difficulty will be experienced in the introduction into the domestic economy of those units of the SI which have so far not been widely used in engineering calculations and for the measurement of which we do not at the present time have adequate instruments, graduated in the corresponding units, e.g., the measurement of force in newtons, the measurement of pressure in newtons/m<sup>2</sup>, the measurement of electrical energy in joules, etc.

Therefore special attention should be paid to the question of transition to SI units for the measurement of force (newtons) and pressure (newtons/m<sup>2</sup>), bearing in mind the presence in the country of an enormous number of machines and devices for the measurement of these quantities in units of kilogram-force and kilogram-force/cm<sup>2</sup>, respectively, and also other units which are widely used at present (kg-force/mm<sup>2</sup>, etc.).

In a number of cases it is necessary to recalculate in order to convert from the units in current use to units of the SI. Thus, for example, in order to convert from kilogram-force to newton, we must use the established relationship between the kilogram-force and the newton, namely 1 kgf = 9.80665 n. However, in the overwhelming majority of cases the conversion may be significantly simplified since within an accuracy of 2% we can assume that 1 kgf = 10 n and we may use this simple conversion in all cases where it is possible to neglect the 2% difference.

Generally speaking, the accuracy of the allowed rounding off used in the various unit conversions for units of the CGS and MKGFS systems and mixed units to units of the SI must be separately established for each particular case taking into account the conditions of application of the given unit.

The entire complex of SI units will be introduced into the scientific, technical, and educational literature (monographs, questionaries, textbooks, etc.) this year and over the next few years (together with the previously used units). The introduction of SI units will also affect all norms and other documentation, such as standards, normals, various objects, technical conditions, etc. Following the order of the Minister of Higher and Intermediate Special Education of the USSR and the Minister of Education of the RSFSR, the SI will be introduced in all educational institutions.

As a result of the introduction into the national economy of units of the SI which have not as yet received widespread practical application and also of the provision in the domestic economy of measures and measuring devices assuring the possibility of making measurements in the units of the SI, units not in the SI will not be used in practical applications (will disappear from the domestic economy). The practical introduction of the units of the SI into the national economy will be assured by the issue of corresponding tables for converting the measuring units being used at present into SI units. The conversion tables will include the permissible degree of rounding off. Published questionaries and textbooks will include methods for converting from one system of units to the other as required for the various physical laws and more expedient methods for replacing the various units now in use with SI units which will be better suited to the various types of measurements.

The units of measurements used in all standards documents must be indicated. For example, if the SI is introduced in making measurements on an object for which measurements were heretofore made in other units, it is necessary to preserve the measurements that were taken in terms of the previously used units. We should also proceed in a similar manner in all cases in which SI units are introduced for technical documentation and means are not available for making the original measurements in SI units.

One of the important steps taken is the introduction of SI units not used heretofore in practical applications as governmental standards for industrial items, raw materials, and general technical and other standards. This step will be put into effect starting this year. The units of the SI will be introduced in the standards along with the units in use heretofore in the national economy (that is, the units of other systems or mixed units).

A basic factor in the success of the transition to SI units will be the existence of measures and measuring devices for all types of measurements in SI units; this is associated with the provision of new scales for measuring devices.

In order to assure the practical use of SI units which have not as yet received wide application it is necessary to expand and improve the popularization of the advantages of the SI, ensure the publication of the necessary questionaries and textbooks, reeducate the personnel, and put into effect a series of other measures. Seminars devoted to the SI would be one way of providing information regarding the SI and of answering questions regarding the practical introduction of the units. The seminars must be conducted by the more qualified specialists.

Bearing in mind the fact that the publication of scientific and technical literature must precede by a certain period the direct introduction of the usage of the SI into the national economic practice, the Committee on Standards, Measures, and Measuring Devices of the Council of Ministers of the USSR directs the attention of the publishers of scientific and technical books to the necessity of notifying the authors and editors that SI units should be used in scientific and technical literature that is about to be published in order to ensure the transition to the new system of units.

In those cases where the newly introduced units of the SI have not as yet received wide application (the newton, newton/m<sup>2</sup>, etc.) and also in the absence of measuring devices that could be used to make measurements in SI

units, the new units should be shown together with the units formerly used. The publication of technical literature and standards documentation and of completed works should not be delayed or re-edited in order to introduce the new units.

The introduction into national economic practice of all the units of the SI permits us to benefit from the full advantages of the use of this system in our country, and its international use will facilitate and improve conditions for scientific, technical, and trade and cultural relations between nations.

A necessary condition for the successful completion of the work involved in the introduction into the national economic practice of SI units is active participation in this work and a responsible attitude on the part of large circles of engineering and technical workers and their searching in each individual case for the most expedient technico-economic solution.

Acting Director of the Committee on Standards, Measures,  
and Measuring Devices of the Council of Ministers of the  
USSR

V. Korotkov

## BIBLIOGRAPHY

## NEW LITERATURE

Translated from *Atomnaya Énergiya*, Vol. 15, No. 1,  
p. 99, July, 1963

## Gosatomizdat (Atom Press) Releases

D. J. Rose and M. Clark. Fizika plazmy i upravlyaemya termoyadernye reaktsii [Plasma physics and controlled fusion]. Translated from the English, *Plasmas and Controlled Fusion*, MIT Press, 1961. 1963, 480 pp., 2 rubles, 37 kopeks.

This item is written as a textbook for seniors and graduate physics students interested in plasma physics and controlled thermonuclear reactions.

The first twelve chapters of the book present the fundamentals of plasma physics, magnetohydrodynamics, the elements of gaseous electronics in combination with the theory of transport processes and electrostatics. The next four chapters elucidate the basic principles and present status of research in the controlled fusion field, and outline the problems involved in extracting energy from hypothetical fusion reactors.

The appendices provide: a glossary of notations used in the book, interrelation of various systems of units, frequently used vector relationships, and frequently encountered physical constants.

Stroenie i svoystva splavov urana, toriya i tsirkoniya [Structure and properties of uranium, thorium, and zirconium alloys]. Symposium edited by O. S. Ivanov, 1963, 380 pages, 1 ruble, 34 kopeks.

Forty articles appear in this symposium. They detail the results of experimental studies on the structure and properties of uranium-, thorium-, and zirconium-base alloys, and on the structure and transformations of several other systems; phase diagrams of binary and ternary systems, and phase transformations are discussed; ample data are provided on the mechanical and corrosion resistance properties, strength, and creep behavior of alloys containing uranium, thorium, and zirconium.

A. I. Bezgubov, Yu. I. Byvshikh, P. K. Dement'ev, Ya. M. Kislyakov, L. V. Kovalev, V. N. Kotlyar, V. G. Kruglova, L. S. Rudnitskaya, and V. M. Tsyru'nikov. Uran v drevnikh konglomeratakh [Uranium in ancient conglomerates]. 1963, 188 pages, 95 kopeks.

This book draws inferences from available data on foreign uranium deposits associated with ancient conglomerates, and points out the governing laws of formation of mineralization as an aid in spotting signs of ore. The first part of the book deals with the Witwatersrand uraniumiferous and auriferous district, and the second part with the Blind River reserves which are in no way inferior to the Witwatersrand. The third portion of the book presents information on the Jacobina ore district in Brazil, while the fourth deals with uranium manifestations in ancient conglomerates of Gabon, Ghana, and some other countries. The fifth and last part presents an analysis of extant hypotheses on the genesis of ancient metalliferous conglomerates.

The literature reference list includes 154 titles.

## ARTICLES FROM THE PERIODICAL LITERATURE

Translated from Atomnaya Énergiya, Vol. 15, No. 1,  
pp. 99-104, July, 1963

I. Nuclear Physics

(Nuclear reactions, neutrons, fission of nuclei)

J. Appl. Phys., 34, No. 1 (1963)

O. Oen, et al., 302-312, Ranges of high-energy atoms in solids.

J. Inorg. and Nucl. Chem., 24 (December, 1962)

M. Ramaniah and A. Wahl, 1185-89, Fission of  $\text{Th}^{232}$  by 9.5 MeV deuterons. The yield/mass curve.

Nucl. Sci. and Engng., 15, No. 2 (1963)

B. Palowitch and F. Franta, 146-57, Measurement of the temperature coefficient of resonance absorption in uranium metal and uranium oxide.

I. Asplund-Nilsson, et al., 213-16, Mean number of fast neutrons emitted in spontaneous fission of  $\text{U}^{238}$  and  $\text{Pu}^{240}$ .

Nucleonics, 21, No. 4 (1963)

J. Waters, 74-76, Measuring particle velocities with Cherenkov rings.

Nuvo Cimento, 27, No. 2 (1963)

H. De Carvalho, et al., 468-74, Fission of uranium, thorium, and bismuth by 20 BeV protons.

II. Plasma Physics

Doklady Akad. Nauk SSSR, 147, No. 5 (1962)

Yu. L. Klimontovich, 1063-66, Note on the statistical theory of homogeneous isotropic turbulence in a relativistic plasma.

L. S. Solov'ev, 1071-74, On the Stability of a cylindrical plasma jet in a magnetic field.

Zhur. tekhn. fiz., 33, No. 3 (1963)

V. E. Golant, 257-62, Effect of collisions between like charged particles on plasma diffusion across a strong field.

A. V. Gurevich and Yu. N. Zhivlyuk, 276-90, On the heating of multiply-charged impurity ions in a plasma.

A. B. Berezin, et al., 291-95, Spectroscopic studies on collective motions of N IV ions in the "Al'fa" machine.

V. B. Gil'denberg and I. G. Kondrat'ev, 301-306, Resonance interaction between an electromagnetic field and higher-order multipole moments of a plasmoid.

V. I. Kogan, 371-73, Gas filter cuts off radiation from particles.

Ahur. eksptl. i teoret. fiz., 44, No. 2 (1963)

L. E. Gurevich, 548-55, Thermomagnetic waves and excitation of the magnetic field in a nonequilibrium plasma.

A. A. Galeev and V. I. Karpman, 592-602, Tub turbulence theory of a weakly nonequilibrium rarefied plasma and shock wave structure.

V. D. Shapiro, 613-25, Contribution to the nonlinear theory of interaction between "monoenergetic" beams and a plasma.

Zhur. eksptl. i teoret. fiz., 44, 3 (1963)

Yu. M. Aleskovskii, 840-45, Investigation of bulk recombination in a cesium plasma.

A. A. Galeev, et al., 903-11, "Universal" instability of a nonuniform plasma in a magnetic field.

A. B. Mikhailovskii and L. I. Rudakov, 912-18, Note on the stability of a spatially inhomogeneous plasma immersed in a magnetic field.

A. B. Mikhailovskii and A. V. Timofeev, 919-21, Cyclotron instability of an inhomogeneous plasma.

Izvestiya vyssh. ucheb. zaved. Radiofizika, 5, No. 6 (1962)

F. V. Bunkin, 1062-71, Emission of a nonequilibrium plasma.

V. N. Tsytovich, 1078-92, Passage of fast particles through a magnetoactive plasma.

L. S. Bogdankevich, et al., 1093-1103, Electromagnetic field noise in a nonequilibrium plasma.

Yu. A. Kirochkin, 1104-14, Contribution to the theory of noise in magnetohydrodynamics.

Nuovo Cimento, 27, No. 5 (1963)

M. Feix, 1130-37, Propagation of a double-stream instability in a plasma.

Phys. Fluids, 5, No. 11 (1962)

W. Bostick, 1406-1409, Measurement of properties of plasma eddies formed by velocity shear in a magnetic field.

C. Pan, 1410-15, Some general characteristics of a two-dimensional incompressible magnetohydrodynamic flow.

R. Levy, 1416-23, Exact solutions to a class of linearized problems of magnetohydrodynamic flow.

J. Menkes, 1414-27, Stability of a heterogeneous shear layer in a magnetic field.

J. Radlow and W. Ericson, 1428-34, Transverse MHD flow past a semiinfinite plane.

N. Krall and M. Rosenbluth, 1435-46, Drift instabilities in a slightly inhomogeneous plasma.

C. Morawetz, 1447-50, Modifications of the structure of a collisionless magnetohydrodynamic wave.

T. Wilson, 1451-55, Structure of collisionless MHD waves.

I. Bohachevsky, 1456-67, Simple waves and shock waves in magnetohydrodynamics.

M. Surdin, 1479-80, Propagation of ultrasonic waves in plasmas.

J. Morris, 1480-81, Damping of quantized longitudinal electron oscillations in a nondegenerate plasma.

K. Halbach, et al., 1482-83, Generation of a hot rotating plasma.

K. Thom and J. Norwood, 1484-85, A new method for measuring electrical conductivity with a magnetic probe.

Plasma Phys., 4, No. 6 (1962)

N. Allen, et al., 375-90, Toroidal discharge in the Spectrum IV.

T. Fowler, 391-94, Integration of Vlasov equation.

G. Landauer, 395-400, Generation of harmonics of the electron cyclotron frequency in a Penning discharge.

J. Taylor, 401-408, Rotation and instability of a plasma in experiments using fast compression of the field  $B_z$ .

S. Edwards and J. Sanderson, 409-414, A new approach to transport problems in a fully ionized plasma II.

H. Teh, 415-16, Pseudoenergetic positive ions in plasma jets.

### III. Acceleration of Charged Particles. Accelerators

Zhur. tekhn. fiz., 33, No. 3 (1963)

V. K. Grishin, 307-16, Interaction between a space charge and the high-frequency field in cyclic accelerators.

G. I. Zhileiko, 317-19, Effect of current of accelerated electrons on the propagation constant of a traveling accelerating wave.

V. P. Bykov, 337-44, Effect of magnetic field inhomogeneities on particle motion in a microtron.

A. I. Pavlovskii, et al., 374-76, Note on the injection energy dependence of betatron intensity.

Pribory i tekhn. éksp., No. 1 (1963)

G. M. Anisimov and V. A. Teplyakov, 21-22, Focusing with an accelerating field.

Atomwirtschaft, 8, No. 2 (1963)

N. Hom, 99-100, The linear accelerator at the Riso research center.

Plasma Phys., 4, No. 6 (1962)

L. Sipek, 417-18, Stabilization of excitation of a betatron or synchrotron magnet.

#### IV. Nuclear Engineering. Nuclear Power

(Neutron physics. Nuclear reactor theory and calculations. Nuclear reactor design. Performance of nuclear reactors and nuclear power stations. Radiation shielding. Disposal of radioactive wastes.)

Avtomatika i telemekh. (Mosk. inzh. fiz. inst.), No. 3 (1962)

Yu. I. Gribanov, et al., 5-15, Test stand for nuclear plant power transients.

Yu. V. Grigor'ev and B. A. Kuvshinnikov, 16-21, Pulsed control of reactor power.

P. I. Popov and V. G. Terent'ev, 22-25, Enhanced reliability of a shielding system in the presence of noise.

Voprosy dozimetrii i zashchity ot izlucheniia, No. 1 (1962)

N. G. Gusev, et al., 7-23, Improved gamma-constant radioisotopes.

V. P. Mashkovich, 24-32, Use of point and slab directed sources in shielding materials studies.

V. I. Popov, 33-36, Note on self-absorption of gamma radiation in extended sources.

V. I. Popov, 37-45, Some experimental data on emission by cylindrical sources.

D. P. Osanov, 46-52, Contribution of emission resulting from multiple scattering in a volume source to the dose on the other side of the shielding.

D. P. Osanov and E. E. Kovalev, 53-54, Determination of buildup factor of scattered emission from extended sources.

A. V. Larichev and V. I. Mitin, 55-56, Buildup factors for low-energy gamma dosage in aluminum.

A. E. Kramer-Ageev and V. P. Mashkovich, 57-65, Dose distribution of fission neutrons in some shielding media.

A. V. Larichev, et al., 66-73, Effect of channels in the shielding on attenuation of gamma emission from extended sources.

A. M. Panchenko, 74-77, Use of standard dosimeters in fields of pulsed gamma radiation.

V. V. Pavlov, 78-80, Note on the use of the Sakharov counter in an abruptly varying gamma field.

Sbornik trud. Mosk. inzh.-stroit. inst. im. Kuibysheva, No. 41 (1962)

S. T. Shershnev, 21-32, Nuclear reactor safety and strength evaluation of containment sheels.

L. N. Zaitsev and M. M. Komochkov, 33-44, Optimum amount of water in concrete reactor shielding.

Teploenergetika, No. 2 (1963)

L. S. Serman and V. D. Mikhailov, 82-87, Determination of burnout in boiling of high-boiling coolant in pipes.

Trudy nauchno-issled. inst. betona i zhelezobetona akad. stroit. i arkhitekt. SSSR, No. 29 (1962)

A. E. Desov and V. I. Nodol'skii, 4-36, Some aspects of heavy concrete technology for radiation shielding.

Atomic Energy Review (IAEA), 1, No. 1 (1963)

E. Proksch, 5-42, Purification of reactor moderators and coolants.

Atomkernenergie, 8, No. 2 (1963)

E. Kern, 41-51, Effect of reflector on reactor temperature coefficients.



A. Jannussis, 52-53, Thermal spectrum in absorbing media.

H. Brauer, 54-61, Heat transfer in annular gaps by forced convection and local boiling (II).

H. Weiss, 70-73, Measurement of reactor pulse power by Cherenkov radiation.

Atompraxis, 9, No. 2 (1963)

Beauge, et al., 52-58, French reactors for studying biological shielding.

F. Reiff, et al., 52-58, Deactivation of tissues with polyphosphate solutions.

H. Bernhardt, 64-67, Study of deactivating action of a filter unit.

Atomwirtschaft, 8, No. 2 (1963)

--, 48-50, Outlook for nuclear power development in the Scandinavian countries.

H. Brynielsson, 51-54, Nuclear power in Sweden.

O. Gimstedt and I. Wivstad, 55-57, Introduction of nuclear electric power generating stations to the Swedish electric power grid.

C. Mileikowsky, et al., 58-62, The Swedish atomic industry.

P. Margen, 63-67, Development of reactor design in Sweden.

E. Laurila, 78-89, Development of nuclear power in Finland.

T. Bjerger, 80-83, The Danish Atomic Energy Commission and the Riso Research Center.

H. Harboe, 84-87, Danish power picture and the Danish nuclear industry program.

S. Werner, 87-88, Nuclear maritime reactor projects in Denmark.

A. Jonsson, 105-108, Pressurized heavy-water reactor and uniform fuel placement.

C. Jacobsen, 112, The Riso plant for processing low-level liquid wastes.

G. Randers, 117-118, Atomic energy in Norway.

F. Moller, 119-120, Norwegian industry and nuclear power.

T. Volledal, 121-22, The Norwegian Atomic Energy Institute.

R. Rose, 123-26, The Halden heavy-water boiling reactor.

V. Eriksen, 127029, The reactor physics research program at the NORA reactor in Norway.

J. Wilhelmsen, 130-32, Development of nuclear seagoing power plants in Norway.

Chem. and Process Engng., 44, No. 3 (1963)

T. Deighton, 138-44, Development of water-moderated reactors.

Énergie nucléaire, 5, No. 1 (1963)

W. Haegi, 26-30, Processing of radioactive wastes and uranium recovery.

Y. Prax, 35-39, The Mol nuclear energy research reactor.

Engineer, 215, No. 5587 (1963)

--, 336-40, Nuclear merchant ship reactor project.

--, 382-84, Present and future costs for large-scale nuclear power stations.

Engineer, 215, No. 5588 (1963)

--, 400-401, Heavy-water steam-generating reactor.

Engineer, 215, No. 5590 (1963)

--, 468-472, Evaluation of gas-cooled reactors.

Engineer, 215, No. 5591 (1963)

--, 509-511, Improved gas-cooled reactor No. 1 at Windscale.

--, 545-48, Core characteristics of the Yankee power station reactor.

Engineer, 215, No. 5592 (1963)

--, 554-58, Commissioning and performance of the AGR reactor at Windscale.

--, 579-582, The improved gas-cooled reactor at Windscale.

Industries Atomiques, 7, No. 1-2 (1963)

R. Darras, 55-65, Corrosive attack on zirconium and zirconium alloys by high-temperature gases.

L. M. Vincent, et al., 67-77, 79-80, Corrosive attack on zirconium and zirconium alloys by uranium hexa-fluoride.

Kernenergie, 5, No. 2 (1963)

G. Bessner, et al., 55-63, Calculation of effective cross sections for uranium-water lattices.

Kerntechnik, 5, No. 2 (1963)

H. Fendler, et al., 41-54, Determination of radiation conditions and effectiveness of biological shielding at the inauguration of the Kahl nuclear reactor power stations.

W. Ullrich, 54-61, Fabrication, assembly, and testing of the main components of the Kahl nuclear reactor power stations.

R. Hemmleb, 62-63, Experience in the construction of the Kahl nuclear reactor power stations.

D. Ulken, 63-65, Heat transfer test stand for maritime reactor components.

H. Müller and H. Uschwa, 66-71, Heat removal system in the DRAGON high-temperature reactor.

H. Acher, 71-75, Development of control rod drives for boiling-water reactors.

B. Schallopp, 76-79, Survey of reactivity measurement techniques.

Nucl. Energy (March, 1963)

P. Egelstaff, 66-69, Scattering of subthermal neutrons by metals.

Nucl. Engng., 8, No. 83 (1963)

--, 115-21, Evaluation of the AGR improved gas-cooled reactor.

G. Hefferon, 122-26, Reliability of a nuclear power station.

--, 127-32, Nuclear power on the line in Sweden.

Nucl. Power, 8, No. 83 (1963)

B. Aler, 34-36, Nuclear power picture in Sweden.

P. Margen, 37-39, The Swedish Marviken nuclear reactor power station project, around a boiling heavy-water reactor.

N. Rydell, 40-42, The Swedish Agesta power station.

O. Hellström, 42-44, Reactor pressure vessel (Agesta).

T. Wykman, 44-46, Heat exchangers (Agesta).

P. Erdhäll, 47-48, Fuel transfer mechanisms (Agesta).

S. Ericsson, et al., 48-50, Control equipment (Agesta).

O. Hedström, 51-53, Installation and assembly of Agesta components.

Nucl. Power, 8, No. 84 (1963)

R. Coombe, 54-56, Neutron energy spectra. III. Measurements in the 0.5-15 MeV energy range.

R. Guard, 51-53, Status of reactor design as of 1962.

A. Wyatt, 57-60, The CANDU reactor and the Canadian power reactor building program.

Nucleonics, 21, No. 4 (1963)

--, 47-52, Reactors on the lines: Indian Point.

D. Harvey, et al., 56-59, Reliability and safety of isotope generator for space missions.

C. Heindl, et al., 80-85, Fission-fragment conversion reactors for space.

Nukleonik, 5, No. 2 (1963)

T. Gozani, 55-62, The reactivity concept and its application to kinetic measurements.

A. Fraude, 62-67, On the solution of kinetics equations for the case of periodic reactivity variations.

C. Hashmi, 67-74, Absorption of energy, transmission, and diffusion of gamma radiation in infinite homogeneous media.

D. Emendörfer, 74-82, Boundary conditions for neutron flow in a cylinder of finite dimensions, according to the  $P_L$ -approximation of the transport equation.

H. Kellner, 85-86, An attempt on an explicit derivation of the Boltzmann equation.

#### V. Nuclear Materials

(Geology. Chemistry. Chemical technology. Metallurgy)

Vestnik Leningrad. Univ., No. 24, Seriya geol. i geograf., No. 4 (1962)

L. F. Syritso, 65-73, Data on uraniferous minerals from one of the pegmatitic deposits.

Doklady akad. nauk SSSR, 147, No. 5 (1962)

N. I. Blinova, et al., 1112-13, On the magnetic properties of  $U_2O_5$ .

Doklady akad. nauk SSSR, 147, No. 6 (1962)

A. V. Nikoläev and Yu. A. Afanas'ev, 1380-81, Mutual effects of thorium nitrate and cerium nitrate (IV) in coextraction by tributylphosphate.

Zhur. anal. khim., 17, No. 9 (1962)

I. A. Berezin and V. I. Malyshev, 1101-1104, Determination of trace amounts of hydrogen and oxygen in uranium metal.

Zhur. strukturn. khim., 3, No. 6 (1962)

A. V. Karyakin and M. P. Volynets, 714-16, Infrared spectra of thorium carbonate complex.

M. E. Dyatkina and Yu. N. Mikhailov, 724-47, Structure of uranyl and its analogs.

Zhur. fiz. khim., 36, No. 11 (1962)

E. D. Kiseleva, et al., 2457-64, Investigation of the radiation stability of ion exchange resins.

E. D. Kiseleva, et al., 2465-68, Effect of ionizing radiations from a stream of accelerated electrons on anion exchange resins.

Izvestiya akad. nauk SSSR, Otdel. tekhn. nauk. Metallurgiya i toplivo, No. 6 (1962)

I. N. Plaksin, et al., 185-91, Extraction of rare earths.

Atomic Energy Revue (IAEA), 1, No. 1 (1963)

S. Bush, 43-92, Special materials used in reactor building and their fabrication technology.

Atomwirtschaft, 8, No. 2 (1963)

L. Hall and S. Brandberg, 101-104, Fabrication of powder from sintered uranium dioxide.

S. Aas, 113-16, Nuclear fuel and reactor materials in Norway.

Chem. and Process Engng., 44, No. 3 (1963)

N. Hassett, 127-31, Areas of application of fluidization (review of patents granted).

Énergie nucléaire, 5, No. 1 (1963)

J. Doumerc, 4-15, Production technology of fuel elements.

P. Faugeras and M. Bourgeois, 16-25, Study of corrosion of uranium oxides and alloys in the gaseous phase, with applications to spent fuel elements.

Industries Atomiques, 7, No. 1-2 (1963)

A. Degeilh and R. Simon, 81-85, Defects in solids bombarded by charged particles. II.

Kernenergie, 5, No. 2 (1963)

S. T. Konobeevsky, 49-55, Present status of knowledge on the nature of radiation damage.

D. Naumann, 73-76, Laboratory investigation of recovery of uranium fuel by the chlorination method.

D. Naumann, 81, Ion exchange separation of plutonium on SBW wofatite in an alcoholic solution of hydrochloric acid.

Nature, 197, No. 4873 (1963)

P. Pauson, et al., 1200, Acid leaching of uranium and thorium carbides.

Nucl. Power, 8, No. 83 (1963)

--, 54-55, The Ronstad uranium mill.

Nukleonik, 5, No. 2 (1963)

C. Keller, 41-48, Investigation of germanates and silicates of tetravalent elements from thorium to americium.

H. Riedel, 48-54, Properties of inorganic ion exchange zirconium-base and clayey mineral resins.

#### VI. Dosimetry and Radiometry. Nuclear Meteorology

Voennyi med. zhur., No. 12 (1962)

I. S. Sobol', 36-37, Gamma shielding in calibration of dosimetric instrumentation.

Izvestiya akad. nauk SSSR, Seriya geofiz., No. 1 (1963)

K. P. Makhan'ko, 183-87, On the shape of the spectrum of particle sizes of radioactive dust of natural origin.

Trudy akad. nauk Litov. SSR, Seriya B., 4 (1962)

B. I. Styro and C. A. Garbaliuskas, 23-40, On the natural radioactivity of atmospheric fallout and some related problems.

Atomkernenergie, 8, No. 2 (1963)

K. Becker, 74-77, Sources of error in neutron personnel dosimetry using nuclear emulsions.

G. Malkowski, 78-79, Arguments on the timely detection of radioactive fallout.

Atompraxis, 9, No. 2 (1963)

L. Distel, et al., 39-44, Practical aspects of the use of radiometers and pocket dosimeters.

H. Hardt, et al., 45-48, Dosimetry using phosphate glass.

Kernenergie, 5, No. 2 (1963)

M. Frank, 76-80, Thermoluminescent dosimetry using the LiF phosphor, and energy dependence of thermoluminescent dosimeters.

Nature, 197, No. 4871 (1963)

T. Mamuro, et al., 964-66, Fractionation of high-level fallout.

Nucleonics, 21, No. 4 (1963)

N. Baily and K. Hoalst, 68, 70, 72-73, Dosimetry of space radiations.

#### VII. Radioactive and Stable Isotopes

(Separation, production, use)

Pribory i tekhnika eksp., No. 1 (1963)

Yu. S. Zaslavskii, et al., 149-52, Measurement of coating thickness by recording scattered betas.

Soobshch. akad. nauk Gruz. SSR, 29, No. 6 (1962)

I. N. Pantskhava, 691-95, Note on the use of radioisotopes to determine the physicommechanical properties of concrete.

Atomic Energy Review, 1, No. 1 (1963)

R. Hara, 93-140, Chemical research performed at nuclear research reactors.

Atomwirtschaft, 8, No. 2 (1963)

C. Osterlundh and L. Erwall, 67, 68, 73, 74, Production and use of radioactive isotopes in Sweden.

K. Heydom, 93-95, Production of radioactive isotopes in Denmark.

E. Somer, 96-98, Technical applications of radioactive isotopes in Denmark.

U. Been, 133-135, Fabrication and use of radioactive isotopes in Norway.

Énergie nucléaire, 5, No. 1 (1963)

A. Loverdo, 31-34, Process control instruments and processes utilizing trace isotopes.

Jaderná Energie, No. 6 (1963)

F. Behounek, K. Barta, and B. Fiser, Rapid monitoring of beta activity in liquid wastes.

J. Silar and O. Nováková, Single-crystal scintillation gamma spectrometer: parameters and applications.

K. Stetina, Cermets: a material for fuel element cladding.

L. Simon, Use of radioactive traces in coal flotation.

J. Boucek, High-voltage source for radiation detectors.



Izv. AN SSSR O(td). Kh(im). N(auk)	Izvestiya Akademii Nauk SSSR: Otdelenie khimicheskikh nauk	Bulletin of the Academy of Sciences of the USSR: Division of Chemical Science	Consultants Bureau	16	1	1952
Izv. AN SSSR O(td). T(ekhn). N(auk): Metall. i top.	(see Met. i top)					
Izv. AN SSSR Ser. fiz(ich).	Izvestiya Akademii Nauk SSSR: Seriya fizicheskaya	Bulletin of the Academy of Sciences of the USSR: Physical Series	Columbia Technical Translations.	18	3	1954
Izv. AN SSSR Ser. geofiz.	Izvestiya Akademii Nauk SSSR: Seriya geofizicheskaya	Bulletin of the Academy of Sciences of the USSR: Geophysics Series	American Geophysical Union	7	1	1957
Izv. AN SSSR Ser. geol.	Izvestiya Akademii Nauk SSSR: Seriya geologicheskaya	Bulletin of the Academy of Sciences of the USSR: Geologic Series	American Geological Institute	23	1	1958
Iz. Vyssh. Uch. Zav., Tekh. Tekh. Prom.	Izvestiya Vysshikh Uchebnykh Zavedeni Tehnologiya Tekstil'noi Promyshlennosti	Technology of the Textile Industry, USSR	The Textile Institute (Manchester)	4	1	1960
Kauch. i rez.	Kauchuk i rezina	Soviet Rubber Technology	Palmerston Publishing Company, Inc.	18	3	1959
Kolloidn. zh(urn).	Kinetika i kataliz	Kinetics and Catalysis	Consultants Bureau	1	1	1960
Metallov. i term.	Koks i khimiya	Coke and Chemistry, USSR	Coal Tar Research Assn. (Leeds, England)	1	8	1959
Met. i top.(gorn.)	Kolloidnyi zhurnal	Colloid Journal	Consultants Bureau	14	1	1952
Mikrobiol.	Kristallografiya	Soviet Physics - Crystallography	American Institute of Physics	2	1	1957
OS, Opt. i spekt.	Metallovedenie i termicheskaya obrabotka metallov	Metals Science and Heat Treatment of Metals	Acta Metallurgica	6	1	1958
Paleontol. Zh(urn)	Metallurg	Metallurgist	Acta Metallurgica	1	1	1957
Pribory i tekhn.	Metallurgiya i toplivo (gornoye delo)	Russian Metallurgy and Fuels(mining)	Scientific Information Consultants, Ltd.	1	1	1960
Eks(perimenta)	Mikrobiologiya	Microbiology	National Science Foundation*	26	1	1957
Prikl. matem. i mekh(an).	Ogneupory	Refractories	Acta Metallurgica	25	1	1960
PTE	Optika i spektroskopiya	Optics and Spectroscopy	American Institute of Physics	6	1	1959
Radiotekh.	Paleontologicheskii Zhurnal	Journal of Paleontology	American Geological Institute	5	1	1962
Radiotekhn. i elektronika)	Pochvovedenie	Soviet Soil Science	National Science Foundation**	53	1	1958
Stek. i keram.	Poroshkovaya Metallurgiya	Soviet Powder Metallurgy and Metal Ceramics	Consultants Bureau	2	1	1962
Svaroch. proiz-vo	Priporostroenie	Instrument Construction	Taylor and Francis, Ltd. (London)	4	1	1959
Teor. veroyat. i prim.	Pribory i tekhnika eksperimenta	Instruments and Experimental Techniques	Instrument Society of America	3	1	1958
Tsvet. metally	Prikladnaya matematika i mekhanika (see Pribory i tekhn. eks.)	Applied Mathematics and Mechanics	Am. Society of Mechanical Engineers	22	1	1958
UFN	Problemy Severa	Problems of the North	National Research Council of Canada	4	1	1958
UKh, Usp. khimi	Radiokhimiya	Radiochemistry	Consultants Bureau	4	1	1962
UMN	Radiotekhnika	Radio Engineering	Am. Institute of Electrical Engineers	16	1	1961
Vest. mashinostroeniya	Radiotekhnika i elektronika	Radio Engineering and Electronic Physics	Am. Institute of Electrical Engineers	6	1	1961
Vop. onk(ol).	Stal'	Stal (in English)	Iron and Steel Institute	19	1	1959
Zav(odsk), lab(oratoriya)	Stanki i instrument	Machines and Tooling	Production Engineering Research Assoc.	30	1	1959
ZhAKh, Zh. anal(it). Khim(ii)	Steklo i keramika	Glass and Ceramics	Consultants Bureau	13	1	1956
ZhETF	Svarochnoe proizvodstvo	Welding Production	Br. Welding Research Assn. (London)	5	4	1959
Zh. eksperim. i teor. fiz.	Teoriya veroyatnostei i ee primeneniye	Theory of Probability and Its Application	Soc. for Industrial and Applied Math.	1	1	1956
ZhFKh	Tsvetnye metally	The Soviet Journal of Nonferrous Metals	Primary Sources	33	1	1960
Zh. fiz. khimii	Uspekhi fizicheskikh nauk	Soviet Physics - Uspekhi (partial translation)	American Institute of Physics	66	1	1958
Zh. neorg(an). khim.	Uspekhi khimii	Russian Chemical Reviews	Chemical Society (London)	29	1	1960
ZhOKh	Uspekhi matematicheskaya nauk	Russian Mathematical Surveys	Cleaver-Hume Press, Ltd. (London)	15	1	1960
ZhPKh	Vestnik mashinostroeniya	Russian Engineering Journal	Production Engineering Research Assoc.	39	4	1959
Zh. obshch. khim.	Voprosy onkologii	Problems of Oncology	National Institutes of Health**	7	1	1961
ZhPKh	Zavodskaya laboratoriya	Industrial Laboratory	Instrument Society of America	24	1	1958
Zh. prikl. khim.	Zhurnal analiticheskoi khimii	Journal of Analytical Chemistry	Consultants Bureau	7	1	1952
ZhSKh	Zhurnal eksperimental'noi i teoreticheskoi fiziki	Soviet Physics - JETP	American Institute of Physics	28	1	1955
Zh. strukt(urnoi) khim.	Zhurnal fizicheskoi khimii	Russian Journal of Physical Chemistry	Chemical Society (London)	33	7	1959
ZhTF	Zhurnal neorganicheskoi khimii	Journal of Inorganic Chemistry	Chemical Society (London)	4	1	1959
Zh. tekhn. fiz.	Zhurnal obshchei khimii	Journal of General Chemistry USSR	Consultants Bureau	19	1	1949
Zh. vyssh. nervn. deyat. (im. Pavlova)	Zhurnal prikladnoi khimii	Journal of Applied Chemistry USSR	Consultants Bureau	23	1	1950
	Zhurnal strukturnoi khimii	Journal of Structural Chemistry	Consultants Bureau	1	1	1960
	Zhurnal tekhnicheskoi fiziki	Soviet Physics - Technical Physics	American Institute of Physics	26	1	1956
	Zhurnal vychislitel'noi matematika i matematicheskoi fiziki	U.S.S.R. Computational Mathematics and Mathematical Physics	Pergamon Press, Inc.	1	1	1962
	Zhurnal vysshei nervnoi deyatelnosti (im I. P. Pavlova)	Pavlov Journal of Higher Nervous Activity	National Institutes of Health**	11	1	1961

\*Sponsoring organization. Translation published by Consultants Bureau.

\*\*Sponsoring organization. Translation published by Scripta Technica.

SIGNIFICANCE OF ABBREVIATIONS MOST FREQUENTLY  
ENCOUNTERED IN SOVIET PERIODICALS

FIAN	Phys. Inst. Acad. Sci. USSR.
GDI	Water Power Inst.
GITI	State Sci.-Tech. Press
GITTL	State Tech. and Theor. Lit. Press
GONTI	State United Sci.-Tech. Press
Gosenergoizdat	State Power Press
Goskhimizdat	State Chem. Press
GOST	All-Union State Standard
GTTI	State Tech. and Theor. Lit. Press
IL	Foreign Lit. Press
ISN (Izd. Sov. Nauk)	Soviet Science Press
Izd. AN SSSR	Acad. Sci. USSR Press
Izd. MGU	Moscow State Univ. Press
LEIIZhT	Leningrad Power Inst. of Railroad Engineering
LET	Leningrad Elec. Engr. School
LETI	Leningrad Electrotechnical Inst.
LEIIZhT	Leningrad Electrical Engineering Research Inst. of Railroad Engr.
Mashgiz	State Sci.-Tech. Press for Machine Construction Lit.
MEP	Ministry of Electrical Industry
MES	Ministry of Electrical Power Plants
MESEP	Ministry of Electrical Power Plants and the Electrical Industry
MGU	Moscow State Univ.
MKhTI	Moscow Inst. Chem. Tech.
MOPI	Moscow Regional Pedagogical Inst.
MSP	Ministry of Industrial Construction
NI ZVUKSZAPIOI	Scientific Research Inst. of Sound Recording
NIKFI	Sci. Inst. of Modern Motion Picture Photography
ONTI	United Sci.-Tech. Press
OTI	Division of Technical Information
OTN	Div. Tech. Sci.
Stroiizdat	Construction Press
TOE	Association of Power Engineers
TsKTI	Central Research Inst. for Boilers and Turbines
TsNIEL	Central Scientific Research Elec. Engr. Lab.
TsNIEL-MES	Central Scientific Research Elec. Engr. Lab.-Ministry of Electric Power Plants
TsVTI	Central Office of Economic Information
UF	Ural Branch
VIESKh	All-Union Inst. of Rural Elec. Power Stations
VNIIM	All-Union Scientific Research Inst. of Metrology
VNIIZhDT	All-Union Scientific Research Inst. of Railroad Engineering
VTI	All-Union Thermotech. Inst.
VZEI	All-Union Power Correspondence Inst.

Note: Abbreviations not on this list and not explained in the translation have been transliterated, no further information about their significance being available to us. — Publisher.



# SOVIET RADIOCHEMISTRY

(RADIOKHIMIYA)

In cover-to-cover translation

A new Soviet journal (first issued in 1959) publishes research works emanating from the Khlopin Radium Institute, Academy of Sciences USSR, and is under the editorial supervision of Academician V. M. Vdovenko, director of the Institute. The other members of the editorial board include such top researchers as I.P. Alimarin, A. I. Brodskii, E. K. Gerling, A. A. Grinberg, V. R. Klokman, L. V. Komlev, B. V. Kurchatov, A. N. Nésmeyanov, A. V. Nikolaev, B. P. Nokol'skii, V. I. Spitsyn, I. E. Starik, and A. P. Vinogradov.

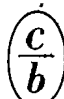
In present-day science and technology, where the radioactive properties of various substances are finding increased application in the study of chemical reactions and properties, it is of great importance that the Western scientific community be cognizant of Soviet progress in radiochemistry. The translations of SOVIET RADIOCHEMISTRY will provide a running account of Soviet progress in the chemistry of atomic elements, methods of research in radiochemistry, the study of radioactivity, the history of radiochemistry, and applied radiochemistry. The information and letters section contains concise accounts of interesting research in radioactivity.

Contributors to the journal include S. Z. Roginskii, I. V. Tananaev, P. I. Kondratov, A. D. Gel'man, Yu V. Egorov, V. P. Zaitseva, V. P. Shvedov, A. N. Ponomarev, V. S. Zlobin, and members of the editorial board.

The journal is issued bi-monthly, as will be the English edition. Translation began with the first issue of 1962.

Study of Coprecipitation of Microimpurities in Isothermal Relief of Supersaturation of a  $K_2SO_4$  Solution. II. Coprecipitation of Lanthanum with  $K_2SO_4$  • Crystallization Coefficients of Some Alkali-Metal Halides with Microconcentrations of One of the Components • Coprecipitation of Microgram Amounts of Molybdenum with Some Inorganic Precipitates • Temperature Dependence of Distribution Coefficients in the Extraction of Uranyl Nitrate from Aqueous Solutions with Diethyl Ether • Salting-Out Action of Group II Metal Nitrates in the Extraction of Uranyl Nitrate with Diethyl Ether • Physicochemical Characteristics of the Dynamics of Sorption of Radioactive Substances • State of Protactinium in Aqueous Solutions. VI. Adsorption Properties of Protactinium • Sorption of Some Radioactive Isotopes from Aqueous Solutions by Active Manganese Dioxide • Adsorption of Yttrium and Zirconium by Zirconium Phosphates • Structure of Uranyl Nitrate Dihydrate • Plutonium Fluorides • Hydrolytic Behavior of Plutonyl in Aqueous Solutions • Elution of Neptunium from the Anionite AM • Use of Ion Exchange to Study the State of a Substance in Solution. VIII. Study of Uranyl Carbonate Solutions by Ion Exchange • Chromatographic Separation of Protactinium from Zirconium, Titanium, and Niobium • Chromatographic Concentration of Astatine • Isolation of a Group of Carrier-Free Rare Earth Fission Products from Uranium and Thorium • Determination of  $M_s ThI$  by  $M_s ThII$   $\beta$ -Particles in the Presence of Radium-226 • Determination of Radioactive Cesium by the Ferrocyanide Method • Determination of Low Levels of Radioactive Contaminants in Water • Reaction of Recoil Tritium Atoms with Benzene • Recoil Effect in Inner-Complex Compounds of Cobalt in the Reaction  $Co^{59}(n, 2n)Co^{58}$  • Yields of Spallation and Fission Reactions Induced by High-Energy Particles • Mechanism of Zirconium Extraction by Organophosphorus Compounds • Effect of Structural Factors on the Thermodynamic Characteristics of the Extraction of Salts of Basic Dyes • Effect of the Amount of Absorbed Ions in a Chromatography Column on the Position of a Peak on the Elution Curve • Diffusion of Strontium-90 in Soil and Sand.

Annual subscription (6 issues): \$95.00

 **CONSULTANTS BUREAU** 227 West 17 St., New York 11, N. Y.

# SOVIET MASER RESEARCH

Edited by Academician D.V. Skobel'tsyn

Reports of four coordinated researches into the theory and applications of masers for frequency standards, Conducted at the P. N. Lebedev Physics Institute under the guidance of Academician A. M. Prokhorov. Transactions (Trudy) No. 21.

## A THEORETICAL STUDY OF THE FREQUENCY STABILITY OF A MASER

by A. I. Oraevskii

The article presents a general analysis of the functioning of a molecular generator or maser operating with a molecular beam of "sorted" molecules. Effects of external perturbations (pressure and magnetic field effects) are treated, and the problem of hyperfine structure of the emission line is considered. Cases treated in detail are those of masers using inversion transitions in ammonia. Some comparisons between theoretical and experimental results are given for such cases.

## INVESTIGATION OF THE CHARACTERISTICS OF MASERS

( $J = 3, K = 3$  in ammonia  $N^{14}H_3$ )

by G. M. Strakhovskii and I. V. Cheremiskii

The authors report experimental investigations into the dependence of frequency and relative power of an ammonium maser,  $N^{14}H_3$ , on the natural frequency of the resonator, the voltage applied to the quadrupole condenser (or to a circular separation system) and the ammonia pressure in the molecular beam source. Also reported on is the dependence of frequency and relative power of a maser with two intersecting beams on ammonia pressure in the molecular beam source.

## THEORY OF THE HYPERFINE STRUCTURE OF THE ROTATIONAL SPECTRA OF MOLECULES

by K. K. Svidzinskii

A theory of the hfs has been developed which allows the calculation of hyperfine effects in rotational spectra of molecules (in a nondegenerate electronic ground state) with an accuracy not lower than 10 cps. By applying methods of group theory, especially the apparatus of irreducible tensor operators and the  $3j$ -symbols, the calculation of hfs has been successfully simplified and standardized.

In order to provide the necessary accuracy (not lower than 10 cps), the present treatment includes, besides the usual dipole and quadrupole interactions, the magnetic octupole and the electric hexadecapole interactions. A general calculation of the energy of the spin-spin interactions of nuclei in a rotating molecule is presented, along with a general expression for the energy of the dipole  $I \cdot J$  interaction in the asymmetric-top molecule.

## THE $ND_3$ MASER

by N. G. Basov, V. S. Zuev, and K. K. Svidzinskii

Reports work aimed at investigating the possibility of making a maser using inversion transitions of heavy ammonia  $ND_3$ , including the accomplishment of a working model. The power output of the  $ND_3$  maser is reported as  $10^{-11}$  watt at 1656.18 mc ( $J=6, K=6$  line in the inversion spectrum of  $ND_3$ ). The absolute stability of the line, according to preliminary data, is of the order of  $10^{-9}$ .

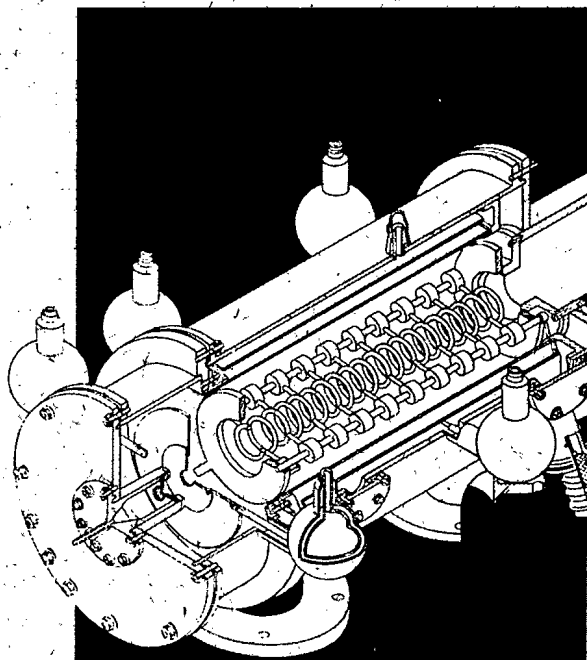
The results of calculations on the hyperfine inversion spectrum of  $ND_3$  are given. Analysis of the hyperfine structure leads to an estimate for the absolute stability of the  $J=6, K=6$  line ( $\sim 10^{-9}$ ).

SOVIET MASER RESEARCH contains a unique bibliography of all work performed in the Laboratory of Oscillations FIAN, P. N. Lebedev Institute from 1935-1961, and covers topics such as: Electron paramagnetic resonance; Quantum electronics; Molecular generators and amplifiers; Time standards; Gas radiospectroscopy; Propagation of radio waves; Statistical radiophysics; Accelerators; and various other problems.

Over 200 pages

Translated from Russian

\$27.50



CONSULTANTS BUREAU  
227 W. 17th St., N. Y. 11, N. Y.